

10 スピントロニクス・マグネティクス | 一般セッション(ポスター講演): 10 スピントロニクス・マグネティクス (ポスター)

[19p-P06-1~50] 10 スピントロニクス・マグネティクス (ポスター)

[19p-P06-1]

Y₂O₃ナノ粒子の磁気特性

○(B)石山 和樹¹、府川 明弘²、中澤 拓斗²、伊藤 風音²、馮 小介²、谷川 哲彦¹、犬井 響熙¹、植木 健太¹、高瀬 浩一¹ (1.日大理工、2.日大院理工)

[19p-P06-2]

MoO₃ナノ粒子の室温強磁性

○中澤 拓斗¹、府川 明弘¹、馮 子介¹、伊藤 風音¹、石山 和樹²、犬井 響熙²、植木 健太²、高瀬 浩一² (1.日大院理工、2.日大理工)

[19p-P06-3]

ZnS、ZnSeナノ粒子の磁気特性

○伊藤 風音¹、府川 明弘¹、中澤 拓斗¹、馮 子介¹、高瀬 浩一² (1.日大院理工、2.日大理工)

[19p-P06-4]

電子および正孔スピンの同時注入下における逆スピンHall効果

○酒井 政道¹ (1.埼玉大理工)

[19p-P06-5]

電子-正孔散乱による運動量緩和の影響を受けたスピン輸送

○酒井 政道¹ (1.埼玉大理工)

[19p-P06-6]

Fe添加CdTe/(Cd,Mg)Te量子井戸におけるFeの電荷揺らぎによる励起子発光スペクトルの分裂

○深海 宏太¹、黒田 真司¹、蓬萊 健志郎¹、古川 園佳¹、Besombes Lucien²、Boukari Herve² (1.筑波大応、2.Néel研)

[19p-P06-7]

Bi(Fe,Co)Oxにおける超軌道分裂の理論的アプローチ

○福島 鉄也¹、新屋 ひかり²、永沼 博^{3,4} (1.産総研、2.東大、3.東北大、4.名古屋大)

[19p-P06-8]

二酸化バナジウム薄膜中のスピン輸送の温度依存性

○(M2)西村 匠¹、神吉 輝夫²、仕幸 英治¹ (1.阪公大院工、2.阪大産研)

[19p-P06-9]

電界印加下における半導体超格子バリアの電子スピン輸送特性

○江藤 亘平¹、樋浦 諭志¹、高山 純一¹、アグス スバギョ¹、末岡 和久¹、村山 明宏¹ (1.北大院情報科学)

[19p-P06-10]

Observation of drain current in carbon nanotube transistor with magnetic electrode for organic spin transistor

○Yuichiro Kurokawa¹, Naoki Tanaka^{2,3}, Masafumi Inaba¹, Naoto Yamashita¹, Hiromi Yuasa¹ (1.ISEE, Kyushu Univ., 2.Grad. Sch. Eng, Kyushu Univ., 3.WPI-I2CNER, Kyusyu Univ.)

[19p-P06-11]

透明導電膜の逆スピンホール効果によるスピン流検出を用いる有機分子薄膜のスピン輸送特性評価

○(M2)松川 裕利¹、山田 奨貴¹、高松 恵人¹、手木 芳男¹、仕幸 英治¹ (1.大阪公大院工)

[19p-P06-12]

Experimentally realizable topological chiral edge spin wave on magnonic crystal

○(D)Juha Do¹, Jae Yong CHO¹, Chun-Yeol YOU¹ (1.Department of Physics and Chemistry, DGIST, Daegu 42988, Republic of Korea)

[19p-P06-13]

マグノニック結晶におけるマグノニックバンドギャップの障壁材料依存性

○(M1)松永 朝成¹、洞口 泰輔¹、眞砂 卓史¹ (1.福岡大理)

[19p-P06-14]

マグノニック結晶のバンドギャップの障壁高さ依存性

○城門 太一¹、洞口 泰輔¹、眞砂 卓史¹ (1.福岡大理)

[19p-P06-15]

有機金属分解法で作製したイットリウム鉄ガーネット薄膜のスピン波の測定

○(M2)今村 圭佑¹、眞砂 卓史¹、笠原 健司² (1.福大理、2.近大産業理工)

[19p-P06-16]

Effects of Magnon Spin-Polarization on Magnon Lifetime in Antiferromagnetic Insulator NiO

○(D)Andi Gumarilang Ahmadi¹, Nawa Kenji¹, Nakamura Kohji¹ (1.Mie Univ.)

[19p-P06-17]

強磁性層状物質CrX₃ (X = Cl, Br, I)の交換相互作用力と結晶磁気異方性の電子論的考察

○村田 尚登¹、Andi Gumarilang¹、名和 憲嗣^{1,2}、中村 浩次¹ (1.三重大院工、2.物材機構)

[19p-P06-18]

Manipulation of the interfacial Dzyaloshinskii-Moriya interaction via the ionic gate voltage adaptation

○(D)Cho Jaeyong¹, Lee Soobeom^{1,2}, Kim Dongryul¹, You Chun-Yeol¹ (1.Department of Physics and Chemistry, DGIST, 2.Basic Science Research Center, DGIST)

[19p-P06-19]

二元系合金の軌道ホール伝導度に関する第一原理的考察

○辻出 裕至¹、名和 憲嗣^{1,2}、中村 浩次¹ (1.三重大院工、2.物材機構)

[19p-P06-20]

Observation of Spin Seebeck Effect in YIG/Rh

○(B)Shuto Sahara¹, Yuichiro Kurokawa¹, Hiromi Yuasa¹ (1.Kyushu Univ.)

[19p-P06-21]

Field-free spin-orbital torque magnetization switching in gallium-doped thulium iron garnet

○山下 尚人^{1,2}、Ngaloy Roselle²、黒川 雄一郎¹、湯浅 裕美¹、Dash Saroj² (1.九大シス情、2.チャルマース工科大)

[19p-P06-22]

Spin-current generation by ultrashort laser pulses in a heavy-metal/rare-earth iron garnet heterojunction

○(M1)Shunsuke Takahashi¹, Yuga You², Kazuto Yamanoi², Yukio Nozaki², Takuya Satoh¹, Kihiro Yamada¹ (1.Tokyo Tech, 2.Keio Univ.)

[19p-P06-23]

MgO(001)上CoFe多層膜の結晶磁気異方性の機械学習と解釈可能性：有効な回帰モデルと記述子の探索から

○名和 憲嗣^{1,2}、萩原 克幸¹、中村 浩次¹ (1.三重大、2.NIMS)

[19p-P06-24]

Magnetism of L1₀-FePd from angle-dependent XMCD: Theory and experiments

○Kenji Nawa^{1,2}, Samuel Vergara^{3,4}, Tetsuro Ueno⁵, Hirofumi Nomachi¹, Kohji Nakamura¹, Hiroshi Naganuma^{4,6} (1.Mie Univ., 2.NIMS, 3.ENS-Paris, 4.Tohoku Univ., 5.QST, 6.Nagoya Univ.)

[19p-P06-25]

第一原理計算によるL1₀合金の角度依存X線磁気円二色性とスピン・軌道磁気モーメントの解析

○野町 宙史¹、名和 憲嗣^{1,2}、中村 浩次¹ (1.三重大院工、2.物材機構)

[19p-P06-26]

第一原理計算による(Mn, Fe, Ni)窒化物の磁気特性の理論的考察

○中村 考志¹、梅津 理恵²、石崎 学³、栗原 正人³ (1.産総研、2.東北大、3.山形大)

[19p-P06-27]

Dynamic magnetic properties in RuO₂/Co-Fe-B stack film

○Anh ThiVan Nguyen^{1,2}, Yoshiaki Saito², Hiroshi Naganuma^{1,2}, Duong Vu³, Shoji Ikeda^{1,2}, Tetsuo Endoh^{1,2,4,5} (1.CSIS, Tohoku Univ., 2.CIES, Tohoku Univ., 3.IoP, VAST, 4.ECEI, Tohoku Univ., 5.RIEC, Tohoku Univ.)

[19p-P06-28]

フェリ磁性Co₂Mn₂C薄膜における侵入炭素サイトの解明

Prabhat Kumar¹、Parasmani Rajput²、阿部 仁³、○磯上 慎二¹ (1.物材機構、2.RRCAT、3.高エネ研)

[19p-P06-29]

Effect of hydrogen annealing in CoFeB/MgO system

○(M1)Noriyuki Seki¹, Toshiaki Morita¹, Daichi Chiba^{1,2,3,4}, Tomohiro Koyama^{1,2,3,5} (1.SANKEN, Osaka Univ., 2.CSRN, Osaka Univ., 3.OTRI, Osaka Univ., 4.SRIS, Tohoku Univ., 5.JST PRESTO)

[19p-P06-30]

CoPt合金ナノ粒子の磁気プラズモニク特性

○(M2)張 晨¹、石田 拓也¹、イ スンヒョク¹、立間 徹¹ (1.東大生研)

[19p-P06-31]

電子ビーム蒸着法で作製した(100)配向β-Sn/M (M = Ni,Cu)積層膜の超伝導と磁性

○熊澤 宏紀¹、山田 啓介¹、嶋 睦宏¹ (1.岐阜大院自)

[19p-P06-32]

Investigation of magnetic properties in gallium-doped epitaxial thulium iron garnet using Brillouin light scattering

○(D)Soojung KIM¹, Naoto YAMASHITA², Soobeom LEE¹, Chun-Yeol You¹ (1.Department of Physics and Chemistry, DGIST, Daegu 42988, Republic of Korea, 2.Faculty of Information Science and Electrical Engineering, Kyushu Univ., Japan)

[19p-P06-33]

スピン偏極電子の生成源のための白金層上へのバリウムフェライト垂直磁化絶縁層の作製

○(M2)足立 亮太¹、田中 雅章¹、小見山 遥²、小野 輝男²、日原 岳彦¹、壬生 攻¹ (1.名工大工、2.京大化研)

[19p-P06-34]

二元化合物Cr_{1-δ}Te薄膜のMBE成長～成長温度による結晶構造変化

○小林 純也¹、仁谷 浩明²、城戸 大貴²、黒田 眞司¹ (1.筑波大数理物質、2.高エネ研)

[19p-P06-35]

希薄磁性半導体粉末における強磁性発現条件の解明

○矢野 智識¹、村山 真理子^{1,2}、趙 新為¹ (1.東理大理、2.東洋大工技研)

[19p-P06-36]

強磁性共鳴下の強磁性金属膜に発生する起電力を利用した充電技術

○(M2)藤井 龍徳¹、辻井 浩佑¹、仕幸 英治¹ (1.大阪公立大学)

[19p-P06-37]

光熱磁気記録を用いた微細磁区の形成条件の検討

○本間 拓真¹、坂口 穂貴¹、野中 尋史²、鷲見 聡³、栗野 博之³、Chafi Fatima Zahra¹、石橋 隆幸¹ (1.長岡技科大、2.愛知工大、3.豊田工大)

[19p-P06-38]

座屈状自己組織化磁性粒子を利用した外部環境記憶マイクロロボット

○井口 恵吾¹、斎木 敏治¹ (1.慶大理工)

[19p-P06-39]

Ni₇₈Fe₂₂/Erq₃/FeCo分子スピントロニクスデバイスにおけるスピン信号の観測

○宮本 龍之介¹、松坂 美月¹、谷口 真理¹、上田 拓海¹、橋本 千佳¹、鹿嶋 倖太郎¹、安藤 和也^{1,2}、海住 英生^{1,2} (1.慶大理工、2.慶大スピンセンター)

[19p-P06-40]

Fabrication of nanoscale magnetoresistance devices using chiral molecules

○Mizuki Matsuzaka¹, Ryunosuke Miyamoto¹, Kotaro Kashima¹, Takumi Ueda¹, Takashi Yamamoto¹, Kohei Sambe², Tomoyuki Akutagawa², Hideo Kaiju^{1,3} (1.Keio Univ., 2.IMRAM, Tohoku Univ., 3.CSRN, Keio Univ.)

[19p-P06-41]

Tunnel Magnetoresistance devices fabricated on polyimide film attached to PDMS

○(M2)Seiya Oishi¹, Yuichiro Kurokawa¹, Naoto Yamashita¹, Hiromi Yuasa¹ (1.Kyushu Univ.)

[19p-P06-42]

磁気渦スピントルク発振器のポテンシャルがダイナミクスに及ぼす影響

○(D)堀住 耕太¹、千葉 貴裕^{2,3}、小峰 啓史¹ (1.茨城大院、2.東北大工、3.東北大学際研)

[19p-P06-43]

磁気トンネル接合を用いた高出力電圧磁気センシング

○若本 瑞葵¹、柴田 有仁¹、Gang Xiao²、海住 英生^{1,3} (1.慶大理工、2.ブラウン大物理、3.慶大スピンセンター)

[19p-P06-44]

Investigation of exchange bias field in magnetic multilayer fabricated by coating

○(M1)Masamune Taguchi¹, Yuichiro Kurokawa¹, Hiromi Yuasa¹ (1.Kyushu Univ.)

[19p-P06-45]

Dielectric constant and VCMA effect of epitaxial MgO tunnel barrier

○Tomohiro Nozaki¹, Hiroshige Onoda¹, Shingo Tamaru¹, Hiroyasu Nakayama¹, Makoto Konoto¹, Takayuki Nozaki¹, Shinji Yuasa¹ (1.AIST)

[19p-P06-46]

Data-writing and shift processes toward a vertical domain wall motion memory with perpendicular magnetic anisotropy

○Feifan Ye¹, Heechan Jang¹, Yoichi Shiota^{1,2}, Hideki Narita¹, Ryusuke Hisatomi^{1,2}, Shutaro Karube^{1,2}, Satoshi Sugimoto³, Shinya Kasai³, Teruo Ono^{1,2} (1.ICR, Kyoto Univ., 2.CSRN, Kyoto Univ., 3.NIMS)

[19p-P06-47]

GdFe磁性細線における電流駆動磁壁の磁気光学検出系の構築

○(M2)鈴木 紀行¹、Mojtaba Mohammadi¹、鷲見 聡¹、田辺 賢士¹、栗野 博之¹ (1.豊田工大)

[19p-P06-48]

GdFe磁性細線メモリにおける磁界記録磁壁と光磁気記録磁壁の電流駆動速度比較

○(M2)和井内 琴理¹、Mojtaba Mohammadi¹、鷲見 聡¹、田辺 賢士¹、栗野 博之¹ (1.豊田工大)

[19p-P06-49]

Effect of Pulse Duration on Domain Wall Motion in Ferrimagnetic GdFe Nanowires

○(P)Mojtaba Mohammadi¹, Satoshi Sumi¹, Kenji Tanabe¹, Hiroyuki Awano¹ (1.Spintronics Laboratory, Toyota Technological Institute, Nagoya 468-8511, Japan)

[19p-P06-50]

3次元デバイスを目指した凹凸構造側面部への垂直磁化膜の作製

○安田 優也¹、黒川 雄一郎²、鷲見 聡¹、栗野 博之¹、田辺 賢士¹ (1.豊田工大工、2.九州大工)

Y₂O₃ ナノ粒子の磁気特性

Magnetic properties of Y₂O₃ nanoparticles

日大理工¹, 日大院理工², °石山 和樹¹, 府川 明弘², 中澤 拓斗², 伊藤 風音², 馮子介²,
谷川 哲彦¹, 犬井 響熙¹, 植木 健太¹, 高瀬 浩一¹

College of Sci. and Tech., Nihon Univ.¹, Graduate School of Sci. and Tech., Nihon Univ.²,

°Kazuki Ishiyama¹, Akihiro Fukawa², Takuto Nakazawa², Kazane Ito², Zijie Feng²,

Tetsuhiko Tanikawa¹, Inui Hibiki¹, Ueki Kenta¹, and Kouichi Takase¹

E-mail : takase.kouichi@nihon-u.ac.jp

この 20 年、磁気モーメントの起源となる d 電子を持たない、または、 d 軌道が全て占有されている半導体ナノ粒子において室温強磁性の発現が報告されている。これらの強磁性が観測されるのは、主に表面効果が顕著になるナノ粒子や薄膜であることから、磁気モーメントの起源はナノ粒子表面の欠陥がもたらす不対電子であると考えられている。

これまで我々の研究では代表的な酸化物半導体である ZnO や TiO₂ ナノ粒子の強磁性について報告してきた。TiO₂ の場合、酸素が欠損することで $3d$ 電子が不対電子になり、これが磁気モーメントの起源となっていると考えられる。では、主役の d 電子の主量子数が変化すると磁氣的性質はどのように変わるのであるか？

そこで本研究では、 $4d$ 電子を持つ Y₂O₃ 絶縁体に注目し、ナノ粒子の磁性について調査した。

本研究では、出発試料をレアメタリックから購入した Y₂O₃ 粉末とした。まず、その出発試料に対して超伝導量子干渉磁束計(SQUID)を用いた磁化測定を行った。強磁性を示さないことが確認できた試料に対して遊星ボールミルを用いて粉碎処理を施した。粉碎後の試料に対して、形状評価を FE-SEM、結晶構造評価を粉末 X 線回折測定(XRD)、磁気特性の評価として磁化測定で行った。

Fig.1 に出発試料(a)と 1 時間粉碎した試料(b)の SEM 画像を示す。購入した試料は、2 μ m 以上の粒子から構成されているが、1 時間粉碎し

た試料では、粒子が全体的に小さく丸みを帯び、凝集している。

Fig.2 に出発試料と 1 時間粉碎した試料の磁化の磁場依存性($M-H$)の結果を示す。出発試料である Y₂O₃ 粉末は、負の傾きを示しており、反磁性であることが確認できる。この結果より、出発原材料には強磁性不純物が混入していないことが確認できた。

1 時間粉碎した試料では、ヒステリシスが見られ、強磁性を示していることがわかる。発表当日は、磁気円二色性測定の結果も紹介し、磁気モーメントの起源や主量子数が強磁性にどのような影響を与えているのかを議論する。

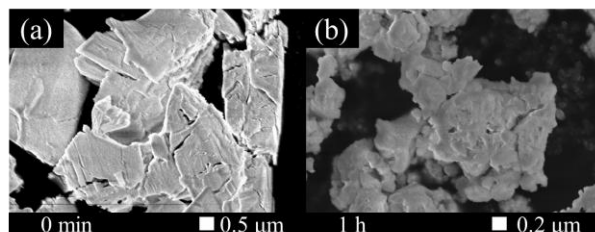


Fig.1 SEM images of the starting powder (a) and the milled powder (1h) (b).

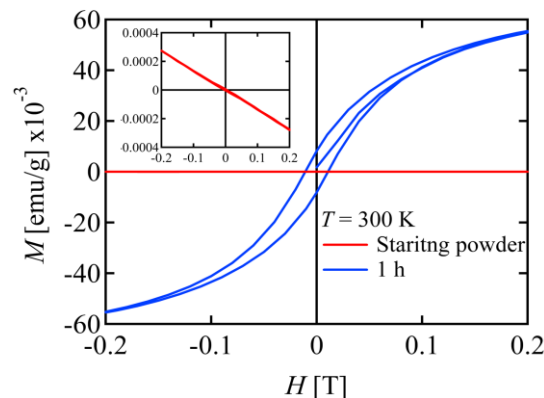


Fig.2 Magnetic field dependences of magnetization ($M-H$) of the starting powder and the milled sample (1h).

MoO₃ ナノ粒子の室温強磁性

Room temperature ferromagnetism of MoO₃ nanoparticles

日大院理工¹, 日大理工²,

◦中澤 拓斗¹, 府川 明弘¹, 馮 子介¹, 伊藤 風音¹,
石山 和樹², 犬井 響熙², 植木 健太², 高瀬 浩一²

Graduate School of Sci. and Tech., Nihon Univ.¹, College of Sci. and Tech., Nihon Univ.²,

◦Takuto Nakazawa¹, Akihiro Fukawa¹, Zijie Feng¹, Kazane Ito¹,

Kazuki Ishiyama², Hibiki Inui², Kenta Ueki², and Kouichi Takase²

E-mail: takase.kouichi@nihon-u.ac.jp

半導体メモリは、電子の自由度の一つである電荷の自由度を利用したメモリで、応答速度の高速化や多値化を考えると、電子のもう一つの自由度であるスピンを利用することが提唱されている。しかし、不対電子をもたない半導体に磁性を与えるのは困難であるため、このような状況を切り開くアイデアとして、GaMnAsのような希釈磁性半導体が提案されたが、キュリー温度が低すぎるがゆえに実用化までは至らなかった。

近年、MgO、ZnO、TiO₂などの磁性元素を含まない酸化物半導体ナノ粒子で室温強磁性が観測されており、注目を集めている。この室温強磁性では、その飽和磁化が試料の粒子径に依存していることから、磁気モーメントの起源は表面に存在する欠陥であると考えられている。

本研究では、触媒、有機太陽電池、リチウム電池など多くの場で応用されている MoO₃ に注目した。これまで、遷移金属元素をドーピングした MoO₃ ナノ粒子で、半導体の性質を維持した状態で強磁性的な振る舞いが観測される報告がなされているが、アンドープ MoO₃ ナノ粒子の室温強磁性に関する報告例はほとんどない。そこで、本研究では市販の MoO₃ 粉末に粉碎処理を施し、ナノ粒子化することで室温強磁性を有する MoO₃ ナノ粒子を作製し、その物性を評価した。

本研究では、高純度化学研究所で購入した MoO₃ (99.9 %)粉末を用いた。ナノ粉末試料合成には、遊星ボールミルによる粉碎処理を実

施した。作製した MoO₃ ナノ粒子に対して、粉末 X 線回折測定、SQUID を用いた磁化測定、電子スピン共鳴(ESR)測定、電界放出型走査電子顕微鏡(FE-SEM)による粉碎状態と粒形の確認を行った。

図 1 に MoO₃ ナノ粒子の磁化の磁場依存性を示す。まず、出発試料は常磁性的な振る舞いを示した。したがって、出発試料には強磁性不純物は含まれていないことが確認できた。この出発試料に対して粉碎処理を施すことで、明確なヒステリシスが観測された。

当日の発表では、磁化の磁場依存性だけでなく、その他の物性測定の結果も含め、MoO₃ ナノ粒子の室温強磁性の起源について議論する予定である。

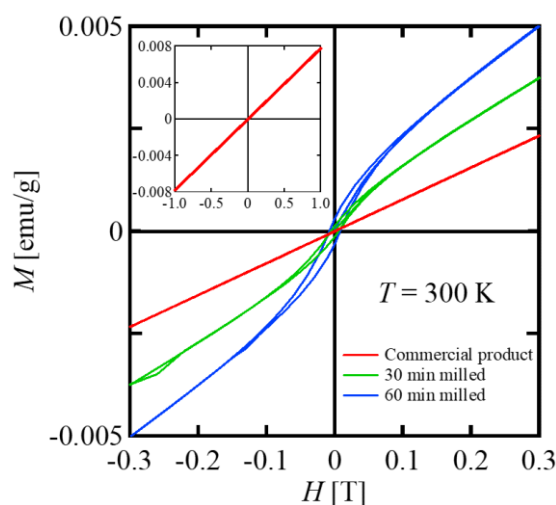


Fig. 1 Magnetic field dependences of magnetization of MoO₃ nanoparticles

ZnS、ZnSe ナノ粒子の磁気特性

Magnetic properties of ZnS and ZnSe nanoparticles

日大院理工¹, 日大理工², 伊藤 風音¹, 府川 明弘¹, 中澤 拓斗¹, 馮 子介¹, 高瀬 浩一²

Graduate School of Sci. and Tech., Nihon Univ.¹, College of Sci. and Tech., Nihon Univ.²,

Kazane Ito¹, Akihiro Fukawa¹, Takuto Nakawaza¹, Zijie Feng¹, Kouichi Takase²

E-mail : takase.kouichi@nihon-u.ac.jp

近年、MgO、TiO₂、HfO₂などの純粋半導体ナノ粒子で室温強磁性が確認されている。この室温強磁性はバルク状態では観測されず、飽和磁化が粒径に依存していることから、表面の欠陥によって強磁性が表れると考えられている。

前回の学会では、ボールミルで粉碎処理を施した酸化亜鉛ナノ粒子の室温強磁性や水素アニール効果について報告した。ZnO ナノ粒子の磁気モーメントの起源は他グループの X 線 MCD の結果より、酸素 2p 電子であることが報告されている。亜鉛カルコゲナイドでは、磁気モーメントの起源は硫黄では 3p、セレンでは 4p、テルルでは 5p となり、波動関数は広がっていくと考えられる。そこで本研究では、磁気モーメントを担う p 電子の軌道の広がりが強磁性にどのような影響を与えるのかを明らかにすることを目的とする。

出発試料には ZnSe (フルウチ化学株式会社、純度 99.99 %)と ZnS (高純度化学研究所、純度 99.99 %)、ZnO (高純度化学研究所、純度 99.9 %)を使用した。出発試料に磁化測定を行い、強磁性不純物がないことを確認した。出発試料に対して大気中で遊星ボールミルによる粉碎処理 (5 min, 10 min, 15 min, 30 min, 45 min, 1 h) を施した。粉碎処理した試料には、結晶構造評価として粉末 X 線回折 (XRD) 測定、表面状態の確認のために電界放出型走査電子顕微鏡 (FE-

SEM) による観察、磁気特性評価として SQUID 磁束計を用いた磁化測定を行った。

Fig.1 にそれぞれの試料の磁化測定の結果を示す。出発試料は全て反磁性を示しており、強磁性不純物が混入していないことが分かる。一方、粉碎した試料には強磁性を示すヒステリシスが観測されている。磁化の大きさに注目すると ZnSe は ZnO や ZnS よりも大きな値を持つことが分かる。磁化の大きさには欠陥量が関与しているので、電子・スピン共鳴測定から欠陥量を求め、この値で磁化の大きさを規格化することで試料間の磁化の大きさを評価し、軌道の広がりの効果を当日議論する予定である。

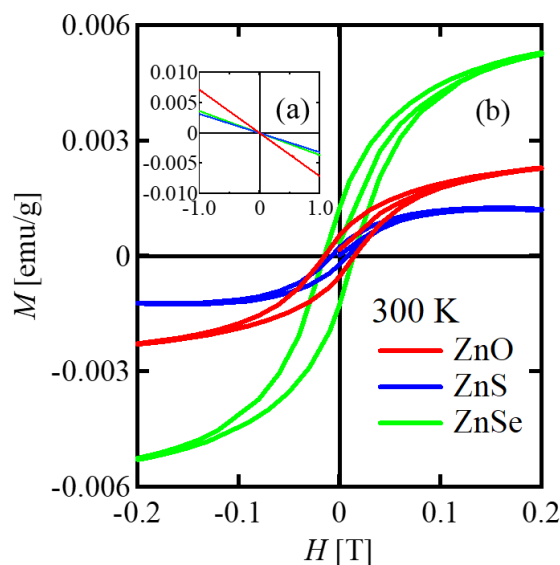


Fig.1 Magnetic field dependences of magnetization of the starting powders (a) and the milled powders(b).

電子および正孔スピンの同時注入下における逆スピン Hall 効果

Inverse spin Hall effect under simultaneous injection of electron and hole spins

埼玉大院理工 酒井 政道

Saitama Univ. M. Sakai

E-mail: sakai@fms.saitama-u.ac.jp

緒言 強磁性金属と非磁性アンビポラ性導体の接合界面を電流が横切れば、非磁性側の電流は電子電流と正孔電流の合計であるから、スピン角運動量の引込みや引抜きには、電子のスピンと正孔のスピンが同時に関与する。先行研究では、非磁性アンビポラ金属(N)を2つの強磁性金属(F)で挟んだ二重ヘテロ構造 F/N/F におけるスピン蓄積界面電位差 (spin-coupled interface voltage) の表式を導出した[1]。本講演では、このヘテロ構造 N 領域のスピン流の表式を導出し、電子スピン流と正孔スピン流の寄与の仕方を明らかにする。そして、それらの逆スピン Hall 効果による Hall 抵抗の表式を導出し、Hall-bar 素子を使った測定結果[2]を解析する。

計算方法 N領域 (チャンネル長 L) を、同一材料の強磁性金属(F)によって挟むが、F 領域の長さは強磁性金属のスピン拡散長に比べて十分大きいとし、F/N 界面によるキャリア散乱やスピン緩和は無いものとする。計算では、電流密度、スピン角運動量の流れ密度、スピンに依存した電気化学ポテンシャル $\varepsilon_v^{(i)}$ ($i = 1$ (electron), 2 (hole), $v = \uparrow, \downarrow$) が、それぞれ F/N 界面において連続的に変化するとした。逆スピン Hall 抵抗の計算は、スピン依存電流密度 $\vec{j}_v^{(i)}$ が、スピン依存電気伝導度 $\sigma_v^{(i)}$ を使って、 $\vec{j}_v^{(i)} = -(1/q_i) \text{grad } \varepsilon_v^{(i)}$ によって与えられることを用いた。 $\varepsilon_v^{(i)}$ は、電流チャンネル方向 (x 方向) のみに依存するとした。

結果と考察 2つの F 領域の磁化が互いに平行 ($\uparrow\uparrow$) $R(+)$ および反平行 ($\uparrow\downarrow$) $R(-)$ な場合について、それぞれ逆スピン Hall 抵抗の表式は以下のように導出された：

$$R(\pm) = 2p \frac{\rho_N}{d_N} \left(\frac{J_c^*}{J_c} \right) \frac{\sum_i \frac{\tan \theta_i}{r_i} \text{csch} \frac{L}{\ell_i} \left(\pm \cosh \frac{x}{\ell_i} + \cosh \frac{x-L}{\ell_i} \right)}{\sum_i \frac{1}{r_i} \left(\coth \frac{L}{\ell_i} \pm \text{csch} \frac{L}{\ell_i} \right) + \frac{1}{r}}$$

ここで、 J_c^* は F/N 界面の電流密度、 J_c は N 領域の電流密度、 x は電流ソース電極からの距離、 p は F 領域のキャリアスピン偏極度、 r は F 領域のスピン抵抗、 ρ_N は N 領域の比抵抗、 d_N は N 領域の厚さ、 r_i は N 領域のスピン抵抗、 ℓ_i は N 領域のスピン拡散長、 θ_i は N 領域のスピン Hall 角である。1 種類のキャリアに対して知られている表式において、キャリアの特徴を表す項をキャリア種分だけ単純に合計する表式である。この表式にもとづいて、文献[2]の測定結果を考察する。文献[2]では、F 領域に希土類遷移金属フェリ磁性体 $\text{Tb}_{0.33}\text{Fe}_{0.67}$ を使い、N 領域 (チャンネル長 $L=80 \mu\text{m}$) に電子-正孔補償金属 YH_2 を使っている。 $x = (1/4)L, (1/2)L, (3/4)L$ の3地点で観測された Hall 抵抗を上記の表式にもとづいて解析した結果は、講演で報告する。

[1] Y. Koinuma, S. Hasegawa, and M. Sakai, J. Phys: Condens. Matter **36** (2024) 135806.

[2] K. Sato et al., Phys. Scr. **98** (2023) 045912.

電子-正孔散乱による運動量緩和の影響を受けたスピン輸送

Spin transport in ambipolar metal undergoing the momentum relaxation due to electron-hole scattering

埼玉大院理工 酒井 政道

Saitama Univ. M. Sakai

E-mail: sakai@fms.saitama-u.ac.jp

緒言 補償金属や半金属に代表される縮退したアンビポーラ性伝導体では、スピン緩和の原因として、スピン交換が伴う異なるスピン同士の電子-正孔散乱を、一方、運動量緩和としてフォノンや不純物散乱を考慮すると、無散逸モードと散逸の有るモードの2種類の固有スピンモードが得られる[1]。さらに、Elliott-Yafet (EY) や D'yakonov-Perel' (DP) などスピン軌道相互作用 (SOI) を介したスピン緩和を考慮すると、散逸の無いモードのスピン拡散距離は通常の常磁性金属と同程度の値に落ち着く[1]。SOIによるスピン緩和は無視できないので、上述の設定では、低温 (2 K) における $\text{Bi}_{0.95}\text{Pb}_{0.05}$ のスピン拡散長 (230 μm) [2] や YH_2 の室温スピン拡散長 (40 μm) [3] を説明できない。本研究では、スピン緩和としても専ら EY 型や DP 型 SOI を考慮し、運動量緩和として、フォノン・不純物散乱に加えて、同じスピン同士の電子-正孔散乱 (Baber 散乱)、および異なるスピン同士の電子-正孔散乱を考慮して、スピン輸送の固有モードを求めた。

計算方法 Boltzmann 方程式は、電子と正孔の2種類の分布関数に、スピンの自由度を加えた4つの方程式から構成される。衝突積分項には電子-正孔散乱項があるため、これらは連立積分方程式であるが、本研究では発見的手法によって、すなわち、電気伝導度が緩和時間近似を超えた厳密な計算結果[4]と一致するように、衝突項に対する緩和時間近似の表式を決めた。線形化した Boltzmann 方程式とガウス則から4種類の粒子密度の非平衡的变化分 $n_{\uparrow}^{(1)}$ 、 $n_{\downarrow}^{(1)}$ 、 $n_{\uparrow}^{(2)}$ 、 $n_{\downarrow}^{(2)}$ に関する連立ドリフト拡散方程式が得られる。ここで、1:電子、2:正孔、 \uparrow :ダウンスピン、 \downarrow :ダウンスピンである。

結果と考察 定常状態におけるスピンモードの固有値 κ^2 が2種類得られるが、そのうちの1つが

$$(\kappa_-)^2 = \frac{1}{2} \left(\frac{1}{D_1 \tau_{\text{SOI}}^{(1)}} + \frac{1}{D_2 \tau_{\text{SOI}}^{(2)}} \right) - \frac{1}{2} \sqrt{\left(\frac{1}{D_1 \tau_{\text{SOI}}^{(1)}} + \frac{1}{D_2 \tau_{\text{SOI}}^{(2)}} \right)^2 - \frac{4(1-\theta_1\theta_2)}{D_1 \tau_{\text{SOI}}^{(1)} D_2 \tau_{\text{SOI}}^{(2)}}}$$

である。ここで $D_{1,2}$ は考慮した諸々の運動量緩和時間にもとづく拡散係数、 $\tau_{\text{SOI}}^{(1,2)}$ は、SOI によるスピン緩和時間である。 $\theta_{1,2}$ は考慮した運動量緩和時間に依存する量であるが、因子 $1 - \theta_1\theta_2$ は緩和時間の選び方に依存して、ゼロを含んだ両極性を示す。特に、 $\theta_1\theta_2 = 1$ では $(\kappa_-)^2 = 0$ となりスピン拡散長 $1/|\kappa_-|$ が無限大である。また、 $\theta_1\theta_2 > 1$ の場合では、 $(\kappa_-)^2 < 0$ となり、非平衡スピン密度が波数 $|\kappa_-|$ で空間的に振動する。

[1] M. Sakai et al., J. Phys., Condens. Matter **34** (2022) 055801.

[2] K.-I. Lee et al., Phys. Rev. B **79** (2009) 195201.

[3] K. Sato et al., Phys. Scr. **98** (2023) 045912.

[4] P. F. Maldague and C. A. Kukkonen, Phys. Rev. B **19** (1979) 6172.

Fe 添加 CdTe/(Cd,Mg)Te 量子井戸における Fe の電荷揺らぎによる 励起子発光スペクトルの分裂

Splitting of excitonic emission spectrum due to charge fluctuation of Fe in

Fe-doped CdTe/(Cd,Mg)Te single quantum well

筑波大数理物質¹, CNRS Néel 研² ○深海宏太¹, 蓬萊健志郎¹, 古川園佳¹

H. Boukari², L. Besombes², 黒田 真司¹

Inst. Mater. Sci., Univ. Tsukuba¹, CNRS Institut Néel²

○K. Fukami¹, K. Hourai¹, M. Kogawa¹, H. Boukari², L. Besombes², S. Kuroda¹

E-mail: s2320369@u.tsukuba.ac.jp

1. Introduction 半導体量子ドット内に遷移金属原子を添加した系に対して、単一磁性原子スピンの制御に注目が集まっている。これまで我々は CdTe 自己形成ドット(SAD)内に Cr 原子 1 個を含む系において、励起子発光の測定を通じてドット中の単一 Cr スピンの振舞いを明らかにしてきた[1]。さらに最近では、CdTe/(Cd,Mg)Te 単一量子井戸(SQW)に Fe を添加した試料において、単一 Fe スピンの振舞いを調べている[2]。CdTe/(Cd,Mg)Te SQW においては励起子は井戸層幅の揺らぎにより零次元に束縛され、また SAD と異なり格子歪がほとんどないという特徴を有する。前回の報告では、単一 Fe スピンとの相互作用により分裂した励起子発光スペクトルを検出し、磁場によるスペクトルの変化および直線偏光特性を調べ、格子歪の有無による Fe スピン状態の違いを比較検討した[2]。今回は、同じ Fe 添加 CdTe/(Cd,Mg)Te SQW において、同じように分裂した形状を示しながら、直線偏光特性の異なるスペクトルを見出し、その分裂の原因として Fe イオンの電荷の揺らぎ[3]を考察したので、報告する。

2. Experimental 試料は分子線エピタキシー(MBE)法によって作製した。GaAs(001)基板上に CdTe buffer 層を介して、CdTe/(Cd,Mg)Te 量子井戸を積層した。CdTe 井戸層厚は 3ML または 4ML とし、微量(~0.7%)の Fe を添加した。

3. Results Fig.1, 2 に井戸層厚 3ML と 4ML の試料における発光スペクトルと直線偏光特性を示す。図に示すように、2 本 1 組の発光線が偏光角の 90° ごとの回転に伴い強弱が入れ替わるという偏光特性を示している。これは、前回報告した単一 Fe スピンとの交換相互作用により分裂した発光線とは異なっており[2]、以前に報告された Cr 添加 CdTe SAD においてドット外部に位置する Cr イオンの電荷揺らぎの影響を受けた発光スペクトル[3]と似た特徴を示している。すなわち、ドット近傍に位置する Cr イオンが光励起により生成された電子ないし正孔を捕獲することで電荷の揺らぎが生じ、ドット内部の励起子エネルギーに影響することで、発光スペクトルに分裂が生じる。今回、CdTe/(Cd,Mg)Te SQW で観測された発光スペクトルも、CdTe 井戸層外に位置する Fe イオンに同様のメカニズムで電荷揺らぎが生じ、分裂したものと考えられる。

Reference

[1] A. Lafuente-Sampietro *et al.*, PRB **93**, 161301(R) (2016).

[2] 安藤他 第 71 回 応用物理学会 春季学術講演会 24a-71B-9.

[3] L. Besombes *et al.*, PRB **99**, 035309 (2019).

謝辞：本研究は大阪大学スピントロニクス学術連携研究教育センター(CSRN)の支援を受けた。

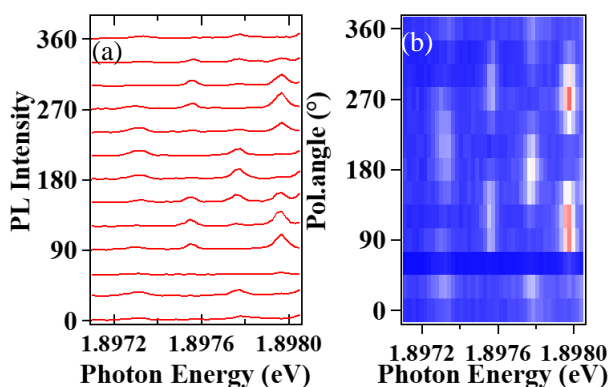


Fig.1(a)PL spectrum (3ML well)
(b)The dependence on the
linear polarization angle

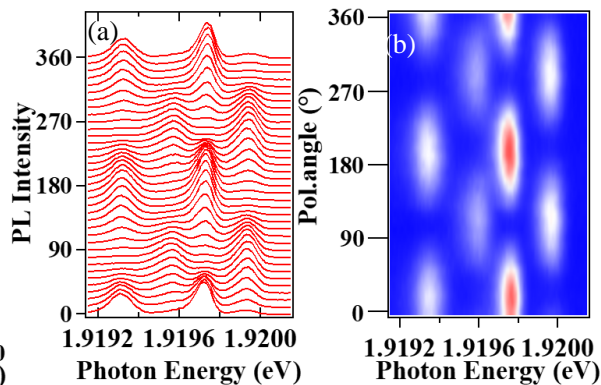


Fig. 2(a)PL spectrum (4ML well)
(b)The dependence on the
linear polarization angle

Bi (Fe, Co) O_x における超軌道分裂の理論的アプローチ

Theoretical approach to super orbital splitting in Bi(Fe,Co)O_x

産総研¹, 東大², 東北大³, 名古屋大⁴, ○福島 鉄也¹, 新屋 ひかり², 永沼 博^{3,4}

AIST.¹, Tokyo Univ.², Tohoku Univ.³, Nagoya Univ.⁴, ° T. Fukushima¹, H. Shinya², H. Naganuma

E-mail: t.fukushima@aist.go.jp

Multiferroics are expected to find applications in next-generation electric devices such as electric-field-driven nonvolatile memories and ultrasensitive magnetic sensors, by utilizing the magneto-electric (ME) coupling combined with tunnel junction structures. However, obtaining a large ME effect at room temperature remains a challenge. It has been reported that a colossal interfacial response (CIR) appears at the interface of the multiferroic Bi(Fe,Co)O_x (BFCO). While cross-sectional structure analysis revealed the formation of an approximately 1 nm thick oxygen-deficient BFCO layer at the interface, the magnetic structure and the origin of the significant CIR remained unclear. Therefore, in this study, before delving into research on the interfacial BFCO layer, we conducted the first-principles studies for the magnetic properties of oxygen-deficient bulk BFCO

First, the spin structure of the Co atoms in BFCO was investigated by using the LDA+U method on the basis of the VASP code. It was found that the Co atoms are stable in the high-spin state regardless of the Co concentration. We speculated that the origin of the colossal response for electric field in BFCO is related to the oxygen vacancies. We performed the exhaustive calculations for all possible arrangements of the oxygen vacancies in the supercell by supercomputer Fugaku and investigated their formation energies and stable magnetic structure. Our calculations indicated that the colossal response is caused by complicated orbital splitting due to the Co doping and O vacancies. In this presentation, we discuss the detail of this complicated orbital splitting.

Reference

- 1) H. Naganuma et al., “Increase of Fe moment of BiFeO₃ in Co/BiFeO₃/LaSrMnO₃ tunnel junctions” (Presentation number: 9p-PB1-38) 9th March 2019.
- 2) H. Naganuma et al, J. Appl. Phys., **109**, 07D917 (2011).
- 3) S. Yasui, et al., Jpn. J. Appl. Phys., 47, 7582 (2008).

Acknowledgements: This work was supported by Grant-in-Aid for Transformative Research Areas (B) Colossal Interface Response No. 23H03803 and by the “Program for Promoting Researches on the Supercomputer Fugaku (Computational Research on Materials with Better Functions and Durability toward Sustainable Development)” project (Grant Number: JPMXP1020230325).

二酸化バナジウム薄膜中のスピン輸送の温度依存性

Temperature dependence of the spin transport in a vanadium dioxide thin film

阪公大院工¹, 阪大産研² ○(M2)西村 匠¹, 神吉 輝夫², 仕幸 英治¹

Osaka Metro. Univ.¹, ISIR Osaka Univ.² °Takumi Nishimura¹, Teruo Kanki², Eiji Shikoh¹

E-mail: si23495g@st.omu.ac.jp

スピン流の実用化には外場を用いた制御技術の確立が必要不可欠である。二酸化バナジウム(VO_2)は温度の変化によって引き起こされる結晶構造の変化を伴う金属絶縁体転移(MIT)を示す[1]。これは VO_2 薄膜中でのスピン輸送が達成できればスピン流を熱的に制御することができることを意味する。即ちスピントロニクスにおけるスピン流スイッチを実現する手段として、 VO_2 の MIT を利用し、温度によってスピン流を制御する熱スイッチング可能なデバイスの創製が期待できる。我々はこれまでに、 $\text{Pt}/\text{VO}_2/\text{Ni}_{80}\text{Fe}_{20}$ の三層試料を作製し、スピンポンピング[2]を用いたスピン注入により、 VO_2 薄膜でのスピン輸送を達成した[3]。本研究では $\text{Pt}/\text{VO}_2/\text{Ni}_{80}\text{Fe}_{20}$ の三層構造試料におけるスピン輸送特性の、 VO_2 膜厚依存性、および温度依存性を評価することを目的とした。

Fig. 1 に VO_2 の膜厚が 60 nm および 80 nm の試料の 300 K における強磁性共鳴(FMR)スペクトルと起電力特性を示す。それぞれの膜厚の強磁性共鳴磁界(H_{FMR})付近において起電力が検出された。試料基板面に対する静磁界の印加方向(θ)の反転に伴い検出された起電力の符号も逆転した。この特性はスピンポンピングによって注入されるスピン流を ISHE により変換して得られる起電力の特性と一致する

[4]。したがって $\text{Pt}/\text{VO}_2/\text{Ni}_{80}\text{Fe}_{20}$ の三層試料においてスピン輸送を達成したと結論づけた。さらに、試料の温度を 300 K~355 K の範囲で変化させ、 VO_2 の MIT 温度前後での起電力の変化を測定し、MIT によるスピン輸送特性への影響を検証した。学会時には研究の詳細について議論する。

[1] S. Wall, et. al., Science, 362, 572 (2018).

[2] S. Mizukami, et. al., Phys. Rev. B, 66, 104413(2002).

[3] T. Nishimura, F. Kishi, S. Yamauchi, T. Kanki, E. Shikoh, 2023 IEEE International Magnetic Conference - Short Papers (INTERMAG Short Papers), Sendai, Japan, 2023, pp. 1-2, doi:10.1109/INTERMAGShortPapers58606.2023.10305026.

[4] E. Saitoh, et. al., Appl. Phys. Lett., 88, 182509 (2006).

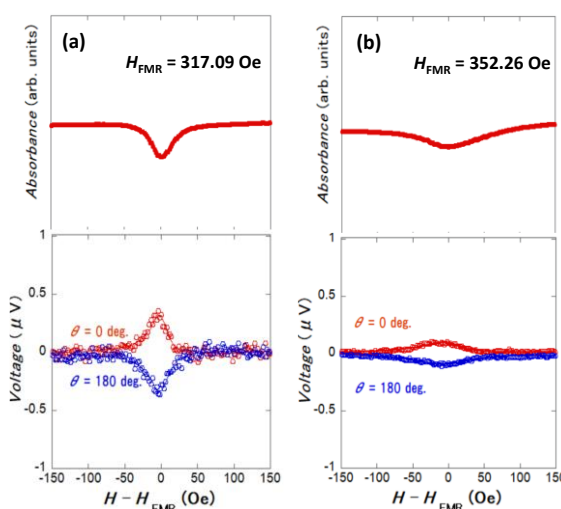


Fig. 1. FMR spectra at 5 GHz and output voltage properties at 300 K of the tri-layer structure samples. The VO_2 film thickness of the samples are (a) 60 nm [3] and (b) 80 nm, respectively.

電界印加下における半導体超格子バリアの電子スピン輸送特性

Electron spin transport properties of semiconductor superlattice barriers

under an applied electric field

Faculty of Information Science and Technology, Hokkaido Univ.

○K. Etou, S. Hiura, J. Takayama, A. Subagyo, K. Sueoka, and A. Murayama

E-mail: eto.kohe@eis.hokudai.ac.jp

ビックデータや IoT を用いた高度情報社会の到来により、情報機器の消費電力増大が喫緊の問題となっている。そこで、光による情報伝送と電子スピンによる情報保持を低消費電力で行う光電スピン情報基盤が注目されている[1]。なかでもスピン偏極発光ダイオード(スピン LED)は、電子スピン偏極の光変換デバイスであるが、実用に必須の室温高電圧条件では、電子スピン偏極のおよそ 9 割が光学活性層への輸送中に失われる[2]。そこで、半導体超格子バリアを用いた電子スピン輸送に着目した。超格子では、電子の量子波を利用することでスピン偏極を保持しながら電子スピンを長距離輸送できる[3]。本研究では、GaAs/AlGaAs 超格子バリアの電子スピン輸送特性を、LED 動作時と同様の電界印加下でフォトルミネッセンス(PL)測定を行うことにより評価した。

図 1(a)に試料構造と伝導帯のバンド構造を示す。試料は p -GaAs(100)基板上に超格子バリアと GaInNAs 量子ドットを含む LED 構造であり、超格子は n -Al_{0.3}Ga_{0.7}As 5 nm/GaAs 5 nm を 6 周期繰り返した。測定には異なる励起エネルギーでの電界印加円偏光 PL を用い、室温で行った。

図 1(b),(c)に印加電圧+4.0 V の条件にて励起エネルギーを 1.72 eV と 1.42 eV としたときの量子ドットの円偏光 PL スペクトルと PL 円偏光度(CPD)を示す。ここで、CPD は左右円偏光 PL の強度比と定義し、量子ドットの電子準位におけるスピン偏極率を反映する。励起エネルギーを量子ドット近傍の GaAs 層を励起する 1.42 eV から、超格子バリア上部の Al_{0.2}Ga_{0.8}As 量子井戸を励起する 1.72 eV に変化させると、20%を超える高い PL 円偏光度を維持しながら PL 強度は大きく増大した。この結果は、電界印加下で高いスピン偏極を保持しながら電子スピンの超格子バリアから量子ドットに輸送注入されていることを示唆している。

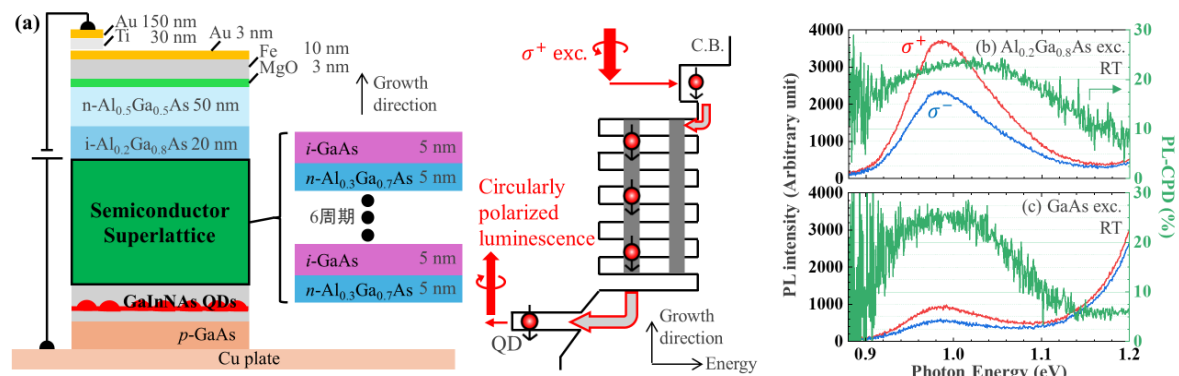


Fig. 1 (a) Schematic image of sample structure with a conduction-band structure. Circularly polarized PL spectra and corresponding CPD of GaInNAs QDs with excitation energies of (b) 1.42 eV and (c) 1.72 eV, at an applied bias voltage of +4.0 V.

References:

- [1] P. Dainone et al., Nature **627**, 783 (2024).
- [2] K. Etou et al., Phys. Rev. Appl. **16**, 014034 (2021).
- [3] S. Hiura et al., Appl. Phys. Lett. **114**, 072406 (2019).

有機スピントランジスタに向けたカーボンナノチューブトランジスタ中ドレイン電流の磁性電極依存性測定

Observation of drain current in carbon nanotube transistor with magnetic electrode for organic spin transistor

九大シス情¹, 九大院工², WPI-I2CNER³, ○黒川 雄一郎¹, 田中 直樹^{2,3}, 稲葉 優文¹,
山下 尚人¹, 湯浅 裕美¹

ISEE, Kyushu Univ.¹, Grad. Sch. Eng, Kyushu Univ.², WPI-I2CNER, Kyusyu Univ.³

○Yuichiro Kurokawa¹, Naoki Tanaka^{2,3}, Masafumi Inaba¹, Naoto Yamashita¹, Hiromi Yuasa¹

E-mail: ykurokawa@ed.kyushu-u.ac.jp

[Introduction] Spin transistor is one of candidates for transistor in beyond CMOS generation. To realize the spin transistor, the spin current needs to inject in a semiconductor. Here, the spin current is easy to decrease in the semiconductor with high spin orbit coupling. Therefore, the semiconducting carbon nanotube (CNT) is a promising material for the spin transistor because the spin current scattering is weak in CNT (spin diffusion length: $\sim 2 \mu\text{m}$ at temperature $T = 0.25 \text{ K}$) [1],[2]. In this study, we investigate the properties of CNT transistor with various magnetic electrodes.

[Experiment] We fabricated the thin CNT film on a thermally oxidized heavy doped Si substrate using a drop cast method. The magnetic electrodes and CNT patterns were obtained by using a photolithography. Thermally oxidized SiO_2 layer with a thickness of 200 nm was used as the gate insulator. The $\text{Fe}_{90}\text{Co}_{10}$ or Gd were used as electrodes. The properties of CNT transistor were measured at $T = 298 \text{ K}$ under the gate voltage which was applied to the back gate on Si substrate.

[Results] Fig. 1(a) and 1(b) show the drain current I_D as a function of the gate voltage V_G for the CNT transistors. The ON-OFF ratio and the I_D of CNT transistor with $\text{Fe}_{90}\text{Co}_{10}$ electrode is higher than those with Gd electrode. It is because the Gd has the lower work function than the $\text{Fe}_{90}\text{Co}_{10}$ [3]. The drain current of CNT transistor with $\text{Fe}_{90}\text{Co}_{10}$ electrode successfully modified by gate voltage.

[Acknowledgements] This study was supported in part by the JST, ACT-X Grant Number JPMJAX21K5, Murata Science and Education Foundation, and Iketani Science and Technology Foundation.

[1] N. Tombros, et al., Phys. Rev. B 73, 233403 (2006). [2] H. Yang et al., Phys. Rev. B 85, 052401 (2012). [3] Y. Nosh, et al., Nanotechnology 17, 3412 (2006).

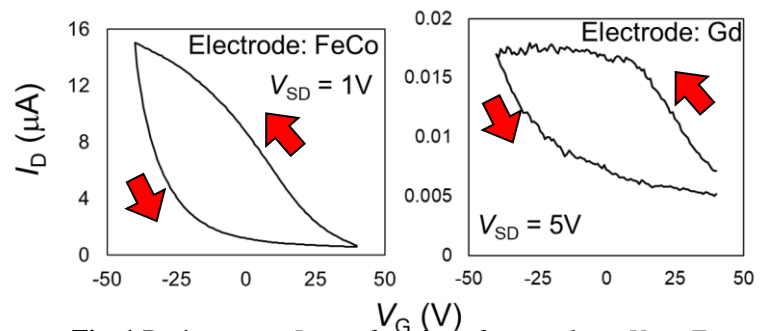


Fig. 1 Drain current I_D as a function of gate voltage V_G at $T = 295 \text{ K}$ for CNT transistor with (a) $\text{Fe}_{90}\text{Co}_{10}$ and (b) Gd electrode. Insets show the source-drain voltage V_{SD} .

透明導電膜の逆スピンホール効果によるスピン流検出を用いる 有機分子薄膜のスピン輸送特性評価

Evaluation of the spin transport properties in organic molecular films using the inverse spin-Hall effect in a transparent conductive film as a spin current detector

大阪公大院工¹ ○(M2)松川裕利¹, (M1)山田奨貴¹, (M1)高松恵人¹, 手木芳男¹, 仕幸英治¹

Osaka Metro. Univ. Eng.¹, ○Yuri Matsukawa¹, Shouki Yamada¹, Keito Takamatsu¹,

Yoshio Teki¹, Eiji Shikoh¹

E-mail: si23502v@st.omu.ac.jp

スピントロニクスにおいて、有機分子材料は主に軽元素で構成されていることから、重金属と比較してスピン軌道相互作用が小さくスピン流の散逸を抑えられると考えられている。これまで様々な有機分子材料において動力学的スピン注入によるスピン輸送の達成が報告されている [1-3]。また、有機分子材料は光を照射することで、電気伝導を担うキャリア数を増加させる光導電性を有している。この特性を用いた外場によるスピン流の制御が見込める点も有機分子材料の魅力である。本研究では、光を有機分子層に照射することを念頭に、透明導電膜ITO層を新たにスピン流検出層とした有機分子薄膜を含む三層構造におけるスピン輸送の実証とその特性評価を目的とした。これまでに同様の試料構造において強磁性共鳴(FMR)スペクトルの線幅の広がり度でスピン輸送特性を評価した研究例があるが[4]、輸送特性を逆スピンホール効果(ISHE)[5]を用いて評価した研究は無い。

RFスパッタリング法、抵抗加熱蒸着法、電子ビーム蒸着法を用い、合成石英基板上にITO(膜厚 60 nm)/PTCDA分子層(30 nm)/Ni₈₀Fe₂₀(25 nm)の三層構造試料 (Fig. 1)を作製した。Ni₈₀Fe₂₀層のFMR励起によるスピンプンピングを用いてPTCDA層にスピン流を注入し、PTCDA層を輸送したスピン流はITO層でISHEによって起電力として変換される。この起電力を観測できればスピン輸送の証拠となる。FMRの励起にはベクトルネットワークアナライザから伝送線に流れる高周波電流による高周波磁界と、電磁石による静磁界を用いた。また、起電力の測定にはナノボルトメータを用いた。

Fig. 2 に(a)FMRスペクトルと(b)FMR磁界付近にてITO層から検出された起電力を示す。強磁性共鳴磁界 H_{FMR} 付近において起電力が検出され、その符号は静磁界の印加方向の反転に伴い逆転した。この特性は、スピンプンピングによって注入されるスピン流をISHEによって変換して得られる起電力の特性と一致する[5]。以上より、PTCDA分子層のスピン輸送に成功したと結論した。学会時には研究の詳細について議論する。

[1] S. Watanabe, et. al., Nature Phys., **10**, 308 (2014)., [2] K. Nishida, et. al., Solid State Commun., **312**, 113898 (2020)., [3] Y. Onishi, et. al., Solid State Commun., **360**, 115035 (2023)., [4] R. Gupta, et. al., Angew. Chem. Int. Ed., **62**, e202307458 (2023)., [5] E. Saitoh, et. al., Appl. Phys. Lett., **88**, 182509 (2006).

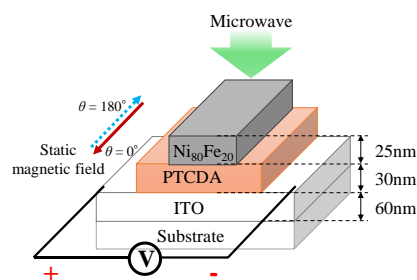


Fig. 1. Schematic illustration of our sample structure.

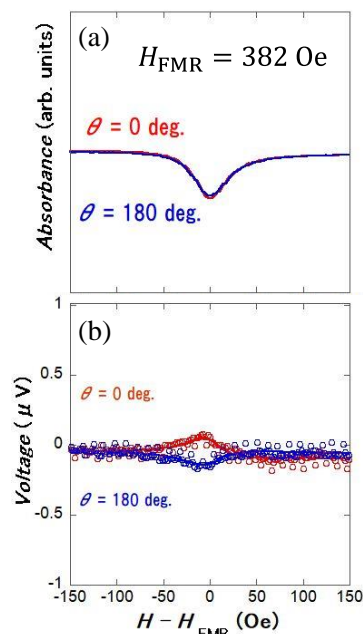


Fig. 2. (a) FMR spectra, and (b) output voltage properties generated in a tri-layer structure sample under the FMR, at 5 GHz.

Experimentally realizable topological chiral edge spin wave on magnonic crystal

Department of Physics and Chemistry, DGIST, Daegu 42988, Republic of Korea¹

^oJuha DO¹, Jae Yong CHO¹, Chun-Yoel YOU¹

E-mail: cyyou@dgist.ac.kr

Topological materials have gained significant attention due to their unique physical properties, including topologically protected edge states that allow for lossless propagation of currents or spin waves. These properties have the potential to impact information storage and transmission technologies. Although topological magnons have been demonstrated in various quantum magnets, direct experimental observation of edge modes remains unachieved. Most proposed topological magnonic crystal structures have been difficult to create experimentally [1, 2]. This study aims to observe chiral edge spin waves in experimentally feasible structures and explore the conditions for realizing and detecting topological edge modes.

Using micromagnetic simulations, we analyzed the topological properties of magnonic crystals, extending previous structures where four bases constitute a single cell. As shown in Figure 1, this shape is distinguished from former studies in that decorated square-lattice model is rotated by 45 degrees. The side of triangle ranges from 20 nm to 120 nm. Cobalt was employed as model parameters for simulation.

Results confirmed the formation of distinct bulk and edge modes in magnonic crystals. A unidirectional mode was observed in the edge modes, indicating a topologically protected state. Analysis of the band topology showed non-zero Chern numbers. Additionally, we examined the dependence of band structures on external magnetic fields and pattern sizes, which enables to control emergence of topological edge mode. This finding clearly indicate experimental feasibility, thus increases the potential for magnon-based information processing technologies such as spin current splitters, and waveguides.



[Figure 1] Figure of the proposed magnonic crystal design with four unit cells.

[1] R. Shindou, J.-i. Ohe, R. Matsumoto, S. Murakami, and E. Saitoh, Phys. Rev. B **87**, 174402 (2013).

[2] J. Feilhaber, M. Zelent, Z. Zhang, J. Christensen, and M. Mruczkiewicz, APL Mater. **11**, 021104 (2023).

マグノニック結晶におけるマグノニックバンドギャップの障壁材料依存性

Wall material dependence of the magnonic band gap in magnonic crystals

福岡大理, [○](M1)松永朝成, 洞口泰輔, 眞砂卓史

Fukuoka Univ. [○]T. Matsunaga, T. Horaguchi, and T. Manago

E-mail: sd241009@cis.fukuoka-u.ac.jp

【研究背景】

我々は、これまでにアンテナ法を用いてパーマロイ(Py)のマグノニック結晶(MC)中を伝搬するスピン波の特性について調べてきた。マグノニック結晶は主に構造周期でその特性が決まるが、MCを用いたスピン波電子デバイスへの応用の観点から、周期変調以外の方法で、マグノニックバンドギャップの周波数やバンドギャップ幅を制御する手段の開発が望まれる。本研究では、マグノニック結晶の障壁材料の観点から、全てPyで作製したマグノニック結晶(Py-MC)とPy導波路上に障壁のみCoを用いて作製したマグノニック結晶(Py-Co-MC)の伝搬特性を比較した。

【計算手法】

スピン波伝搬の計算はMumax3を用いて行った。長さ×幅×膜厚が $81.92\text{ }\mu\text{m} \times 6\text{ }\mu\text{m} \times 20\text{ nm}$ のPy導波路直上に、高さ 20 nm 、幅 $1\text{ }\mu\text{m}$ (周期 $2\text{ }\mu\text{m}$)の凹凸障壁をもつMCを作製した。この時、障壁材料にPyとCoを用いる二種類のモデルに対して計算を行った。アンテナによって生成される磁場の空間分布をMATLABを用いて計算し、これをMumax3に取り込み、Gaussian Pulse波形(パルス幅 50 ps)で印加することでスピン波励起用磁場とした。スピン波の波数ベクトルと磁化が直交するMSSWモード条件で計算を行うため、 20 mT の静磁場を短辺方向に印加した。パルス磁場印加後の磁化の時間発展データから、スピン波の分散関係やスペクトルを解析した。

【結果】

Figure 1(a)はPy-MC, Figure 1(b)はPy-Co-MCにおけるスピン波スペクトルであり、黄色の領域でスピン波強度の減衰が確認できる。この減衰がマグノニックバンドギャップを表している。マグノニックバンドギャップの周波数領域は、Py-MCでは 5.7 GHz から 6.0 GHz でバンドギャップ幅は 0.3 GHz , PyCo-MCでは 5.8 GHz から 6.6 GHz でバンドギャップ幅は 0.8 GHz であることが確認できる。このように障壁材料をPyからCoに変更することで、バンドギャップの中心の周波数と、バンドギャップ幅が増大していることが分かった。バンドギャップの中心周波数の増加は、Co障壁によってMCの平均飽和磁化の増大に起因すると考えられる。ギャップ幅増大の原因については、さらなる考察が必要である。これらの結果により、マグノニック結晶の障壁材料を変更することでバンドギャップの幅や位置を制御することが可能であることが分かった。

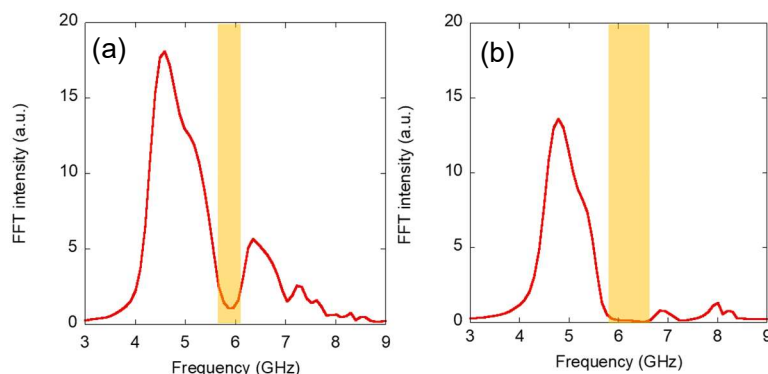


Figure 1 (a)Py-MC と(b)PyCo-MC におけるスピン波スペクトル。黄色網掛けはバンドギャップを示す。

マグノニック結晶のバンドギャップの障壁高さ依存性

Wall height dependence of band gaps in magnonic crystals

福岡大理 [○](M2)城門太一, 洞口 泰輔, 眞砂卓史

Fukuoka Univ. [○]T. Kido, T. Horaguchi, and T. Manago

E-mail: sd231008@cis.fukuoka-u.ac.jp

【研究背景】

近年, スピン波の伝搬を制御するマグノニック結晶 (MC) についての研究に注目が集まっている。MC によるスピン波電子デバイスへの応用を考えると, スピン波に効率的に周期構造の影響を与える MC 構造の探索や, 構造周期以外にバンドギャップの幅や位置を制御する手段の開発が望まれる。我々はこれまで, マグノニック結晶の形状依存性の観点から, 周期的な壁の高さ変調によるスピン波の伝搬特性を実験的に調べた。本研究では, mumax³ を用いたマイクロマグネティックシミュレーションを行い, 実験的に得たデータと比較した。

【計算方法】

スピン波伝搬の計算には mumax³ を用いた。縦×横×膜厚が $81.92\ \mu\text{m} \times 6\ \mu\text{m} \times 20\ \text{nm}$ の Py 細線に, 凹凸幅 = $1\ \mu\text{m}$ の壁(周期 $D=2\ \mu\text{m}$)を, 壁の高さ $h=20, 40, 60\ \text{nm}$ で配置したマグノニック結晶を仮定した。磁場印加用アンテナ形状と, 印加電流 $1\ \text{mA}$ を設定した条件下でのスピン波励起用パルス磁場の空間分布係数は Python プログラムであらかじめ計算し, mumax³ に取り込んだ。その後, mumax³ 上で $50\ \text{ps}$ のガウシアンパルスを設定し, 取り込んだ磁場分布係数を乗じて印加することによりスピン波励起を実現した。静磁場の印加方向は Py の短辺方向 ($+20\ \text{mT}$) とし, スピン波の伝搬方向は Py の長辺方向とした (MSSW モード)。

【結果】

Figure 1 はスピン波分散関係のシミュレーション結果であり, それぞれ障壁の高さが (a) $h=20\ \text{nm}$ (b) $h=40\ \text{nm}$ (c) $h=60\ \text{nm}$ の場合における分散関係を表している。それぞれ $6\ \text{GHz}$ 付近でマグノニックバンドギャップが見られ, 壁の高さの増大とともにバンドギャップの拡大が確認された。これは, 我々が実験的に得た結果^[1]を裏付けるものとなり, 周期的な壁の高さ変調によってギャップ幅制御が可能であることが明らかとなった。

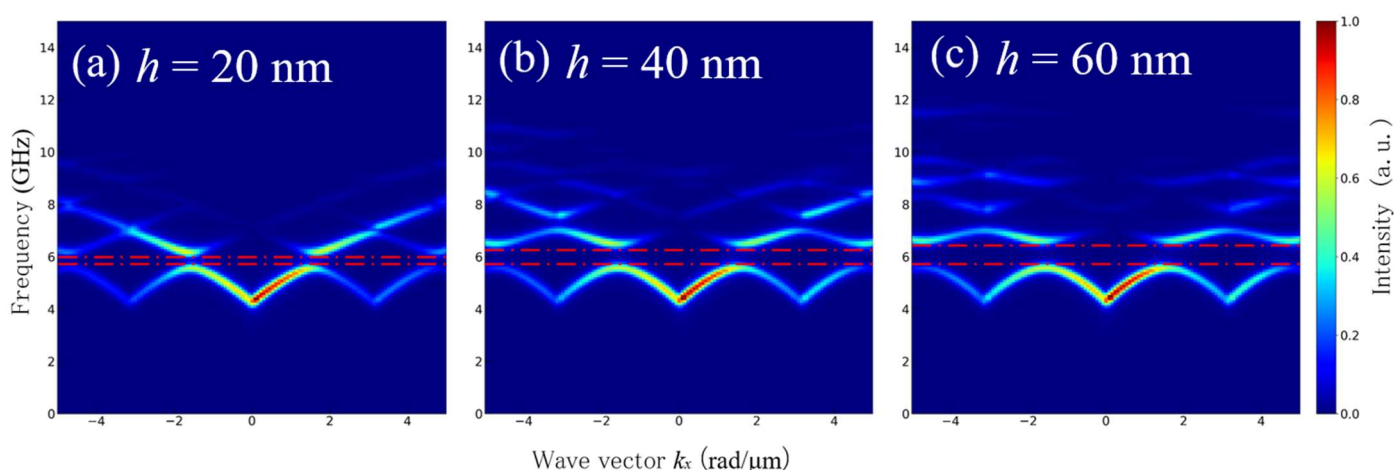


Figure 1 MCにおける分散関係の壁高さ依存性 (a) $h=20\ \text{nm}$ (b) $h=40\ \text{nm}$ (c) $h=60\ \text{nm}$

【参考文献】

[1] スピン波伝搬におけるマグノニック結晶の壁高さ依存性, 第84回応用物理学会 春季学術講演会 講演番号 25a-P01-28

有機金属分解法で作製した イットリウム鉄ガーネット薄膜のスピン波の測定

Spin wave measurements of YIG thin film deposited by MOD method.

福大理¹, 近大産業理工², [○](M2) 今村圭佑¹, 眞砂卓史¹, 笠原健司², 洞口泰輔¹

Fukuoka Univ.¹, Kinki Univ.², [○]K. Imamura¹, T. Manago¹, K. Kasahara², T. Horaguchi¹

E-mail: sd231002@cis.fukuoka-u.ac.jp

【研究背景】

イットリウム鉄ガーネット(YIG)は、スピン波デバイスなどの高周波デバイスに応用できる素材として期待されている。また、YIG 薄膜などの磁性酸化膜を簡便に作製できる手法として有機金属分解法(MOD 法)が注目されているが、スピン波伝搬を観測できる YIG 薄膜の報告例はない。これまでに我々は、MOD 法を用いて鋭い共鳴ピークをもつ強磁性共鳴が観測可能な YIG 薄膜の作製に成功した。将来のスピン波デバイスへの応用を考慮し、本研究では、MOD 法で作製した YIG 薄膜を用いてアンテナ法によるスピン波の検出を試みた。

【実験手法】

GGG(111)基板上に、MOD 溶液〔オクチル酸塩(Y:Fe=3:5)、濃度 3%〕をスピスコート後、200 °Cで 30 分間乾燥ベーク、350 °Cで 30 分間分解ベークを行い、その後 950 °Cで 3 時間アニールして YIG 薄膜を作製した。さらに、薄膜上に励起・検出アンテナとして Au/Cr のコプレーナウェーブガイドを形成した。また、ベクトルネットワークアナライザーと磁場可変高周波プローバーを用いて、静磁表面波の透過信号を測定した。

【実験結果】

Figure. 1 に(a)測定から得られた MSSW 信号と(b)信号強度の距離依存性を示す。Fig. 1(a)より、磁場に応じた MSSW 信号を確認でき、磁場とスピン波周波数の関係は、Kittel の式によくしたがっていることを確認した。また Fig. 1(b)に示すように、信号強度は、伝搬距離の増大につれて指数関数的な減衰が見られ、これは理論的な強度減衰に一致する。以上のことから、MOD 法で作製した YIG 薄膜のスピン波の観測に成功したと考えられる。

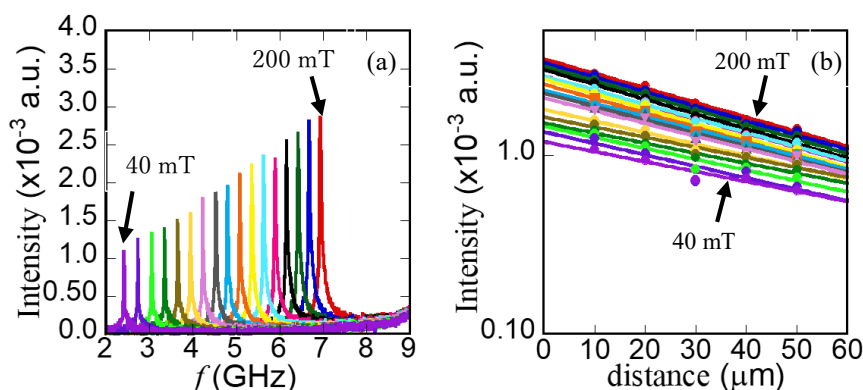


Figure 1 (a) MSSW signals and (b) antenna distance dependence of signal intensities.

Effects of Magnon Spin-Polarization on Magnon Lifetime in Antiferromagnetic Insulator NiO

Mie Univ.¹, (D2) °Andi Gumaring¹, K. Nawa¹, K. Nakamura¹

E-mail: 423db01@m.mie-u.ac.jp

Long lifetime signal propagation is essential for modern THz signal processing devices. Antiferromagnetic insulator NiO allows long-lifetime THz signal to propagate via two non-degenerate magnon modes [1,2] that carry non-integer spin-polarization [3], in contrast to stereotypical beliefs of $\pm 1 \hbar$ for antiferromagnetic magnons. Due to weak spin-orbital effects and insulating properties, the main channel that gives rise to magnon lifetime in NiO is four-magnons interactions, rather than relativistic effects [4]. However, the mechanism in which magnon spin-polarization impacts magnon lifetimes in NiO has been unaddressed. Previously, we investigated magnon frequencies of NiO comprising of magnetic dipole-dipole interactions, single-ion anisotropy, and spin-exchange interactions. In this presentation, we extend our model to investigate the effects of magnon spin-polarization on magnon lifetime driven by four-magnon interactions. Fourth order magnon Hamiltonian is treated as a perturbation term, and the inverse of imaginary part of self-energy in many-body Green's functions is calculated.

First, we calculate room-temperature magnon lifetime at Γ and obtain 1.04×10^{-12} s, which is in the same order of magnitude as in experiment results in monocrystalline NiO, 7.65×10^{-12} s. [1]. We find that intra-mode contribution dominates magnon lifetime at Γ , while at the edge of Brillouin zone (BZ), inter-mode contribution becomes comparable in magnitude to intra-mode one. Magnon lifetime at the edge of BZ decreases as the applied static magnetic field increases to 0.1 T. Second, we calculate magnon spin-polarization to understand the origin of the magnon lifetimes. At the edge of BZ, non-integer magnon spin-polarization at the high symmetry \mathbf{k} -points are observed, and application of static magnetic field up to 0.1 T breaks the equivalence between two Ni sublattices and enhances the magnon spin-polarization up to $|\hbar|$. Since transition probability at the edge of BZ is governed by spin-conserving contribution in fourth order magnon Hamiltonian, the enhancement of magnon spin-polarization increases transition probability from one magnon state to another, which thus leads to the decrease of magnon lifetimes in one magnon state.

References:

- [1] T. Moriyama, et. al., Phys. Rev. Mater. **3**, 051402 (2019).
- [2] T. Kampfrath, et. al., Nat. Photon. **5** 31 (2011).
- [3] A. Kamra, et. al., Phys. Rev. B **96** 020411 (2017)
- [4] S. M. Rezende, et. al., J. Phys. D: Appl. Phys. **51**, 174004 (2018).

強磁性層状物質 CrX_3 ($X = \text{Cl}, \text{Br}, \text{I}$) の 交換相互作用力と結晶磁気異方性の電子論的考察 Analysis of exchange interactions and magnetocrystalline anisotropy in ferromagnetic layered CrX_3 ($X = \text{Cl}, \text{Br}, \text{I}$)

三重大院工¹, NIMS², [○](M1)村田 尚登¹, Andi Gumarilang¹, 名和 憲嗣^{1,2}, 中村 浩次¹
Mie Univ.¹, NIMS², Naoto Murata¹, Andi Gumarilang¹, Kenji Nawa^{1,2}, Kohji Nakamura¹
E-mail: 423M250@m.mie-u.ac.jp

層状物質の中でも CrI_3 や $\text{Cr}_2\text{Ge}_2\text{Te}_6$ は単層で強磁性を発現する新物質である [1,2]。ファンデルワールス力による欠陥のないヘテロ界面形成が容易であること、歪みや磁場などにより電氣的・磁気的特性を幅広く変調可能であることが層状物質のメリットであり、強磁性を示す層状物質の発見は、2次元磁性の研究領域をさらに拡大させた。最近では単層 CrX_3 ($X = \text{Br}, \text{I}$) におけるトポロジカルマグノンの存在が理論的に予測される [5] など、スピントロニクスへの応用に向けた研究も進んでいる。本研究では第一原理計算から、単層 CrX_3 ($X = \text{Cl}, \text{Br}, \text{I}$) の交換相互作用力と結晶磁気異方性を評価し、その起源を解析した。これら基礎的な磁気特性は、 CrX_3 の2次元スピン波（マグノン）予測にも重要な磁気パラメータである。 CrX_3 中の第1～3近接の Cr-Cr 間にはたらく交換相互作用力 (J_1, J_2, J_3) をハイゼンベルグモデルに基づき表現した強磁性 (FM) と反強磁性 (Neel-AFM, Stripy-AFM, Zigzag-AFM) の磁気構造 (図1) の全エネルギーから算出した。結晶磁気異方性エネルギー (E_{MCA}) は層表面に対して面内磁化 ([001]) と面直磁化 ([111]) のエネルギー差 ($E_{MCA} = E_{[001]} - E_{[111]}$) として定義し、Force 理論から算出した。第一原理計算にはフルポテンシャル線形化補強平面波法 [4] を用い、また Cr 3d 軌道に+U法を用いた (GGA+U 近似)。 CrI_3 において、全エネルギー計算から FM の磁気構造が基底状態であった。交換相互作用力は $J_1=4.27$ meV, $J_2=0.55$ meV, $J_3=-0.27$ meV となり、第一近接 Cr-Cr 間の交換相互作用が支配的であった。さらにこのときの $E_{MCA}=0.36$ meV から面直の磁化容易軸を示し、実験の報告 [3] と一致した。発表では、 CrCl_3 と CrBr_3 の交換相互作用定数と結晶磁気異方性の結果も示し、これら磁気特性の X 種依存性の観点からその起源を考察する。

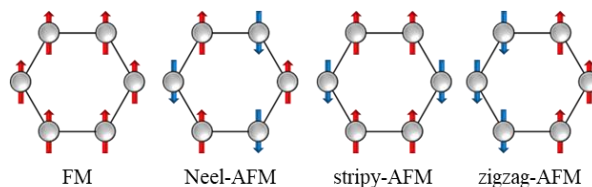


図 1 CrX_3 における 4 種の磁気構造

- [1] B. Huang, *et al.*, Nature **546**, 270 (2017).
- [2] C. Gong, *et al.*, Nature **546**, 265 (2017).
- [3] P. Delugas, *et al.*, Phys. Rev. B **107**, 214452 (2023)
- [4] K. Nakamura, *et al.*, Phys. Rev. B **67**, 014420 (2003).
- [5] M. Soenen, *et al.*, Phys. Rev. Materials **7**, 084402 (2023).

Manipulation of the interfacial Dzyaloshinskii-Moriya interaction via the ionic gate voltage adaptation

Department of Physics and Chemistry, DGIST, Daegu 42988, Republic of Korea¹

Basic Science Research Center, DGIST, Daegu 42988, Republic of Korea²

◦Jae Yong CHO¹, Soobeom LEE^{1,2}, Dongryul Kim¹, Chun-Yeol YOU¹

E-mail: cyyou@dgist.ac.kr

Changing the properties of magnetic materials through electrical methods has long been of interest to spintronics[1]. Among them, ionic gating technique using electrolytes, which are non-conducting materials in the form of molten salts, have attracted much attention because they can create a structure with a large capacitance on the surface of the material through a structure called an electric double layer (EDL). Much effort has been made to modulate the magnetic properties of various magnetic layers using EDL[2,3]. We focus on electrical modulation of the interfacial Dzyaloshinskii-Moriya interaction (iDMI), which is the asymmetric interaction between neighboring spins. The change of iDMI could affect various topological magnetic structures affected by iDMI, such as domain wall motion with chirality or the formation of skyrmions.

We utilize a trilayer structure of perpendicularly magnetized Pt/Co/Pt. This structure exhibits relatively small iDMI due to symmetry of the top and bottom heavy metal (HM) layers. Previously, we have observed changes in spin-orbit torque of Pt/Co/Pt trilayer through ionic gating[4]. In this study, we investigate the change in iDMI by using ionic gating. Effective field of iDMI is evaluated by measuring shift of anomalous Hall curve with an applied in-plane magnetic field[5]. The detail will be discussed in the presentation.

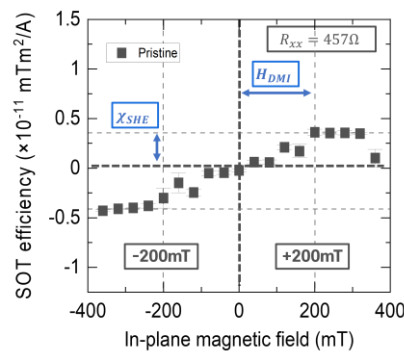


[Figure 1] Measurement of effective DMI field in the pristine sample.

- [1] M. Weisheit *et al.*, Science 315, 349-351 (2007).
- [2] S. Zhao *et al.*, Advanced Materials 30, 1801639 (2018).
- [3] C. Li *et al.*, Current Applied Physics 20, 883-887 (2020).
- [4] S. Lee, J. Cho, C.-Y. You *et al.*, in preparation for submission
- [5] C.-F. Pai *et al.*, Physical Review B 93, 144409 (2016).

二元系合金の軌道ホール伝導度に関する第一原理的考察

Ab-initio insights into orbital Hall conductivity for binary alloys

三重大院工¹, 物材機構² °(M2)辻出 裕至¹, 名和 憲嗣^{1,2}, 中村 浩次¹

Mie Univ.¹, NIMS² °Yushi Tsujide¹, Kenji Nawa^{1,2}, Kohji Nakamura¹

E-mail: 423M230@m.mie-u.ac.jp

軌道分極した電子が固体中を流れる軌道ホール効果(OHE)は Kontani[1]らの理論予測をきっかけに盛んに研究が行われている。OHE はスピン軌道相互作用(SOC)を必要としないため軽元素を含む幅広い元素で発現し、その伝導度はスピホール伝導度と比較して数桁大きい。スピンオービトロニクスデバイスにおいては、この軌道流は SOC を介してスピン軌道トルクを生じさせることで、強磁性体中の磁化を反転させると考えられており、純スピン流由来のスピン軌道トルクと組み合わせることで磁化反転効率の向上が期待できる。実験的には 2023 年に遷移金属の Ti[2]をはじめとして軌道流の観測が複数報告されている。また理論計算では Ru で約 $9000(\Omega\text{ cm})^{-1}$ と遷移金属元素の中で最大の軌道ホール伝導度(OHC)を持つことなどが報告されている[3]。一方、OHC とバンド構造を対応づけた解析は不十分な現状にある。

我々は単金属系から多元系の合金や多層膜構造までの様々な系を対象に OHC の第一原理計算を進めてきており、元素種や組成比に対する OHC の変調性を系統的に調べてきた[4]。本発表では OHE とバンド構造の一対一対応の理解を目的に、その解析結果を報告する。第一原理計算には一般化勾配近似に基づく全電子フルポテンシャル線形化補強平面波法[5]を用い、内因性 OHC を久保公式から評価した。

OHC の第一原理計算から、二元系合金 $\text{Ru}_{1-x}\text{Pt}_x$ の OHC は組成比に対して線形に変化し、 $\text{Ru}(x=0)$ 、 $\text{Ru}_{0.75}\text{Pt}_{0.25}$ ($x=0.25$)、 $\text{Ru}_{0.25}\text{Pt}_{0.75}$ ($x=0.75$)、 $\text{Pt}(x=1)$ のそれぞれで $\text{OHC}=8014, 7721, 5838, 4402(\Omega\text{ cm})^{-1}$ を得た。バンド構造解析から、例えば $\text{Ru}_{0.75}\text{Pt}_{0.25}$ ($x=0.25$)の OHC の起源となるバンド構造は、フェルミ準位では波数空間の R 点近傍に現れることが分かった。この R 点近傍のバンドは主に Pt の $d_{x^2-y^2}$ 及び d_{xy} 軌道で形成されており、また p 軌道との混成軌道も確認できた。 $\text{Ru}_{0.25}\text{Pt}_{0.75}$ ($x=0.75$)の場合、類似のバンド構造はフェルミ準位から約 1eV 低いエネルギー帯に位置していることが分かった。以上のバンド構造解析から、 $\text{Ru}_{1-x}\text{Pt}_x$ 合金の OHC がリジッドバンド的におおよそ振る舞うことが明らかになり、スピホール伝導度と同様の傾向を示すことが分かった。

[1] H. Kontani, *et al.*, J. Phys. Soc. Jpn. **76**.103702 (2007).

[2] Y. G. Choi, *et al.*, Nature **619**, 52 (2023).

[3] L. Salemi, *et al.*, Phys. Rev. Mater **6**, 095001 (2022).

[4] Y. Tsujide, *et al.*, The 84th JSAP Autumn Meeting, 22a-P01-22, Kumamoto, Sep. 2023;

Y. Tsujide, *et al.*, The 71th JSAP Spring Meeting, 25a-P01-36, Tokyo, Mar. 2024.

[5] K. Nakamura, *et al.*, Phys. Rev. B **67**, 014420 (2003).

YIG/Rh におけるスピンゼーベック効果の観測

Observation of Spin Seebeck Effect in YIG/Rh

九大シス情¹, 佐原 脩飛¹, 黒川 雄一郎¹, 湯浅 裕美¹

Kyushu Univ.¹, S. Sahara¹, Y. Kurokawa¹, H. Yuasa¹

E-mail: sahara@mag.ed.kyushu-u.ac.jp

[Introduction]

Spintronic devices require heavy metals with large spin-orbit interactions and low resistivity, and Pt is a typical material. In order to expand the selection of materials, we focus on the properties of Rh because Rh has the same fcc crystal structure as Pt and has half the electrical resistivity of Pt. In this study, we investigate spin Seebeck voltage of YIG/Rh.

[Experiment]

We prepared YIG/Pt and YIG/Rh samples where YIG 50 nm was deposited on thermally oxidized Si substrate and annealed at 1023 K in an atmosphere. The Pt and Rh with thickness of 3 nm or 5 nm are deposited on YIG by DC sputtering. Next, spin Seebeck voltage was measured while applying a temperature gradient from 5 K to 25 K between top and bottom surfaces in the perpendicular direction to the layers and a magnetic field from -0.3 T to 0.3 T in the vertical direction.

[Result]

The thermoelectromotive force $\frac{\Delta V}{\Delta T}$ originated from spin Seebeck voltages are shown in Figure 1. It was found that the YIG/Rh showed about half $\frac{\Delta V}{\Delta T}$ of YIG/Pt, which corresponds to the difference in the resistivity between Pt and Rh. This means that there is no difference between Pt and Rh in charge current obtained by the inverse spin-Hall effect. Therefore, we were able to increase the choice of materials depending on whether we focused on ΔV or ΔI .

[Reference]

[1] K. Uchida et al., Appl. Phys. Lett. 97, 172505 (2010)

[2] H. Adachi et al., Rep. Prog. Phys. 76, 036501(2013)

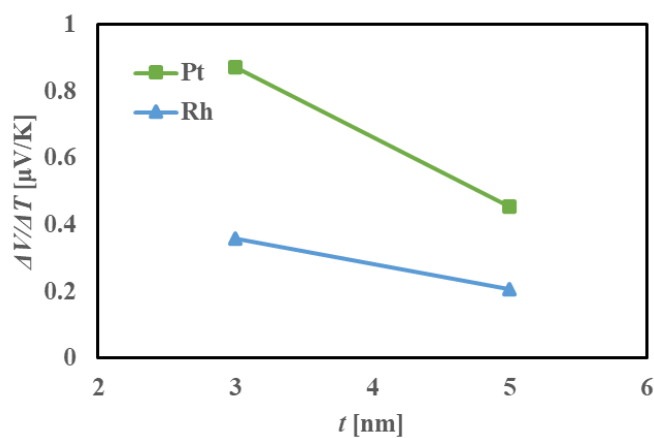


Fig.1. The result of The spin Seebeck voltages

Field-free spin-orbital torque magnetization switching in gallium-doped thulium iron garnet

Kyushu Univ.¹, Chalmers²,

Naoto Yamasahita^{1,2}, Roselle Ngalyo², Yuichiro Kurokawa¹, Hiromi Yuasa¹, Saroj Prasad Dash²

E-mail: yamashita.naoto.952@m.kyushu-u.ac.jp

Current-induced magnetization switching in a perpendicularly magnetized ferrimagnetic insulator - $\text{Tm}_3\text{Fe}_5\text{O}_{12}$ (TmIG) has attracted much attention for the expectation of energy-efficient and ultrafast switching^{1,2}. Whilst Ga^+ ions are often applied to modulate the magnetic properties in Co/Pt system³, the effects on TmIG are yet to be investigated. Here, we investigate the effect of Ga^+ ion irradiation on the spin-orbital torque in TmIG.

The films of Pt(3 nm)/TmIG(6 nm) were prepared using on-axis RF magnetron sputtering on a $\text{Gd}_3\text{Ga}_5\text{O}_{12}$ substrate⁴. After the sputtering deposition of TmIG, Ga^+ ions were irradiated by using a focused ion beam followed by thermal annealing. Hall-cross devices were determined by photolithography and ion milling.

The Ga-doped area appears black in the scanning electron microscopy image (Fig. 1a). The effective spin Hall angle $\theta_{\text{SHE}}^{\text{DL}}$ was evaluated by harmonic measurements¹. The charge current density J_C dependence of the effective field generated by the damping-like torque H_{DL} was fitted using the following equation¹): $\theta_{\text{SHE}}^{\text{DL}} = (2e/\hbar)(H_{\text{DL}}/J_C)M_S t$, where e is an elementary charge, \hbar is the reduced Planck constant, M_S is the saturation magnetization, and t is the thickness of Pt. A tiny difference in $\theta_{\text{SHE}}^{\text{DL}}$ was observed between the Ga-doped and non-doped TmIG samples. $\theta_{\text{SHE}}^{\text{DL}}$ of 5 pC/ μm^2 Ga-doped and non-doped samples were 0.012 and 0.015, respectively, both are in line with the previous study¹. Accordingly, current-induced magnetization switching was successfully demonstrated in both samples without applying magnetic field (Fig. 1b). These results disclosed the notable robustness of TmIG as a material platform in spin-orbitronics study.

This work was supported by JSPS KAKENHI Grant Number JP22K14292, JST ACT-X JPMJAX23KJ, Nippon Sheet Glass Foundation for Materials Science and Engineering, Murata Science and Education Foundation, and Scandinavia-Japan Sasakawa Foundation.

Reference

- 1) C. O. Avci *et al.*, *Nat. Mater.* **16**, 309 (2017).
- 2) J. Ke *et al.*, *Adv. Mater. Interfaces* **10**, 2300632 (2023).
- 3) A. Aziz *et al.*, *J. Appl. Phys.* **99**, 08C504 (2006).
- 4) M. N. Agusutrisno *et al.*, *Thin Solid Films* **788**, 140176 (2024).

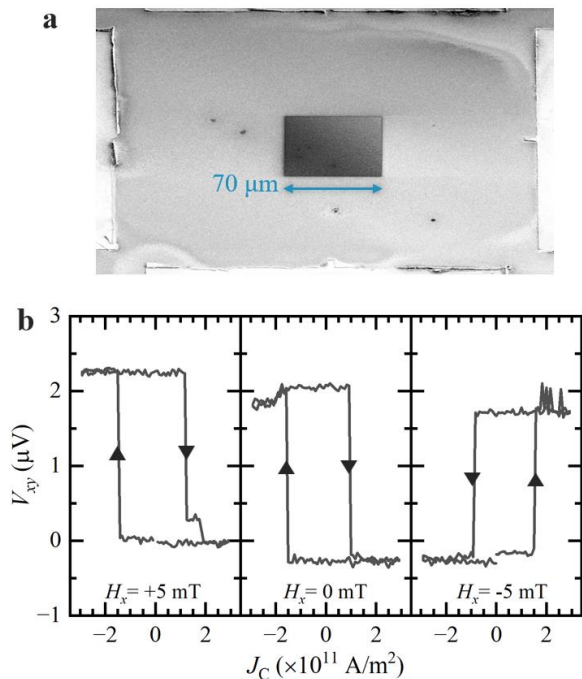


Figure1: Current-induced magnetization switching in $\text{Tm}_3(\text{Fe}_{1-x}\text{Ga}_x)_5\text{O}_{12}$.

a. Scanning electron microscopy image of Ga-doped area.

b Demonstration of current-induced magnetization switching.

Spin-current generation by ultrashort laser pulses in a heavy-metal/rare-earth iron garnet heterojunction

Tokyo Tech¹, Keio Univ.², °Shunsuke Takahashi¹, Yuga You², Kazuto Yamanoi², Yukio Nozaki²,

Takuya Satoh¹, and Kihiro T. Yamada¹

E-mail: Takahashi.s.by@m.titech.ac.jp

The generation of spin currents is one of the central research topics in spintronics. Microwaves are commonly used for generation spin currents by resonantly exciting magnetization dynamics. On the other hand, in this research, we explored the potential of ultra-short optical pulses for spin-current generation. We irradiated femtosecond laser pulses, with a central wavelength of 800 nm and duration of 60 fs, to a $\text{Gd}_{3/2}\text{Yb}_{1/2}\text{BiFe}_{3/2}\text{O}_{12}$ single crystal covered with a heavy-metal electrode for generating spin currents. The spin currents were converted to electric currents in an adjacent electrode of heavy metal, such as Pt and Ta, through the inverse spin Hall effect. The electric-current waveforms were measured using an oscilloscope in conjunction with a trans-impedance amplifier.

We observed electric-current waveforms of which polarity inverted depending on the polarities of the spin Hall effect and in-plane magnetic field (Fig. 1). Furthermore, increasing the thickness of the electrode significantly reduces the peak amplitudes of the electric currents. These results suggest that the direct excitation of the hereto-interface plays a crucial role in the spin-current generation using femtosecond laser pulses.

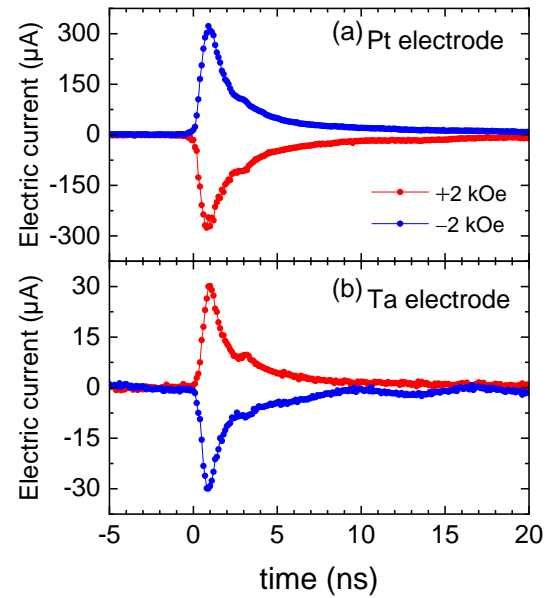


Fig. 1. Electric-current waveforms for Pt (a) and Ta (b) electrodes.

MgO(001)上 CoFe 多層膜の結晶磁気異方性の機械学習と解釈可能性：

有効な回帰モデルと記述子の探索から

Machine learning and interpretability of magnetocrystalline anisotropy in CoFe multilayers on MgO(001): Search for effective regression models and descriptors

三重大¹, NIMS², 名和 憲嗣^{1,2}, 萩原 克幸¹, 中村 浩次¹

Mie Univ.¹, NIMS², °K. Nawa^{1,2}, K. Hagiwara¹, K. Nakamura¹

E-mail: nawa@elec.mie-u.ac.jp

材料科学におけるデータ駆動型手法であるマテリアルズ・インフォマティクス (MI) は、従来材料の物性向上や新規材料の探索など、その応用は多岐に渡り、理論・実験の両方で主流のアプローチとなりつつある。MI に基づく材料設計のボトルネックとして、材料・物性に関するデータベースが不十分であることや、辿り着いた物質において所望する物性の発現メカニズムの解釈困難さなどが挙げられる。我々はこれまでに、前者の課題に対してデータ拡張法とアンサンブル学習を組み込んだ機械学習により、スモールデータであっても構造に基づく物性の予測精度が向上することを MgO(001)上に積層した CoFe 多層膜モデル [(Vac.)/bcc-Co_{9-n}Fe_n/MgO(001)] を例に示してきた[1]。

本発表では、後者の課題解決に向けて、CoFe 多層膜モデルの様々な特徴量を抽出した記述子の観点から、機械学習の予測精度向上と物性の発現メカニズムの解釈可能性を調査した。特徴量には従来の単純な Co と Fe の単層単位の位置情報に加え、多層膜中で隣接する原子層 (2 層ペア) の配列やその数、位置情報などを考慮して記述子を定義した。これら記述子を用いて、結晶磁気異方性エネルギー (E_{MCA}) の予測精度の変化を調べるとともに、 E_{MCA} と原子層配列との関係性を、高い予測精度を示す記述子をもとに解析した。

例えば l_2 正則化によるノンパラメトリック回帰モデル (L2REG) による E_{MCA} 予測では、単層単位だけでなく 2 層ペアの配列の位置情報を組み合わせた記述子を用いることで、最も高い予測精度が得られた。この 2 層ペアに注目した統計的なデータ分析から、Co_{9-n}Fe_n 多層膜が特に 2 層ペア Fe/Fe 配列を表界面に、Co/Co 配列を多層膜中心付近にもつとき、大きな E_{MCA} を示すことを確認した。さらに第一原理計算による解析から、表界面の 1 層の Fe ではなく、 \cdots /Fe/Fe/MgO(001)や (Vac.)/Fe/Fe/ \cdots のように 2 層の連続した Fe/Fe 配列に由来して顕著に大きな E_{MCA} を発現していることが明確になった。以上の結果は、機械学習の記述子の観点から金属多層膜の物理起源が解釈可能であることを示唆している[2]。発表では、L2REG 以外の回帰モデルを用いた場合の予測精度の差異についても報告する。

[1] K. Nawa, K. Hagiwara, K. Nakamura, Comput. Mater. Sci. **219**, 112032 (2023).

[2] K. Nawa, K. Hagiwara, K. Nakamura, under review.

Magnetism of $L1_0$ -FePd from angle-dependent XMCD: Theory and experiments

Mie Univ. ¹, NIMS ², ENS-Paris ³, Tohoku Univ. ⁴, QST ⁵, Nagoya Univ. ⁶

[○]K. Nawa ^{1,2}, S. Vergara ^{3,4}, T. Ueno ⁵, H. Nomachi ¹, K. Nakamura ¹, H. Naganuma ^{4,6}

E-mail: nawa@elec.mie-u.ac.jp

Analysis of microscopic magnetism in alloys, superlattices, and surface/interface is of importance to control magnetic properties such as magnetocrystalline anisotropy for spintronics applications. X-ray absorption spectrum (XAS) and X-ray magnetic circular dichroism (XMCD)—with varying incident angles of X-ray and applied magnetic fields—have been powerful techniques for element-specific probing of electronic and magnetic structures of materials. So far, we implemented the angle-dependent XMCD into first-principles calculations based on density functional theory (DFT). [1] In this work, focusing on $L1_0$ -FePd, for which a heterogeneous interface with two-dimensional graphene was achieved [2], we investigated the XMCD spectra and its variations depending on X-ray incident angle from both theory and experiments. The lattice parameters of FePd, $a = 3.905 \text{ \AA}$ and $c/a = 0.93$ (degree of order, $S = 0.97$), were obtained from experimental sample, which was fabricated by two-steps heating method using r.f. magnetron sputtering. [3]

From the DFT calculations, XMCD spectra of Fe site, normalized at L_3 edge, show clear variations depending on X-ray incident angle from $[100]$ ($\theta = 0^\circ$) to $[001]$ ($\theta = 90^\circ$); the intensity of L_2 edge signal becomes smaller and its position moves to higher energy. This tendency is in quite good agreement with experimentally measured XMCD results, in which the θ varies from 30° to 90° . From the sum rule using the XMCD spectra obtained from the DFT, the orbital magnetic moment (m_{orb}) was theoretically deduced. The results show that m_{orb} is $0.048 \mu_B$ at $\theta = 0^\circ$ and this value increases up to $0.053 \mu_B$ at $\theta = 90^\circ$. The non-negligible variation of m_{orb} ($\Delta m_{\text{orb}} \sim 0.006 \mu_B$) follows the variation of magnetocrystalline anisotropy energy, confirming satisfaction of the Bruno relationship with respect to θ . In the presentation, the comparative results of theory and experiments in XAS/XMCD spectra, spin/orbital magnetic moments, and magnetocrystalline anisotropy will be discussed.

This work is partly supported by the JSPS KAKENHI (No. JP22K14290 and JP21K03444) and JSPS Core-to-Core Program (No. JPJSCCA2023005), Nagoya University Program for Research Enhancement, QST-Tohoku University Matching Research Support Program, and Cooperative Research Project of the Research Institute of Electrical Communication, Tohoku University. XMCD experiments were performed under the approval of the Photon Factory Program Advisory Committee (Proposal No. 2022G516).

[1] H. Nomachi, K. Nawa, K. Nakamura, The 71st JSAP Spring Meeting, 25a-P01-7, Tokyo, March 2024.

[2] H. Naganuma *et al.*, ACS Nano **16**, 4139 (2022).

[3] S. Vergara, T. V. A. Nguyen, H. Naganuma, The 71st JSAP Spring Meeting, 25a-P01-6, Tokyo, March 2024.

[4] K. Nakamura *et al.*, Phys. Rev. B **67**, 014420 (2003).

第一原理計算による L1₀ 合金の角度依存 X 線磁気円二色性と スピン・軌道磁気モーメントの解析

Analysis of angle-dependent X-ray magnetic circular dichroism and spin/orbital magnetic
moments in L1₀ alloys by first-principles calculations

三重大院工¹, 物材機構² ○(M2)野町 宙史¹, 名和 憲嗣^{1,2}, 中村 浩次¹

Mie Univ¹, NIMS². °Hirofumi Nomachi¹, Kenji Nawa^{1,2}, Kohji Nakamura¹

E-mail: 423M237@m.mie-u.ac.jp

X 線磁気円二色性 (XMCD) は、総和則から元素選択的にスピン磁気モーメント (m_{spin}) および軌道磁気モーメント (m_{orb}) を評価できる強力な実験手法であり、磁性材料研究で幅広く利用されている。スピン磁気モーメントに関する総和則は実際には、磁気双極子モーメント (m_{T}) 項を含む有効スピン磁気モーメント ($m_{\text{spin}}^{\text{eff}} = m_{\text{spin}} + 7/2 \cdot m_{\text{T}}$) を与え、角度依存 XMCD (AD-XMCD) を応用すれば m_{T} 項の評価も可能となる[1]。近年では、強磁性体中の結晶磁気異方性[2]だけでなく、反強磁性体の磁気構造の理解においても m_{T} 項が重要な役割を担うことが分かってきた[3]。我々はこれまで、全電子手法の FLAPW 法を用いて、AD-XMCD 計算を第一原理計算に組み込み、L1₀ 型合金系を中心に AD-XMCD スペクトルと d 軌道電子状態の関係性やその元素種依存性を報告してきた[4]。本発表では、さらに総和則に基づいてスピン・軌道磁気モーメントの角度依存性を調べた。L1₀ 型の $3d-5d$ 合金 (FePt, CoPt) と $3d-3d$ 合金 (FeNi, CoNi) に対して、X 線入射方向を [001] ($\theta = 0^\circ$) から [100] ($\theta = 90^\circ$) へと変化させながら、AD-XMCD スペクトル強度をフェルミの黄金率に従って全電子 FLAPW 法[5]から計算した。

計算の結果、スピン磁気モーメントに関する総和則から、FeNi, FePt (CoNi, CoPt) の Fe (Co) サイトの $m_{\text{spin}}^{\text{eff}}$ は $\theta = 0^\circ \rightarrow 90^\circ$ の角度変化に対して増加 (減少) したことから、 θ に対して異方的な変化を示した。一方で、第一原理計算より得られた $m_{\text{spin}}^{\text{DFT}}$ (スピン角運動量演算子の期待値) は θ に対して等方的に、 $m_{\text{T}}^{\text{DFT}}$ 項 (磁気双極子演算子の期待値) は異方的に変化した。従って、総和則から算出される $m_{\text{spin}}^{\text{eff}}$ の角度依存性は m_{T} 項に起因すると解釈できる。さらに軌道磁気モーメントについて、総和則から得られた合金中のそれぞれの原子サイトの m_{orb} も $\theta = 0^\circ \rightarrow 90^\circ$ の角度変化に対して異方的な変化が見られ、この傾向は第一原理計算で得られる $m_{\text{orb}}^{\text{DFT}}$ (軌道角運動量演算子の期待値) と一致した。発表では、 θ に対する XMCD スペクトルの変化とスピン・軌道磁気モーメントとの関連性についても報告する。

[1] J. Stöhr and H. König, Phys. Rev. Lett. 75, 3748 (1995).

[2] G. Shibata, *et al.*, npj Quantum Materials 3, 3 (2018).

[3] N. Sasabe, *et al.*, Phys. Rev. Lett. 131, 216501 (2023).

[4] H. Nomachi, *et al.*, The 71th JSAP Spring Meeting, 25a-P01-7, Tokyo, Mar. 2024.

[5] K. Nakamura, *et al.*, Phys. Rev. B 67, 014420 (2003).

第一原理計算による (Mn, Fe, Ni) 窒化物の磁気特性の理論的考察

Theoretical study of magnetic properties of (Mn, Fe, Ni) nitrides
by first-principles calculations

産総研¹, 東北大², 山形大³, [○]中村 考志¹, 梅津 理恵², 石崎 学³, 栗原 正人³

AIST¹, Tohoku Univ.², Yamagata Univ.²,

[○]Takashi Nakamura¹, Rie Umetsu², Manabu Ishizaki³, Masato Kurihara³

E-mail: nakamura-mw@aist.go.jp

我々は多孔性配位高分子を前駆体を利用した新たな金属窒化物の合成法を提案している。多孔性配位高分子の一つであるプルシアンブルー類似体 (PBA) を利用することで、金属窒化物の任意の元素を任意の比率で合成できることが本法の特徴である。我々はこれまで、本法を用いて、窒化鉄ニッケルにマンガンを導入することに成功し、マンガンを全遷移金属元素に対して 5 ~ 10 % 添加した時、最も飽和磁化が高くなることを発見し、報告した (第 84 回応用物理学会秋季学術講演会、発表番号 : 22a-P01-12、2023 年)。発表では XRD 等による構造解析を行ったが、なぜ透磁率の向上の原因が不明であった。

本発表では、第一原理計算によるアプローチから飽和磁化向上の原因を考察したので発表する。計算は Materials Studio の CASTEP モジュールを利用し、一般化勾配近似 (GGA) —PBE 交換汎関数により、バンド構造と部分状態密度の計算を行った。k 点は 7x7x7、カットオフエネルギーは 300 eV で行った。図 1 に示す M₄N (M は金属元素) 基本構造における金属元素の位置 a, b, c について、表 1 の組み合わせで計算を行った。

当日は各構造のバンド構造及び状態密度を基に磁気特性に関する議論を行う。

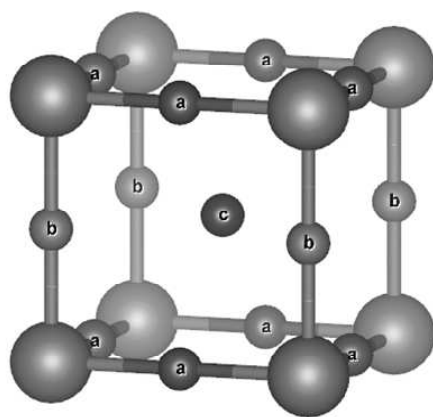


図 1 . M₄N の結晶構造モデル.

表 1 .組成と元素の配置

通し番号	系統	組成	元素と配置		
			a ^{*1}	b	c
			2 ^{*2}	1	1
1	(Fe, Ni) ₄ N	Fe ₄ N	Fe	Fe	Fe
2		Fe ₃ NiN	Fe	Fe	Ni
3		Fe ₃ NiN	Fe	Ni	Fe
4		Fe ₂ Ni ₂ N	Fe	Ni	Ni
5		Fe ₂ Ni ₂ N	Ni	Fe	Fe
6		FeNi ₃ N	Ni	Ni	Fe
7		FeNi ₃ N	Ni	Fe	Ni
8		Ni ₄ N	Ni	Ni	Ni
9	(Mn, Fe, Ni) ₄ N	MnFe ₂ NiN	Fe	Ni	Mn
10		MnFe ₂ NiN	Fe	Mn	Ni
11		MnFeNi ₂ N	Ni	Fe	Mn
12		MnFeNi ₂ N	Ni	Mn	Fe
13		Mn ₂ FeNiN	Mn	Ni	Fe
14		Mn ₂ FeNiN	Mn	Fe	Ni

*1:図 1 に対応する元素の位置

*2:単位格子内の元素数

Dynamic magnetic properties in RuO₂/Co-Fe-B stack film

°T. V. A. Nguyen^{1,2}, Y. Saito², H. Naganuma^{1,2}, D. Vu³, S. Ikeda^{1,2}, T. Endoh^{1,2,4,5}

CSIS¹, CIES², , Tohoku Univ., IoP, VAST³, Vietnam ,Grad. School of Eng. ⁴, RIEC⁵, Tohoku Univ.

E-mail: nguyen.thi.van.anh.e7@tohoku.ac.jp

Spin-split effect (SSE)-induced spin current generation in altermagnetic RuO₂ [1, 2] has been attractive for potential applications in spintronics devices such as spin-orbit torque magnetic random-access memory (SOT-MRAM) [3]. Recent works have reported SSE-induced SOT in RuO₂/Ferromagnetic bilayers with various crystal orientations [2, 4]. However, a detailed study on the dynamic magnetic properties, such as the damping constant (α) and effective magnetization ($4\pi M_{s, \text{eff}}$) in these stacking structures has not been reported. Herein we choose the stacking structures consisting of RuO₂ and Co-Fe-B and investigate the Co-Fe-B layer's thickness (t_{CFB}) and RuO₂ layer thickness (t_{RuO_2}) dependence of α and $4\pi M_{s, \text{eff}}$ by a broadband ferromagnetic resonance (FMR) measurement technique.

RuO₂ (t_{RuO_2})/Co-Fe-B (t_{CFB})/MgO (1.3 nm)/Ta (1.0 nm) stacking structures were fabricated on an α -Al₂O₃ (0001) substrate by DC/RF sputtering. The RuO₂ (100) film was grown on the substrate by RF sputtering at 300°C, while other layers were prepared at room temperature. Each stacking film possesses an in-plane magnetic anisotropy.

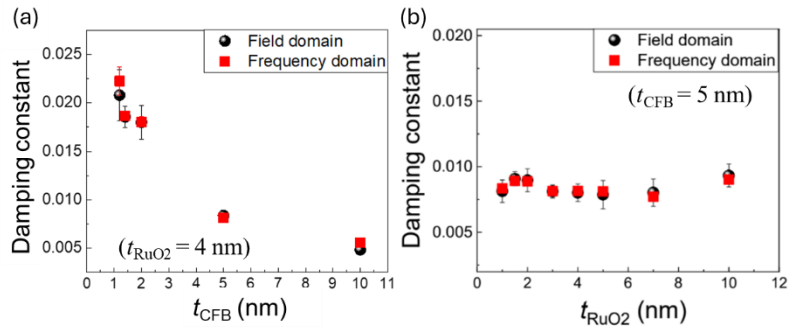


Fig. 1: t_{CFB} (a) and t_{RuO_2} (b) dependences of the damping constant.

Figures 1 (a) and (b) show t_{CFB} and t_{RuO_2} dependences of α for the stacking films evaluated from the FMR spectra measured in the field and frequency domains. α increases with the decrease of t_{CFB} . For a stack film with $t_{\text{CFB}} = 10$ nm, $\alpha = 0.0056$ which is close to the bulk value of a Co-Fe-B [5]. Then α increases to 0.022 when t_{CFB} reduces to 1.2 nm. The increase of α might be attributed to the spin pumping, and/or the magnetic inhomogeneity such as the anisotropy dispersion, and/or the two-magnon scattering, and so on. On the other hand, α is around 0.008 and is almost saturated at t_{RuO_2} range above 1 nm, which suggests that using RuO₂ would enable the retention of a low α value in a wide range of the RuO₂ thickness. The results would be helpful for the on-going research and application of altermagnet-based spintronics.

The authors acknowledge the JSPS Core-to-Core Program (No. JPJSCCA20230005), X-NICS (No. JPJ011438), JSPS KAKENHI Grants 21K18189, 24H000300, Core Research Cluster program, the MRAM program in CIES, TU-MUG start-up Project, Tohoku Univ.

Refs: [1] R. González-Hernández *et al.*, Phys. Rev. B **126**, 127701 (2021). [2] A. Bose *et al.*, Nature Electronics **5**, 267 (2022). [3] H. Honjo *et al.*, IEDM Technical Digest 28.5, 2019. [4] H. Bai *et al.*, Phys. Rev. Lett. **128**, 197202 (2022). [5] M. Belmeguenai *et al.*, J. Phys. D: Appl. Phys. **51**, 045002 (2018).

Possible site occupation of interstitial carbon in ferrimagnetic $\text{Co}_2\text{Mn}_2\text{C}$ thin film

Prabhat Kumar¹, Parasmani Rajput², Hitoshi Abe³ and ^oShinji Isogami¹

¹NIMS, Tsukuba 305-0047 Japan

²INDUS-2, Synchrotron Radiation, RRCAT, Indore 452013, India

³Synchrotron Radiation Science Div.2 (PF), KEK, Tsukuba 305-0801, Japan

E-mails: KUMAR.Prabhat@nims.go.jp

Although anomalous Hall effect (AHE) can be scaled by the saturation magnetization for many magnetic materials, it has been reported that some materials are beyond such scaling. For example, Mn_3Sn antiferromagnet is one of the attractive materials to show large AHE for negligible net magnetic moment, and which is explained by the enhanced spin Berry curvature near the band crossing points called Weyl points [1]. Recently, transition-metal nitrides, e.g. Mn_4N , Co_4N , and Fe_4N , have attracted attention in spintronics [2]; on the other hand, C and B have a potential to be promising materials as for the nitrides. In the previous results, $L1_0$ type $\text{Co}_2\text{Mn}_2\text{C}$ epitaxial thin film showed relatively high AHE for its saturation magnetization, the AHE value for which was one order of magnitude higher than that for CoMn (without C). Similar to N, C occupies the interstitial sites in the host lattice, possibly impacting magnetic and electronic properties due to the p - d hybridization [3]. We thus infer that the interstitial C in the $\text{Co}_2\text{Mn}_2\text{C}$ plays a crucial role to enhance AHE, leading to a universal way to boost AHE. However, the preferential site of C in the realistic epitaxial film is still unclear. Therefore, in this work, we aim to explore the realistic site occupation of C in $L1_0$ type $\text{Co}_2\text{Mn}_2\text{C}$ compound from a magnetic materials development viewpoint.

We deposited SiO_2 sub.// CoMn (35 nm)/ MgO (2 nm) thin film using the DC/RF magnetron sputtering, and subsequent heat treatment was performed at the 500 °C for 1 hour, in the $Q = \text{C}_2\text{H}_2/(\text{Ar}+\text{C}_2\text{H}_2)$ gas environment [3]. A pure $L1_0$ -type $\text{Co}_2\text{Mn}_2\text{C}$ phase is observed at the $Q = 50$ %. The detailed interstitial site occupation was investigated using the X-ray absorption spectroscopy (XAS) measurement. Figure 1(a) shows the three possible sites of C. Figure 1(b) shows the simulation of Co K -edge near-edge XAS spectra for three sites (shown by red, green, and orange) and experimental spectrum (black). The spectrum for the $\text{Co}_2\text{Mn}_2\text{C}$ with occupation of C at the 1st site is very similar to the experimental spectrum, and the edge *A* also appears at the same energy. However, occupation at the other two sites is not consistent with the experimental result which suggests body-centered occupation of C. Furthermore, such site occupation and detailed structure will be discussed by combining the far-edge XAS spectra.

References:

- [1] Nakatsuji et al., Nature 527, 212 (2015).
- [2] Isogami et al., Adv. Electron. Mater. 9, 2200515 (2023).
- [3] Isogami, et al., Phys. Rev. Mater., 7, 014411 (2023).

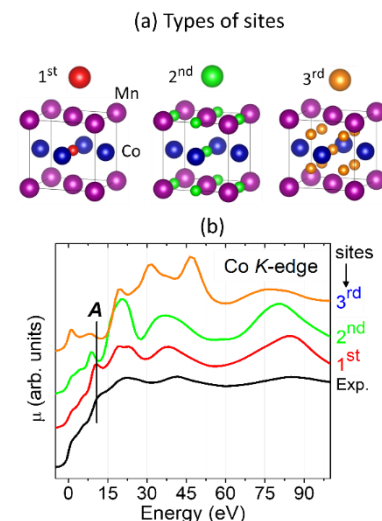


Fig 1: (a) Types of interstitial sites in the $L1_0$ type $\text{Co}_2\text{Mn}_2\text{C}$, and corresponding (b) theoretical near-edge XAS spectra along with the experimental spectrum of $\text{Co}_2\text{Mn}_2\text{C}$ obtained after heat treatment at $Q = 50$ %.

CoFeB/MgO 構造における水素アニールの影響

Effect of hydrogen annealing in CoFeB/MgO system

阪大産研¹, 阪大 CSRN², 阪大 OTRI³, 東北大 SRIS⁴, JST さきがけ⁵

○関 憲行¹, 森田 利明¹, 千葉 大地^{1,2,3,4}, 小山 知弘^{1,2,3,5}

SANKEN, Osaka Univ.¹, CSRN, Osaka Univ.², OTRI, Osaka Univ.³, SRIS, Tohoku Univ.⁴, JST

PRESTO⁵, [○]Noriyuki Seki¹, Toshiaki Morita¹, Daichi Chiba^{1,2,3,4}, Tomohiro Koyama^{1,2,3,5}

E-mail: sekinoriyuki11@sanken.osaka-u.ac.jp

Magnetic tunnel junctions based on the CoFeB/MgO structure are known to exhibit a high tunnel magnetoresistance ratio [1]. Furthermore, in this structure, a strong perpendicular magnetic anisotropy can be obtained by making the CoFeB layer thin due to the interfacial magnetic anisotropy at the CoFeB/MgO interface [2]. To obtain these properties, the system needs to be annealed, which is generally performed in a high vacuum. In this study, we investigate how the magnetic properties of the CoFeB/MgO system affected when the annealing is conducted under hydrogen gas atmosphere.

Ta(2 nm)/CoFeB(t_{CFB})/MgO(1.5) tri-layer structures ($t_{\text{CFB}} = 0.6, 0.8, 1.0$ nm) were deposited on a thermally oxidized Si substrate using sputtering. The samples were fabricated into a Hall bar structure and then, annealed in a vacuum chamber with and without introducing an Ar/H₂ gas mixture. The annealing temperature and time were 300 °C and 1 hour, respectively. Figure 1 shows the results of anomalous Hall resistance R_{Hall} measurement under perpendicular external magnetic field H_{\perp} for $t_{\text{CFB}} = 0.8$ nm sample. The perpendicularly magnetized state was obtained in the sample annealed without H₂ (conventional vacuum annealing), as previous studies. On the other hand, in the H₂-annealed sample, R_{Hall} linearly depends on H_{\perp} when $|H_{\perp}| < \sim 50$ mT and no hysteresis was observed, indicating that the easy axis of the sample is in-plane. Since hydrogen is the smallest atom, the anisotropy change may be relevant to the modulation of electron state at the CoFeB/MgO interface caused by the interstitial hydrogen atoms.

This work is supported by JSPS KAKENHI Grant Number 23K17902, the PRESTO from JST (JPMJPR21B5), MEXT Initiative to Establish Next-Generation Novel Integrated Circuits Centers (X-NICS) and the Spintronics Research Network of Japan.

[1] S. Yuasa *et al.*, *Nat. Mater* **3**, 868 (2004).

[2] S. Ikeda *et al.*, *Nat. Mater* **9**, 721 (2010).

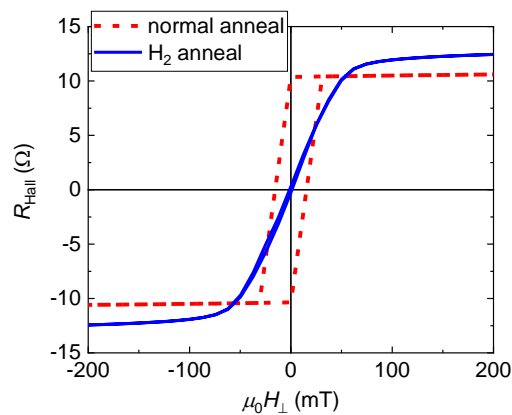


Figure 1: R_{Hall} as a function of H_{\perp} obtained for the conventional vacuum annealing (red dashed) and annealing under H₂ gas atmosphere (blue solid).

CoPt 合金ナノ粒子の磁気プラズモニック特性

Magneto-Plasmonic Properties of CoPt Alloy Nanoparticles

東大生研, °(M2)張 晨, 石田拓也, イ スンヒョク, 立間 徹

IIS, the Univ. of Tokyo, °Chen Zhang, Takuya Ishida, Seung Hyuk Lee, Tetsu Tatsuma

E-mail: tatsuma@iis.u-tokyo.ac.jp

Fe、Co、Ni などの磁性金属を含む材料は、入射光の偏光状態に影響を与える磁気光学効果を示すため、光磁気メモリや磁気検出器、光アイソレータなど多岐に渡り応用されている。これらの磁性材料をナノ粒子化することで、素子の小型化や高速化が可能になり、またプラズモン共鳴に基づく磁気光学効果も期待し得る。磁性金属特有の大きな磁気モーメントを維持しつつ、化学的な不安定性を改善する戦略の一つとして、異なる電子状態やスピン状態を持つ原子のドーピングやそれとの合金化による磁気モーメントの増強が挙げられる^[1]。

本研究では、超常磁性を示す CoPt 合金ナノ粒子を化学的手法により液相合成し、紫外-可視領域で強い MCD を観測した^[2]。CoPt ナノ粒子は、室温、空気中において、 ± 1.6 T の磁場下で MCD の非対称因子 g_{MCD} が 0.034 であった (Fig. 1)。Co ナノ粒子は表面から酸化が進行したために、低い g_{MCD} 値しか示さなかったが、CoPt 合金ナノ粒子は化学的に安定な Pt との合金化によりあまり酸化が進行しなかったことが、高い g_{MCD} 値を示した原因の一つと考えられる。実際、酸素プラズマにより強制的に酸化することにより、 g_{MCD} 値は低下した。また、大きな磁気モーメントを有する Co と、重金属である Pt との間のスピン-軌道相互作用による磁性の強化も、CoPt ナノ粒子の顕著な MCD 応答に寄与したと考えられる。この MCD の起源は、CoPt 合金ナノ粒子内で円偏光によって誘起される Circular Magneto-Plasmonic Mode^[3]に起因する可能性がある。

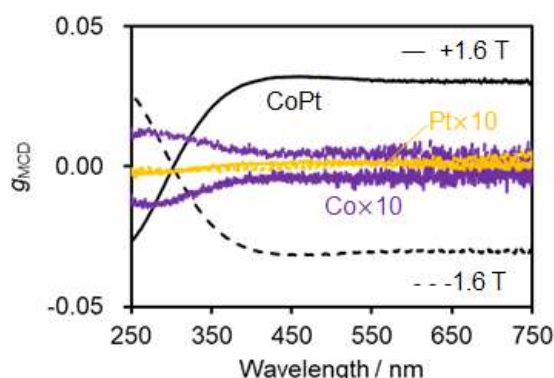


Figure 1. Spectra of g_{MCD} of CoPt, Co, and Pt nanoparticles.

[1] D. Weller, H. Brändle, G. Gorman, C.-J. Lin, and H. Notarys, *Appl. Phys. Lett.* **61**, 2726 (1992).

[2] C. Zhang, T. Ishida, S. H. Lee, and T. Tatsuma, *Appl. Phys. Lett.*, in press.

[3] F. Pineider, G. Campo, V. Bonanni, C. d. J. Fernández, G. Mattei, A. Caneschi, D. Gatteschi, and C. Sangregorio, *Nano Lett.* **13**, 4785 (2013).

電子ビーム蒸着法で作製した(100)配向 β -Sn/M ($M = \text{Ni, Cu}$) 積層膜の超伝導と磁性

Superconductivity and Magnetic Properties of

(100)-textured β -Sn/M ($M = \text{Ni, Cu}$) Multilayer Films Fabricated by Electron Beam Evaporation

岐阜大学大学院¹ 熊澤宏紀¹, 山田啓介¹, 嶋睦宏¹

Gifu Univ.¹ H. Kumazawa¹, K. Yamada¹, M. Shima¹

E-mail: kumazawa.hiroki.k1@s.gifu-u.ac.jp

【背景と目的】 強磁性体と超伝導体のハイブリッド構造では界面でスピン流が長距離伝搬可能なスピン三重項クーパー対を生成しうることから、超伝導とスピントロニクスを組み合わせた新たなデバイス応用への展開が期待されており、超伝導と磁性の相関に関する更なる解明が求められている^[1]。本研究では、電子ビーム蒸着法により超伝導 β -Sn 層及び磁性・非磁性 M ($M = \text{Ni, Cu}$) 層からなる Sn/M/Sn 積層膜を作製し、各層厚 (d_{Sn} , d_{M}) 及び層界面を含む積層構造が超伝導及び磁性に及ぼす影響を解明することを目的とした。

【実験方法】 Sn 層厚を各々 25 nm で固定し M 層厚 d_{M} を 0~5 nm の範囲で変化させた積層膜を電子ビーム蒸着法で作製し、結晶構造を XRD、微細構造を SEM、磁気特性を VSM 及び SQUID、電気伝導特性を SQUID を用いて四端子法で温度、印加磁場、印加電流を変化させて測定した。

【結果と考察】 M 層を Ni とした Sn/Ni/Sn (各 $d_{\text{Sn}} = 25$ nm, $d_{\text{Ni}} = 0\sim 5$ nm) 三層膜の結晶構造を XRD で評価したところ、いずれの試料においても Sn 層は β 相で(100)配向していることを確認した。また VSM による磁化測定の結果、Ni 層は室温で強磁性であることを確認した。SQUID を用い電気抵抗測定を行ったところ、Fig. 1 に示すように Sn/Ni/Sn 膜の d_{Ni} を 0 nm から 5 nm まで変化させたとき、臨界温度 T_{C} は 3.73 K から 2.49 K まで単調に低下する傾向を示した。また Fig. 2 に示す Sn/Ni/Sn 膜の臨界磁場 H_{C} の温度依存性測定結果をもとに理論フィッティング解析を行い、Sn 単層膜や Sn/Cu/Sn 多層膜の結果とも比較したところ、超伝導コヒーレンス長や磁場侵入長は、Ginzburg-Landau のバルクモデルに従う傾向を示した。

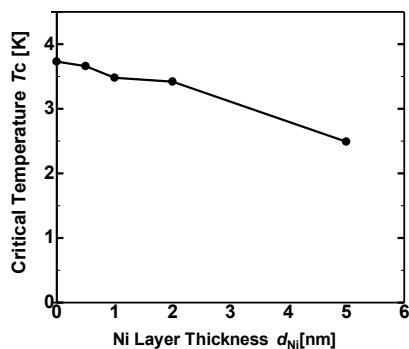


Fig.1: Variation of T_{C} with d_{Ni} in Sn/Ni/Sn.

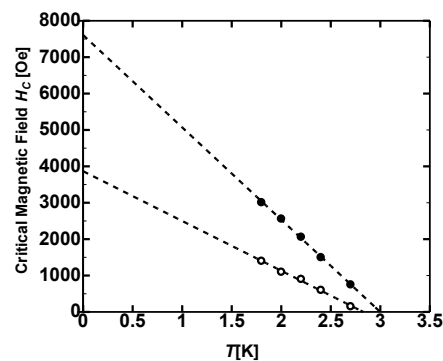


Fig.2: Variation of H_{C} with T in Sn/Ni/Sn.

【参考文献】 [1] J. Linder and J. W. A. Robinson, Nat. Phys. 11, 307 (2015).

【謝辞】 本研究の一部は、文部科学省「マテリアル先端リサーチインフラ」事業（課題番号 JPMXP1223MS1006）の支援を受け自然科学研究機構 分子科学研究所で実施された。

Investigation of magnetic properties in gallium-doped epitaxial thulium iron garnet using Brillouin light scattering

Department of Physics and Chemistry, DGIST, Daegu 42988, Republic of Korea.¹

Faculty of Information Science and Electrical Engineering, Kyushu Univ., Japan²

°Soo-Jung KIM¹, Naoto YAMASHITA², Soobeom LEE¹, Chun-Yeol YOU¹

E-mail: tnwjd8252@dgist.ac.kr

Manipulating the magnetic properties is one of great interest in spintronics. Numerous studies aim to change the magnetic anisotropy, spin-charge interconversion and Dzyaloshinskii-Moriya interaction using annealing, non-metal insertion, alloying and ion irradiation[1, 2]. Especially, the gallium (Ga) ion irradiation using focused ion beam (FIB) is effective in modifying the crystalline structure. Thulium iron garnet ($\text{Tm}_3\text{Fe}_5\text{O}_{12}$ or TmIG) is ferrimagnetic insulator with perpendicular magnetic anisotropy, originating from lattice mismatch strain. This characteristic makes TmIG well-suited for modification of its magnetic properties using FIB. Here, we locally modify the magnetic properties of TmIG film using FIB and analyze the resonance frequency of spin wave via Brillouin light scattering.

We deposited epitaxial TmIG with a thickness of 22 nm using on-axis RF magnetron sputtering on $\text{Gd}_3\text{Ga}_5\text{O}_{12}$ (GGG) substrate [3]. The thickness and crystallinity of TmIG are confirmed by using X-ray reflection and X-ray diffraction, respectively. Figure 1 shows the spin wave frequencies in BLS measurements as a function of applied in-plane magnetic field with incident angle of 10° . We can see the clear difference between non-doped and Ga-doped TmIG. It indicates that the magnetic properties of TmIG are modified by the Ga^+ ion irradiation. A more detailed discussion will be given in the presentation.

This work was supported by JSPS KAKENHI Grant Number JP22K14292, JST ACT-X PMJAX23KJ,

Nippon Sheet Glass Foundation for Materials Science and Engineering and National Research

Foundation of Korea Grant Number NRF-2021MA3F3A2A01037522

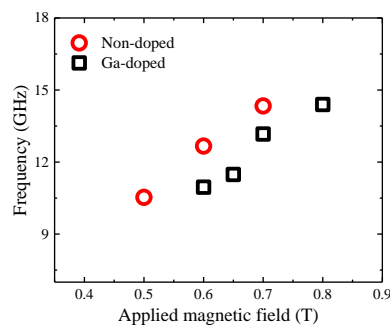


[Figure 1] BLS frequency depends on the applied magnetic field at GGG/TmIG(22 nm) sample with non-doped and Ga-doped (acceleration voltage = 30 kV, dose = 2 pC/ μm^2)

[1] J. Cho, C.-Y. You *et al.*, IEEE Trans. Mang. **54**, 1500104 (2018).

[2] S. An, C.-Y. You *et al.*, Sci. Rep. **12**, 3465 (2022).

[3] M. N. Agusutrino, N. Yamashita *et al.*, Thin Solid Films **788**, 140176 (2024).

スピン偏極電子の生成源のための 白金層上へのバリウムフェライト垂直磁化絶縁層の作製

Preparation of perpendicularly magnetized insulating barium ferrite layers on Pt layers
for the generation of spin polarized electrons

○(M2) 足立 亮太¹, 田中 雅章¹, 小見山 遥²,

小野 輝男², 日原 岳彦¹, 壬生 攻¹ (名工大工¹, 京大化研²)

○R. Adachi¹, M. A. Tanaka¹, H. Komiyama²,

T. Ono², T. Hihara¹, and K. Mibu¹ (Nagoya Inst. Tech.¹, Kyoto Univ.²)

E-mail: r.adachi.082@stn.nitech.ac.jp

研究背景・目的

強磁性絶縁体薄膜を用いたトンネル接合では、トンネルバリアの高さが電子のスピンにより異なり、電子のトンネル確率がスピンに依存して異なるため、スピン偏極した電流を生成することができる。この現象はトンネル型スピンフィルター効果と呼ばれ、強磁性金属を用いない新しいスピン注入源として期待できる。我々はマグネトプランバイト構造を持ちキュリー温度が高い強磁性絶縁体のバリウムフェライト(BaFe₁₂O₁₉, BaM)に注目した。Pt(111)上で(0001)方向に結晶成長することで大きな垂直磁気異方性を示すが、トンネル接合に用いる 10 nm 以下の薄膜での研究はあまりない^{2~3)}。本研究では、アニール方法や組成等の作製条件を変えて垂直磁化を持つ BaM 薄膜の作製を試み、BaM 薄膜を用いたトンネル接合素子の作製を行った。

実験方法

Al₂O₃(0001)基板上に電子ビーム蒸着法で Pt を、パルスレーザー堆積法で BaM を順に製膜した。試料の製膜後に赤外線アニール処理を行い結晶成長させた。X 線回折装置による結晶配向性評価、SQUID 磁束計による垂直磁気異方性の評価、及び原子間力顕微鏡(AFM)による表面平坦性の評価を行った。また BaM 薄膜をトンネル接合とする直径数 μm の MTJ 素子をフォトリソグラフィ及び Ar イオンミリングで作製して、伝導特性の評価を行った。

実験結果

Fig. 1 に 300℃で製膜し 900℃で 90 分間の赤外線アニール処理を行った Pt (20 nm)/BaM (7 nm) 薄膜の X 線回折測定の結果を示す。(000 n)方向のピークを観測することができ、BaM は c 軸方向の結晶成長することがわかった。Fig. 2 に同じ試料の膜面垂直および面内方向の磁化曲線を示す。BaM 層の垂直磁気異方性を確認することができた。また、AFM 観察から Pt/BaM 薄膜のラフネスは 0.5 nm 程度であり平坦性が良いことが分かった。

発表では、作製条件(蒸着条件、アニール条件)の変更に伴う結晶配向性や磁化測定、表面平坦性の影響及び、トンネル伝導の結果についても議論する。

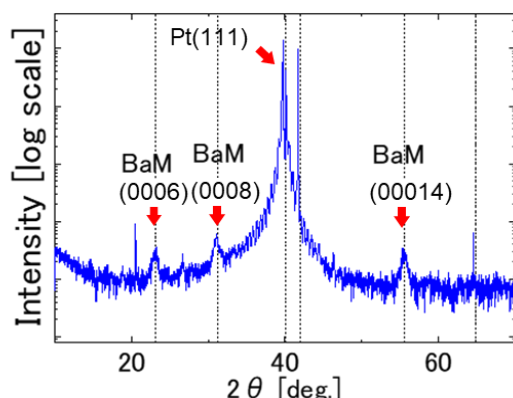


Fig. 1 X-ray diffraction pattern of BaM film

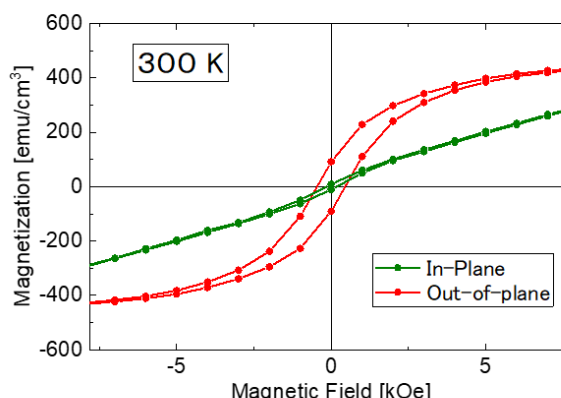


Fig. 2 Hysteresis loops of BaM film

参考文献

- 1) J. S. Moodera *et al.*, Phys. Rev. Lett. **61**, 637 (1988).
- 2) M. Ichinose *et al.*, J. Magn.Soc.Jpn. **23**, 1205 (1999).
- 3) A. Morisako *et al.*, J. Magn.Soc.Jpn. **23**, 1217 (1999).

二元化合物 $\text{Cr}_{1-\delta}\text{Te}$ 薄膜の MBE 成長～成長温度による結晶構造変化

MBE Growth of Binary Compound $\text{Cr}_{1-\delta}\text{Te}$ ~ Growth Temperature Dependence of Crystal Structure

筑波大数理物質¹, 高エネ研², ○小林 純也¹, 仁谷 浩明², 城戸 大貴², 黒田 眞司¹

Univ. Tsukuba¹, KEK², ○J. Kobayashi¹, H. Nitani², D. Kido², S. Kuroda¹

E-mail: s2320345@u.tsukuba.ac.jp

1. Introduction

スピントロニクス分野では、メモリの小型化や低消費電力化に向けて、二次元強磁性体の研究がされている。デバイスへの応用のため、磁気異方性やキュリー温度の調節は重要な要素となっている。本研究で対象とする二元化合物 $\text{Cr}_{1-\delta}\text{Te}$ は、Cr 空孔の量 δ により様々な結晶構造をとり、磁氣的性質も変化することが報告されている[1,2]。我々は MBE 法により様々な成長条件下で $\text{Cr}_{1-\delta}\text{Te}$ 薄膜を作成し、その構造・磁化特性について調べている。

2. Experimental

MBE 法により InP(111)基板上に $\text{Cr}_{1-\delta}\text{Te}$ を成長させた。Flux 比は Cr:Te=1:30 の Te 過剰雰囲気(Te-rich)の下で成長した。 $\text{Cr}_{1-\delta}\text{Te}$ 成長時の基板の温度 T_s を 250~400°Cまで変化させ、また膜厚 20nm と 40nm の2種類の値の薄膜を作成し、その構造特性を評価した。

3. Result

作成した一連の薄膜に対し、XRD ω -2 θ 測定を行った。その結果、NiAs 型 $\text{Cr}_{1-\delta}\text{Te}$ (00n)面の回折ピークのみが見られ、この面に配向した NiAs 型 $\text{Cr}_{1-\delta}\text{Te}$ が成長していることが分かった。Fig. 1 に NiAs 型 $\text{Cr}_{1-\delta}\text{Te}$ の(002)面の回折ピーク付近の拡大図を示す。異なる T_s で成長した膜厚 40nm の薄膜で比較すると、 T_s の上昇とともに回折ピークは高角側にシフトし、面直方向の格子定数が小さくなっていることが分かった。これは T_s の上昇と共に $\text{Cr}_{1-\delta}\text{Te}$ の Cr 空孔量が増加していることを示しているが、これまで報告されている[1,2]のとは逆の傾向である。また $T_s=400^\circ\text{C}$ で成長した膜厚 40nm と 20nm の薄膜の結果を比較すると、膜厚 20nm の薄膜では回折ピークは低角側に位置し、成長の最初の段階では格子定数の大きい相が支配的であることを示唆している。Fig. 2 にそれぞれの薄膜の Cr 吸収端の XANES スペクトルを示す。膜厚 40nm の薄膜では $T_s=250\sim 400^\circ\text{C}$ の範囲でスペクトルはほぼ同じ形状を示し、Cr の価数は変化していないと考えられる。一方、 $T_s=400^\circ\text{C}$ で成長した膜厚 20nm の薄膜では 5996eV 付近の吸収の立ち上がりが小さくなっており、高い成長温度においては成長初期には Cr の価数の異なる状態となっていることを示唆している。詳細は講演で議論したい。

[1] Y.Fujisawa *et al.*, Phys. Rev. Materials **4**, 114001 (2020)

[2] F. S. Luo, *et al.*, J. Magn. Magn. Mater. **550**, 169084 (2022)

謝辞: 本研究は大阪大学スピントロニクス学術連携研究教育センター(CSRN)の支援を受けて行われた。

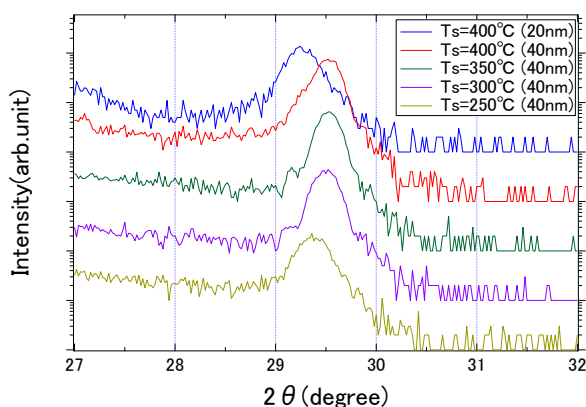


Fig. 1 Profiles of XRD ω -2 θ scan of $\text{Cr}_{1-\delta}\text{Te}$ films.

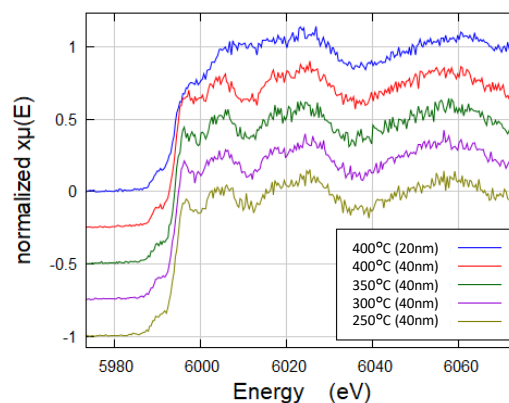


Fig. 2 Normalized Cr K-edge XANES spectra of $\text{Cr}_{1-\delta}\text{Te}$ films.

希薄磁性半導体粉末における強磁性発現条件の解明

Elucidation of the Conditions for Ferromagnetism in Dilute Magnetic Semiconductor Powder

東理大理¹, 東洋大工技研², [○]矢野 智識¹, 村山 真理子^{1,2}, 趙 新為¹

Tokyo Univ. of Sci¹, Toyo Univ. Research Institute of Industrial Technology²

[○]S. Yano¹, M. Murayam^{1,2}, X. Zhao¹

E-mail: xwzhao@rs.tus.ac.jp

【はじめに】

近年、電子のスピンを利用したスピントロニクスが注目を浴びている。希土類元素を含む希薄磁性半導体 (DMS) はスピントロニクス材料に適しており、キュリー温度の低さを克服した室温 DMS の研究が進んでいる。酸化物半導体ベースの磁性半導体では、酸素欠損が重要な役割を果たしており、BMP モデルによって強磁性の発現が説明されている。しかし、薄膜に比べて粉末の形状では多くが常磁性を示すため、理想的な強磁性を持った磁性半導体粉末の作製にはさらなる統一的な理解が必要である。

本研究では、ゾルゲル法で合成した Sm 添加 TiO₂ 粉末およびそれを大気中と窒素中でアニールした試料の磁気特性評価を行った。

【実験】

Sm 添加 TiO₂ 粉末はゾルゲル法で作製した。まず、エタノールにテトライソプロポキシチタン (TTIP) を溶解した。その後、酢酸を加え、混合物を 15 分間かき混ぜた。それとは別に、脱イオン水 (DI 水) に硝酸サマリウム (III) 六水和物を加え、15 分間かき混ぜた。この 2 つの溶液を混合し、80℃で 1 時間かき混ぜた後、110℃で 24 時間乾燥させ、乾燥した粉末を空气中 600℃と窒素中 600℃でそれぞれ 4 時間アニールして結晶性を向上させた。作製した試料は、XRD 測定と RAMAN 測定を用いて結晶性を評価し、XPS 測定を用いて酸素欠損を評価した。さらに、UV-Vis ではバンドギャップや格子乱れを評価し、磁気特性は SQUID 測定を用いて測定した。XAFS 測定では Sm 周りの局所構造を評価した。

【実験結果】

Sm 添加 TiO₂ 粉末では、すべて常磁性を示した。大気中アニール(W-TS)に比べて、窒素アニール(B-TS)のサンプルでは弱い強磁性を示した。また、Sm の添加濃度が増加するに従

って、常磁性成分が増加した。XRD、RAMAN、XPS、UV-Vis および XAFS の結果については当日発表する。

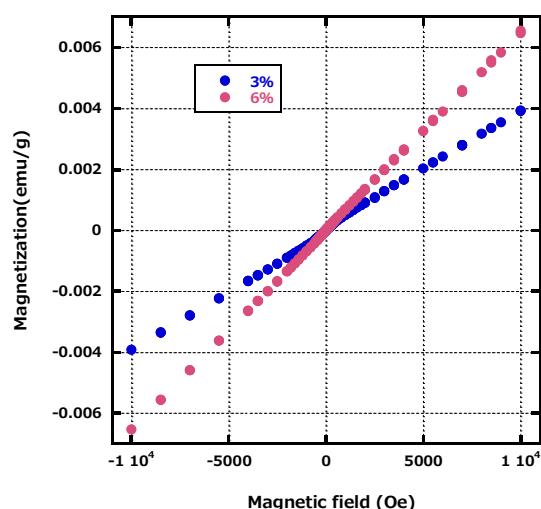


Fig.1 SQUID Result (by concentration)

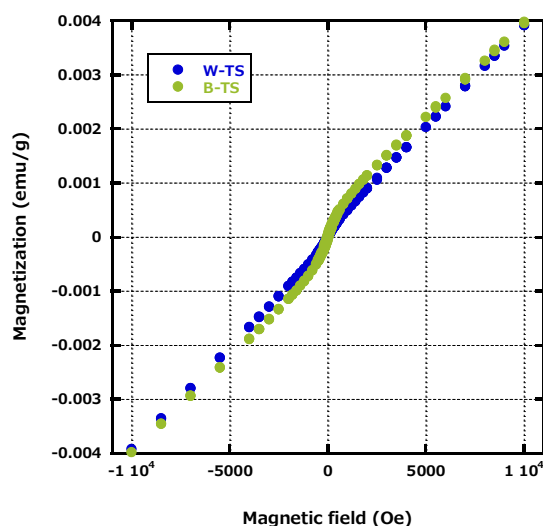


Fig. 2 SQUID Result (by annealing atmosphere)

強磁性共鳴下の強磁性金属膜に発生する起電力を利用した充電技術

A charging technology using the electromotive force generated in a ferromagnetic metal film under the ferromagnetic resonance

阪公大院工¹, °藤井 龍徳¹, 辻井 浩佑¹, 仕幸 英治¹

Osaka Metro. Univ.¹, °Ryutoku Fujii¹, Kousuke Tsujii¹, Eiji Shikoh¹

E-mail: si23473c@st.omu.ac.jp

エネルギーハーヴェスティングは地球上の資源を効率よく利用するための重要な技術である。本研究室では、強磁性共鳴 (FMR) 下の強磁性金属 (FM) 膜における起電力 (EMF) の生成現象[1,2]を利用したエネルギーハーヴェスティング技術の開発を行っている[3]。今回使用した FM 膜 ($\text{Ni}_{80}\text{Fe}_{20}$ および $\text{Co}_{50}\text{Fe}_{50}$) は 10^{-6} Pa 未満の真空下で、熱酸化膜付きシリコン基板上に電子ビーム蒸着法を用いて形成した。評価には電子スピン共鳴装置、もしくはベクトルネットワークアナライザに接続されたコプレーナ線路と電磁石で構成された実験系を使用した。また、FM 試料とコンデンサを含む電気回路をリード線で接続した。Fig. 1 に $\text{Co}_{50}\text{Fe}_{50}$ の典型的な FMR スペクトル (挿入図) と FMR 下の同試料に生成された出力電圧特性を示す。FMR 下の $\text{Co}_{50}\text{Fe}_{50}$ 膜において起電力の生成に成功したことが分かる。Fig. 2 に $\text{Co}_{50}\text{Fe}_{50}$ 膜による充電量の FMR 持続時間依存性を示す。ここで充電量はコンデンサ両端子間の電圧値として評価した。Fig. 2 から FMR 持続時間の増加に伴う、 $\text{Co}_{50}\text{Fe}_{50}$ 膜による充電量の直線的な増加を確認できる[3]。一方で $\text{Ni}_{80}\text{Fe}_{20}$ を用いた場合、FMR 下での起電力の生成には成功したが、FMR 持続時間に対する充電量が時間に比例することなく飽和する傾向がみられた。その原因は試料温度の上昇による飽和磁化の低下、すなわち共鳴条件が FMR の初期設定から離れたため、と考察した[3]。以上より、FMR 下の $\text{Co}_{50}\text{Fe}_{50}$ 膜内に生成された起電力による充電に成功し、かつ今回確認された起電力生成現象をエネルギーハーヴェスティング技術として利用できることと結論付けた[3]。学会時には以上の内容に加え、本研究室でのエネルギーハーヴェスティング関連の研究の詳細について議論する。

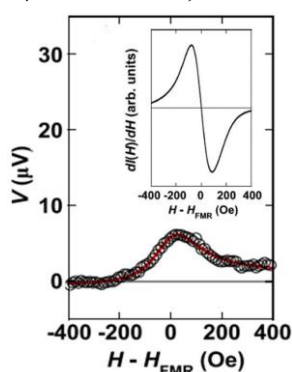


Fig. 1. An EMF property generated in a $\text{Co}_{50}\text{Fe}_{50}$ film itself under the FMR. The inset shows the FMR spectrum of the same $\text{Co}_{50}\text{Fe}_{50}$ film

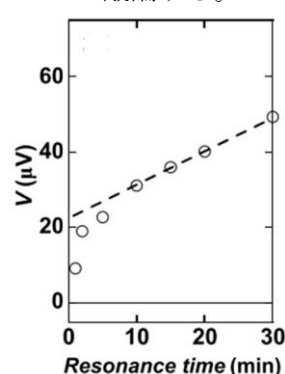


Fig. 2. The FMR duration time dependence of the amount of charge from the $\text{Co}_{50}\text{Fe}_{50}$ film.

- [1] A. Tsukahara, Y. Ando, Y. Kitamura, H. Emoto, E. Shikoh, M.P. Delmo, T. Shinjo, and M. Shiraishi, Phys. Rev. B, 89, 235317 (2014).
- [2] K. Kanagawa, Y. Teki, and E. Shikoh, AIP Advances, 8, 055910 (2018).
- [3] Y. Nogi, Y. Teki, and E. Shikoh, AIP Advances, 11, 085114 (2021).

光磁気記録を用いた微細磁区の形成条件の検討

Examination of conditions for record of fine magnetic domains by MO-recording

長岡技科大¹, 愛知工大², 豊田工大³ ○(M2)本間 拓真¹, 坂口 穂貴¹,

野中 尋史², 鷲見 聡³, 栗野 博之³, Fatima Zahra Chafi¹, 石橋 隆幸¹

Nagaoka Univ. of Tech.¹, Aichi Inst. of Tech.², Toyota Tech. Inst.³, °T. Homma¹, H. Sakaguchi¹,

H. Nonaka², S. Sumi³, H. Awano³, F. Z. Chafi¹, T. Ishibashi¹

はじめに 近年、ディープニューラルネットワークで問題となっている消費電力の大幅な低減や演算の高速化に向けて、光の回折現象を用いたニューラルネットワークが研究されている。我々は、光の回折と磁性体の磁気光学効果を利用した磁気光学回折型ディープニューラルネットワーク(MO-D²NN)を提案し、可視光動作が可能であることやその作製技術について報告した^{1,2)}。今回は、サブミクロンサイズの磁区の書き込みを目的とし、磁区の書き込み条件の検討を行った。

実験方法 磁区書き込みには、有機金属分解法により Gd₃Ga₅O₁₂(111)基板上に作製した、Y_{0.5}Bi_{2.5}Fe₄GaO₁₂ 薄膜 (保磁力: 約 300 Oe) を用いた。波長 405nm のレーザーパルスを対物レンズ(Mitsutoyo 製, G Plan Apo 50×, NA = 0.50)で集光し、磁区の形成を行った。ガルバノミラーを用い 100 μm × 100 μm の範囲に等間隔でレーザーパルス照射し、磁区サイズと収差の影響を評価した。このとき、書き込みの条件としてレーザーの照射強度、パルス幅、外部磁場をパラメータとした。磁区の直径は、磁気光学像から得られた光強度の 2 次元分布を積分し、磁化飽和時の光強度で正規化することで求めた³⁾。

結果と考察 Fig. 1 に書き込み時のパラメータと磁区サイズの関係を示す。パラメータを最適化することで 1 μm 以下の磁区を書き込めることが可能になった。Fig. 2 に計算で求めた磁区パターンと実際に書き込んだ磁区パターンの磁気光学像を示す。実験で書き込んだパターンは目的のパターンを概ね正確に再現できているが、細部を見るとまだ書き込み不良が見られる結果となった。より正確なパターンの書き込みには、レーザー書き込み条件やガーネット膜の磁気異方性を最適化する必要がある。今後は、書き込んだ磁区パターンを用いた手書き数字分類などの実験を行う予定である。

謝辞 本研究の一部は JSPS 科研費 JP23H04803 の助成を受けて実施した。

参考文献 1) T. Fujita et al., *Optical Express.*, 30, 36889 (2022).
2) H. Sakaguchi et al., *IEEE Trans. Magn.*, 59, 1 (2023).
3) I.V. Soldatov et al., *Appl. Phys. Lett.*, 112, 262404 (2018).

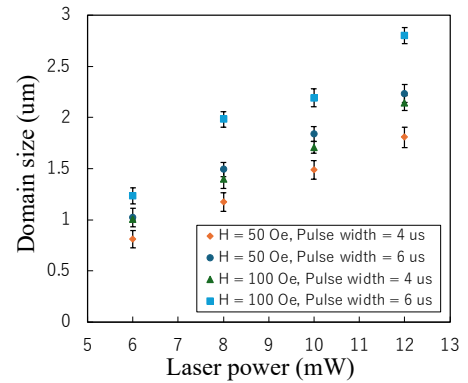


Fig. 1 Laser power dependence of recorded magnetic domain sizes.

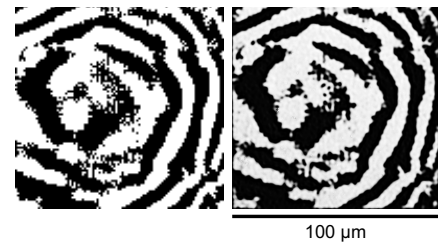


Fig. 2 (a) Magnetic domain pattern obtained by a simulation and (b) Kerr image of experimentally recorded magnetic domain pattern.

座屈状自己組織化磁性粒子を利用した外部環境記憶マイクロロボット

Microrobot with external environment memory
using buckled self-assembling magnetic particles

慶大理工¹, °井口 恵吾¹, 斎木 敏治¹

Keio Univ.¹, °Keio Iguchi¹, Toshiharu Saiki¹

E-mail: keigo.ca_dr@keio.jp

生物は外部の環境を感知／処理し、最適な行動を行う。これは現在の環境に対してのみならず、過去の情報をもとに学習／遺伝する。これにより、生物は多様な進化を遂げてきた。このような生物の適応能力を参考に、物理的／化学的手法を用いて再現することで、非ノイマン型コンピュータの作成や、機能性材料の開発が試みられている。特にマイクロスイマーと呼ばれる、生物の基本的な機能である指向性運動を持った微小ロボットの開発は、ドラッグデリバリーや集団知解明のため、盛んに研究が行われている。このような微小ロボットの推進システムと、エネルギー供給／センシング／信号処理／メモリなどの複雑な機能を統合する点が課題として挙げられる。

そこで本研究では、指向性のある運動とメモリ機能を搭載したマイクロロボットの開発を目標に、Unity3D を用いた物理シミュレーションを行った。マイクロロボット外装には、自由に変形して様々な地形を移動でき、生体適合性が高く生体応用も期待できる脂質二重膜を想定した膜構造体を使用し、内部には推進のための磁性粒子を搭載した。また、メモリ機能は、磁性粒子直径の1.5~2.0 倍で発生する座屈状自己組織化を利用した(図1)。この特異な自己組織化は、磁性粒子間の磁気双極子相互作用によるもので、長距離では微弱な斥力が、近距離では強力な引力へと変化することで、外部刺激に対してヒステリシスを示す(図2)。これにより、過去に受けた外部刺激や通過した外部環境に応じて、物理的特性の変化に伴った移動速度が変化する。これは推進とメモリ機能を両立したマイクロスイマーとして、本マイクロロボットの有用性を示している。

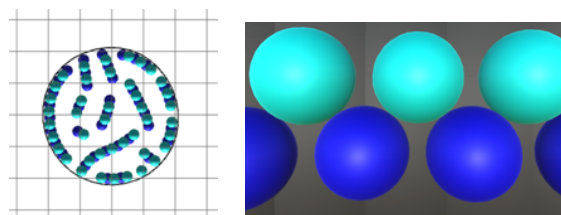


図1.膜構造体内磁性粒子の座屈状自己組織化(左:上面図、右:側面図)

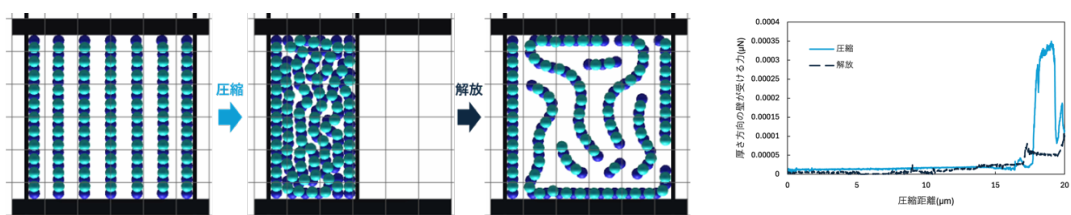


図2.外部からの圧縮によるヒステリシスの発現

Ni₇₈Fe₂₂/Erq₃/FeCo分子スピントロニクスデバイスにおける スピン信号の観測

Observation of spin signal in Ni₇₈Fe₂₂/Erq₃/FeCo molecular spintronic devices

慶大理工¹, 慶大スピンセンター²

○宮本 龍之介¹, 松坂 美月¹, 谷口 真理¹, 上田 拓海¹,

橋本 千佳¹, 鹿嶋 倅太郎¹, 安藤 和也^{1,2}, 海住 英生^{1,2}

Keio Univ.¹ and CSRN, Keio Univ.²

○Ryunosuke Miyamoto¹, Mizuki Matsuzaka¹, Mari Taniguchi¹, Takumi Ueda¹,

Chika Hashimoto¹, Kotaro Kashima¹, Kazuya Ando^{1,2} and Hideo Kaiju^{1,2}

E-mail: mryunosuke@keio.jp

分子材料は軽元素で構成されているため、スピン軌道相互作用が小さく、スピン拡散長が長くなることが期待されている。そのため、スピン輸送材料として適しており、近年注目を集めている。さらに、第一原理計算によると強磁性体と分子の軌道混成由来の巨大な磁気抵抗(MR)効果が予測されている[1]。しかし、現状の分子スピントロニクスデバイスにおいてMR比は11 Kで40%程度[2],[3]と高くない。そこで、本研究では、先行研究[2],[3]で用いられた tris-(8-hydroxyquinoline) aluminum (Alq₃)中の Al を Er に置換した tris-(8-hydroxyquinoline) erbium (Erq₃)に注目した。Al の核スピンは 5/2 である一方、Er の核スピンは 0 であることから、超微細相互作用が小さく、スピン散乱の抑制が期待できる。本研究では Ni₇₈Fe₂₂/Erq₃/FeCo デバイス(Fig. 1)を作製し、MR 効果を観測することを目的とした。

デバイスの作製にはスパッタ法と真空蒸着法を用いた。磁気特性評価には集光型磁気光学カー効果を用いた。また、デバイスにおける MR 効果は磁場中直流 4 端子法を用いて測定を行った。

Fig. 2 にデバイスにおける Ni₇₈Fe₂₂ 電極と FeCo 電極の磁化曲線を示す。Ni₇₈Fe₂₂ 電極と FeCo 電極の保磁力差から本デバイスにおいて MR 効果の発現に必要な磁化平行・反平行状態が実現できていると考えられる。Fig. 3 に 200 K におけるデバイスの MR 効果を示す。本デバイスにおいて負の MR 効果が観測された。これは Erq₃ を介したスピン信号の観測に初めて成功したことを意味する。

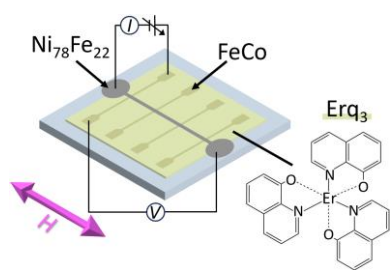


Fig. 1 Schematic illustration of Ni₇₈Fe₂₂/Erq₃/FeCo devices.

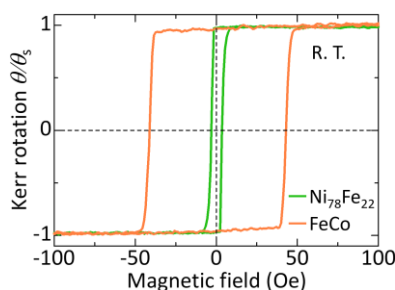


Fig. 2 Magnetization curves of Ni₇₈Fe₂₂ and FeCo in the devices.

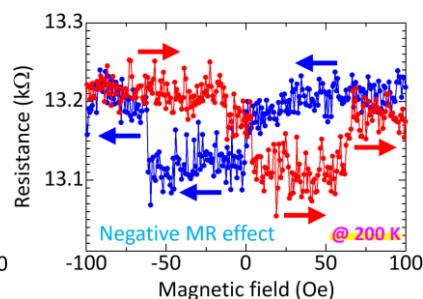


Fig. 3 Negative MR effect observed in the devices.

[1] A. R. Rocha *et al.*, *Nat. Mater.* **4** (2005) 335.

[2] Z. H. Xiong *et al.*, *Nature* **427** (2004) 821.

[3] I. Angervo *et al.*, *Appl. Surf. Sci.* **589** (2022) 152854.

Fabrication of nanoscale magnetoresistance devices using chiral molecules

[○]Mizuki Matsuzaka¹, Ryunosuke Miyamoto¹, Kotaro Kashima¹, Takumi Ueda¹,

Takashi Yamamoto¹, Kohei Sambe², Tomoyuki Akutagawa², and Hideo Kaiju^{1,3}

¹ Keio Univ., ² IMRAM, Tohoku Univ. and ³CSRN, Keio Univ.

E-mail: m.matsuzaka@keio.jp

Molecular spintronic devices are attractive owing to the expected long spin diffusion lengths in organic molecules. Nanosized devices are expected to provide a high spin polarization, leading to a large magnetoresistance (MR) effect [1]. We have successfully observed MR effect in nanojunctions using high-mobility molecules sandwiched between two Ni₇₈Fe₂₂ thin-film edges at room temperature [2]. Recently, chirality induced spin selectivity (CISS) effect has been observed in the chiral molecules [3, 4] and attractive for the application to the MR devices. CISS effect was observed in the Au/chiral molecules/ferromagnetic materials (FM) micro-devices under a high magnetic field H of ~ 5000 Oe [5, 6]. Here, in this study, towards the observation of MR effect owing to CISS effect under low magnetic field, we fabricate nanoscale MR devices, which consist of chiral molecules, *N*-(3*S*)-3,7-dimethyloctyl[1]benzothieno[3,2-*b*]benzothiophene-2-carboxamide (*S*-BTBT-CONHR) sandwiched between Au and FM thin films with their crossed edges (Fig. 1), and evaluate their structural, electrical and magnetic properties.

Prior to fabricating the devices, we investigated the current–voltage (I – V) curves of *S*-BTBT-CONHR by conductive atomic force microscopy (c-AFM) using CoPtCr tips magnetized along the up or down direction. In these measurements, *S*-BTBT-CONHR chiral molecules were spin-coated on highly oriented pyrolytic graphite (HOPG) substrates. The fabrication method of our proposed devices mainly consists of sputtering, thermal pressing, mechanical cutting, polishing and spin-coating techniques [2]. The electric features of the electrodes were examined by c-AFM. The magnetic properties of the FM electrodes were evaluated by magneto-optic Kerr effect spectroscopy (MOKE).

As shown in Fig. 2, the current through a tip with down magnetization is larger than that with up magnetization in c-AFM studies using magnetized tips. The obtained I – V curves indicate that using *S*-BTBT-CONHR can lead to the observation of a large MR effect due to CISS effect in the nanoscale MR devices. Fig. 3 shows a c-AFM image of the surface of the Au electrodes (glass/Au/glass). A uniform electrical conduction along the Au edges is observed. MOKE study reveals that FM electrodes show small coercivities (< 100 Oe). By using these electrodes for the device, we could observe MR effect based on CISS effect observed under a low magnetic field of ~ 100 Oe. This study can lead to the realization of the nanoscale MR device with high magnetic sensitivity.

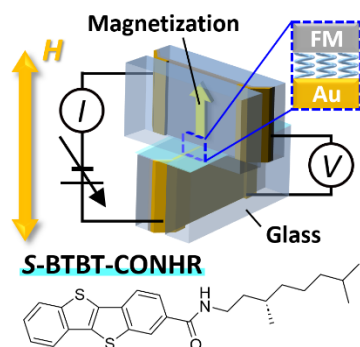


Fig. 1 Schematic of FM/*S*-BTBT-CONHR/Au devices.

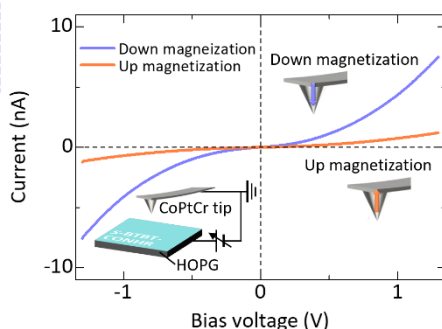


Fig. 2 I – V characteristics of *S*-BTBT-CONHR by a magnetized CoPtCr tip.

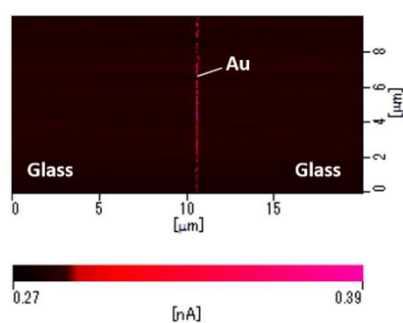


Fig. 3 c-AFM image of the surfaces of the Au electrodes.

[1] C. Barraud *et al.*, Nat. Phys. **6**, 615 (2010). [2] M. Matsuzaka *et al.*, Nanoscale Adv. **4**, 4739 (2022).

[3] B. Göhler *et al.*, Science **331**, 894 (2011). [4] Z. Xie *et al.*, Nano Lett. **11**, 4652 (2011).

[5] M. Suda *et al.*, Nat. Commun. **10**, 2455 (2019). [6] C. Kulkarni *et al.*, Adv. Mater. **32**, 1904965 (2020).

PDMS に接合したポリイミド膜上に作製したトンネル磁気抵抗素子 Tunnel Magnetoresistance devices fabricated on polyimide film attached to PDMS

九大シス情¹ ○大石 晟矢¹, 黒川 雄一郎¹, 山下 尚人¹, 湯浅 裕美¹

Kyushu Univ.¹, ○Seiya Oishi¹, Yuichiro Kurokawa¹, Naoto Yamashita¹, Hiromi Yuasa¹

E-mail: oishi@mag.ed.kyushu-u.ac.jp, ykurokawa@ed.kyushu-u.ac.jp

[Introduction] Spintronics devices with sufficient flexibility are very useful because it can be used on a curved surface like human body. In fact, there have been reports on strain gauges based on spintronics technology.[1] Flexible applications require the device to be mounted on a film with sufficient flexibility. However, to use spintronics device on human body, the film needs to have biocompatibility. In this study, we used a polyimide (PI) film and a PDMS (dimethylpolysiloxane) instead of a rigid Si substrate to fabricate a flexible and biocompatible magnetic tunnelling junction (MTJ).

[Experiment] First, the PI varnish was coated on the Si substrate by a spin coating. Next, the PI film was annealed to polymerize PI varnish. Then, the multilayered film, bottom electrode/Ru/IrMn/CoFeB/MgO/CoFeB/top electrode, was deposited on the PI film by a sputtering method. The multilayer on the PI film was annealed in a field of 500 mT at 593 K for 1 hour to pin the magnetization of the pinned layer. The multilayer was patterned into a MTJ by a photolithography and Ar ion milling. Then, the PI film with the Tunnel Magnetoresistance (TMR) device was peeled from the Si substrate. Finally, the PI film and PDMS were bonded by attaching them.[3] Magnetoresistance (MR) of samples was measured by the four-terminal method.

[Results] Figure 1 shows MR curves for MTJs on the PI/Si substrate and the PI/PDMS, where they are normalized by MR ratio of MTJ on the PI/Si substrate. They showed good agreement in MR ratio and magnetic properties, that indicates that there is no damage in MR ratio even after peeling process. Therefore, the PI film fabricated by spin coating method has sufficient flatness and flexibility, and the devices on the PI film has a high resistance against stress during peeling.

[Acknowledgements] This study was supported in part by the JST, ACT-X Grant Number JPMJAX21K5., KAKENHI JP22KK0056, JP24H00030, JP24H02235

[Reference] [1] K. Saito, et al., Appl. Phys. Lett, 120, 072407 (2022).

[2] T. P. O. Nguyen, et al., Lab on a Chip, 16, 3251 (2016).

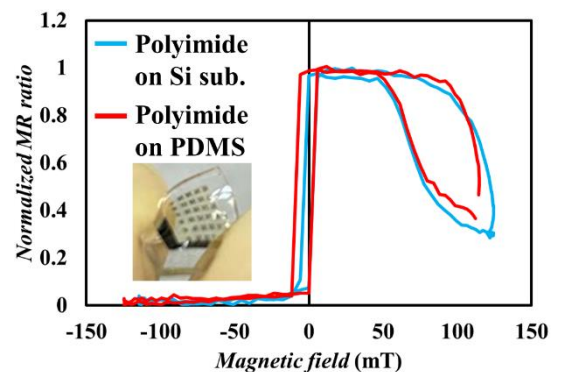


Fig. 1 MR curves for TMR devices of PI film on Si sub. and that on PDMS

磁気渦スピントルク発振器のポテンシャルがダイナミクスに及ぼす影響

Influence of potential on vortex spin torque oscillator dynamics

○堀住 耕太¹, 千葉 貴裕^{2,3}, 小峰 啓史¹ (1. 茨城大院, 2. 東北大工, 3. 東北大学際研)

○Kota Horizumi¹, Takahiro Chiba^{2,3}, and Takashi Komine¹

(1. Ibaraki Univ., 2. Tohoku Univ., 3. FRIS)

E-mail: 24nd253n@vc.ibaraki.ac.jp

磁気渦スピントルク発振器 (Vortex Spin Torque Oscillator, VSTO) は磁気渦構造がスピントルクにより運動し、高周波電圧を出力するナノスケールの発振器である [1]. VSTO において、磁気渦コアが運動する閾値電流が存在することが知られており、閾値電流は VSTO のダンピングや静磁気エネルギーを反映したポテンシャル形状に依存する [2]. 本研究では、磁気トンネル接合における自由層の構造に細工することでポテンシャル形状の制御を行い、ポテンシャル形状が磁気渦コアのダイナミクスに及ぼす影響を数値解析により調べた。

半径 $R = 187.5$ nm, 厚さ 5 nm の自由層を持つ VSTO の磁気渦コアの運動を Thiele 方程式 [3, 4] の数値解析により調べた。

$$-G \times \dot{X} - D(s)\dot{X} - \frac{\partial W}{\partial s}X + a_J J p_z e_z \times X + c a_J J R_0 p_x e_x = 0$$

ここで、 X は磁気渦コアの位置、 R_0 は磁気渦コアの半径 (10nm), G はジャイロベクトル, $D(s)$ は非線形を含むダンピング係数, a_J はスピントルク, J は電流密度, $(p_x, 0, p_z)$ は参照層の磁化ベクトルの向き, c はカイラリティ, s は規格化された磁気渦コアの変位 $s = |X|/R$ である. $W(s)$ は磁気渦コアに対するポテンシャルであり、VSTO における自由層のディスク形状を反映した静磁気エネルギー及び電流磁場の影響を加味した $W(s) = \frac{1}{2}(\kappa - \kappa_1)s^2 + \frac{1}{4}\kappa' s^4$ という関数でしばしばモデル化される. 本研究では、自由層を 2 枚のディスク形状とすることで磁気渦コアに対するポテンシャル $W(s)$ を変化させた。

マイクロマグネティックスにより計算したポテンシャル、及び、モデル化したポテンシャルを Fig.1 に示す. 付与したディスクエッジはポテンシャルの極小値を形成すると同時に、ポテンシャルにおける s^2 の係数 $(\kappa - \kappa_1)$ を小さくする効果があることがわかる. 本研究では、ポテンシャルの形状の影響を定性的に調べるため、 $W(s)$ における κ_1 を変えて磁気渦のダイナミクスを解析した. パラメータ κ_1 を変えて磁気渦コアの運動を調べた結果を Fig.2 に示す. 従来の VSTO では閾値電流 I_c が存在し、閾値電流以上で磁気渦の規格化距離 s が一定となる周回運動となる. 一方、ポテンシャル形状を変えることで閾値電流が大幅に低減されることがわかる. 講演では、様々な自由層形状に対して計算したポテンシャルが磁気渦ダイナミクスに及ぼす影響を議論する.

[1] V. S. Pribiag, *et al.*, *Nat. Phys.* **3**, 498 (2007).

[2] K. Y. Guslienko, *et al.*, *J. Phys.: Conf. Ser.* **292**, 012006 (2011).

[3] A. V. Khvalkovskiy, *et al.*, *Phys. Rev. B* **80**, 140401(R) (2009).

[4] Y. Imai, *et al.*, *Sci. Rep.* **12**, 21651 (2022).

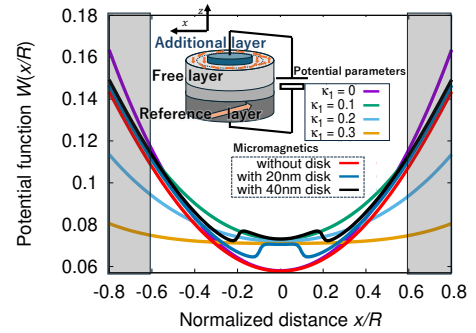


Fig.1 Model potentials for various potential parameters κ_1 . The inset illustrates VSTO with a double-disk free layer.

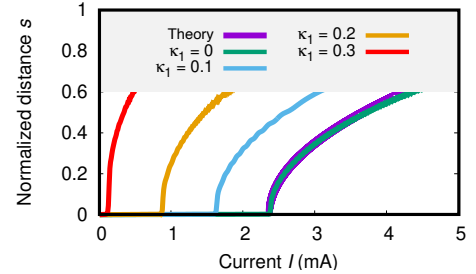


Fig.2 Current dependence of normalized vortex core distance s for various potential parameters κ_1 , and a theoretical trend for a single free layer [4] was also shown. Only the range of data adequately represented by the model was shown here.

磁気トンネル接合を用いた高出力電圧磁気センシング

High-output-voltage magnetic sensing using magnetic tunnel junctions

慶大理工¹, ブラウン大物理², 慶大スピンセンター³

○若本 瑞葵¹, 柴田 有仁¹, Gang Xiao², 海住 英生^{1,3}

¹Keio Univ., ²Brown Univ., and ³CSRN, Keio Univ.

○Mizuki Wakamoto¹, Yuto Shibata¹, Gang Xiao², and Hideo Kaiju^{1,3}

E-mail: mizuki_wakamoto@keio.jp

磁気トンネル接合 (MTJ) は、室温で巨大なトンネル磁気抵抗 (TMR) 効果を示すことから、高感度磁気センサや磁気ランダムアクセスメモリ (MRAM) に応用されている[1]。最近では、CoFe/MgO/CoFe MTJ において、界面の高度な制御により 631%の巨大 TMR 比が観測されており[2]、絶縁体に MgO を用いた高性能な MTJ が注目されている。しかし、MTJ には絶縁層が存在し、大きなセンス電流を流すことができないため、従来のセンシング方法では大きな出力電圧を得ることができない。そこで、本研究では、MTJ を用いた高出力電圧磁気センシングの実現を目的とした。

Fig. 1 に磁気センシング回路を示す。MTJ をハートレー発振回路の帰還部に挿入し、磁場による発振電圧を出力電圧として検出した。増幅部には接合型 FET とダイオードを用いた。MTJ は SiO₂/Ta(5)/Co₅₀Fe₅₀(2)/IrMn(15)/Co₅₀Fe₅₀(2)/Ru(0.8)/Co₄₀Fe₄₀B₂₀(3)/MgO(2)/Co₄₀Fe₄₀B₂₀(3)/contact layer (nm) で構成される。

Fig. 2 に交流周波数 320 kHz における TMR 曲線を示す。TMR 比は 133%、抵抗変化分 ΔR は最大で 1.2 k Ω を示した。Fig. 3 に本磁気センシングによる発振出力電圧、及び、従来のセンス電流型磁気センシングにおける出力電圧の ΔR 依存性を示す。出力電圧は ΔR に依存し、 ΔR が 200–930 Ω の範囲において、従来のセンス電流型磁気センシングを大きく上回る高出力電圧を観測した。

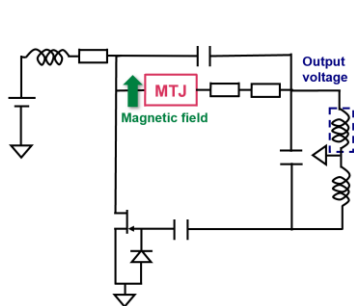


Fig. 1 Magnetic sensing circuit using MTJs.

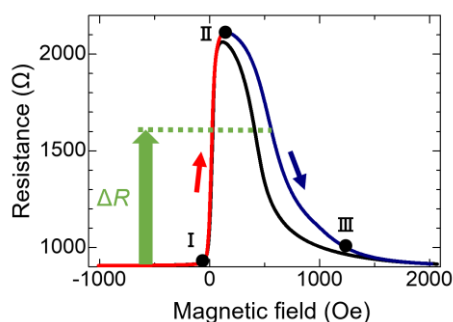


Fig. 2 TMR effect at a frequency of 320 kHz.

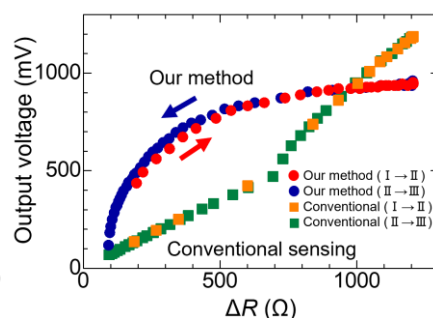


Fig. 3 Resistance change ΔR dependence of output voltage.

[1] S. Yuasa, T. Nagahama, A. Fukushima, Y. Suzuki, and K. Ando, *Nat. Mater.* **3**, 868 (2004).

[2] T. Scheike, Z. Wen, H. Sukegawa, and S. Mitani, *Appl. Phys. Lett.* **112**, 112404 (2023).

塗布による作製が可能な磁性多層膜の交換バイアス磁場の観察

Investigation of exchange bias field in magnetic multilayer fabricated by coating

九大シス情^{1, °}田口 正宗¹, 黒川 雄一郎¹, 湯浅 裕美¹

Kyushu Univ.¹, [°]Masamune Taguchi¹, Yuichiro Kurokawa¹, and Hiromi Yuasa¹

E-mail: taguchi@mag.ed.kyushu-u.ac.jp

[Introduction]

Flexible spintronics devices that can be placed anywhere, for example the human body or curved surfaces, are very useful. Giant magnetoresistance (GMR) is one of magnetoresistance that can be used as a magnetic field sensor. Highly sensitive magnetic sensors can be used as compasses, magnetocardiographs, or magnetoencephalographs, expanding their applications by introducing flexibility. To use GMR effect, we need to fix magnetization in a pinned layer by exchange bias. In this study, we fabricated IrMn/CoFeB bilayer by a simple coating process and observe exchange bias field to realize flexible GMR sensors with high sensitivity.

[Experiment]

First, we coated a resist which can be removed in organic solvents onto a Si substrate. Next, an IrMn/CoFeB bilayer was prepared on the resist film using DC magnetron sputtering. Sequentially, the IrMn/CoFeB bilayer was dissolved with the resist in acetone using an ultrasonic cleaner. Then, the IrMn/CoFeB bilayer flakes dispersed solution was applied onto the Si substrate. Finally, they were annealed in an in-plane magnetic field to generate an in-plane exchange bias field. The magnetization curves before and after annealing were measured with a vibrating sample magnetometer (VSM).

[Result]

Figure 1 is a photo for the IrMn/CoFeB bilayer flakes on Si substrate. The size of flake is a few 100 μm and they get twisted. In addition, some flakes rolled up to shape like cylinder with a diameter around 100 μm . It is necessary to increase the flake population to electrically connect them. On the other hand, the magnetization curve measured by VSM shows that the magnetization of the CoFeB is sufficiently pinned by the IrMn through the exchange coupling even the flake is not perfectly parallel to the bias field during annealing. In addition, exchange bias field was found to develop even in the presence of films with roll-up structures. In the future, MR will be measured to verify its practicality as a sensor.

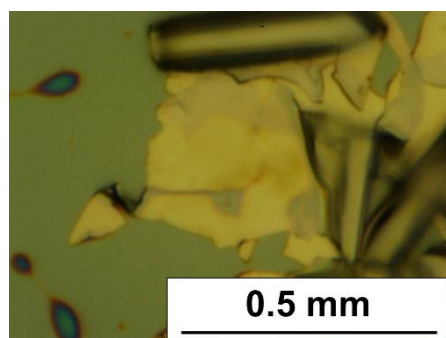


Fig. 1 Optical microscope image of IrMn/CoFeB flakes.

[Acknowledgements] This study was supported in part by

the JST, ACT-X Grant Number JPMJAX21K5, KAKENHI (JP22KK0056, JP24H00030, and JP24H02235), and Iketani Science and Technology Foundation.

エピタキシャル MgO トンネル障壁の誘電率と VCMA 効果

Dielectric constant and VCMA effect of epitaxial MgO tunnel barrier

産総研 ○野崎友大, 小野田浩成, 田丸慎吾, 中山裕康, 甲野藤真, 野崎隆行, 湯浅新治

AIST, °T. Nozaki, H. Onoda, S. Tamaru, H. Nakayama, M. Konoto, T. Nozaki, and S. Yuasa

E-mail: nozaki.tomohiro@aist.go.jp

Voltage controlled magnetic anisotropy (VCMA) effect has received much attentions as a magnetization control technique with ultra-low power consumption. Toward practical applications, further enhancement of VCMA coefficient has been desired. One approach to further enhance VCMA coefficient is to use high- k dielectrics for the tunnel barrier. Thus far, incorporation of high- k dielectrics such as HfO_2 , ZrO_2 , $\text{Pb}(\text{Zr}_x\text{Ti}_{1-x})\text{O}_3$, and SrTiO_3 has been attempted^[1]. However, achieving both a large dielectric constant (ϵ_r) and a large tunnel magnetoresistance (TMR) ratio is challenging. On the other hand, MgO tunnel barrier itself has the potential for a larger ϵ_r : strain induced enhancement of ϵ_r has demonstrated for rocksalt-type dielectrics in the past^[2]. In this study, we investigated the ϵ_r of MgO tunnel barrier in epitaxial stacks (MgO sub./MgO (5 nm)/Cr (50 nm)/Fe (0.9 nm)/Ir (0.06 nm)/Co (0.1 nm)/MgO (t_{MgO} nm)/cap structure) and demonstrated large $\epsilon_r > 15$, which is more than 50 % larger than that of bulk MgO ($\epsilon_r = 10$). We found that the ϵ_r increases with decreasing t_{MgO} . From in-plane XRD measurements, we clarified that lattice parameter a of epitaxial MgO tunnel barrier decreases with decreasing t_{MgO} . We interpreted the large ϵ_r of epitaxial MgO tunnel barrier in terms of the compressive strain induced enhancement of ϵ_r . We also investigated the VCMA coefficient of the epitaxial stacks and confirmed that the VCMA coefficient increases as the ϵ_r increases. This study provides a new perspective to the large VCMA effect of the epitaxial stacks and also demonstrates the importance of the strain engineering.

This work was partly based on results obtained from a project, JPNP16007, commissioned by the New Energy and Industrial Technology Development Organization (NEDO).

Reference: [1] H. Onoda *et al.*, Phys. Rev. Materials **6**, 104406 (2022). [2] E. Bousquet *et al.*, Phys. Rev. Lett. **104**, 037601 (2010).

Table 1. Comparison of dielectric constant ϵ_r , lattice parameter a , and VCMA coefficient of the epitaxial stacks with varied t_{MgO} .

t_{MgO}	ϵ_r	a	VCMA coefficient
4 nm	15.9	4.147 Å (−1.5 %)	−256 fJ/Vm
6 nm	14.6	4.165 Å (−1.1 %)	−238 fJ/Vm
8 nm	14.1	4.174 Å (−0.9 %)	−226 fJ/Vm
10 nm	13.6	4.186 Å (−0.6 %)	−216 fJ/Vm

Data-writing and shift processes toward a vertical domain wall motion memory with perpendicular magnetic anisotropy

ICR, Kyoto Univ.¹, CSRN, Kyoto Univ.², NIMS³, [○]Feifan Ye¹, Heechan Jang¹, Yoichi Shiota^{1,2},

Hideki Narita¹, Ryusuke Hisatomi^{1,2}, Shutaro Karube^{1,2}, Satoshi Sugimoto³, Shinya Kasai³, Teruo

Ono^{1,2}

E-mail: ye.feifan.56e@st.kyoto-u.ac.jp

Domain wall motion memory is promising to achieve high-density and non-volatile storage as a candidate of the next-generation memory. In this memory, logic bits are stored in domains and separated by domain walls in a ferromagnetic nanowire. By injecting electric current, the logic bits can be carried to desired storage position due to the domain wall motion. A novel vertical domain wall motion memory (Figure 1) was designed in our previous work [1, 2]. Micromagnetic simulations showed that it is possible to obtain a low critical current density J_c ($<10^{11}$ A m⁻²) and a high thermal stability ($\Delta > 60$, $\Delta = E_B/k_B T$) by tuning properties of each layer. In this research, we investigated the data-writing and shift processes in a 300 nm nanopillar to show the feasibility of the vertical memory structure.

Multilayers of Si-SiO₂/Ta(5)/Pt(10)/Co(1.4)/Cu(3)/Co(t_1)/Pt(t_2)/Co(t_1)/Cu(3)/Pt(3) with wedge-shaped Co and Pt were deposited using sputtering. Here, t_1 and t_2 in the parentheses indicate the thickness gradients. Pt was selected as the material for the bottom electrode to induce spin-orbit torque (SOT). Nanopillars are fabricated by electron beam lithography and Ar etching. A sudden resistance change in the hysteresis measured by the giant magnetoresistance (GMR) effect indicated a perpendicular easy axis of each layer. A canted-magnetic-field-assisted SOT switching of the downmost layer was observed for the data writing. When out-of-plane current pulses are injected into the nanopillar, the data in the writing layer can be further transferred to the second layer by spin-transfer torque (STT). Continuous data writing and shift can be achieved by repeating these two operations.

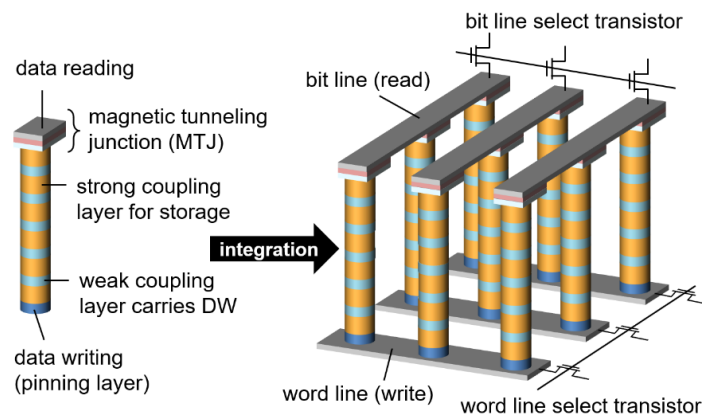


Figure 1. A vertical domain wall motion memory cell and integrated high-density storage arrays.

[1] Y. Hung et al., J. Magn. Soc. Jpn., **45**, 6 (2020). [2] Y. Hung et al., Appl. Phys. Express, **14**, 023001 (2021).

GdFe 磁性細線における電流駆動磁壁の磁気光学検出系の構築

Construction of MO detection for current-driven domain walls in GdFe magwires

豊田工業大学 [○](M2)鈴木 紀行, Mojtaba Mohammadi, 鷲見 聡, 田辺 賢士, 栗野 博之Toyota Technological Institute, [○]N. Suzuki, M. Mohammadi, S. Sumi, K. Tanabe, H. Awano

E-mail: sd23425@toyota-ti.ac.jp

磁性細線を用いたレーストラックメモリは超省電力かつ高速動作可能な次世代記録媒体として盛んに研究されている[1]. しかし, 研究報告のほとんどは電流による磁壁駆動に関するもので, その動的な記録磁区の検出報告は少ない. そこで, リアルタイムに動的な磁区の動きを観察可能な磁気光学 (MO) 効果検出に取り組んでいる. 昨年の国際会議 (MMM2023) において検出器にアバランシェフォトダイオード (APD) を用いて磁壁移動をリアルタイム観測した結果が 500 m/sec であることを報告した[2]. これは偏光顕微鏡で観察した磁壁移動距離から算出した磁壁移動速度と一致していた. しかし, この APD の帯域は 800 MHz と狭い. そこで, 信号は小さくなるが帯域が 10 GHz と広い差動検出システムを立ち上げることにした.

Figure 1 に MO 差動検出システムを示す. MO 信号検出には波長 780 nm のレーザを用い, 記録膜構造は Pt(5 nm)/GdFe(20 nm)/SiN(10 nm)である. Figure 2 には細線幅 3 μm の細線中央に 1 MHz の連続パルス光を照射したときの MO 信号の測定結果を示す. 2 つのフォトダイオードの差動検出にはデジタルオシロの引き算機能を用いた. その結果, レーザの変調に同期した MO 信号が得られた. 更に差動アンプを用いれば信号を改善できると考えられる. また MO 信号の細線幅依存性を Figure 3 に示す. 細線幅 2 μm まで信号強度が一定で, 細線幅 1 μm になると低下している. これはレーザスポットのエアリー直径が 1.9 μm であることに起因していると考えられ, 今後高速駆動磁壁のリアルタイム測定を行う予定である.

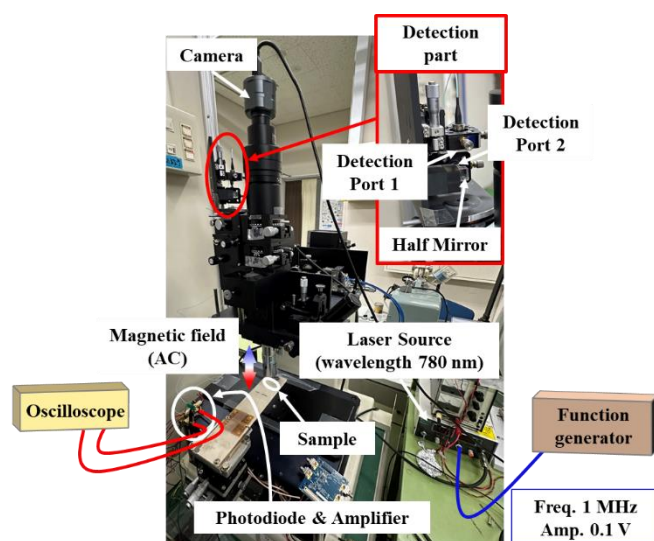


Figure 1 MO differential detection system.

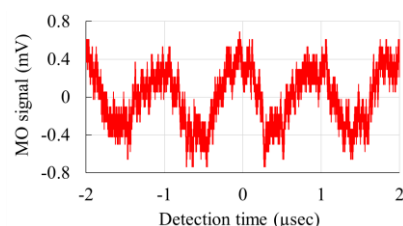
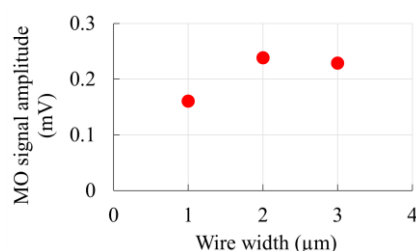
Figure 2 Detected MO signal in the wire of 3 μm width.

Figure 3 Dependence of MO signal amplitude on wire width.

[1] Caretta et al., Nature Nanotechnology **13**, 1154 (2018).

[2] N. Suzuki et al., The 68th Annual Conference on Magnetism and Magnetic Materials SP-05, 2023.

GdFe 磁性細線メモリにおける磁界記録磁壁と光磁気記録磁壁の 電流駆動速度比較

Comparison of current-driven DW velocity of GdFe wire between magnetic field recording and
magneto-optical recording

豊田工業大学, [○](M2)和井内零理, M. Mohammadi, 鷲見聡, 田辺賢士, 栗野博之,

Toyota Tech Inst., K. Wainai, M. Mohammadi, S. Sumi, K. Tanabe and H. Awano

E-mail: sd22442@tti-j.net

低消費電力で不揮発な、磁性細線メモリはデータ記録速度の大幅な向上を期待されている。これまでに磁性細線メモリを実現するため、細線形状[1]や細線端部の磁気異方性エネルギー変調[2]の観点から、磁壁(DW)駆動の高速化に成功した成果が報告されている。磁性細線メモリにデータを書き込む代表的な方法は、電流から発生する磁界を利用する方法である。この方法では、電流を流すための複雑な配線が必要となる。一方、レーザ光の熱を照射してデータを記録できれば、配線不要なためより単純な構成で済む。そこで、レーザを利用した磁区形成と磁壁駆動を行った。

まず、Pt(5 nm)/Gd₂₅Fe₇₅(20 nm)/SiN(10 nm)を積層した構造で幅 1 μm の細線に、レーザを照射し、熱磁化反転によって磁壁（光磁気記録磁壁）を形成した。また、外部磁場を調整することで、レーザを用いずに磁壁（磁界記録磁壁）を形成した。次に、細線にパルス電流を印加し、磁壁駆動速度を測定した。結果を Fig. 2 に示す。Fig. 2 より、光磁気記録磁壁の速度が最も速いことがわかる。Fig. 1 に示すように、光磁気記録による磁壁形成は一度磁壁エネルギーが下がることで磁壁のスピンの向きが揃いやすくなり、外部磁界で形成した磁壁よりも電流駆動しやすくなったと考えることができる。

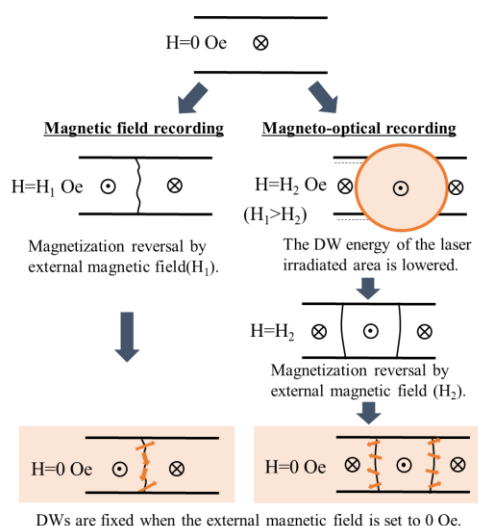


Fig. 1 Formation process of two types of DWs.

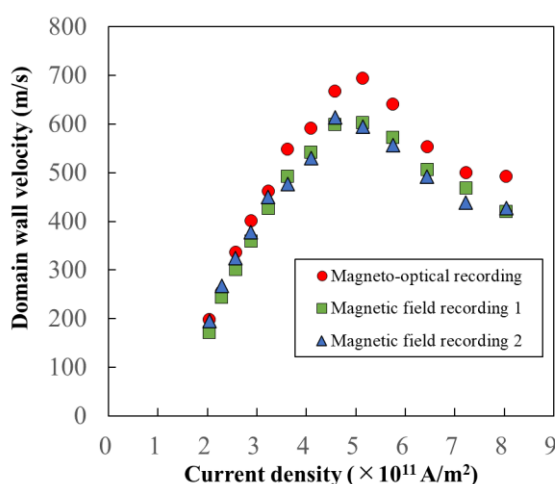


Fig. 2 Comparison of DW velocity between two types of DWs. Magnetic field recording 1 is an isolated magnetic domain. Magnetic field recording 2 is a non-isolated magnetic domain.

[1] S. Ranjbar et al., Materials Advances 3, 7028-7036 (2022).

[2] M. Mohammadi et al., Applied Physics Letters, 123, 202403 (2023)

Effect of Pulse Duration on Domain Wall Motion in Ferrimagnetic GdFe Nanowires

Mojtaba Mohammadi*, Satoshi Sumi, Kenji Tanabe, and Hiroyuki Awano

Spintronics Laboratory, Toyota Technological Institute, Nagoya, Japan

*E-mail: mojtaba_mohammadi@toyota-ti.ac.jp

The advancement of low-energy memory devices necessitates the exploration of novel materials and fabrication techniques [1,2]. Here, we report on the fabrication and characterization of nanowires composed of ferrimagnetic GdFe thin films, deposited on a naturally oxidized Pt sublayer, and with a SiN protective layer. Utilizing electron-beam lithography and a lift-off method, we successfully fabricated nanowires with a width of $1\mu\text{m}$. The primary focus of this study was to investigate the domain wall motion (DWM) within these nanowires under the application of voltage pulses of varying durations (1, 3, 5, 10, 20, and 30 ns). Our measurements revealed that the maximum DW velocity of around 1800 m/s was achieved with a 1 ns pulse duration. This high velocity is attributed to the effective spin-orbit torque (SOT) induced by the Pt under-layer, which enhances the efficiency of current-driven DWM. Notably, the current threshold for initiating DWM was approximately $7 \times 10^{10} \text{ A/m}^2$. The presence of the Pt under-layer is crucial in achieving this low current threshold, as it promotes a strong spin Hall effect, thereby increasing the spin current density and reducing the required charge current. Interestingly, our results demonstrated that while DW velocity generally increases with current density, a deviation occurs for pulse durations of 20 ns and 30 ns. In these cases, the DW velocity increases with current density up to a maximum point, beyond which further increases in current density result in a decrease in velocity. This phenomenon may be attributed to the onset of the Joule heating effect [3] that impedes DWM at higher current densities over longer pulse durations. The results of this study demonstrate the feasibility of using ferrimagnetic GdFe nanowires, coupled with a Pt under-layer, for high-speed, low-energy memory applications.

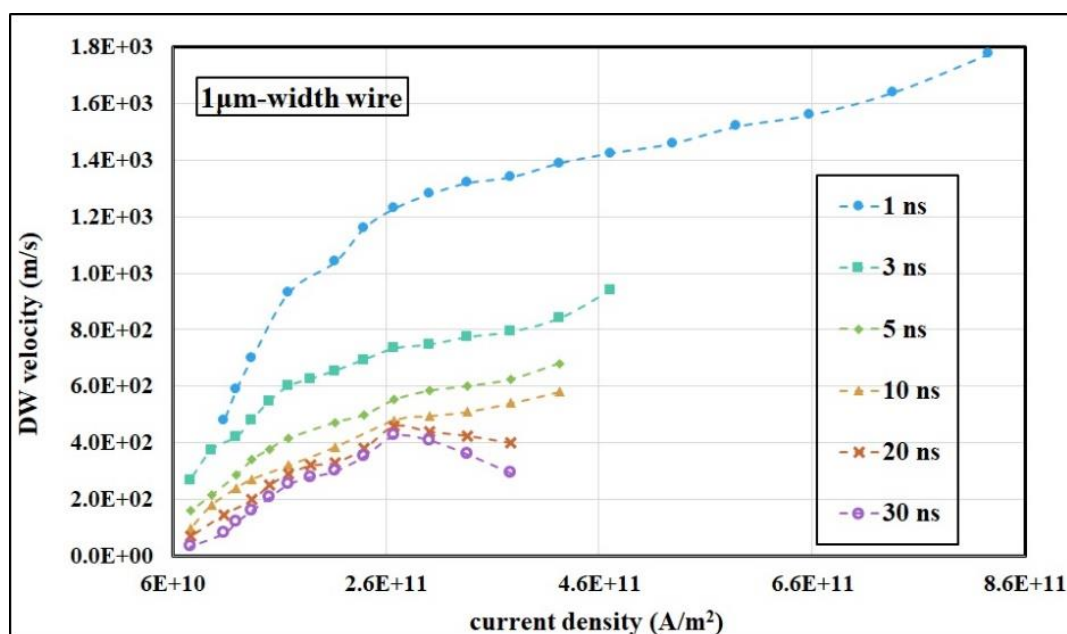


Fig. 1. DW velocity vs. current density for a wire with $1\mu\text{m}$ width and under pulse durations of 1, 3, 5, 10, 20, and 30 ns.

Acknowledgment: This research was partially funded by the research center for smart photons and materials of Toyota Technological Institute.

References: [1] S. S. Kim, *et al.*, Nat. Mater., **21** (2022) 24. [2] K. Cai, *et al.*, Nat. Electron., **3** (2020) 37. [3] S. Ranjbar, *et al.*, Mater. Adv. **3** (2022) 7028.

3次元デバイスを目指した凹凸構造側面部への垂直磁化膜の作製

Fabrication of perpendicular magnetic anisotropic films on the side of uneven structures toward 3-dimensional devices

豊田工大¹, 九大², [○](M1)安田優也¹, 黒川雄一郎², 鷲見聡¹, 栗野博之¹, 田辺賢士¹

Toyota Tech Inst.¹, Kyushu Univ.², Y. Yasuda¹, Y. Kurokawa², S. Sumi¹, H. Awano¹ and K. Tanabe¹

E-mail: sd24448@tti-j.net

近年、スピントロニクス分野では3次元ナノ磁石[1]や3次元磁気メモリデバイス[2]、3次元マグノニックデバイス[3]の研究に注目が集まっている。特に磁壁駆動型メモリであるレーストラックメモリはParkinらが2008年に提案した当初から、3次元構造が示唆されてきた[4]。レーストラックメモリは、不揮発性(待機電力ゼロ)、高速動作、高安定性かつ安価なメモリとして期待されており、3次元化によってさらに超高密度化というアドバンテージも有することになる。しかし、3次元レーストラックを実現するためには、3次元の構造物の側面部分にも垂直磁化膜を作製する必要がある。そこで我々は、ナノインプリント法を用いて基板の凹凸構造側面部への垂直磁化膜の作製に成功したのでここで報告する。

マグネトロンスパッタ装置を用いて、Pt(5 nm)/Tb₁₈Co₇₂(40 nm)/Pt(5 nm)の多層膜を、平坦なプラスチック基板(日本ゼオン zeonorfilm)上に成膜した。その後、ナノインプリント法を用いて、薄膜ごと基板表面に凹凸構造を作製した。凹凸構造はFig. 1のような、5 μm の周期で凹部と凸部があり、高さは5 μm である。参照試料として、先にプラスチック基板表面に凹凸構造を作製し、その上から薄膜を成膜した試料も同時に作製した。磁化測定には磁場勾配型磁力計を用いた。基板の凹凸構造の側面に対して垂直方向(面内方向)に磁場を印加した(Fig. 2)。ゼロ磁場近傍に注目すると、ヒステリシスが開いており、2.5 kOe程度の保持力が存在する。このことは、側面部分の磁化膜が側面に対し垂直方向に磁化していることを意味している。一方、参照試料ではこのような大きな保磁力は確認できなかった(Fig. 2)。加工プロセスに依存して、垂直磁化膜の作製が可能になることを示している。

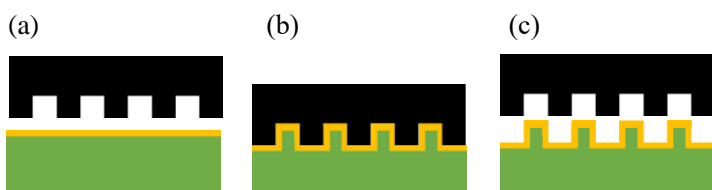


Fig. 1 Sample fabrication procedure for nanoimprinting

- (a) Prepare a sample and a mold
- (b) Crimp the sample and the mold
- (c) Transfer the mold structure to the sample

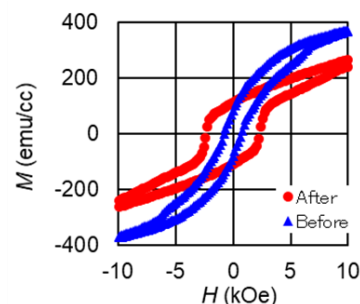


Fig. 2 M - H curves and schematic of magnetization directions. Red circle and blue triangle indicate the samples nanoimprinted after and before sputtering, respectively.

[1] A. Fernández-Pacheco et al., Nature Communications **8**, 15756 (2017).

[2] R. Lavrijsen et al., Nature **493**, 647 (2013).

[3] G. Gubbiotti, *Three-Dimensional Magnonics*, Jenny Stanford Publishing (2019).

[4] S. S. P. Parkin et al., Science **320**, 190 (2008).

10 スピントロニクス・マグネティクス | 一般セッション(口頭講演) : 10.1 新物質・新機能創成 (作製・評価技術)

[20a-D61-1~9] 10.1 新物質・新機能創成 (作製・評価技術)

[20a-D61-1]

Room-temperature flexible manipulation of the quantum-metric structure in a topological chiral antiferromagnet

○Jiahao Han^{1,2}, Tomohiro Uchimura^{1,3}, Yasufumi Araki⁴, Ju-Young Yoon^{1,3}, Yutaro Takeuchi², Yuta Yamane^{1,5}, Shun Kanai^{1,2,3,6,7,8,9}, Junichi Ieda⁴, Hideo Ohno^{1,2,3,8,10}, Shunsuke Fukami^{1,2,3,8,11} (1.RIEC, Tohoku Univ., 2.AIMR, Tohoku Univ., 3.Eng., Tohoku Univ., 4.ASRC, JAEA, 5.FRIS, Tohoku Univ., 6.PRESTO, JST., 7.DEFS, Tohoku Univ., 8.CSIS, Tohoku Univ., 9.QST, 10.CIES, Tohoku Univ., 11.InaRIS)

[20a-D61-2]

Magnetic Phase Diagram of Non-Collinear Antiferromagnet $\text{Mn}_{3+x}\text{Sn}_{1-x}$ Thin Films

○Katarzyna Gas^{1,2}, Ju-Young Yoon^{3,4}, Yuma Sato^{3,4}, Hiroki Kubota^{3,4}, Jaroslaw Z. Domagala², Piotr Dluzewski², Yadhu K. Edathumkandy², Yutaro Takeuchi^{3,5,6}, Shun Kanai^{1,3,4,5,7,8,9}, Hideo Ohno^{1,3,5,10}, Maciej Sawicki^{2,3}, Shunsuke Fukami^{1,3,4,5,10} (1.CSIS, Tohoku Univ., 2.Institute of Physics PAS, 3.Laboratory for Nanoelectronics and Spintronics, RIEC, Tohoku Univ., 4.Graduate School of Engineering, Tohoku Univ., 5.WPI-AIMR, Tohoku Univ., 6.ICYS, NIMS, 7.PRESTO, JST, 8.DEFS, Tohoku Univ., 9.NIQST, 10.CIES, Tohoku Univ)

[20a-D61-3]

Improved magnetic properties in CoFeB/MgFeO multilayers with Fe segregated interfaces

○Tomohiro Ichinose¹, Tatsuya Yamamoto¹, Takayuki Nozaki¹, Kay Yakushiji¹, Shingo Tamaru¹, Shinji Yuasa¹ (1.AIST)

[20a-D61-4]

Characterization of spin polarization in ordered Co-based full Heusler $\text{Co}_2\text{FeAl}_{0.33}\text{Si}_{0.67}$ alloy thin films using nano-contact Andreev reflection technique

○(M2)Syunki Kameoka¹, Togo Miyake¹, Jin Ow¹, Yota Takamura¹, Shigeki Nakagawa¹ (1.Tokyo Tech.)

[20a-D61-5]

Large Magnetoresistance and High Spin-Transfer Torque Efficiency of $\text{Co}_2\text{Mn}_x\text{Fe}_{1-x}\text{Ge}$ ($0 \leq x \leq 1$) Heusler Alloy Thin Films Obtained by High-Throughput Compositional Optimization Using Combinatorially Sputtered Composition-Gradient Film

○(PC)Vineet Barwal¹, Hirofumi Suto¹, Ryo Toyama¹, Taisuke Sasaki¹, Yuya Sakuraba¹ (1.NIMS)

[20a-D61-6]

Positive and negative anomalous Nernst coefficients in 2-dimensional layered MnAlGe thin films with large magnetic anisotropy

○(P)Nanhe Kumar Gupta¹, Ryo TOYAMA¹, Benugopal BAIRAGYA¹, Keisuke MASUDA¹, Yuya SAKURABA¹ (1.Research Center for Magnetic and Spintronic Materials, National Institute for Materials Science)

[20a-D61-7]

Direct-Contact Seebeck-Driven Transverse Magneto-Thermoelectric Generation in Magnetic / Thermoelectric Bilayers

○Weinan Zhou¹, Taisuke Sasaki¹, Ken-ichi Uchida¹, Yuya Sakuraba¹ (1.NIMS)

[20a-D61-8]

Anomalous Nernst effect and magnetic structures of Pd/Co multilayers

○(M2)Hayato Kudo¹, Yasuo Takeichi², Shohei Yamashita³, Bowen Qiang¹, Toshio Miyamachi¹, Kanta Ono², Masaki Mizuguchi¹ (1.Nagoya Univ., 2.Osaka Univ., 3.KEK-IMSS)

[20a-D61-9]

Observation of the giant anomalous Nernst effect in the Weyl ferromagnet Co₂MnGa polycrystalline films

○(P)Ryota Uesugi^{1,2}, Tomoya Higo^{1,2,3}, Satoru Nakatsuji^{1,2,3,4,5} (1.Dep. of Phys., Univ. of Tokyo, 2.ISSP, Univ. of Tokyo, 3.CREST, JST, 4.TSQS, Univ. of Tokyo, 5.IQM, JHU)

Room-temperature flexible manipulation of the quantum-metric structure in a topological chiral antiferromagnet

Jiahao Han^{1,2*}, Tomohiro Uchimura^{1,3}, Yasufumi Araki⁴, Ju-Young Yoon^{1,3}, Yutaro Takeuchi², Yuta Yamane^{1,5}, Shun Kanai^{1,2,3,6,7,8,9}, Jun'ichi Ieda⁴, Hideo Ohno^{1,2,3,8,10} & Shunsuke Fukami^{1,2,3,8,10,11}

¹RIEC, Tohoku Univ. ²AIMR, Tohoku Univ. ³Grad School of Eng., Tohoku Univ. ⁴ASRC, JAEA. ⁵FRIS, Tohoku Univ. ⁶PRESTO, JST. ⁷DEFS, Tohoku Univ. ⁸CSIS, Tohoku Univ. ⁹QST. ¹⁰CIES, Tohoku Univ. ¹¹InaRIS. *Presenter email: jiahao.han.c8@tohoku.ac.jp

The quantum metric and Berry curvature are two fundamental and distinct factors that describe the geometry of quantum eigenstates. While the role of the Berry curvature in governing various condensed-matter states has been investigated extensively [1,2], the quantum metric, which was also predicted to induce topological phenomena of equal importance [3], has rarely been studied. Recently, a breakthrough has been made in observing the quantum-metric nonlinear transport in a van der Waals magnet [4,5], but the effect is limited at cryogenic temperature and is tuned by strong magnetic fields of several teslas. In our study [6], we demonstrate room-temperature manipulation of the quantum-metric structure of electronic states through its interplay with the interfacial spin texture in a topological chiral antiferromagnet/heavy metal $\text{Mn}_3\text{Sn}/\text{Pt}$ heterostructure (Fig. 1a), which is manifested in a time-reversal-odd second-order Hall effect (ScHE) (Figs. 1b and 1c). We show the flexibility of controlling the quantum-metric structure with moderate magnetic fields and verify the quantum-metric origin of the observed ScHE by theoretical modeling (Fig. 1c). Our results open the possibility of building applicable nonlinear devices by harnessing the quantum-metric structure of electronic states.

A portion of this work is supported by JSPS Kakenhi Grant Nos. 19H05622, 22K03538, and 22KF0035, MEXT Initiative to Establish Next-Generation Novel Integrated Circuits Centers (X-NICS) Grant No. JPJ011438, and Casio Science and Technology Foundation Grant No. 40-4.

[1] D. Xiao, et al. *Rev. Mod. Phys.* **82**, 1959 (2010). [2] L. Šmejkal, et al. *Nat. Phys.* **14**, 242 (2018). [3] Y. Gao, et al. *Phys. Rev. Lett.* **112**, 166601 (2014). [4] A. Gao, et al. *Science* **381**, 181 (2023). [5] N. Wang, et al. *Nature* **621**, 487 (2023). [6] J. Han, et al. *Nat. Phys.* <https://doi.org/10.1038/s41567-024-02476-2> (2024).

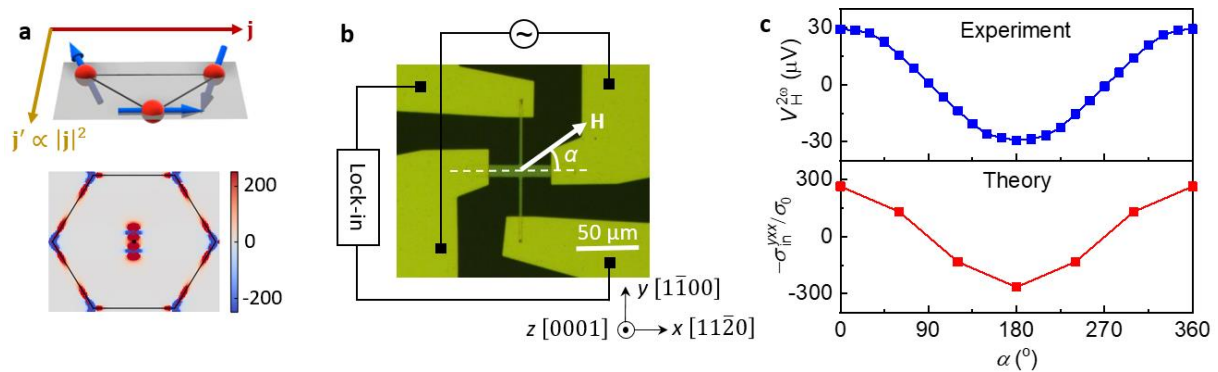


Fig. 1. **a**, Chiral-spin structure with out-of-plane canting in $\text{Mn}_3\text{Sn}/\text{Pt}$ (upper panel), which leads to specific quantum-metric structure (lower panel) as the origin of the ScHE, that is, the Hall current \mathbf{j}' is quadratic to the applied current \mathbf{j} . **b**, Device connected to an alternating current source and a lock-in amplifier to measure the second-harmonic Hall signal to probe the ScHE. A magnetic field \mathbf{H} that can rotate in the sample plane is applied. **c**, Experimental and theoretical ScHE as a function of the applied magnetic field angle. The field strength is fixed at 0.4 T.

Magnetic Phase Diagram of Non-Collinear Antiferromagnet $\text{Mn}_{3+x}\text{Sn}_{1-x}$ Thin Films

°K. Gas^{1,2}, J.-Y. Yoon^{3,4}, Y. Sato^{3,4}, H. Kubota^{3,4}, J. Z. Domagala², P. Dłużewski²,

Y. K. Edathumkandy², Y. Takeuchi^{3,5,6}, S. Kanai^{1,3,4,5,7,8,9}, H. Ohno^{1,3,5,10},

M. Sawicki^{2,3}, and S. Fukami^{1,3,4,5,10}

¹ CSIS, Tohoku Univ., ² Institute of Physics PAS, ³ Laboratory for Nanoelectronics and Spintronics,

RIEC, Tohoku Univ., ⁴ Graduate School of Engineering, Tohoku Univ., ⁵ WPI-AIMR, Tohoku

Univ., ⁶ ICYS, NIMS, ⁷ PRESTO, JST, ⁸ DEFS, Tohoku Univ., ⁹ NIQST, ¹⁰ CIES, Tohoku Univ.

E-mail: gas.katarzyna.a2@tohoku.ac.jp

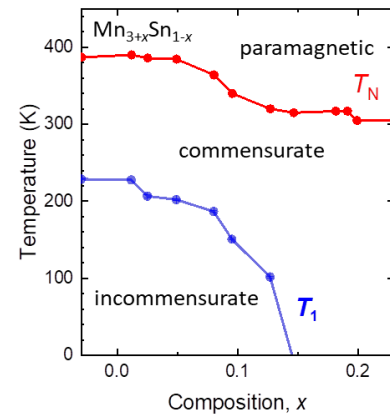
Non-collinear antiferromagnetic $D0_{19}\text{-Mn}_{3+x}\text{Sn}_{1-x}$ exhibits various intriguing properties akin to ferromagnets, such as a large anomalous Hall effect (AHE) arising from the Berry curvature associated with Weyl points [1]. Since its properties are expected to significantly change with the Mn content x through the position of the Fermi level [2] as well as other factors [3,4], the development of systematic knowledge on the role of x in $\text{Mn}_{3+x}\text{Sn}_{1-x}$ on its physical properties is timely and important.

We comprehensively study structural (XRD, TEM), magnetic, and magnetotransport (AHE) [with different temperatures (4 – 400 K)] properties of m -plane-oriented epitaxial $\text{Mn}_{3+x}\text{Sn}_{1-x}$ ($-0.03 \leq x \leq +0.23$) thin layers deposited by magnetron sputtering [5]. This effort allows us, for example, to construct x -dependent magnetic phase diagram (Figure), in which the most profound feature is the disappearance of the transition (at temperature T_1) between an anti-chiral commensurate phase (inverse triangular antiferromagnetic order) to a non-coplanar modulated incommensurate phase [6] for $x \geq +0.15$. This indicates that the inverse triangular antiferromagnetic order exhibiting large AHE can be stabilized down to the liquid He temperatures in thin layers of Mn-rich $\text{Mn}_{3+x}\text{Sn}_{1-x}$. We also find that the Néel temperature (T_N) depends on the Mn composition and correlates with the simultaneous change in the lattice parameter. Our work broadens the understanding of the correlation between the structural and magnetic characteristics of Mn_3Sn thin films towards developing novel devices.

Acknowledgments: This study has been partly supported by TUMUG Support Program from Center for Diversity, Equity, and Inclusion, Tohoku University, and by JSPS Kakenhi 19H05622, 21J23061, 24KJ0432, and 24H00039.

Acknowledgments: This study has been partly supported by TUMUG Support Program from Center for Diversity, Equity, and Inclusion, Tohoku University, and by JSPS Kakenhi 19H05622, 21J23061, 24KJ0432, and 24H00039.

[1] S. Nakatsuji *et al.*, Nature, **527**, 212 (2015). [2] K. Kuroda *et al.*, Nat. Mater., **16**, 1090 (2017). [3] J.-Y. Yoon *et al.*, AIP Advances 11, 065318 (2021). [4] T. Uchimura *et al.*, Appl. Phys. Lett. 120, 172405 (2022). [5] J.-Y. Yoon *et al.*, Appl. Phys. Express, **13**, 013001 (2020). [6] Y. Chen *et al.*, arXiv:2306.07822v3



Improved magnetic properties in CoFeB/MgFeO multilayers with Fe segregated interfaces

AIST¹, [○]Tomohiro Ichinose¹, Tatsuya Yamamoto¹, Takayuki Nozaki¹, Kay Yakushiji¹, Shingo Tamaru¹, Shinji Yuasa¹

E-mail: tomohiro.ichinose@aist.go.jp

Introduction Large perpendicular magnetic anisotropy (PMA) and low magnetic damping (α) in CoFeB/MgO junctions are necessary for magnetoresistive random-access memory applications to realize a long data retention time and low writing energy. Since the PMA and α are sensitive to quality of the CoFeB/MgO interface, various approaches have been attempted to modify the CoFeB/MgO interface. An interesting example is the use of MgFeO instead of MgO; it has been revealed that Fe atoms in the MgFeO layer segregated at the CoFeB/MgFeO interface after annealing. [1] Although the segregated Fe may play a key role on the PMA observed in CoFeB/MgFeO, the chemical and magnetic properties of the segregated Fe remain undefined. In this work, we investigated the properties of Fe segregated from MgFeO and its influence on magnetic properties of CoFeB/MgFeO. [2]

Experiments Co₄₀Fe₄₀B₂₀(*t*_{CoFeB})/MgO(*t*_{MgO})/Mg₄₀Fe₁₀O₅₀(*t*_{MgFeO}) multilayers were deposited by sputtering on Si/SiO₂ wafers with buffer layers. The multilayers were annealed at 300 – 400°C in a vacuum furnace. X-ray photoelectron spectroscopy (XPS) measurements were conducted to evaluate the chemical states of Fe in the multilayers. Magnetic properties of the multilayers were measured with vibrating sample magnetometry and vector network analyzer ferromagnetic resonance.

Results Figure 1 shows Fe-2*p* XPS profiles taken from the multilayer annealed at 300°C. As had been expected, the Fe-2*p* XPS profiles showed that Fe atoms in the CoFeB layer were metallic whereas the MgFeO layer consisted of FeO. In contrast, XPS profiles taken from the MgFeO/Ru interface exhibited peaks corresponding to metallic Fe, which revealed that FeO in the MgFeO layer was reduced to metallic Fe associated with interfacial segregation. As for the magnetic properties, the CoFeB/MgFeO based multilayers exhibited 1.2 times larger PMA compared with CoFeB/MgO multilayers. We also report clear reduction of α in the CoFeB/MgFeO multilayers.

Acknowledgements This presentation was partly based on results obtained from a project, JPNP16007, subsidized by the New Energy and Industrial Technology Development Organization (NEDO).

References [1] K. Yakushiji *et al.*, AIP Adv. **8**, 055905 (2018). [2] T. Ichinose *et al.*, APEX **16**, 113002 (2023).

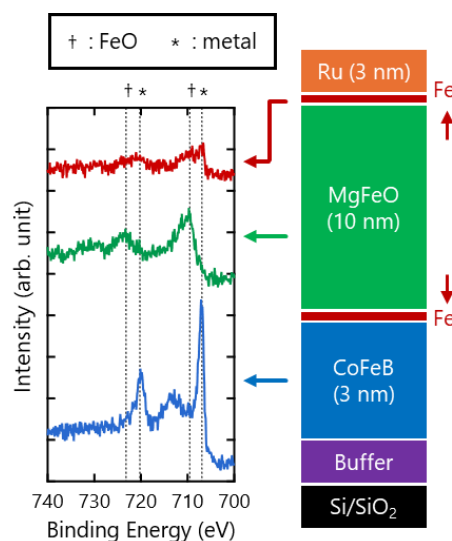


Fig. 1 XPS spectra in CoFeB/MgFeO

ナノコンタクトアンドレーエフ反射を用いた規則相 Co 基フルホイスラ ー合金 $\text{Co}_2\text{FeAl}_{0.33}\text{Si}_{0.67}$ のスピン分極率評価

Characterization of spin polarization in ordered Co-based full Heusler $\text{Co}_2\text{FeAl}_{0.33}\text{Si}_{0.67}$ alloy thin films using nano-contact Andreev reflection technique

東工大¹, [○](M2) 亀岡 俊貴¹, 三宅 玄梧¹, 歐 晋¹, 高村 陽太¹, 中川 茂樹¹

Tokyo Tech¹, [°]S. Kameoka¹, T. Miyake¹, J. Ow¹, Y. Takamura¹, and S. Nakagawa¹

E-mail: kameoka.s.aa@m.titech.ac.jp

The performance of spintronics devices such as magnetoresistive random access memory and highly sensitive sensor, requires the use of ferromagnetic materials with a high spin polarization ratio. The half-metallic nature of Co-based full Heusler $\text{Co}_2\text{FeAl}_{0.33}\text{Si}_{0.67}$ (CFAS) alloys is promising for such devices. The spin polarization of Co-based full Heusler alloys depends on the atomic order in the ordered structures characterized by degree of order^[1] and thus both measurement for the same films is necessary to develop highly spin polarized full-Heusler alloy films. Spin polarization can be accurately measured using nano-contacts Andreev reflection (NCAR) technique^[2] because, the cleanliness contact interface between ferromagnets and superconductors can be kept. In this study, we fabricate nano-contacts junction of CFAS and superconductor Nb by microfabrication, and measured spin polarization of the B2-phase CFAS thin film by NCAR technique.

The $\text{Co}_2\text{FeAl}_{0.33}\text{Si}_{0.67}$ /Nb junctions was fabricated from a structure of MgO(001) substrate/CFAS(70 nm)/Nb(70 nm)/Cr(25 nm)/W(120 nm)/Cr(25 nm), which is formed using a facing target sputtering system. The CFAS layer was deposited at a substrate temperature of 400°C to form the B2 structure. The degree of B2 order was approximately 100%. Figure 1 shows the device structure and measurement configuration. The device was patterned into a 50 nm diameter of pillar using electron beam lithography technique to increase the junction resistance of the CFAS/Nb interface. Additionally, the pillar was headed by etch-back Benzocyclobutene insulating layer by reactive-ion etching to ensure sufficient contact between the pillar and electrodes. The differential conductance dI/dV of the device was measured with lock-in amplifier at 4.2 K in LHe. Figure 2 shows normalized dI/dV as a function of voltage applied to the sample. The residual and parasitic resistances were numerically subtracted. The obtained curve was fitted by an improved Blonder-Tinkham-Klapwijk (BTK) model^[3] to evaluate the spin polarization P . From fitting the spin polarization was determined to be $P = 0.54$ with $\Delta = 3.00$ meV, $Z = 0.15$.

Acknowledgements: We thank ARIM at Tokyo Institute of Technology for help microfabrication system.

Refs: 1. Y. Takamura et al., J. Appl. Phys. **105**, 07B109 (2009). 2. I. Shigeta et al., Appl. Phys. Lett. **112**, 072402 (2018). 3. G. J. Strikers et al., Phys. Rev. B **63**, 104510 (2001).

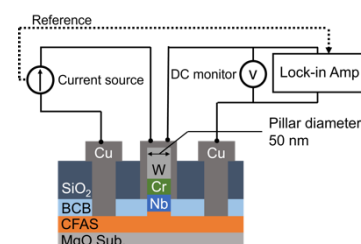


Fig. 1 Device structure and measurement configuration

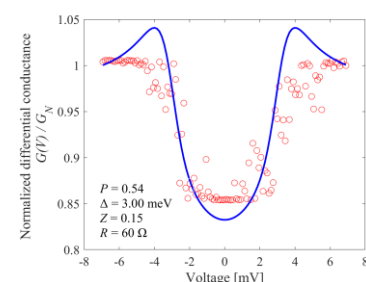


Fig. 2 Normalized differential conductance dI/dV of CFAS/Nb interface at 4.2 K



Large Magnetoresistance and High Spin-Transfer Torque Efficiency of $\text{Co}_2\text{Mn}_x\text{Fe}_{1-x}\text{Ge}$ ($0 \leq x \leq 1$) Heusler Alloy Thin Films Obtained by High-Throughput Compositional Optimization Using Combinatorially Sputtered Composition-Gradient Film

Vineet Barwal, Hirofumi Suto, Ryo Toyama, Taisuke Sasaki and Yuya Sakuraba

Research Center for Magnetic and Spintronic Materials,

National Institute for Materials Science (NIMS), Tsukuba, 305-0047, Japan

E-mail: BARWAL.Vineet@nims.go.jp

Half-metallic ferromagnetic Heusler alloys having high spin polarization have been studied for their potential spintronic applications [1,2]. For certain applications such as current-perpendicular-to-plane giant magnetoresistance (CPP-GMR) read heads, achieving low process temperature, typically below 350°C , is crucial. Moreover, composition tuning is known to be an important factor to enhance the magnetic properties of the Heusler systems, and we developed an experimental method for detailed high-throughput composition optimization using combinatorially sputtered composition-gradient film [3]. In this study, we apply the developed method to $\text{Co}_2\text{Mn}_x\text{Fe}_{1-x}\text{Ge}$ ($0 \leq x \leq 1$) and report high-performance CPP-GMR properties obtained at lower process temperature. Figure (a) shows the deposition process of the composition-gradient thin film. The CPP-GMR stacks shown in Fig. (b), containing composition-gradient $\text{Co}_2\text{Mn}_x\text{Fe}_{1-x}\text{Ge}$ were deposited and processed at different post-annealing (PA) temperatures. Figure (c) shows the position dependence of the atomic concentration in the $\text{Co}_2\text{Mn}_x\text{Fe}_{1-x}\text{Ge}$ film. The XRD measurement revealed the epitaxial and largely single-phase structure throughout the composition range and improved atomic ordering with annealing temperature. The change in MR ratio with Mn content for the stacks annealed at different temperatures is shown in Fig. (d). In the as-deposited sample, the MR ratio exhibited gradual change with Mn content. The CFG side showed lower MR ratio $\sim 2.5\%$ and the CMG side showed slightly higher MR ratio $\sim 5\%$. In the 250°C PA sample, the MR was greatly enhanced and exhibited the following clear composition dependence. The MR ratio was $\sim 22\%$ at $x = 0$, increased gradually with increasing x , and showed a maximum MR ratio of $\sim 35\%$ at around $x = 0.85$. Then it decreased to the CMG side. In the 350°C PA sample, MR was further enhanced with maximum MR ratio of $\sim 45\%$ in the broad x range. The trend of MR ratio versus x changed from the case of 250°C PA sample. First, it increased in the x range of $0-0.2$, stayed almost constant in broad x range of $0.2-0.7$, and then abruptly decreased near the CMG side. The optimal composition for the highest MR changed with annealing temperature because of the stability of the GMR stack being higher in the lower x range. We achieved record high MR for the CPP-GMR devices at relatively low annealing temperature of 250°C by the present composition optimization method. The results provide comprehensive guidance on the composition optimization to obtain large MR ratio and high STT efficiency in the CPP-GMR devices employing $\text{Co}_2\text{Mn}_x\text{Fe}_{1-x}\text{Ge}$ at relatively low process temperature. In the presentation, the results related to high STT efficiency will also be discussed. The authors acknowledge the support from Advanced Storage Research Consortium (ASRC) and JST CREST Grant No. JPMJCR21O1.

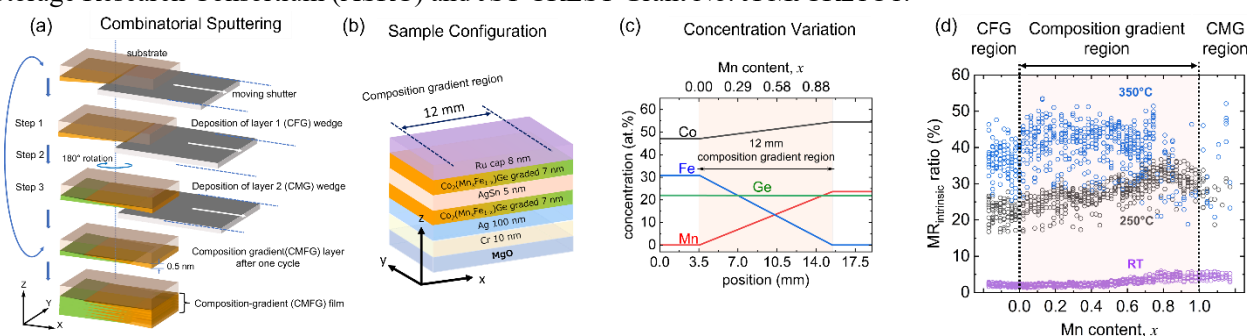


Figure: (a) Schematic showing the Combinatorial sputtering process. (b) Configuration for the CPP-GMR stack. Post-annealing was done after the deposition of the upper $\text{Co}_2\text{Mn}_x\text{Fe}_{1-x}\text{Ge}$ layer. (c) Variation of atomic concentration in $\text{Co}_2\text{Mn}_x\text{Fe}_{1-x}\text{Ge}$ composition-gradient film. (d) Change in intrinsic MR ratio with Mn content for the CPP-GMR stack with different annealing temperatures.

References

- [1] T. Nakatani, Z. Gao, and K. Hono, MRS Bull. **43**, 106 (2018).
- [2] T. Kubota, Z. Wen, and K. Takamashi, J. Magn. Mater. **492**, 165667 (2019).
- [3] V. Barwal, H. Suto, T. Taniguchi, and Y. Sakuraba, Sci. Technol. Adv. Mater. Methods **3**, 1 (2023).

Positive and negative anomalous Nernst coefficients in 2 - dimensional layered MnAlGe thin films with large magnetic anisotropy

Nanhe Kumar Gupta¹, R. Toyama¹, B. Bairagya¹, K. Masuda¹ and Y. Sakuraba¹

¹Research Center for Magnetic and Spintronic Materials, National Institute for Materials Science (NIMS),

Tsukuba, 305-0047, Japan

E-mail: GUPTA.Nanhe Kumar@nims.go.jp

Ferromagnets with remarkable transverse transport properties, low saturation magnetization (M_s), and high uniaxial magneto crystalline anisotropy constant (K_u) are attracting attention for application in thermopower devices [1]. MnAlGe is an emerging material class with various interesting properties owing to a layered topological nodal line. Reports on the temperature dependence anomalous Nernst effect (ANE) and anomalous Nernst conductivity (α_{xy}) in this class of materials are, however, very limited [2-3]. In this study, the ANE in MnAlGe film with a pseudo-two-dimensional structure consisting of Mn and Al-Ge layers was investigated over a wide temperature range (10-400 K). Using sputtering, the $\text{Mn}_{1.02}\text{Al}_{0.93}\text{Ge}_{1.04}$ films were grown epitaxially on single-crystal MgO (001) substrates. The M_s was as low as ~ 260 emu/cc and K_u was as high as ~ 6 Merg/cc. The relatively large anomalous Hall angles of ~ 0.032 (0.02) were obtained in the film at 25 (300) K, which could be attributed to layered topological nodal lines in these materials [2]. The observed anomalous Nernst coefficient (S_{ANE}) of ~ 2.0 (-0.5) $\mu\text{V/K}$ [Fig. 1(a)] and anomalous Hall conductivity (σ^A_{xy}) of 656 (138) S/cm [Fig. 1(b)] yielded α_{xy} of 4.5 (-0.17) A/(m K) at 25 (300) K [Fig. 1(b)], respectively. The sign change in S_{ANE} occurs at 125 K, which was not observed in the anomalous Hall effect of the film. We performed the first-principles calculation of α_{xy} at 300K and found α_{xy} shows the negative sign which agrees with the experimental observation.

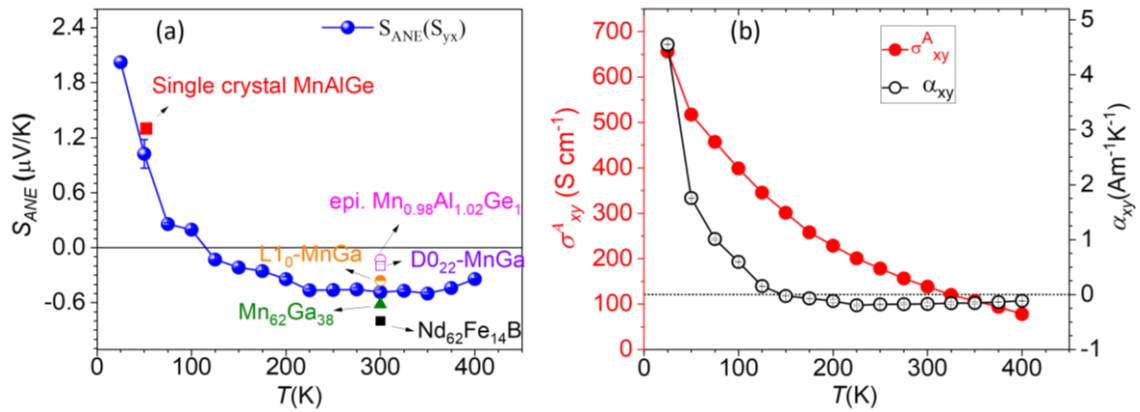


Figure: (a), (b) Temperature dependence of anomalous Nernst coefficient (S_{ANE}), anomalous Nernst conductivity (α_{xy}), anomalous Hall conductivity (σ^A_{xy}) and comparison with existing S_{ANE} values for different material in the literature [4] at 300K.

[1] K. Uchida, *et.al.* Appl. Phys. Lett. 118, 140504 (2021).

[2] S. N. Guin, *et. al.* Adv. Mater. 33,2006301 (2021).

[3] K. Ito, *et. al.* Phys. Rev. Applied 21, 054012 (2024).

[4] W. Zhou, *et.al.* Appl. Phys. Lett. 118, 152406 (2021).

Direct-Contact Seebeck-Driven Transverse Magneto-Thermoelectric Generation in Magnetic / Thermoelectric Bilayers

NIMS, °Weinan Zhou, Taisuke Sasaki, Ken-ichi Uchida, Yuya Sakuraba

E-mail: ZHOU.Weinan@nims.go.jp

Transverse thermoelectric generation can convert temperature gradient (∇T) in one direction into electric field (\mathbf{E}) perpendicular to that direction, where the anomalous Nernst effect (ANE) observed in magnetic materials is a well-known example. The orthogonal relationship between ∇T and \mathbf{E} allows the thermoelectric module to have a simple two-dimensional structure made of connecting wires on a surface, which is beneficial for better flexibility and scalability while avoiding some challenging problems facing modules based on the Seebeck effect (SE) [1]. However, the transverse thermopower of ANE is still small compared to the longitudinal thermopower of SE of thermoelectric materials, and further enhancement is strongly required for applications. Recently, significant enhancement of transverse thermopower is observed in closed circuits consisting of magnetic and thermoelectric materials, which is referred to as the Seebeck-driven transverse magneto-thermoelectric generation (STTG). The strong SE of the thermoelectric material generates a large longitudinal charge current in the magnetic material, which is then converted to the transverse direction by its anomalous Hall effect, leading to a giant transverse thermopower [2]. However, the formation of a closed circuit requires electrical connection only at the two ends along the direction of ∇T but insulation in between, which could be a complicated structure to fabricate and hinder its wide adoption. In this study, we realize STTG in the simplest way to combine magnetic and thermoelectric materials, namely, by stacking a magnetic layer and a thermoelectric layer together to form a bilayer. Different from the closed circuit used in previous studies of STTG, the magnetic and thermoelectric layers are in direct contact over the entire interface. We model the magnetic / thermoelectric bilayer and derive the expression for its transverse thermopower, which varies with changing layer thicknesses and peaks at a much larger value under an optimal thickness ratio (Fig. 1). We reproduced this behavior in the experiment. We measured the transport properties of a serial of samples, which are prepared by depositing Fe-Ga alloy thin films of various thicknesses onto n -type Si substrates. Here, the Fe-Ga film is the magnetic material, while the n -type Si is the thermoelectric material. The predicted tendency of transverse thermopower is nicely reproduced by the measured results as shown in Fig. 1. The value obtained from the sample with optimized layered structures reaches $15.2 \pm 0.4 \mu\text{V K}^{-1}$, which is a fivefold increase from that of Fe-Ga alloy and much larger than the current room temperature record observed in Weyl semimetal Co_2MnGa . Our findings highlight the potential in combining magnetic and thermoelectric materials for transverse thermoelectric applications [3].

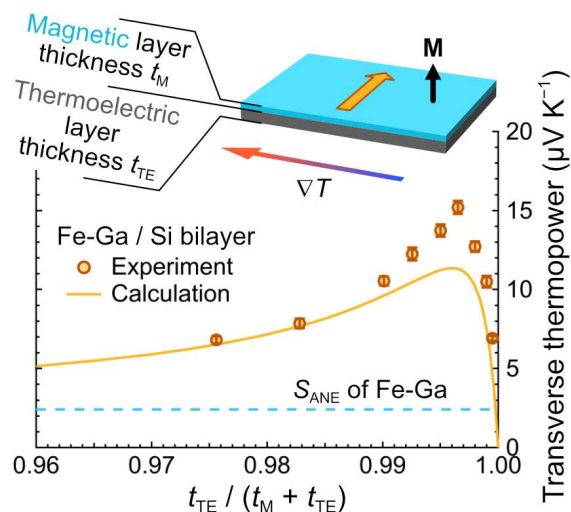


Fig. 1 Transverse thermopower of Fe-Ga / Si bilayer as a function of thickness ratio between the magnetic layer thickness (t_M) and the total thickness of bilayer ($t_M + t_{TE}$).

[1] K. Uchida *et al.*, *Appl. Phys. Lett.* **118**, 140504 (2021).

[2] W. Zhou *et al.*, *Nat. Mater.* **20**, 463 (2021).

[3] W. Zhou *et al.*, *Adv. Sci.* **11**, 2308543 (2024).

Anomalous Nernst effect and magnetic structures of Pd/Co multilayers

(M2)^oHayato Kudo¹, Yasuo Takeichi², Shohei Yamashita³,

Bowen Qiang¹, Toshio Miyamachi¹, Kanta Ono², Masaki Mizuguchi¹

Nagoya Univ.¹, Osaka Univ.², KEK-IMSS³

E-mail: mizuguchi.masaki@material.nagoya-u.ac.jp

Abstract

In recent years, the anomalous Nernst effect (ANE) has been attracting attention because of its application to a sustainable energy source. The ANE, the thermal counterpart of the AHE, is phenomenon that converts heat flow into transverse voltage in magnetic materials and therefore magnetic structures and their dynamics are thought to be greatly important. Actually, there have been many interesting reports such as observation of topological contributions to the AHE and ANE^[1] with chiral magnetic structures like magnetic skyrmions and prediction of transverse magnon-drag effect^[2]. We have presented the ANE in chiral magnetic samples and discussed their magnetic structures and the ANE. In this talk, we focus on the magnetic structure at each point in a magnetic hysteresis loop and investigate relationship between their magnetic structures and the AHE and ANE.

Experimental method

[Pd (t_{Pd} nm) / Co (0.2 nm)]₁₅ (t_{Pd} = 1.0, 1.5, 2.0, 2.5, and 3.0) films were grown onto thermally oxidized Si substrates by using magnetron sputtering at room temperature. After the growth, we applied some optional magnetic fields to films and characterized their magnetic structures by magnetic force microscopy (MFM). Then, we performed the AHE and ANE measurements by Physical Properties Measurement System (PPMS). We also conducted Scanning Transmission X-ray Microscopy (STXM) measurements for a [Pd (1.0 nm) / Co (0.2 nm)]₅₀ film grown on a SiN membrane and observed its magnetic structures.

Result

Figure 1 shows a STXM image of a [Pd (1.0 nm) / Co (0.2 nm)]₅₀ film. As shown in the figure, the film exhibits an obvious particle-like magnetic structure and this looks same as that observed by MFM. In our presentation, we will focus on the evolution of magnetic structures with magnetic field and discuss relation with the AHE and ANE.

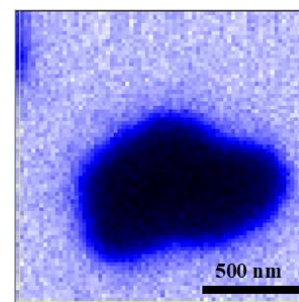


Fig 1 STXM image of [Pd (1.0 nm) / Co (0.2 nm)]₅₀ film.

Reference

- [1] Max Hirschberger *et al.*, Phys. Rev. Lett. **125**, 076602(2020).
- [2] Jun-ichiro Ohe *et al.*, Appl. Phys. Lett. **117**, 062404(2020).

Observation of the giant anomalous Nernst effect in the Weyl ferromagnet Co₂MnGa polycrystalline films

°Ryota Uesugi^{1,2}, Tomoya Higo^{1,2,3}, Satoru Nakatsuji^{1,2,3,4,5}

1. Dep. of Phys., Univ. of Tokyo, 2. ISSP, Univ. of Tokyo, 3. CREST, JST, 4. TSQS, Univ. of Tokyo, 5. IQM, Johns Hopkins Univ.

E-mail: rusg@g.ecc.u-tokyo.ac.jp

Recently, topological band structures have been extensively studied, and their unique properties have attracted attention in a wider field, especially in spintronics. In particular, magnetic Weyl materials such as Mn₃Sn and Co₂MnGa show large anomalous Nernst effect (ANE) due to the enhancement of transverse transport properties by the Berry curvature[1]. Moreover, ANE has a role as a probe of the topological band structure, which reflects the Berry curvature near the Fermi energy[2,3].

On the other hand, polycrystalline films that can be fabricated on amorphous templates should contribute to the realization of embedded and/or flexible thermoelectric devices such as heat flux sensors using ANE[4–6]. Transport properties derived from the topological band structure are resilient to disorder and impurities in the required crystal structure, and even polycrystalline samples may exhibit a large transverse response comparable to that of single crystals if the quality of each crystallite is sufficiently high. However, the largest ANE grown on an amorphous template is only ~3 μV/K for the Fe–Al thin film grown on a SiO₂/Si substrate[4]. Relatively large ANE has been observed in Co₂MnGa using a stacked structure with AlN to promote crystal growth[7], but there have been issues such as the unavailability of interfaces that are important in spintronics.

In this study, we report the largest ANE of −5.4 μV/K in Co₂MnGa film on the amorphous template of the SiO₂/Si substrate directly by successfully fabricating polycrystalline film with high-quality crystal grains using a sputtering method[8]. Establishing a thin-film fabrication technique capable of producing a giant ANE facilitates not only thermoelectric devices but also spintronic applications of the Weyl ferromagnet.

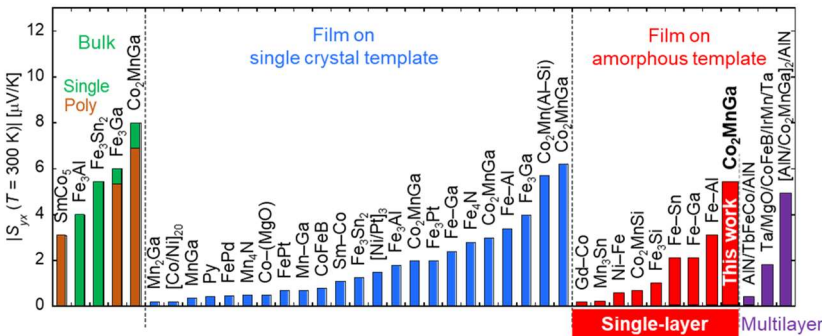


Figure: Comparison of the size of the room temperature ANE[8].

[1] S. Nakatsuji and R. Arita, *Annu. Rev. of Cond. Mat. Phys.* **13**, 119 (2022).
[2] D. Xiao, M.-C. Chang, and Q. Niu, *Rev. Mod. Phys.* **82** 1959 (2010).
[3] G. Sharma, P. Goswami, and S. Tewari, *Phys Rev. B* **92** (2016).
[4] W. Zhou and Y. Sakuraba, *Appl. Phys. Express* **13**, 043001 (2020).
[5] T. Higo *et al.*, *Adv. Funct. Mater.* **31**, 2008971 (2021).
[6] H. Tanaka *et al.*, *Adv. Mater.* **35**, 2303416 (2023).
[7] J. Wang *et al.*, *Adv. Electron. Mater.* **8**, 2101380 (2022).
[8] R. Uesugi, T. Higo, S. Nakatsuji, *Appl. Phys. Lett.* **123**, 252401 (2023).

10 スピントロニクス・マグネティクス | 一般セッション(口頭講演): 10.1 新物質・新機能創成 (作製・評価技術)

[20p-D61-1~14] 10.1 新物質・新機能創成 (作製・評価技術)

[20p-D61-1]

Magnetic compensation of epitaxial $\text{Mn}_{4-x}\text{Cu}_x\text{N}$ at room temperature

○安田 智裕¹、旗手 蒼¹、雨宮 健太²、末益 崇¹ (1.筑波大、2.高エネ研)

[20p-D61-2]

Anomalous Nernst effect in heavy-metal-substituted Fe_4N films

○Keita Ito¹, Takeshi Seki^{1,2} (1.IMR, Tohoku Univ., 2.CSIS, Tohoku Univ.)

[20p-D61-3]

All-in-one evaluation method for transverse thermoelectric properties of a single magnetic thin film device

○Takumi Yamazaki¹, Norihiko L. Okamoto¹, Tetsu Ichitsubo¹, Takeshi Seki^{1,2} (1.IMR, Tohoku Univ., 2.CSIS, Tohoku Univ.)

[20p-D61-4]

Low-temperature measurements of the anomalous Ettingshausen effect using lock-in thermography

○Takumi Imamura^{1,2}, Takamasa Hirai², Ken-ichi Uchida^{1,2,3} (1.Univ. of Tsukuba, 2.NIMS, 3.Univ. of Tokyo)

[20p-D61-5]

Detecting Compensated Magnetic Moments in Altermagnetic RuO_2

○Jun Okabayashi¹, Zhenchao Wen², Cong He², Yoshio Miura³, Seiji Mitani² (1.UTokyo, 2.NIMS, 3.Kyoto Inst. Tech.)

[20p-D61-6]

X-ray helicity-dependent ultrafast demagnetization in a Pt/Co/Pt multilayer

○Kihiro Yamada¹, Rei Kobayashi², Itaru Sugiura³, Yuya Kubota^{4,5}, Aoi Gocho⁶, Yusuke Akiyama², Kaiki Takemura², Sota Sasakura⁶, Keisuke Kaneshima⁶, Takuo Ohkouchi^{4,6}, Iwao Matsuda⁷, Teruo Ono³, Tadashi Togashi^{4,5}, Yoshihito Tanaka⁶, Motohiro Suzuki² (1.Tokyo Tech, 2.Kuwansei Univ., 3.ICR, Kyoto Univ., 4.JASRI, 5.RIKEN, 6.Hyogo Univ., 7.U Tokyo)

[20p-D61-7]

イオン注入によりSi中に形成した強磁性マンガンスリサイドナノ粒子

○大杉 廉人¹、河野 慎¹、若林 勇希¹、クロッケンバーガー ヨシハル¹、角倉 久史¹、登坂 仁一郎¹、西口 克彦¹ (1.NTT物性研)

[20p-D61-8]

Hydrogen annealing effect on ferromagnetic ultra-thin films

○Tomohiro Koyama^{1,2,3,4}, Noriyuki Seki¹, Daichi Chiba^{1,3,4,5} (1.SANKEN, Osaka Univ., 2.JST PRESTO, 3.CSRN, Osaka Univ., 4.OTRI, Osaka Univ., 5.SRIS, Tohoku Univ.)

[20p-D61-9]

Strain induced reversible sign change of the anomalous Hall effect

○Toshiaki Morita¹, Tomohiro Koyama^{1,2,3,4}, Daichi Chiba^{1,2,3,5} (1.SANKEN, Osaka Univ., 2.CSRN, Osaka Univ., 3.OTRI, Osaka Univ., 4.PRESTO, JST, 5.SRIS, Tohoku Univ.)

[20p-D61-10]

Preparation and characterization of Fe₃O₄ thin films on graphene

○Shodai Iwasaki¹, Agus Subagyo¹, Eko Ishihara¹, Katsuyuki Yagi¹, Koki Nakane¹, Hidehiro Jonai¹, Eiji Hatta¹, Kazuhisa Sueoka¹ (1.IST, Hokkaido Univ.)

[20p-D61-11]

Perspective high-temperature oxides: theoretical study

○(D)Martin Heczko¹, Masao Obata², Renaud Patte³, Denis Ledue³, Tatsuki Oda², Martin Zeleny¹ (1.Brno Univ. of Tech., 2.Kanazawa Univ., 3.Univ. Rouen Normandy)

[20p-D61-12]

L10秩序合金/ 2次元物質界面の原子スケール構造の第一原理計算

○遠藤 竜佑¹、植本 光治¹、松本 尚弥¹、ヴェルガラ サミュエル^{2,3}、新屋 ひかり⁴、永沼 博^{3,5}、小野 倫也¹ (1.神戸大工、2.パリ高等師範、3.東北大、4.東京大、5.名古屋大)

[20p-D61-13]

第一原理計算によるFeNi/2D materials界面の原子構造予測

○(M1)松本 尚弥¹、植本 光治¹、遠藤 竜佑¹、小野 倫也¹ (1.神戸大工)

[20p-D61-14]

First-principles study of magnetostriction and damping in Fe_{4x}Co_{4-4x}N

○(P)Ivan Kurniawan¹, Keita Ito², Takeshi Seki^{2,3}, Yoshio Miura¹ (1.NIMS, 2.IMR, Tohoku Univ., 3.CSIS, Tohoku Univ.)

Magnetic compensation of epitaxial $\text{Mn}_{4-x}\text{Cu}_x\text{N}$ at room temperature

1. Univ. of Tsukuba, 2. KEK

T. Yasuda¹, A. Hatate¹, K. Amemiya², and T. Suemasu¹

E-mail: ytrp108@gmail.com

【Introduction】 Anti-perovskite Mn_4N -based compounds have attractive characteristics such as magnetic compensation (MC) compositions of ferrimagnetism and noncollinear magnetic components^[1] (Fig. (b)) which can contribute to efficient magnetization dynamics^[2,3] and out-of-plane spin polarization^[4]. $\text{Mn}_{4-x}\text{Cu}_x\text{N}$ is one candidate that has such an MC composition. R. Zhang *et al.* reported the MC composition of bulk polycrystalline $\text{Mn}_{4-x}\text{Cu}_x\text{N}$ ^[5]. However, the MC composition of $\text{Mn}_{4-x}\text{Cu}_x\text{N}$ film is not clear. In this work, we investigate the magnetic properties of *c*-axis oriented epitaxial films at room temperature (RT).

【Experiment】 10-nm-thick $\text{Mn}_{4-x}\text{Cu}_x\text{N}$ films ($x = 0.0\text{--}1.0$) were prepared on $\text{SrTiO}_3(001)$ substrates by molecular beam epitaxy method. Epitaxial growth was confirmed by reflection high-energy electron diffraction (RHEED). The magnetic properties were measured using a vibrating sample magnetometer (VSM) at RT. The field was applied in the $[001]$ direction.

【Results and discussion】 Figure 2 shows RHEED images for $\text{Mn}_{4-x}\text{Cu}_x\text{N}$ films taken along the $[001]$ and $[110]$ azimuths. These sharp and streaky patterns indicate the epitaxial growths of $\text{Mn}_{4-x}\text{Cu}_x\text{N}$ layers on $\text{SrTiO}_3(001)$. Figure 3 shows the composition dependence of the magnetic properties of $\text{Mn}_{4-x}\text{Cu}_x\text{N}$ films at RT. The minimum value of the saturation magnetization M_s and the maximum value of the coercivity $\mu_0 H_c$ were observed around $x = 0.1$. This result means the MC composition is between $x = 0.1$ and 0.15 . The reduction of M_s and $\mu_0 H_c x \geq 0.6$ is thought to be caused by the decrease in the Néel temperature. In the presentation, we will show the results of X-ray magnetic circular dichroism (XMCD) and anomalous Hall effect (AHE) measurements.

【Acknowledgement】 The XMCD measurements were performed at BL-16A of KEK-PF with the approval of the Photon Factory Program Advisory Committee (Proposal No. 2022G036). The magnetic properties obtained using a VSM and the AHE measurements were measured with the help of Professor H. Yanagihara and Mr. T. Takahashi of the University of Tsukuba.

【References】

- [1] V. N. Antonov *et al.*, Low Temp. Phys. **40**, 641–648 (2014).
- [2] S. Ghosh *et al.*, Nano Lett. **21**, 2580 (2021).
- [3] T. Hajiri *et al.*, Appl. Phys. Lett. **115**, 052403 (2019).
- [4] Y. You *et al.*, Nat. Commun. **12**, 6524 (2021).
- [5] R. Zhang *et al.*, Acta Mater. **234**, 118021 (2022).

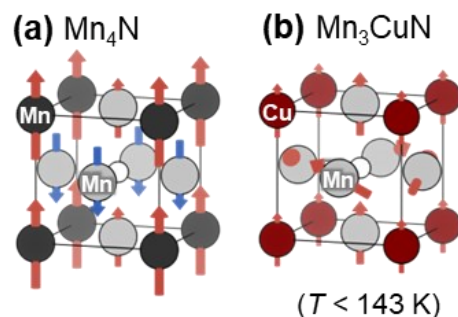


Fig. 1. Crystal and Magnetic structure of (a) Mn_4N and (b) Mn_3CuN .

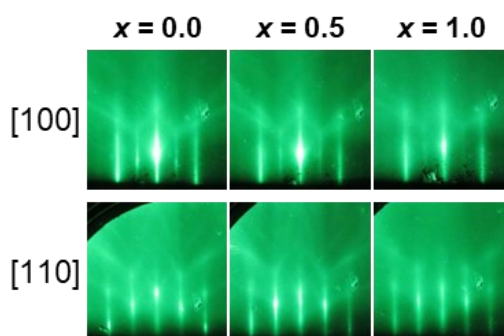


Fig. 2. RHEED images of $\text{Mn}_{4-x}\text{Cu}_x\text{N}$ taken along $[001]$ and $[110]$ azimuth.

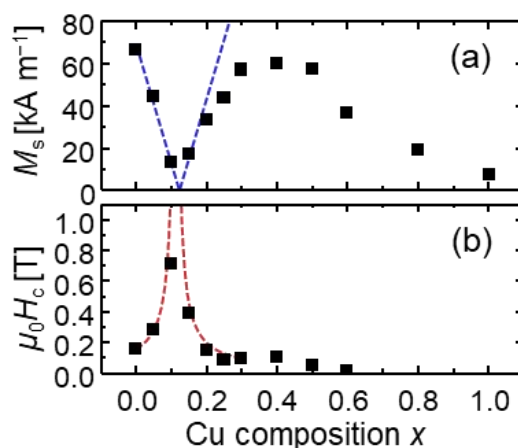


Fig. 3. (a) Saturation magnetization M_s , and (b) coercivity $\mu_0 H_c$ of $\text{Mn}_{4-x}\text{Cu}_x\text{N}$.

Anomalous Nernst effect in heavy-metal-substituted Fe₄N films

IMR, Tohoku Univ.¹, CSIS, Tohoku Univ.², °Keita Ito¹, Takeshi Seki^{1,2}

E-mail: keita.ito.e3@tohoku.ac.jp

Thermoelectric conversion using the anomalous Nernst effect (ANE) in ferromagnetic materials has attracted attention as a new energy harvesting technology. However, one crucial problem is that the thermoelectric power is lower than that of thermoelectric conversion using the Seebeck effect (SE) in semiconductor materials. Therefore, the development of novel ferromagnetic materials that exhibit a large anomalous Nernst coefficient (S_{ANE}) is essential for improving the power output of ANE. Fe₄N is a ferromagnetic material having a relatively large S_{ANE} (1.4 ~ 2.2 $\mu\text{V/K}$) [1,2]. Substitutions of the part of Fe atoms in Fe₄N with other metals are an effective method to tune the electrical and magnetic properties of Fe₄N [3]. This idea also gives us the possibility of enhancing the magnitude of S_{ANE} in Fe₄N by the substitution of Fe. In this study, Fe_{4-x}Ru_xN and Fe_{4-y}Pt_yN films were grown and the substitution effect for Fe by small amount heavy metals, which possess large spin-orbit interaction, on S_{ANE} was investigated.

Fe₄N, Fe_{4-x}Ru_xN ($x = 0.02, 0.10$) and Fe_{4-y}Pt_yN ($y = 0.04, 0.13$) films (~21 nm) were grown at 450 °C on MgO(001) substrates by molecular beam epitaxy. Fe, Ru, Pt, and radio-frequency radical N were simultaneously supplied. The sample structure was characterized by x-ray diffraction (XRD). The grown films were fabricated into Hall-bar-shaped devices, and the ANE, SE, and anomalous Hall effect were measured at 300 K. In the thermoelectric effect measurements, temperature gradients (∇T) were applied in the in-plane [100] direction of the nitride films, and external magnetic fields were applied in the out-of-plane direction. On-chip thermometers fabricated on the device were used to measure ∇T [2].

From the results of XRD measurements, the epitaxial growth on the MgO(001) substrate was confirmed for all the nitride films. The S_{ANE} values of the Fe₄N, Fe_{3.98}Ru_{0.02}N, Fe_{3.90}Ru_{0.10}N, Fe_{3.96}Pt_{0.04}N, and Fe_{3.87}Pt_{0.13}N films were evaluated to be 1.33, 1.28, 1.09, 1.36, and 1.54 $\mu\text{V/K}$, respectively. S_{ANE} decreased with x , while a slight increase was obtained with increasing y , indicating that the Pt substitution might be effective to enhance S_{ANE} of Fe₄N. S_{ANE} is represented by the following equation: $S_{ANE} = \rho_{xx}\alpha_{xy} - S_{SE}\tan\theta_{AHE}$, where ρ_{xx} is the longitudinal resistivity, α_{xy} is the transverse thermoelectric conductivity, S_{SE} is the Seebeck coefficient, and θ_{AHE} is the anomalous Hall angle. By substituting the experimentally obtained S_{ANE} , ρ_{xx} , S_{SE} , and $\tan\theta_{AHE}$ into this equation, the α_{xy} values of the samples were derived. The α_{xy} values of the Fe₄N, Fe_{3.98}Ru_{0.02}N, Fe_{3.90}Ru_{0.10}N, Fe_{3.96}Pt_{0.04}N, and Fe_{3.87}Pt_{0.13}N films were 1.02, 0.99, 1.02, 1.12, and 1.31 A/K·m, respectively. The enhancement of S_{ANE} in the Fe_{4-y}Pt_yN films is mainly due to the increase of α_{xy} . In the presentation, the S_{ANE} values of Fe_{4-z}Pd_zN films will be also shown.

This work was supported by JSPS KAKENHI (JP21K04859) and E-IMR in Tohoku University.

[1] S. Isogami *et al.*, Appl. Phys. Express **10**, 073005 (2017). [2] K. Ito *et al.*, J. Appl. Phys. **132**, 133904 (2022). [3] K. Ito *et al.*, Nanotechnology **33**, 062001 (2022).

All-in-one evaluation method for transverse thermoelectric properties of a single magnetic thin film device

IMR, Tohoku Univ.¹, CSIS, Tohoku Univ.²

°Takumi Yamazaki¹, Norihiko L. Okamoto¹, Tetsu Ichitsubo¹, and Takeshi Seki^{1,2}

E-mail: takumi.yamazaki.d5@tohoku.ac.jp

Transverse thermoelectric conversion, in which a temperature gradient leads to a transverse electric field, is a promising phenomenon for realizing the next-generation energy harvesting technology [1]. The anomalous Nernst effect (ANE) is a representative transverse thermoelectric effect in magnetic materials. The performance of transverse thermoelectric conversion for the ANE is characterized using the figure of merit $z_T T (= S_T^2 \sigma_{yy} T / \kappa_{xx})$, where S_T , σ_{yy} , κ_{xx} and T denote the transverse thermoelectric coefficient, electrical conductivity, thermal conductivity, and temperature, respectively. Although thin film forms offer advantages from the viewpoint of practical thermoelectric applications, the precise evaluation of their thermoelectric figure of merit is quite challenging. Recently, we have demonstrated that $z_T T$ in thin films can be precisely quantified by the combined use of heat-flux method, time-domain thermoreflectance, and four-terminal method [2]. However, the samples specialized for each evaluation method are required, which slows down the throughput speed and prevents the rapid materials development.

In this study, we propose an all-in-one method to evaluate S_T , σ_{yy} , and κ_{xx} of thin films. The device features a multilayer structure comprising of substrate/magnetic film sample/insulator/transducer. The device structure was fabricated by photolithography and Ar ion milling, enabling the simultaneous measurement of these three parameters with a single device. Herein, κ_{xx} is determined by fitting the temperature response of Joule heating to a theoretical curve derived from a one-dimensional heat conduction model, known as the 2ω method [3]. S_T is obtained from the relation of $S_T = \kappa_{xx} \Delta T_{AEE} / (d j_c T)$ [4], where d and j_c represent the sample thickness and applied charge current density, respectively. ΔT_{AEE} denotes the temperature change induced by the anomalous Ettingshausen effect (AEE), which is the reciprocal phenomenon of the ANE. σ_{yy} is measured using the four-terminal method. To detect the temperature response induced by Joule heating and ΔT_{AEE} , the lock-in thermoreflectance is employed, which is an optical thermometry based on the temperature dependence of reflectivity [5]. To verify the accuracy of the developed 2ω method, κ_{xx} of an Al-O insulating film was measured, yielding a value of $1.15 \pm 0.22 \text{ W m}^{-1} \text{ K}^{-1}$, which is consistent with values reported in the previous study [6]. Subsequently, the magnetic field dependence of ΔT_{AEE} of CoFeB film was measured. The obtained response reflects the magnetization curve of the CoFeB film, successfully evaluating the AEE. In the presentation, the details of each measurement method will be explained.

[1] K. Uchida and J. P. Heremans, *Joule* **6**, 2240 (2022). [2] T. Yamazaki *et al.*, *Phys. Rev. Applied* **21**, 024039 (2024). [3] Y. Nakamura *et al.*, *Nano Energy* **12**, 845 (2015). [4] A. Miura *et al.*, *Appl Phys. Lett.* **115**, 222403 (2019). [5] T. Yamazaki *et al.*, *Phys. Rev. B* **101**, 020415(R) (2019). [6] S.-M. Lee *et al.*, *Int. J. Thermophys.* **38**, 176 (2017).

ロックインサーモグラフィを用いた異常エッチングスハウゼン効果の低温測定

Low-temperature measurements of the anomalous Ettingshausen effect using lock-in thermography

筑波大¹, NIMS², 東京大³

○今村拓未^{1,2}, 平井孝昌², 内田健一¹⁻³

Univ. of Tsukuba¹, NIMS², Univ. of Tokyo³

○Takumi Imamura^{1,2}, Takamasa Hirai², and Ken-ichi Uchida¹⁻³

E-mail: IMAMURA.Takumi@nims.go.jp

The anomalous Ettingshausen effect (AEE) refers to the conversion of a charge current into a transverse heat current in a magnetic conductor¹. Since AEE works as a temperature modulator with simple structure and versatile scaling, it may pave the way for thermal management technologies for electronic and spintronic devices². In recent years, the experimental studies of AEE have been accelerated since the measurement method based on the lock-in thermography (LIT)^{3,4} has been established. While LIT makes it possible to estimate the AEE-induced temperature modulation quantitatively with high reliability and reproducibility, LIT measurements were performed only at room and high temperatures⁵⁻⁸. For further comprehension of AEE, it is important to verify the applicability of LIT for AEE measurements at low temperatures.

Here, we report low-temperature measurements of AEE in a polycrystalline Co₂MnGa slab⁹ using LIT, which is expected to show large AEE-induced signals, and estimate the limit of the temperature range available for LIT. Since LIT is applicable to various materials and phenomena, this work will stimulate materials science and physics studies on spin caloritronics and thermoelectrics.

References:

- [1] P. W. Bridgman, Phys. Rev. **24**, 644 (1924).
- [2] K. Uchida and R. Iguchi, J. Phys. Soc. Jpn. **90**, 122001 (2021).
- [3] S. Daimon, R. Iguchi, T. Hioki, E. Saitoh, and K. Uchida, Nat. Commun. **7**, 13754 (2016).
- [4] T. Seki, R. Iguchi, K. Takanashi, and K. Uchida, Appl. Phys. Lett. **112**, 152403 (2018).
- [5] K. Uchida, S. Daimon, R. Iguchi, and E. Saitoh, Nature **558**, 95 (2018).
- [6] A. Miura, K. Masuda, T. Hirai, R. Iguchi, T. Seki, Y. Miura, H. Tsuchiura, K. Takanashi, and K. Uchida, Appl. Phys. Lett. **117**, 082408 (2020).
- [7] A. Takahagi, T. Hirai, R. Iguchi, K. Nakagawara, H. Nagano, and K. Uchida, Appl. Phys. Express. **15**, 063002 (2022).
- [8] R. Modak, T. Hirai, S. Mitani, and K. Uchida, Phys. Rev. Lett. **131**, 206701 (2023).
- [9] W. Zhou, A. Miura, T. Hirai, Y. Sakuraba, and K. Uchida, Appl. Phys. Lett. **122**, 062402 (2023).

Detecting Compensated Magnetic Moments in Altermagnetic RuO₂

Jun Okabayashi,^{1*} Zhenchao Wen,² Cong He,² Yoshio Miura,^{3,2} and Seiji Mitani²

¹Research Center for Spectrochemistry, The University of Tokyo, Bunkyo-ku, Tokyo 113-0033, Japan

²Research Center for Magnetic and Spintronic Materials, National Institute for Materials Science (NIMS), Tsukuba, Ibaraki 305-0047, Japan

³Kyoto Institute of Technology, Kyoto 606-8585, Japan

*E-mail: jun@chem.s.u-tokyo.ac.jp

Altermagnetism has been developed recently using time-reversal symmetry breaking spintronic and spin-splitting phenomena in materials with collinear-compensated magnetic order [1]. It originates from the unique band structures splitting up and down spin bands, which is different from ferromagnetic exchange splitting and antiferromagnetic compensation. Some materials such as RuO₂, MnTe, and Mn₅Si₃ have been classified as an altermagnetism. In particular, RuO₂ has unique spin-dependent ellipse Fermi surfaces, which is regarded as an origin of spin-splitting effect [2]. However, recent topical issues of altermagnetism in RuO₂ is the existence or absence of the magnetic moments in the Ru sites. Although recent μ SR measurements for bulk RuO₂ reported the absence of the magnetic moments [3], the RuO₂ film includes the local strain, which might be essential for the finite Ru magnetic moments and altermagnetic properties. To access these controversial issues, we employ the x-ray magnetic linear dichroism (XMLD), which probes the square of the magnetization. The x-ray magnetic circular dichroism (XMCD) does not work for the detection of compensated spins. To separate the magnetic and structural contributions, we propose the temperature-dependent XMLD.

We prepared the sample of a 20-nm-thick rutile-type RuO₂ (101) layer, which is conductive, grown on single-crystal Al₂O₃ (1 $\bar{1}$ 02) substrates by reactive rf-sputtering of Ru. The Néel temperature of the sample was determined to be \sim 400 K. The magnetic moments in RuO₂ are aligned along [001] or [00 $\bar{1}$] direction, which is 35° tilted from sample surface normal. The Neel vector direction was determined from the previous angular-dependent XMLD [4]. The XMCD and XMLD measurements for Ru *M*-edge were performed at BL-7A and BL-16A in the Photon Factory (KEK). The total-electron-yield mode was adopted at 80 K and room temperature. For the XMLD, horizontally and vertically linear polarized beams were injected into the sample and difference is defined as a linear dichroism.

The x-ray absorption spectra in 4*d* transition-metal element *M*-edge consists of not only 3*p* to 4*d* but also 3*p* to 5*s* transition peaks. There was no XMCD signal because of the complete compensation in the total magnetization (*M*). To detect *M*², the XMLD was performed in the geometry of strong coupling between electric field in the incident beam and Neel vector in the sample. Temperature-dependent XMLD exhibits the changes of intensities; at low temperature, XMLD signal intensity is enhanced, which originates from the magnetic components. At room temperature, small signal intensity is detected. Therefore, finite *M* in the Ru sites can be confirmed. The appearance of *M* might come from the thin film cases. The XMLD magneto-optical sum rules provide the quantitative estimation of element-specific quadrupole through the charge distribution in the same manner for the XMCD sum rules [5]. Since the integrals of XMLD spectra are related to the sign of quadruples, the Ru 4*d* states form the 3*z*² − *r*² type quadrupole charge distribution along the spin orientation direction, which is also reproduced by the first-principles calculations.

This work was partly supported by JSPS KAKENHI No. JP22H04966.

References: [1] L. Šmejkal *et al.*, [Phys. Rev. X **12**, 040501 \(2022\)](#). [2] S. Karube *et al.*, [Phys. Rev. Lett. **129**, 137201 \(2022\)](#).

[3] M. Hiraishi *et al.*, [Phys. Rev. Lett. **132**, 166702 \(2024\)](#). [4] C. He, Z. Wen, J. Okabayashi *et al.*, to be submitted.

[5] J. Okabayashi *et al.*, [Appl. Phys. Lett. **115**, 252402 \(2019\)](#).

X-ray helicity-dependent ultrafast demagnetization in a Pt/Co/Pt multilayerTokyo Tech ¹, Kuwansei Gakuin Univ. ², ICR, Kyoto Univ. ³,JASRI ⁴, RIKEN ⁵, Hyogo Univ. ⁶, U Tokyo ⁷°K. T. Yamada ¹, R. Kobayashi ², I. Sugiura ³, Y. Kubota ^{4,5}, A. Gocho ⁶, Y. Akiyama ²,K. Takemura ², S. Sasakura ⁶, K. Kaneshima ⁶, T. Okouchi ^{4,6}, I. Matsuda ⁷, T. Ono ³,T. Togashi ^{4,5}, Y. Tanaka ⁶, and M. Suzuki ²

E-mail: yamada@phys.titech.ac.jp

When a femtosecond optical pulse irradiates a ferromagnetic metal, the magnetization dramatically decreases on a sub-picosecond time scale. This phenomenon, known as ultrafast demagnetization, results from optically pumping electrons in the outer-most electron shell, in the visible to near-infrared (NIR) spectral ranges. On the other hand, the advent of x-ray free electron lasers has provided new possibilities for studying ultrafast demagnetization induced by the resonance excitation of core-to-valence electric dipole transitions [1]. We are currently exploring new ultrafast magnetic phenomena triggered by intense hard x-ray pulses using the SACLA facility.

Here, we studied ultrafast demagnetization in a Pt/Co/Pt multilayer triggered by circularly polarized hard x-ray pulses. A magnetic multilayer of Ta(2.0 nm)/Pt(0.5 nm)/[Co(0.5 nm)/Pt(0.5 nm)]₁₀/Pt(0.5 nm)/Ta (2.0 nm) on a SiN membrane was prepared using dc sputtering. The Co layers force the Pt layers in the proximity to be ferromagnetically polarized. We performed x-ray-pump and NIR-probe experiments using SACLA beamline 3 in the experimental hutch 2, where 10-fs wide hard x-ray pulse and 40-fs wide NIR pulse are available in synchronization. In the hutch, a polarized optical microscope was constructed with two cameras, which simultaneously capture magneto-optical and transmittance images by synchronizing to the SACLA system. The repetition rates of the pump and probe pulses were 30 Hz and 60 Hz, respectively, to obtain images with/without pump pulses. We excited the $2p_{3/2}$ core electrons to the $5d$ empty valence states of Pt using circularly polarized hard x-ray pulses under an out-of-plane magnetic field and captured magneto-optical and transmittance images for each NIR probe pulse at an arbitrary optical delay. We observed that the amplitude and recovery of the ultrafast demagnetization changes depending on both the helicity and the initial magnetization direction. In this presentation, we would like to present details of the original measurement system and the obtained results with discussions.

References

[1] X. Liu et al., *Opt. Express* **29**, 32388-32403 (2021).

イオン注入法により Si 中に形成した強磁性 Mn シリサイドナノ粒子 Ferromagnetic manganese silicide nanoparticles formed by ion implantation in silicon

NTT 物性研 ○大杉 廉人、河野 慎、若林 勇希、Krockenberger Yoshiharu、
角倉 久史、登坂 仁一郎、西口 克彦

NTT BRL ○R. Ohsugi, M. Kawano, Y. K. Wakabayashi, Y. Krockenberger, H. Sumikura,
J. Noborisaka, and K. Nishiguchi
E-mail: rento.oosugi@ntt.com

薄膜中に埋め込まれた磁性ナノ粒子は、その粒径や分布によって様々な磁気特性を示す。個々の磁性ナノ粒子の磁気モーメントが常磁性として振る舞う状態を超常磁性という。十分低温においては、磁性ナノ粒子間の磁気的な障壁エネルギーの存在により磁化の向きが揃った状態で凍結し、見かけ上膜全体が強磁性のように振る舞う。この超常磁性から強磁性に転移する温度をブロッキング温度という。このような磁気状態を示す磁性ナノ構造を用いたスピントロニクスデバイスが報告されているが[1]、磁性ナノ粒子をそのようなデバイスに応用するためには、粒径や磁気特性の制御が不可欠となる。マンガン(Mn)シリサイドはバルクのキュリー温度(T_C)が約 40 K の強磁性体であり[2]、シリコン(Si)中への Mn イオン注入およびアニールプロセスによってナノ粒子を形成可能である[3,4]。イオン加速エネルギー(E_{acc})はナノ粒子を形成する上で重要な条件であるため、 E_{acc} によって Mn シリサイドの形成や磁気特性が制御可能であると期待される。そこで、本研究では、 E_{acc} に対する Mn シリサイドナノ粒子の Si 薄膜中での粒径とその磁気特性の変化を系統的に調べた。

Mn シリサイドナノ粒子は p -Si (001) 基板への Mn イオン注入により作製した。ドーズ量を $5 \times 10^{15} \text{ cm}^{-2}$ で一定とした下で、 E_{acc} が異なる 4 種類の試料 ($E_{acc} = 50, 100, 150$, および 300 keV) を作製した。イオン注入後、試料は窒素雰囲気中で 700°C 、30 分間アニールした。図 1 (a) は、 $E_{acc} = 50 \text{ keV}$ で作製した試料中で観察された代表的なナノ粒子の透過型電子顕微鏡 (TEM) 像と局所電子線回折 (SAED) 像である。このナノ粒子は直径が約 5 nm の正方晶の単結晶であり、(2-20) および (0-14) の格子面間隔 d はそれぞれ 0.196 nm および 0.344 nm であった。この SAED 像と d は、正方晶の $\text{MnSi}_{1.7}$ 単結晶の [441] 方向に向かって電子線を照射した場合に得られる SAED 像と d [5] と一致することから、形成された Mn シリサイドナノ粒子は $\text{MnSi}_{1.7}$ であると考えられる。

図 1 (b) および 1 (c) は、 $E_{acc} = 150 \text{ keV}$ で作製した試料の磁化-磁場 (M - H) 曲線および磁化-温度 (M - T) 曲線である。測定温度が 3 K のとき、明瞭なヒステリシスが観測された。これは、Mn シリサイドナノ粒子が膜全体として強磁性となっていることを示す。零磁場冷却 (ZFC) および磁場中冷却 (FC) 下で測定した M - T 曲線を比較すると、20 K 付近で分岐が見られた。これは磁性ナノ粒子由来の強磁性-超常磁性転移を意味する。以降、 T_B は ZFC 曲線のピーク位置の温度として定義する。図 1 (d) は、各 E_{acc} で作製された試料の ZFC 曲線から見積もられた T_B をナノ粒子のメディアン径 (R_{medi}) の 3 乗に対してプロットしたものである。ここで、 R_{medi} は断面 TEM 像で観測されたナノ粒子の粒径分布を対数正規分布関数でフィッティングすることで求めた。 T_B は R_{medi} の 3 乗に対して線形に増加しており、磁性ナノ粒子の磁気異方性とサイズの関係を表す Néel の緩和理論[6]でよく説明できた。また、 R_{medi} は E_{acc} の増加に伴って単調増加した。以上の結果から、 E_{acc} によりナノ粒子のサイズを調整でき、それによって磁気特性を制御できることが明らかになった。

[1] J. Grollier *et al.*, Nat. Electron. **3**, 360 (2020). [2] U. Gottlieb *et al.*, J. Alloys Compd. **361**, 13 (2003). [3] S. Zhou *et al.*, Phys. Rev. B **75**, 085203 (2007). [4] S. Yabuuchi *et al.*, Jpn. J. Appl. Phys. **47**, 4487 (2008). [5] Y. Xu, M. Yamazaki, and P. Villars, Jpn. J. Appl. Phys. **50**, 11RH02 (2011). [6] L. Néel *et al.*, Annales de géophysique **5**, 99 (1949).

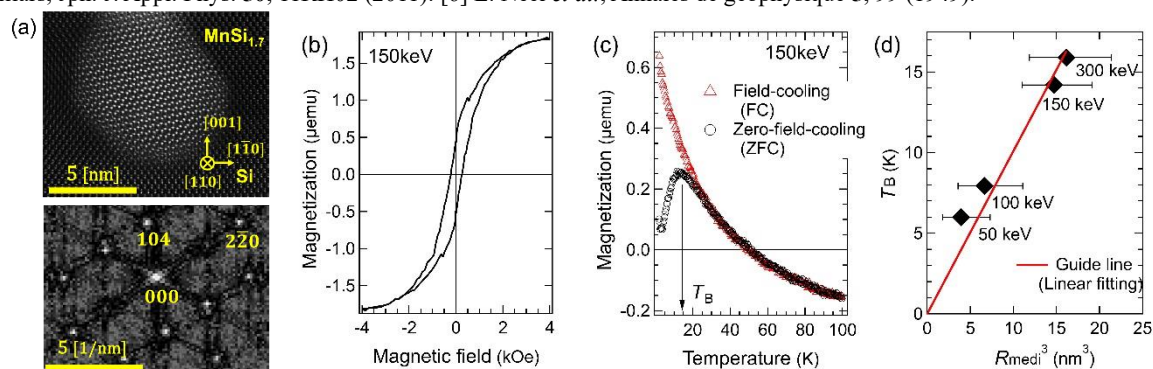


Fig. 1 (a) Cross-sectional TEM (top) and SAED (bottom) images of a Mn silicide nanoparticle with E_{acc} of 50 keV. (b) M - H curve of the sample with E_{acc} of 150 keV measured at 3 K. (c) M - T curves of the sample with E_{acc} of 150 keV measured under FC (triangle) and ZFC (circle) conditions, respectively. (d) T_B as a function of R_{medi}^3 . The guideline represents a linear fitting of the data.

強磁性超薄膜における水素アニール効果

Hydrogen annealing effect on ferromagnetic ultra-thin films

阪大産研¹, JST さきがけ², 阪大 CSRN³, 阪大 OTRI⁴, 東北大 SRIS⁵,

○小山 知弘^{1,2,3,4}, 関 憲行¹, 千葉 大地^{1,3,4,5}

SANKEN, Osaka Univ.¹, JST PRESTO², CSRN, Osaka Univ.³, OTRI, Osaka Univ.⁴, SRIS, Tohoku

Univ.⁵ ○Tomohiro Koyama^{1,2,3,4}, Noriyuki Seki¹, Daichi Chiba^{1,3,4,5}

E-mail: tkoyama@sanken.osaka-u.ac.jp

Ferromagnetic thin film (FM) is widely used in spintronics research. Contribution of the interfacial magnetic anisotropy is pronounced in this system. The interfacial Rashba effect [1] and interfacial DMI [2] in thin films with structural inversion asymmetry has been intensively investigated. Recently, ferromagnetic 2D materials are also attracting attention. However, in the thin-film systems, it is often pointed out that the degradation of magnetic properties is caused by oxidization through air exposure or process-damage [3]. In order to resolve this problem, we investigate a new device process: annealing under hydrogen (H₂) gas.

A Ta(2.0 nm)/Pt(2.5)/Co(1.4)/MgO(3.4) multilayer was deposited on a thermally oxidized Si substrate using sputtering. The films were annealed in a vacuum chamber with introducing an Ar/H₂ gas mixture. The annealing temperature and time were 150 °C and 1 hour, respectively. Figure 1 shows the magnetic moment per unit area $M_s t$ as a function of perpendicular external magnetic field H_{\perp} . No ferromagnetic behavior was observed in the as-deposited film because the MgO layer was formed with high sputtering power (120 W), resulting in an excessive oxidization damage to the Co layer. On the other hand, a clear hysteresis was observed in the H₂-anneal film. This result indicates that the ferromagnetic state is restored by the H₂-annealing in the Pt/Co/MgO structure with deeply oxygen-damaged Co. No clear change occurs in the $M_t - H_{\perp}$ curve after no-H₂-anneal. Thus, H₂ plays a crucial role in changing the magnetic property.

This work is supported by JSPS KAKENHI Grant Number 23K17902, the PRESTO from JST (JPMJPR21B5), MEXT Initiative to Establish Next-Generation Novel Integrated Circuits Centers (X-NICS) and the Spintronics Research Network of Japan.

[1] I. M. Miron *et al.*, *Nat. Mater* **9**, 230 (2010).

[2] T. Koyama *et al.*, *Sci. Adv.* **4**, eaav0265 (2018). [3] H.-K. Gweon *et al.*, *Sci. Rep.* **8**, 1266 (2018).

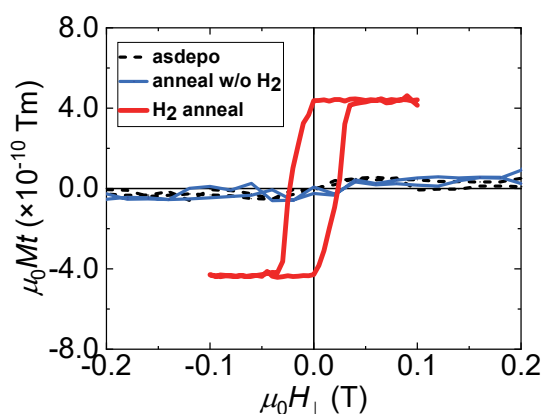


Figure 1: Magnetic moment per unit area M_t as a function of perpendicular field H_{\perp} . The results for the films annealed under different conditions (asdepo, annealed without H₂ flow, and annealed in H₂ gas) are shown.

Strain induced reversible sign change of the anomalous Hall effect

阪大産研¹, 阪大 CSRN², 阪大 OTRI³, JST PRESTO⁴, 東北大 SRIS⁵

○森田 利明¹, 小山 知弘^{1,2,3,4}, 千葉 大地^{1,2,3,5}

SANKEN, Osaka Univ.¹, CSRN, Osaka Univ.², OTRI, Osaka Univ.³,

PRESTO, JST⁴, SRIS, Tohoku Univ.⁵

○Toshiaki Morita¹, Tomohiro Koyama^{1,2,3,4}, and Daichi Chiba^{1,2,3,5}

E-mail: tmorita11@sanken.osaka-u.ac.jp

The anomalous Hall effect (AHE) is a fundamental physics related to spin-dependent transport. It is reported that a sign change of the AHE depending on the temperature and the layer structure[1,2]. The origin of the sign change of the AHE is attributed to band filling effect[3]. Recently, flexible spintronics utilizing the inverse magnetostriction effect has attracted attention[4]. The magnetostriction effect is a well-known phenomenon that combines strain and magnetism, but the modulation of magnetism by strain is still not fully understood. In this study, we observed strain induced reversible sign change of the AHE in Co/Ni multilayered film.

We deposited a [Co/Ni]_n multilayer on a flexible substrate by magnetron sputtering. Hall measurement was conducted without (w/o) and with (w/) application of a uniaxial strain in various temperatures. The small tensile jig was used to apply a strain. The results of Hall measurement are shown in Figure 1. Blue and red plots represent the results w/o and w/ strain, respectively. In w/o strain, the sign of the AHE is positive; Hall resistance is positive under positive magnetic field. In contrast, in w/ strain, the sign of the AHE reverses to negative. When the strain is removed, the sign of the AHE returns to positive (dashed blue plot). Our data suggest that band filling can be controlled by strain. We will discuss in more detail the effect of strain on the sign change in the AHE.

The authors thank S. Ota for technical support. This work is supported by Program for Leading Graduate School: “Interactive Materials Science Cadet Program”, JSPS KAKENHI (Grant No. 24KJ1613 and 23H00183), JST A-Step (Grant No. JPMJTR233A), JST CREST (Grant No. JPMJCR20C6), MEXT X-NICS, and the Spintronics Research Network of Japan.

- [1] Z.B. Guo *et al.*, *Phys. Rev. B* **86**, 104433 (2012).
 [2] V. Keskin *et al.*, *Appl. Phys. Lett.* **102**, 022416 (2013). [3] I. Turek *et al.*, *Phys. Rev. B* **86**, 014405 (2012). [4] S. Ota *et al.*, *Nat. Electron.* **1**, 124 (2018).

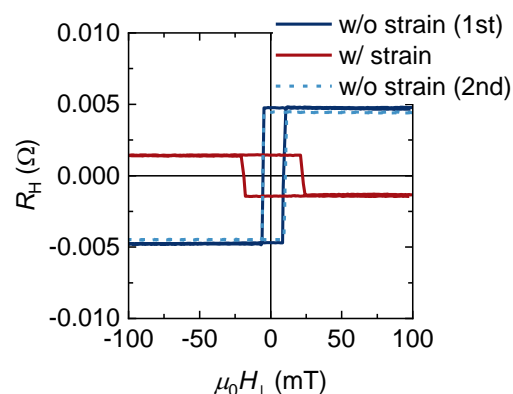


Figure 1: The results of Hall measurement. Blue and red plots represent the result w/o and w/ strain, respectively.

Preparation and characterization of Fe₃O₄ thin films on graphene

Graduate School of IST, Hokkaido Univ.

[○](M2)Shodai Iwasaki, Agus Subagyo, Eko Ishihara, Katsuyuki Yagi,

Koki Nakane, Hidehiro Jonai, Eiji Hatta and Kazuhisa Sueoka

E-mail: siwasaki@eis.hokudai.ac.jp; agus_subagyo@ist.hokudai.ac.jp

Since the first reports of spin injection and detection in graphene in 2007^[1,2], graphene has emerged as an ideal choice for spintronics materials. This is due to its extremely long spin diffusion lengths, reaching the micrometer scale at room temperature, which are attributed to its weak spin-orbit interaction^[1-4]. Additionally, graphene exhibits long spin relaxation times, ranging from microseconds to milliseconds, high mobility down to a single molecular layer, and outstanding scalability. These properties enable the transmission of pure spin currents over long distances, significantly reducing Joule heating losses in graphene spin devices. This has sparked the development of various groundbreaking next-generation devices, such as lateral spin valves, magnetic tunnel junctions (MTJs), and spin filter devices in spin tunnel transistors^[5,6]. To inject spin-polarized electrons into graphene and control spin currents within it, graphene is typically brought into contact or junction with ferromagnetic materials. As with general organic and molecular devices, the interfacial properties between graphene and the ferromagnetic material play a significant role in device characteristics^[7]. In this study, we investigate the use of Fe₃O₄, a half-metal, as the injection electrode for spin-polarized electrons into graphene, aiming to fabricate high-quality single-crystal Fe₃O₄ on graphene and achieve a high-quality Fe₃O₄/graphene interface.

First, we attempted growth of Fe₃O₄ on an HOPG surface. As a result, we found that a stoichiometric composition of Fe₃O₄ could be obtained by depositing Fe at a rate of approximately 0.1 nm/min in an oxygen atmosphere (vacuum level of 7.0×10^{-7} mbar) at a substrate temperature of 320°C, followed by post-annealing in an oxygen atmosphere at 400°C for 30 minutes (Fig.1). However, LEED and XRD measurements revealed that the resulting Fe₃O₄ was polycrystalline. Next, we attempted to grow Fe₃O₄ under same conditions using commercially available graphene, but the desired single crystal was not obtained. Since the LEED pattern was not observed with commercially available graphene, it is suspected that the crystallinity of the commercial graphene is the cause. Therefore, to improve the crystallinity of Fe₃O₄, we plan to conduct in-situ fabrication of graphene and the growth of Fe₃O₄. Additionally, we plan to fabricate graphene spin devices using the produced graphene.

References :

- [1]. N. Tombros *et al.*, Nature **448**, 571 (2007).
- [2]. M. Ohishi *et al.*, Jpn. J. Appl. Phys. **46**, L605 (2007).
- [3]. M. Drögeler *et al.*, Nano Lett., **16**, 3533 (2016).
- [4]. J. Panda *et al.*, ACS Nano **14**, 12771 (2020).
- [5]. E. C. Ahn, 2D Mater. Appl. **4**, 17 (2020).
- [6]. G. Hu, Nanoscale Res. Lett. **15**, 226 (2020).
- [7]. M. Cinchetti *et al.*, Nat. Mat. **16**, 507 (2017).

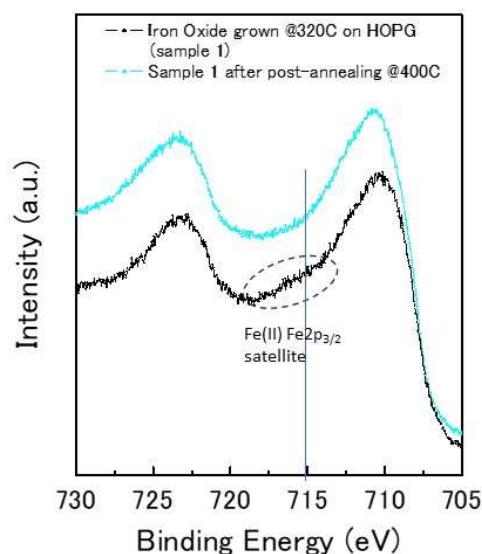


Fig. 1 Fe2p spectra of iron oxide

Perspective high-temperature oxides: theoretical study

Martin Heczko¹, Masao Obata², Renaud Patte³, Denis Ledue³, Tatsuki Oda², and Martin Zelený¹

¹ Institute of Material Science and Engineering, Brno University of Technology, Czech Republic

² Graduate School of Natural Science and Technology, Kanazawa University, Japan

³ Groupe de Physique des Matériaux, University of Rouen Normandy, France

E-mail: martin.heczko1@vutbr.cz

A wide range of physical properties like various magnetic orders, ferroelectricity, multiferroicity and possible half-metallicity makes $A_2BB'O_6$ oxides very promising for example in magnetic data storages [1] or spintronics. The possibility of combining different A, B and B' elements in many ways open the doors to designing materials with higher Curie temperatures and various band gaps at Fermi level in order to obtain a material usable in advanced applications.

Here we present calculations of various $A_2BB'O_6$ oxides performed using the spin-polarized DFT method implemented in the Vienna Ab Initio Simulation Package (VASP) [2,3] to obtain magnetic exchange interaction parameters J_{ij} [4]. The electron-ion interaction was described by the potential based on projector augmented-waves [5]. R²SCAN MetaGGA [6] approximation was employed for exchange-correlation contribution to total energy. Then, the electronic structure was confirmed using very precise QSGW approach together with spin-orbit coupling [7]. Curie temperatures were obtained by Metropolis Monte Carlo algorithm [8]. All compositions were modelled by rhombohedral cells containing 10 atoms.

Our results show that the Curie temperature increases proportionally to increasing magnetic moments of B and B' elements. Similar effect can be seen with decreasing A element ionic radius, because it decreases the cell volume, which leads to stronger magnetic interactions.

References

1. M. Azuma, K. Takata, T. Saito, S. Ishiwata, Y. Shimakawa and M. Takano, J. Am. Chem. Soc. **127**, 8889 (2005).
2. Kresse, G. and Furthmüller, J., Phys. Rev. B **54**, 11169–11186 (1996)
3. Kresse, G. and Furthmüller, J., Comput. Mater. Sci **6**, 15–50 (1996).
4. He, X., Helbig, N., Verstraete, M. J. and Bousquet, E., Comput. Phys. Commun. **264**, 107938 (2021).
5. Blöchl, P. E., Phys. Rev. B **50**, 17953–17979 (1994).
6. Furness, J. W., Kaplan, A. D., Ning, J., Perdew, J. P. & Sun, J., J. Phys. Chem. Lett. **11**, 8208–8215 (2020).
7. M. van Schilfgaarde, Takao Kotani, and S. Faleev, Phys. Rev. Lett. **96**, 226402 (2006).
8. Metropolis, N., Rosenbluth, A. W., Rosenbluth, M. N., Teller, A. H. and Teller, E., J. Chem. Phys. **21**, 1087–1092 (1953).

L1₀ 秩序合金/ 2 次元物質界面の原子スケール構造の第一原理計算

First-principles study on the atomic scale structure properties

of L1₀ alloy/2D material hetero-interface

神戸大工¹, パリ高等師範², 東北大³, 東大工⁴, 名古屋大⁵

○遠藤 竜佑¹, 植本 光治¹, 松本 尚弥¹, サミュエル・ヴェルガラ^{2,3}, 新屋 ひかり⁴,
永沼 博^{3,5}, 小野 倫也¹

Kobe Univ.¹, ENS-Paris², Tohoku Univ.³, Univ. Tokyo⁴, Nagoya Univ⁵

○Ryusuke Endo¹, Mitsuharu Uemoto¹, Naoya Matsumoto¹, Samuel Vergara^{2,3} Hikari Shinya⁴

Hiroshi Naganuma^{3,5}, Tomoya Ono¹

E-mail: uemoto@eedept.kobe-u.ac.jp

L1₀ 秩序相の鉄パラジウム合金(FePd)は高い磁気異方性と低い磁気減衰定数をもつ強磁性金属であり、スピントロニクス用途向け材料として注目されている。FePd ベースの磁気トンネル接合 (Magnetic Tunnel Junction: MTJ) 素子における絶縁層材料として、これまで MgO などの酸化物結晶が考えられてきたが、近年ではグラフェン(Gr)などの二次元物質によるヘテロ界面も検討され、実際に FePd/Gr 界面が実験的に作成・観察されている[1-2]。これまで、本研究では第一原理計算による FePd/Gr 界面構造および電子状態・磁気状態・スピン伝導特性の解析を行っており、FePd と多層グラフェン(*m*-Gr)による MTJ 構造である FePd/*m*-Gr/FePd では、磁気抵抗(Magneto-resistance: MR)比は MR~100%~300%に達すること[4]を示した。

今回の発表では、合金表面と二次元物質界面の詳細な原子スケールの構造と組成に注目する。真空中に面した FePd では、通常は Pd 原子層が表面となると安定となるが知られている。しかしながら、FePd/Gr 界面の実験による観察では Fe 原子が最表面となっている。このような結果は Fe と二次元物質間の相互作用の結果として理解され、第一原理計算からも再現できる。また、試料作成時の表面の酸化の存在が Fe 表面の形成を引き起こすと予想でき、表面酸化の存在は最近行われた XPS の測定と整合する。本研究ではさらに、遷移金属カルコゲナイド系二次元物質 PdSe₂ と FePd の界面原子構造についても議論する予定である。

参考文献 : [1] H. Naganuma, M. Nishijima, H. Adachi, M. Uemoto, H. Shinya *et al.*, ACS Nano **16**, 3, 4139-4151 (2022); [2] H. Naganuma, M. Uemoto, H. Adachi, H. Shinya *et al.*, J. Phys. Chem. C (2023). [3] M. Uemoto, H. Adachi, H. Naganuma, T. Ono, J. Appl. Phys. **132**, 095301 (2022); [4] H Adachi, R. Endo, H. Shinya, H. Naganuma, T. Ono, M. Uemoto J. Appl. Phys. **135**, 043902 (2024)

謝辞 : 科研費学術変革 A(JP22H05463)、JSPS Core-to-Core Program (JPJSCCA20230005)による研究助成、および Nagoya University Program for Research Enhancement による支援のもと実施された。また、本計算の一部は筑波大 CCS の学際共同利用(Wisteria-O)をもちいた。

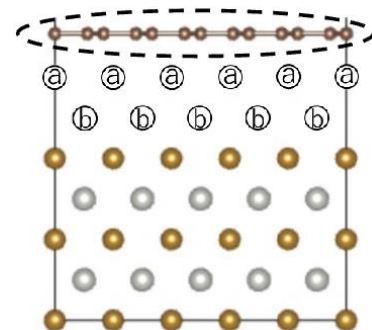


図: FePd/Gr モデルの例
表面金属層 ab の組成を調整

第一原理計算による FeNi/2D materials 界面の原子構造予測

First-principles study on atomic structures of FeNi/2D materials interfaces

神戸大工¹

○松本 尚弥¹, 植本 光治¹, 遠藤 竜佑¹, 小野 倫也¹

Kobe Univ.¹

○Naohiro Matsumoto¹, Mitsuharu Uemoto¹, Ryusuke Endo¹, Tomoya Ono¹

E-mail: 246t257t@eedept.kobe-u.ac.jp

近年、磁気トンネル接合におけるトンネル障壁層の材料として二次元物質が注目されている。このような物質系として我々は強磁性合金(FePd)とグラフェンのファンデルワールス異種界面[1]についてこれまで調査を行っている。また、最近では同じく強磁性合金である FeNi 上への h-BN の合成も報告 [2] されている。

本研究では、第一原理計算を用いて FeNi と二次元物質の界面における原子構造の詳細を明らかにする。まず、バルク FeNi 表面における Fe または Ni 終端の安定性を評価するために形成エネルギーを調べており、最表面金属層は Ni 75%の組成比をもつ表面が最も安定することが分かった。次に、二次元物質であるグラフェン(Gr)と六方晶窒化ホウ素(h-BN)で表面を覆われた FeNi 界面として FeNi/Gr および FeNi/h-BN のケースについても同様の解析を行い、Ni 0%の界面がエネルギー的に最も安定していることが示された。さらに、二次元物質側の吸着サイトを変化させると、最表面の Fe 原子, Ni 原子の直上に C 原子や B, N 原子が位置する構造が安定構造となることが確認された。

FeNi/Gr

FeNi/h-BN

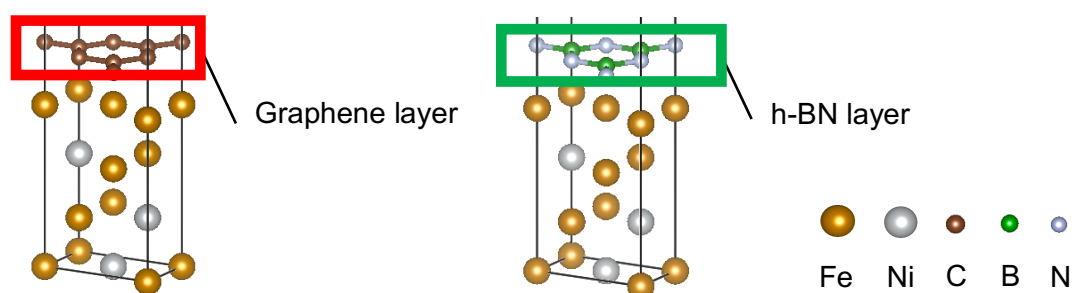


図: FeNi/Gr および FeNi/h-BN 計算モデル

電子状態密度(DOS)の計算からは、金属基板からグラフェンへの電子移動や Fe 原子と C 原子間の軌道混成の様子が見られた。これは、Fe 原子と C 原子間の引力相互作用に起因していると考えられる。本研究から得られる知見は、二次元物質・強磁性金属による磁気トンネル接合素子の設計に応用できる可能性がある。

[1] M. Uemoto, H. Adachi, H. Naganuma, T. Ono, J. Appl. Phys. 132, 095301 (2022)

[2] S. Emoto, H. Kusunose *et al.* Appl. Mater. Interfaces, (2024)

First-principles study of magnetostriction and damping in $\text{Fe}_{4x}\text{Co}_{4-4x}\text{N}$

NIMS¹, IMR, Tohoku Univ.², CSIS, Tohoku Univ.³

[○]Ivan Kurniawan¹, Keita Ito², Takeshi Seki^{2,3}, Yoshio Miura¹

E-mail: kurniawan.ivan@nims.go.jp

The magnetostriction effect corresponds to the change in lattice dimension parallel to the applied magnetic field. This property is important for applications in soft magnets, flexible spintronics, sensors and actuators. A recent paper reported a large and negative magnetostriction of Fe_4N (-121 ppm) [1]. Interestingly, it was also found that the replacement of Fe by Co resulted in a sign change of magnetostriction from negative to positive value. A strong correlation between magnetostriction and damping constant was also found. Therefore, in this study, we focus on the theoretical explanation of the relationship between magnetostriction and damping in $\text{Fe}_{4x}\text{Co}_{4-4x}\text{N}$.

The magnetostriction was calculated from the derivative of the total energy E and the magnetocrystalline anisotropy energy (MAE) on the strain ε ($dE/d\varepsilon$ and $d\text{MAE}/d\varepsilon$) [2]. Note that the sign of magnetostriction is always equal to the sign of $d\text{MAE}/d\varepsilon$. The values of total energy and MAE were obtained by including the spin-orbit interaction in a self-consistent calculation considering different strained structures. Furthermore, using second-order perturbation analysis [3], we clarify the dominant contribution to $d\text{MAE}/d\varepsilon$ based on spin states, atomic sites, and atomic orbitals. On the other hand, the damping constant was calculated using the torque correlation model from noncollinear calculation [4]. In comparison, the fcc- $\text{Ni}_x\text{Co}_{1-x}$ was also studied theoretically because fcc-Ni (Co) is known to have a negative (positive) magnetostriction value [2].

We confirm the good agreement of magnetostriction and damping trend found in experiments [1] and theoretical study for $\text{Fe}_{4x}\text{Co}_{4-4x}\text{N}$ despite the “shifted” behavior. The good agreement is also observed for the fcc- $\text{Ni}_x\text{Co}_{1-x}$. In addition, the face-centered Fe atoms and the orbital symmetry play an important role in the sign change of the magnetostriction of $\text{Fe}_{4x}\text{Co}_{4-4x}\text{N}$. Importantly, we found that the sign of magnetostriction depends on the competing terms of the negative sign of $d\text{MAE}(\downarrow\downarrow)/d\varepsilon$ and the positive sign of $d\text{MAE}(\uparrow\downarrow)/d\varepsilon$, which was confirmed for a range of $0 < x < 1$. The relationship between magnetostriction and damping can be understood from the large minority-spin density of states (DOS) around the Fermi level. The minority-spin DOS give the dominant contribution of damping value and also $d\text{MAE}(\downarrow\downarrow)/d\varepsilon$, which determines the sign and value of magnetostriction. Thus, these findings lead to the possible material design guideline for simultaneous tuning of magnetostriction and damping constant in magnetic materials.

This work was partly supported by Grants-in-Aid for Scientific Research (Grants No. 22H04966) from the Japan Society for the Promotion of Science and the Japan Science and Technology Agency (JST) CREST (Grant No. JPMJCR2101).

[1] K. Ito, *et al.* arXiv:2403.16679 [cond-mat.mtrl-sci]

[2] R. Wu, *et al.* JMMM 170, 103 (1997)

[3] P. Bruno, PRB 39, 865(R) (1989)

[4] V. Kamberský, Can. J. Phys. 48, 2906 (1970)

10 スピントロニクス・マグネティクス | 一般セッション(口頭講演) : 10.2 スピン基盤技術・萌芽的デバイス技術

[16a-D61-1~8] 10.2 スピン基盤技術・萌芽的デバイス技術

[16a-D61-1]

Growth and evaluation of highly textured BiSb(001) topological insulator on Si/SiO_x

○(M1)Wentao Li¹, Huy H.H.¹, S. Takahashi², Y. Hirayama², Y. Kato², Nam Hai Pham¹ (1.Tokyo Tech, 2.Samsung Japan Corp.)

[16a-D61-2]

Spin Hall effect in annealed BiSb topological thin films deposited on Si/SiO_x substrates

○(D)HOANGHUY HO¹, WENTAO L.¹, TAKAHASHI S.², HIRAYAMA Y.², KATO Y.², NAM HAI PHAM¹ (1.Tokyo Tech., 2.Samsung Japan Corp.)

[16a-D61-3]

Enhancement of SOT-driven domain wall motion in wide heavy metal width structure

○(DC)Kim Dongryul¹, Sooboem Lee¹, Chun-Yeol You¹ (1.DGIST)

[16a-D61-4]

piezoelectronic magnetic resistance element in a ring-type piezoelectric structure that induces strain of the limited element analysis

○(M2)山田 海衆¹、高村 陽太¹、中川 茂樹¹ (1.東工大)

[16a-D61-5]

[第56回講演奨励賞受賞記念講演] 非線形電気伝導におけるキラルな軌道テクスチャ

○廣部 大地¹、奥村 卓¹、田中 隆太郎¹ (1.静岡大理)

[16a-D61-6]

電圧制御された単一磁性体による連想記憶

○谷口 知大¹、今井 悠介² (1.産総研、2.東大)

[16a-D61-7]

Reservoir Computing Utilizing Transient Dynamics of Spin-Hall Nano-Oscillators

○Aakanksha Sud^{2,1}, Akash Kumar^{3,6}, Maha Khademi⁷, Johan Akerman^{1,6}, Shunsuke Fukami^{1,3,4,5} (1.RIEC,Tohoku Univ., 2.FRIS,Tohoku Univ., 3.CSIS,Tohoku Univ., 4.CIES,Tohoku Univ., 5.WPI-AIMR, 6.Univ. of Gothenburg, 7.Chalmers Univ.)

[16a-D61-8]

Investigating the origin of cluster spin glass behavior in low-damped garnet-based ferrimagnet towards neuromorphic computation

○(PC)shamim sarker¹, Haining Li¹, EMK Ikball Ahamed¹, Hiroyasu Yamahara¹, Siyi Tang¹, Zhiqiang Liao¹, Tetsuya Iizuka¹, Munetoshi Seki¹, Hitoshi Tabata¹ (1.Tokyo Univ)

Growth and evaluation of highly textured BiSb(001) topological insulator on Si/SiO_x

¹Tokyo Tech., ²Samsung Japan Corp.

L. Wentao ¹, H. H. Huy¹, S. Takahashi², Y. Hirayama², Y. Kato², P. N. Hai¹

E-mail: li.w.ao@m.titech.ac.jp

BiSb topological insulator is a promising spintronic material because of its giant spin Hall effect [1] and high electrical conductivity [2], which can be applied to various spin-orbit torque (SOT) devices, such as ultrafast [3] and ultralow power [4] SOT-MRAM and SOT domain-wall memory. However, high crystal quality BiSb thin films have been grown so far on single crystalline substrates, such as GaAs(111) [2], GaAs(001) [5], sapphire(0001) [6], and BaF₂(111) [7], mostly by molecular beam epitaxy. For realistic spintronic devices applications, it is essential to grow high quality BiSb by the magnetron sputtering technique on top of amorphous SiO_x, which is frequently used as the insulating material for the BEOL process of Si wafers.

In this work, we demonstrate that by using a combination of TiO_x seed and MgO buffer layers, we can grow highly textured BiSb(001) on SiO_x by the magnetron sputtering technique. Figure 1(a) shows the schematic structure of our sample. First, we deposited a TiO_x seed layer on top of a thermally oxidized Si/SiO_x substrate by reactive sputtering of a Ti target using Ar and O₂ mixing gas. Next, we deposited a 2 nm-thick MgO buffer layer on top of the TiO_x layer. Then, we deposited a 10 nm-thick BiSb on top of the MgO layer. Finally, we deposited a 3 nm-thick Ta cap layer. All layers were deposited at room-temperature. Figure 1(b) shows an out-of-plane θ -2 θ X-ray diffraction (XRD) spectrum of our sample, which shows that BiSb grown with the (001) orientation. The BiSb(001) full width at half maximum is comparable or even better than those grown on sapphire substrates, indicating the high crystal quality of BiSb. Figure 1(c) shows the in-plane XRD spectrum of our sample, which shows sharp in-plane peaks corresponding to the BiSb(100) or BiSb(110) planes, indicating that our sample is highly textured. Our results show that by using TiO_x/MgO buffer, we can grow highly textured BiSb(001) even on amorphous SiO_x.

References:

- [1] N. H. D. Khang, Y. Ueda, P. N. Hai, *Nature Mater.* **17**, 808 (2018).
- [2] Y. Ueda, N. H. D. Khang, K. Yao, and P. N. Hai, *Appl. Phys. Lett.* **110**, 062401 (2017).
- [3] N. H. D. Khang, T. Shirokura, T. Fan, M. Takahashi, N. Nakatani, D. Kato, Y. Miyamoto, and P. N. Hai, *Appl. Phys. Lett.* **120**, 152401 (2022).
- [4] H. Wu, A. Chen, P. Zhang, H. He, J. Nance, Ch. Guo, J. Sasaki, T. Shirokura, P. N. Hai, B. Fang, S. A. Razavi, K. Wong, Y. Wen, Y. Ma, G. Yu, G. P. Carman, X. Han, X. Zhang, K. L. Wang, *Nature Commun.* **12**, 6251 (2021).
- [5] K. Yao, N. H. D. Khang, P. N. Hai, *J. Cryst. Growth* **511**, 99 (2019).
- [6] T. Fan, M. Tobah, T. Shirokura, N. H. D. Khang, and P. N. Hai, *Jpn. J. Appl. Phys.* **59**, 063001 (2020).
- [7] K. Ueda, Y. Hadate, K. Suzuki, H. Asano, *Thin Solid Films* **713**, 1383 (2020).

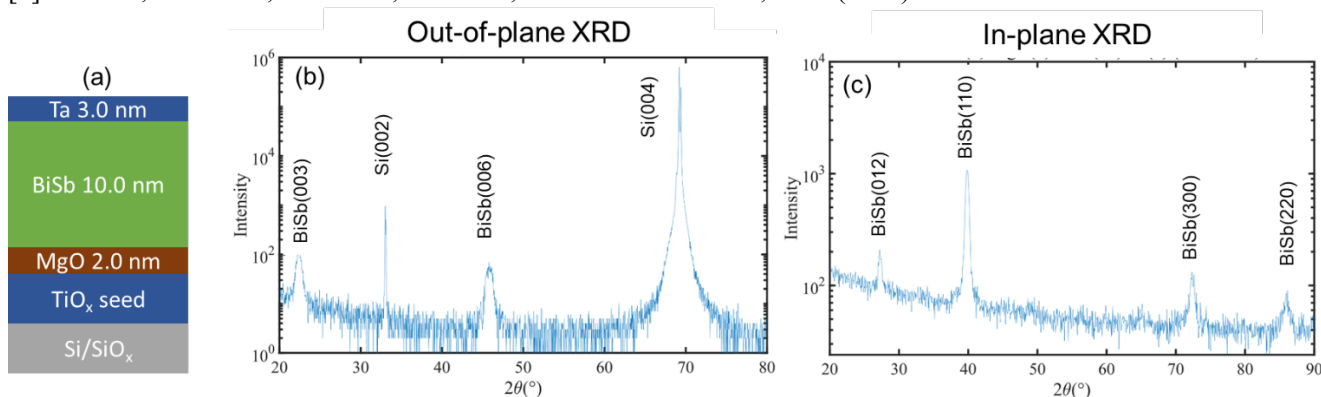


Fig. 1. (a) Schematic stacking structure of our sample. (b) Out-of-plane XRD and (c) In-plane XRD spectrum of our sample.

Spin Hall effect in annealed BiSb topological thin films deposited on Si/SiO_x substrates

¹Tokyo Tech., ²Samsung Japan Corp.

H. H. Huy¹, L. Wentao¹, S. Takahashi², Y. Hirayama², Y. Kato², P. N. Hai¹

E-mail: ho.h.ab@m.titech.ac.jp

BiSb topological insulator has attracted attention as a promising spin-orbit torque (SOT) material owing to its giant spin Hall effect [1] and high electrical conductivity [2] for ultrafast [3] and ultralow power [4] SOT-MRAM and SOT domain-wall memory. Although high crystal quality BiSb thin films have been studied so far on single crystalline substrates, such as GaAs(111) [2], GaAs(001) [5], sapphire(0001) [6], and BaF₂(111) [7], realizing high quality of BiSb with high spin Hall angle and high electrical conductivity on amorphous SiO_x is essential to realize realistic SOT spintronic devices.

In this work, we aim to realize BiSb topological insulator thin films with high spin Hall angle and high electrical conductivity on amorphous SiO_x using oxide buffer layers and post annealing. Figure 1(a) the schematic structure of our sample. We first deposited an oxide buffer layer (1) and an optional oxide buffer layer (2) on thermally oxidized Si/SiO_x substrates. The oxide buffer layer (1) is typically a TiO_x layer which prevents oxygen diffusion from the SiO_x layer to BiSb during high temperature thermal annealing, while the optional oxide layer (2) is typically TaO_x, both are deposited by reactive sputtering of a Ti/Ta target using Ar and O₂ mixing gas. Next, we deposited a 10 nm-thick BiSb on top of the oxide layers. Finally, we deposited a 3 nm-thick Ti cap layer. The stack was then annealed at high temperature for 1 hour and cooled in ultrahigh vacuum to low temperature, after that we deposited the ferromagnetic (FM) multilayers for SOT evaluation. Here we used Pt/Co/Pt or Ta/CoFeB/MgO as the FM multilayers. Figure 1(b) and 1(c) show wide-view and narrow-view θ -2 θ X-ray diffraction (XRD) spectra of a sample with TiO_x buffer and Pt/Co/Pt FM layers, which show that BiSb grown with the (012) orientation. By high temperature annealing, we can improve the BiSb conductivity up to $1.1 \times 10^5 \Omega^{-1}\text{m}^{-1}$ and achieve a relatively high spin Hall angle of $\theta_{\text{SH}} \sim 1.7 - 5$. Our results show that utilizing oxide buffer layers and post-annealing is an effective way to achieve high performance BiSb on Si/SiO_x substrates.

References:

- [1] N. H. D. Khang, Y. Ueda, P. N. Hai, Nature Mater. **17**, 808 (2018).
- [2] Y. Ueda, N. H. D. Khang, K. Yao, and P. N. Hai, Appl. Phys. Lett. **110**, 062401 (2017)..
- [3] N. H. D. Khang, T. Shirokura, T. Fan, M. Takahashi, N. Nakatani, D. Kato, Y. Miyamoto, and P. N. Hai, Appl. Phys. Lett. **120**, 152401 (2022).
- [4] H. Wu, A. Chen, P. Zhang, H. He, J. Nance, Ch. Guo, J. Sasaki, T. Shirokura, P. N. Hai, B. Fang, S. A. Razavi, K. Wong, Y. Wen, Y. Ma, G. Yu, G. P. Carman, X. Han, X. Zhang, K. L. Wang, Nature Commun. **12**, 6251 (2021).
- [5] K. Yao, N. H. D. Khang, P. N. Hai, J. Cryst. Growth **511**, 99 (2019).
- [6] T. Fan, M. Tobah, T. Shirokura, N. H. D. Khang, and P. N. Hai, Jpn. J. Appl. Phys. **59**, 063001 (2020).
- [7] K. Ueda, Y. Hadate, K. Suzuki, H. Asano, Thin Solid Films **713**, 1383 (2020).

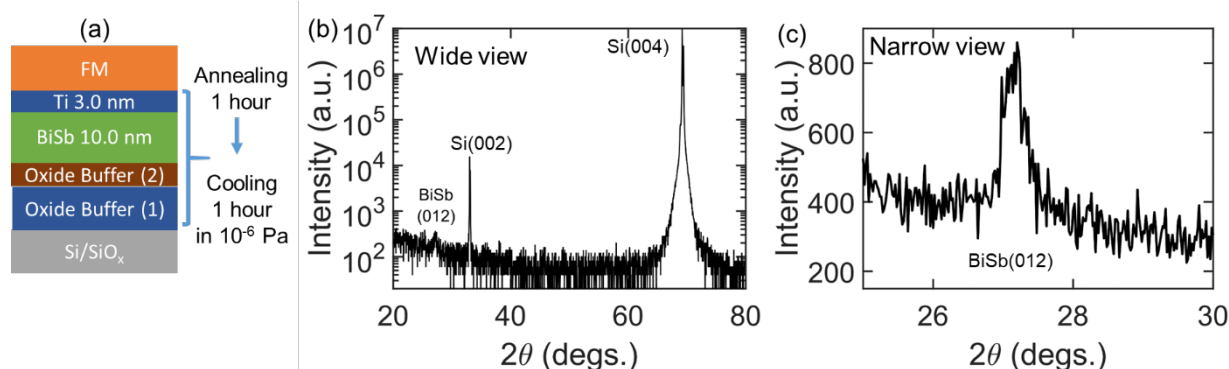


Fig. 1. (a) Schematic stacking structure of our sample. (b) Wide view and (c) Narrow view XRD spectra of a sample with TiO_x and Pt/Co/Pt FM layers.

Enhancement of spin-orbit torque-driven domain wall mobility in wide-width heavy metal structure

(D) Dongryul KIM¹, Sooboem LEE^{1,2}, Chun-Yeol YOU¹

¹Department of Physics and Chemistry, DGIST, Daegu 42988, Republic of Korea

²Basic Science Research Center, DGIST, Daegu 42988, Republic of Korea

E-mail: decalog2@dgist.ac.kr

Magnetic domain wall devices such as a racetrack memory[1] and a spin torque majority gate[2] have attracted significant attention recent decades owing to their non-volatile and uniaxial anisotropic features. In these devices, logic states of ‘1’ or ‘0’ is described by domain polarities of ‘up’ or ‘down’. Furthermore, the velocity of the domain wall (DW) is directly related to the speed of information processing. Therefore, enhancement of DW velocity can improve the performance of magnetic domain wall devices. In this study, we improved mobility of spin-orbit torque (SOT)-driven domain wall motion by modifying a structure of ferromagnetic (FM) and heavy metal (HM) wires, where the bottom HM wire width is wider than the top FM wire.

Ta(3)/Pt(5)/Co(1.2)/Ta(2) (in nanometer unit) heterostructure which exhibits considerable Dzyaloshinskii–Moriya interaction and SOT is exploited for investigation of SOT-induced domain wall motion. We fabricated FM wires with various line widths from 2 to 20 μm . Unlike the conventional single FM wire, only the width of FM layer is modified with fixing the width of the underneath HM (shown in Fig.1(a)). DW mobility which is defined as the slope of DW velocity versus applied current density at each FM wire width was evaluated by using Kerr microscopy. Harmonic Hall measurement is also conducted in the same geometry to investigate efficiencies of SOT. Interestingly, as shown in Fig.2 (b), DW mobility and SOT efficiency decrease as the FM wire width increases, with similar trends. The detailed discussion will be given in the presentation.

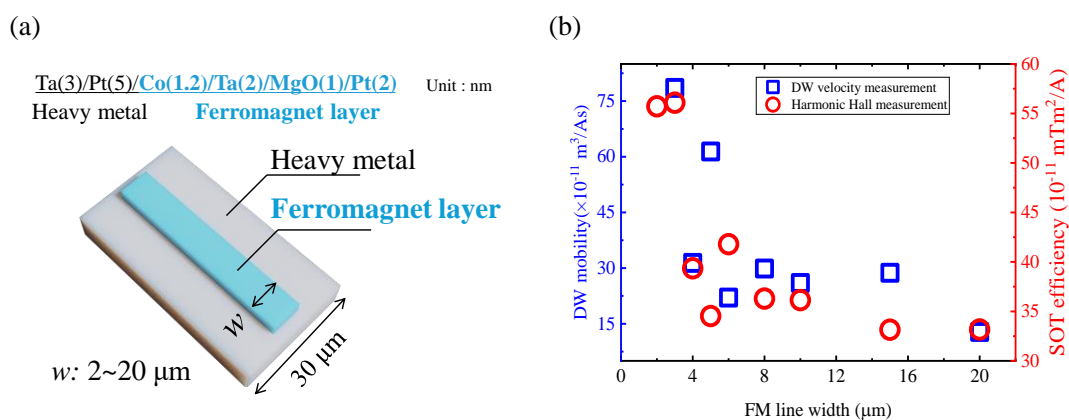


Fig. 1. (a) Schematic and structure of wide HM wire system (b) SOT efficiency (red circles) and DW mobility (blue squares) in various FM wire widths.

ピエゾエレクトロニック磁気抵抗素子における 円環型圧電印加構造が誘起する応力の有限要素法解析

FEM analysis of induced stress in the piezoelectric ring structure of piezoelectronic MTJ

1 東工大電気電子 ○(M2) 山田 海衆, 高村 陽太, 中川 茂樹

Tokyo Tech, ○Kaishu Yamada, Yota Takamura, Shigeki Nakagawa

E-mail: yamada.k.ca@m.titech.ac.jp

Stress-assist magnetization reversal (SAMR) is highly effective in reducing magnetization switching energy in ultra-low power consumption nonvolatile memories [1]. The piezo-electronic magnetic tunnel junction (PE-MTJ) has been proposed as a memory element capable of realizing SAMR [1]. This device consists of an MTJ with a magnetostrictive free layer surrounding a piezoelectronic ring. Induced stress applied to the MTJ pillar in a PE-MTJ has been previously calculated using an analytical model for simplified structure with a uniform pillar model [2]. To analyze stress in more complex structure, such as a layered structure of a MTJ, the finite elemental method (FEM) is necessary. In this study, induced stress in a SmFe_2 pillar is analyzed by FEM for a uniform pillar model with a piezoelectric ring as a first step. FEM calculations are compared with analytical results.

The FEM simulation was carried out using the commercially available software Femtet by MURATA Software. Figure 1 shows the model structure used for both analytical and FEM calculations. The standard size parameters and materials for both calculations are also described in Fig. 1. Figure 2 shows induced compressive stress at the center of the pillar as a function of the voltage difference between the top and bottom of the piezoelectric ring. Both calculation results exhibit the same trend, showing linear dependence. However, the slope calculated by FEM is approximately half of analytical result. This difference may arise from the rectangular approximation described in Ref. [3]. Figure 3 shows stress distribution in SmFe_2 along radial axis (y axis in in Fig. 1). The induced compressive stress decreases from the outside to the center and then increases. This stress distribution can be explained by strain at the interface of $\text{SmFe}_2/\text{PMN-PT}$ ($y = R$). These results facilitate the analyze of switching current reduction in actual PE-MTJ devices.

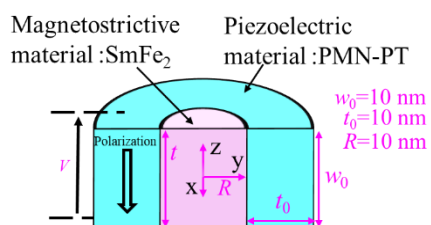


Fig. 1 Schematic of model structure with standard parameters for calculation.

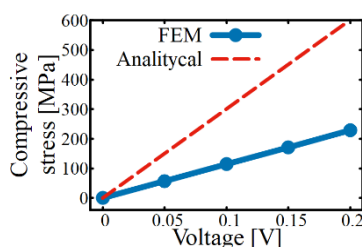


Fig. 2 Stress at the center of the SmFe_2 pillar as a function of applied voltage.

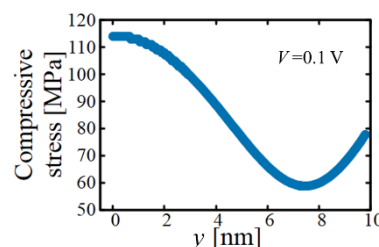


Fig. 3 Stress distribution from the center to the outside of the SmFe_2 pillar.

Refs: [1] N. Saito, et al., J. Appl. Phys. **103**, 07A706 (2008). [2] Y. Takamura, et al., Solid-State Electron. **128**, 194 (2017). [3] Y. Shiotsu, et al., IEEE Trans. on Electron Devices. **67**, 3852(2020).

非線形電気伝導におけるキラルな軌道テクスチャ

Chiral orbital texture in nonlinear electrical conduction

静岡大理¹ °廣部 大地¹, (M2)奥村 卓¹, 田中 隆太郎¹

Shizuoka Univ.¹, °Daichi Hirobe¹, Suguru Okumura¹, Ryutaro Tanaka¹

E-mail: hirobe.daichi@shizuoka.ac.jp

反転対称性や鏡映対称性の破れた系は、多自由度間の結合を単一材料で可能にする。そのような低い対称性は波数空間におけるエネルギーバンドの分裂として現れる。たとえば、スピン軌道結合で分裂したスピン分裂バンドではスピンと擬運動量が結合し、生じる電気-磁気間の交差物性はスピン・エレクトロニクスの基礎である。**単一材料における非線形電気伝導（バルク電荷整流と呼ばれる）もその一例であり、磁場印加で電気伝導が整流性を得る現象である。その整流効率はバンド構造の対称性の破れを定量化するものであり、pn接合を要しない整流素子の原理としても重要である。非線形電気伝導を示す典型的な材料がキラル半導体テルル[1, 2]であり、特にその薄膜結晶テルリン[3-5]は非線形電気伝導のゲート制御性も提供する。**しかしながら、第一原理計算等で予言される非線形電気伝導の選択則はテルリンで再現されておらず、更に実験研究グループ間でも実験結果が一致していない。これらの不一致がテルルにおける非線形電気伝導の機構解明を妨げてきた。

本研究では、デバイス作製条件と高調波電圧測定法を最適化することで、異種接合界面におけるバンド湾曲や熱電効果を抑制した、非線形電気伝導の純粹測定を試みた。その結果、非線形電気伝導の選択則をテルリンで初めて観測することに成功した。さらに、この選択則に基づいて非線形コンダクタンス・テンソルの単一成分を高精度に決定し、そのキャリア濃度依存性を明らかにした。以上の結果と半古典的なボルツマン方程式を組み合わせることで、波数空間におけるキラルな軌道テクスチャが非線形伝導の主要因であると結論付けた。講演当日は、実験結果とモデル計算の比較に基づき、テルルの非線形電気伝導の微視的機構について議論する。

1. G. L. J. A. Rikken & N. Avarvari, Strong electrical magnetochiral anisotropy in tellurium. *Phys. Rev. B* **99**, 245153 (2019).
2. K. Sudo, *et al.*, Valley polarization dependence of nonreciprocal transport in a chiral semiconductor. *Phys. Rev. B* **108**, 125137 (2023).
3. F. Calavalle, *et al.*, Gate-tuneable and chirality-dependent charge-to-spin conversion in tellurium nanowires. *Nat. Mater.* **21**, 526-532 (2022).
4. DH, *et al.*, Chirality-induced intrinsic charge rectification in a tellurium-based field-effect transistor. *Phys. Rev. B* **106**, L220403 (2022).
5. C. Niu, *et al.*, Tunable Chirality-Dependent Nonlinear Electrical Responses in 2D Tellurium. *Nano. Lett.* **18**, 8445-8453 (2023).

電圧制御された単一磁性体による連想記憶

Associative memory by a voltage controlled ferromagnet

産総研¹, 東大² ○ 谷口知大¹, 今井悠介²

AIST¹, The University of Tokyo² ○ Tomohiro Taniguchi¹, Yusuke Imai²

近年、スピントロニクス素子を用いた脳型演算の研究が盛んに行われている [1,2,3]。スピントロニクス素子にはエッジ端末にも搭載可能な小型化かつ集積化可能であるという利点や、ニューロンが示す発火などの非線形応答を模倣できるという利点がある。一方で脳内活動のように多数のニューロンが相互作用するような状態を再現することは難しい。そこで近年、連想記憶のような、従来であれば多体系を用意して実行されていた脳型演算を、単一素子の仮想ネットワークで模倣しようという試みが成されている。実際、単一のスピントルク発振素子を用いて白黒の 60 ピクセル画像を連想記憶する試みが 2022 年に報告された [4]。この研究では単一のスピントルク発振素子からの出力を 60 個の部分に分割し、それぞれを 60 個のニューロンからの出力とみなすことで仮想的な多体系を構築している。そしてそれら出力に適当な重みを掛けて線形結合させた信号を再度、スピントルク発振素子に入力し、その応答を再び分割することで、ニューロンの状態を更新する。この動作を繰り返すと、やがて 60 個の分割された出力は互いに同位相もしくは逆位相の同期状態に落ち着き、それが連想したい画像のピクセルの色 (白もしくは黒) と一対一の対応を持つようになることで連想記憶が成立する。我々はその動作原理の理論的根拠について明らかにしてきた [5]。

この単一のスピントルク発振素子による連想記憶に要するエネルギーは従来の多体系の連想記憶のそれと同程度である。しかしそもそもスピントルク発振素子がジュール発熱によるエネルギー損失が大きいことに加え、60 個の仮想ニューロンの状態とみなしている振動データを記憶しておくためにも多くのメモリを要する。そこで本研究では電圧誘起磁気異方性効果によって制御されたスピントロニクス素子によって仮想ネットワークを構築することを提案する [6]。この方法では磁性体の垂直磁気異方性エネルギーの符号を制御することで磁化が垂直もしくは面内の 2 つの状態のどちらかにする。この 2 状態をピクセルの色 (白もしくは黒) に対応させる。スピントロニクス素子に連続して電圧を印可し、出力を 60 個に分割する点ではスピントルク発振素子による連想記憶と似ているが、メモリに記憶しておかなければならない情報は磁化の終状態 (垂直もしくは面内) のみであり、その状態に緩和するまでの過程は必要無い、という点で、スピントルク発振素子による連想記憶に比べ利点がある。また電圧誘起磁気異方性効果によって素子を制御するためジュール発熱が比較的小さいというのも利点である。講演ではこれらアルゴリズムの詳細について説明する。

本講演は科研費 JSPS 20H05655 の支援を受けて行われた。

1. W. A. Borders *et al.*, Appl. Phys. Express **10**, 013007 (2017).
2. J. Torrejon *et al.*, Nature **547**, 428 (2017).
3. K. Kudo and T. Morie, Appl. Phys. Express **10**, 043001 (2017).
4. 常木澄人ら, 第 83 回応用物理学会秋季学術講演会 (講演番号: 20a-M206-2) (2022).
5. Y. Imai and T. Taniguchi, Sci. Rep. **13**, 15809 (2023).
6. T. Taniguchi and Y. Imai, Sci. Rep. **14**, 8188 (2024).

Reservoir Computing Utilizing Transient Dynamics of Spin-Hall Nano-Oscillators

°Aakanksha Sud^{1,5}, Akash Kumar^{2,3}, Maha Khademi⁴, Johan Åkerman^{3,5} and Shunsuke Fukami^{2,5,6,7}

¹FRIS, Tohoku Univ., ²CSIS, Tohoku Univ., ³Univ. of Gothenburg, Sweden, ⁴Chalmers Univ. Of

Technology, Sweden, ⁵RIEC, Tohoku Univ., ⁶CIES, Tohoku Univ., ⁷WPI-AIMR, Tohoku Univ.

E-mail: sud.aakanksha.c3@tohoku.ac.jp

Reservoir computing (RC) [1] is an emerging computational paradigm that leverages the transient dynamics of physical systems to perform complex tasks such as pattern recognition and time-series prediction. In this work, we explore the use of Spin Hall nano-oscillators (SHNOs) [2] as a novel medium for RC. Spin Hall nano-oscillators are nanoscale devices that exploit the Spin Hall Effect to generate and manipulate magnetization oscillations, which can be harnessed for computational purposes.

We present an experimental demonstration of a Physical Reservoir Computing scheme employing a SHNO. By utilizing the dynamic states of the SHNO, we tackle tasks such as waveform classification and prediction, achieving accuracies comparable to state-of-the-art neural networks. Our experiments involve a detailed analysis of the magnetization dynamics, and we pinpoint the specific regime that yields optimal performance. This regime is characterized by a delicate balance between non-linearity and memory capacity, essential for effective reservoir computing. We specify these regimes based on measurements conducted at different magnetic fields, highlighting the influence of magnetic field strength on SHNOs' computational capabilities. Metric calculations are employed to assess the computational effectiveness of our approach. The implications of our findings are significant: they lay the groundwork for developing swift, parallel, and energy-efficient computing systems based on oscillator networks.

Our work suggests that SHNOs can serve as a foundational technology for future advancements in spintronic-based computation, providing a versatile and scalable alternative to conventional electronic processors.

This research contributes to the broader field of neuromorphic computing, highlighting the potential of leveraging physical systems' intrinsic properties for advanced computational tasks. By bridging the gap between spintronics and reservoir computing, we open new avenues for exploring high-performance, low-power computing architectures.

[1] K. Nakajima and I. Fischer, *Reservoir computing* (Springer, 2021).

[2] T. Chen et al, *Proc. IEEE* **104**, 1919-45 (2016).

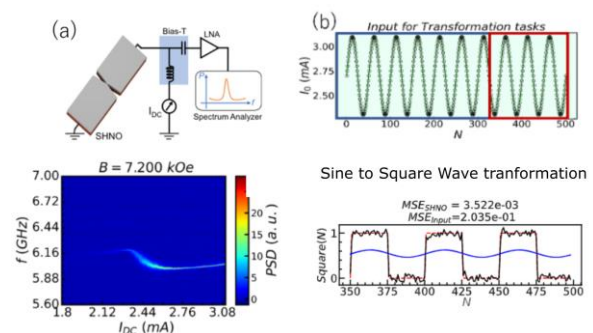


Fig. 1. (a) A schematic illustration of SHNO measurement set-up. The bottom panel of (a) shows 2D plot colorplot of Power Spectral density (PSD) as a function of applied frequency and input current. The measurement is done at different current cycles as shown in (b) and output of PSD spectra is used to form a reservoir. The bottom panel of (b) shows performance of SHNO-RC for a transformation task where a sine wave is converted to square wave.

Investigating the origin of cluster spin glass behavior in low-damped garnet-based ferrimagnet towards neuromorphic computation

Univ. Tokyo, ° (PC) Md Shamim Sarker*, Haining Li, E M K Ikball Ahamed, Hiroyasu Yamahara, Siyi Tang, Zhiqiang Liao, Tetsuya Iizuka, Munetoshi Seki, and Hitoshi Tabata

*E-mail : sarker@g.ecc.u-tokyo.ac.jp

A spin glass (SG) is characterized by a frozen spin state at low temperatures, resulting from competing randomness and frustration of magnetic interactions. This state also demonstrated photoinduced magnetism and an aging memory effect: that is creates a history-dependent property. This unique feature presents an opportunity to replicate the functions of the human brain, leveraging a similar Hamiltonian framework. Our aim is to study the spin dynamics based ultra-low power data carrier (magnon) in the spin glass system at frozen state to implement a reservoir computing system mimicking the ultra-low power operation as human brain. However, the spin frozen state in spin glasses (SG) only manifests at extremely low temperatures, limiting their practical and low-power applications. Consequently, this research primarily aims to explore the potential for developing optimal room temperature spin glass materials by manipulating the disorder within garnet-based ferromagnetic materials. Considering the dynamics of magnetization for further study, we began with yttrium iron garnet (YIG:Y₃Fe₅O₁₂) due to its exceptionally low Gilbert damping constant.

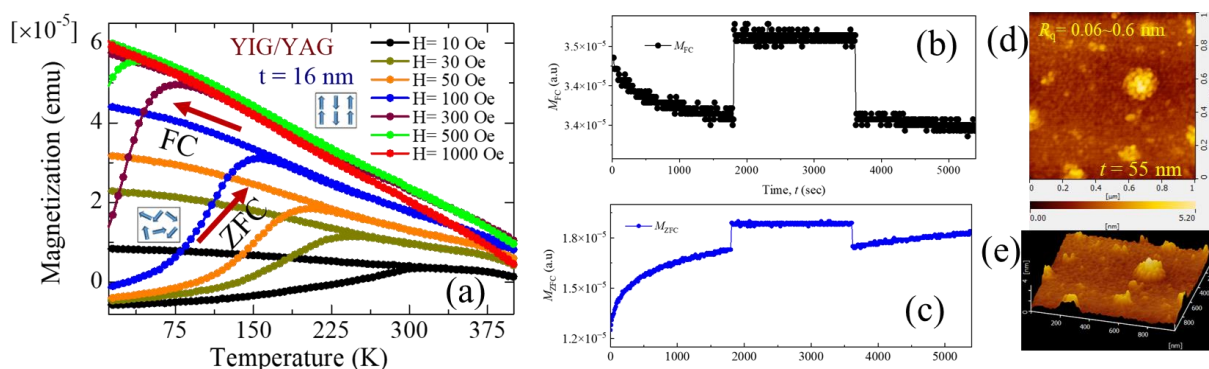


Figure 1. (a) Zero field cooling (ZFC)-Field cooling (FC) behavior under different DC magnetic field in YIG/YAG films. Characteristics of aging memory effect for (b) FC and (c) ZFC. (d) 2D and (e) 3D AFM image of the film surface signifying the surface modification due to crystal dislocation effect.

We have prepared 16 nm thick YIG thin films on the (001)-oriented YAG substrate using pulsed laser deposition. We have investigated field cooling (FC) and zero field cooling (ZFC) properties of the YIG/YAG using standard protocol and have observed the characteristic bifurcation behavior at near room temperature than previous report [1]. From AC susceptibility measurement we calculated the Mydosh parameter as $k = \Delta T_p / T_p \Delta(\log_{10} f) \sim 0.023$ signifying the material as cluster spin glass. We further have confirmed the characteristic aging memory effect for negative heat cycle using standard FC-ZFC protocol which is shown in Figure 1(b) and (c). Magnetization relaxation can be used as the fading memory for reservoir computation. We have identified the dislocation induced defect as the origin of the presence of frustrated spin state in the ferromagnetic YIG film. As the critical thickness of YIG/YAG is less than 10 nm due to large lattice mismatch (2.9%) the film gets relaxed during growth. We have confirmed this by RSM mapping. This film relaxation generates a significant amount of dislocation which can be evident by the extremely rough surface morphology. This film relaxation generates a significant amount of dislocation which can be evident by surface aggregation shown in the atomic force microscopy imaging in Figure 1(d) and (e). These dislocations result in frustrated states which induce the spin freezing effect at room temperature. Further investigation will be conducted using XMCD and STEM measurement to confirm the crystal deformation in terms of orbital momentum and atomic imaging, respectfully.

Acknowledgement

This research was partially supported by Institute for AI and Beyond for the University of Tokyo and JST-CREST Grant Number JPMJCR22O2, Japan. JSPS KAKENHI (Grant Number, 23KF0139).

References

[1] H. Yamahara et al. JMMM, 501, 166437(2020)

10 スピントロニクス・マグネティクス | 一般セッション(口頭講演) : 10.2 スピン基盤技術・萌芽的デバイス技術

[16p-D61-1~13] 10.2 スピン基盤技術・萌芽的デバイス技術

[16p-D61-1]

MgO thickness dependence of the intrinsic Gilbert damping in the V/Fe/MgO multilayer

○(D)Jieyi Chen¹, Shoya Sakamoto¹, Hidetoshi Kosaki¹, Erkang Wei¹, Tempei Hatajiri¹, Shinji Miwa^{1,2} (1.ISSP, Univ. Tokyo, 2.TSQS, Univ. Tokyo)

[16p-D61-2]

Magnetic damping of epitaxial Fe/Pt/MgO and Pt/Fe/MgO multilayers

○(M2)Erkang Wei¹, Shoya Sakamoto¹, Jieyi Chen¹, Hidetoshi Kosaki¹, Tempei Hatajiri¹, Shinji Miwa^{1,2} (1.ISSP-UTokyo, 2.TSQS-UTokyo)

[16p-D61-3]

Magnetic damping of NiFe thin films grown on two-dimensional chiral hybrid lead-iodide perovskites

Tempei Hatajiri¹, Shoya Sakamoto¹, Hidetoshi Kosaki¹, Zikang Tian¹, Miuko Tanaka¹, Toshiya Ideue¹, Keiichi Inoue¹, Daigo Miyajima^{2,3}, ○Shinji Miwa^{1,4} (1.ISSP, Univ. Tokyo, 2.CEMS, RIKEN, 3.CUHK, 4.TSQS, Univ. Tokyo)

[16p-D61-4]

静磁モードスピン波におけるマグノンホール効果の観測

○谷口 卓也¹、Riedel Christian²、Vilsmeier Franz²、岡本 聡^{1,3,4}、Back Christian² (1.東北大、2.ミュンヘン工科大、3.東北大CSIS、4.NIMS)

[16p-D61-5]

イットリウム鉄ガーネットを用いた完全バンドギャップを示す二次元マグノンニック結晶

○後藤 太一¹、森 冠太¹、渡邊 聡明²、高口 拓己¹、宮下 響¹、井上 光輝¹、石山 和志¹ (1.東北大通研、2.信越化)

[16p-D61-6]

Dynamic control of spin wave propagation by electric field in space inversion symmetry broken Iron Oxide Garnet thin films

○(D)EMK IKBALL AHAMED¹, Md Shamim Sarker¹, Hiroyasu Yamahara¹, Haining Li¹, Siyi Tang¹, Munetoshi Seki¹, Hitoshi Tabata¹ (1.Univ. of Tokyo)

[16p-D61-7]

Magnonic Band Gap Control by The Wall Width Modulation in a 1D Magnonic Crystal

○Taisuke Horaguchi¹, Yuma Takeda¹, Takushi Manago¹ (1.Fukuoka Univ.)

[16p-D61-8]

Enhanced non-linear growth of magnon transconductance in a Bi-doped YIG with a perpendicular anisotropy

○河野 竜平¹、Kyongmo An¹、Eric Clot¹、Vladimir Naletov¹、Nicolas Thiery¹、Laurent Vila¹、Richard Schlitz²、Nathan Beaulieu³、Jamal Ben Youssef³、Abdelmadjid Anane⁴、Vincent Cros⁴、Hugo Merbouche⁴、Thomas Hauet⁵、Vlad Demidov⁶、Sergej Demokritov⁶、Gregoire de Leubens⁴、Olivier Klein¹ (1.グルノーブル・アルプ大、2.スイス連邦工科大学チューリッヒ校、3.ブルターニュ・オキシダンタル大、4.パリ・サクレ大、5.ロレーヌ大、6.ミュンスター大)

[16p-D61-9]

Magnetoelastic transmission of surface acoustic-waves on a YIG/GGG substrate

○Daiki Hatanaka¹, Motoki Asano¹, Megumi Kurosu¹, Yoshitaka Taniyasu¹, Hajime Okamoto¹, Hiroshi Yamaguchi¹ (1.NTT BRL)

[16p-D61-10]

Anomalous Nernst effect in Fe/Au/Fe trilayers

○(D)JUNUEI CHAN¹, BOWEN QIANG¹, Toshio Miyamachi¹, Masaki Mizuguchi¹ (1.Nagoya university)

[16p-D61-11]

Thickness dependence of the anomalous Nernst effect in Co thin films studied by local laser heating

○Soichiro Mochizuki¹, Itaru Sugiura², Tetsuya Narushima¹, Teruo Ono², Takuya Satoh¹, Kihiro Yamada¹ (1.Tokyo Tech, 2.Kyoto Univ.)

[16p-D61-12]

熱流センシングのためのGd-Co合金における異常ネルンスト効果

○田辺 賢士¹、小田切 美穂¹、今枝 寛人¹、Yagmur Ahmet^{1,2}、黒川 雄一郎³、鷲見 聡¹、栗野 博之¹ (1.豊田工大、2.リーズ大、3.九大)

[16p-D61-13]

複合構造を利用した高感度異常ネルンスト型熱流センサの無磁場動作

○(M2)今枝 寛人¹、樋田 怜史¹、竹内 恒博¹、栗野 博之¹、田辺 賢士¹ (1.豊田工大)

MgO thickness dependence of the intrinsic Gilbert damping in the V/Fe/MgO multilayer

ISSP-UTokyo¹, TSQS-UTokyo²

°Jieyi Chen¹, Shoya Sakamoto¹, Hidetoshi Kosaki¹, Erkang Wei¹, Tempei Hatajiri¹, and Shinji Miwa^{1,2}

E-mail: jieyi@issp.u-tokyo.ac.jp

The Gilbert damping constant is associated with the spin current generation via the spin-pumping effect [1], and materials with strong spin-orbit coupling, such as *5d* heavy metals, are usually studied. Recently, materials with weak spin-orbit coupling have attracted attention in the emerging field of orbital current physics [3-4]. Previously, we observed that the *effective* Gilbert damping of the V/Fe/MgO multilayer is controlled by the V and MgO thickness [2]. However, the influence of the V and MgO thickness on the *intrinsic* Gilbert damping needs to be elucidated. In this study, we carefully characterized the intrinsic Gilbert damping of the V/Fe/MgO multilayer.

We fabricated epitaxial V/Fe/MgO multilayers using molecular beam epitaxy [Fig. 1(a)]. The magnetization dynamics were characterized by the time-resolved magneto-optical Kerr effect (TR-MOKE). The setup of the TR-MOKE system and the measured magnetization dynamic for MgO 0.2 and 0.5 nm thickness are shown in Fig. 1(b) and 1(c). We found that not only the effective but also the intrinsic Gilbert damping is modulated by variations in MgO thickness. The relationship between the intrinsic Gilbert damping of Fe and the perpendicular magnetic anisotropy at the Fe/MgO interface will be discussed.

This work was partly supported by JSPS KAKENHI (Grants Nos. JP22H00290, JP22H04964, JP22K18320, and JP23H01833), Spin-RNJ, JST-Mirai Program (JPMJMI20A1), JST-ASPIRE (No. JPMJAP2317), X-NICS (No. JPJ011438), and JST-SPRING (No. JPMJSP2108).

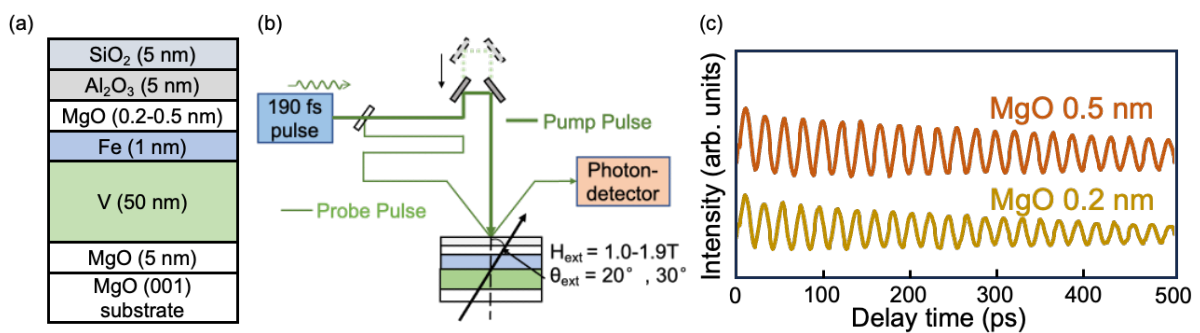


Fig. 1. (a) Schematic of the multilayers. (b) Setup of the TR-MOKE. (c) Magnetization dynamics of Fe/MgO (0.2 nm) and Fe/MgO (0.5 nm).

- [1] S. Mizukami *et al.*, Phys. Rev. B **66**, 104413 (2002).
- [2] J. Chen *et al.*, *The 71st JSAP Spring Meeting*, 23a-12D-6, Tokyo, 2024, 3 (2024).
- [3] H. Hayashi *et al.*, Commun. Phys. **6**, 32 (2023).
- [4] Y.-G. Choi *et al.*, Nature **619**, 52 (2023).

Magnetic damping of epitaxial Fe/Pt/MgO and Pt/Fe/MgO multilayers

ISSP-UTokyo¹, TSQS-UTokyo²

Erkang Wei¹, Shoya Sakamoto¹, Jieyi Chen¹, Hidetoshi Kosaki¹, Tempei Hatajiri¹, Shinji Miwa^{1,2}

E-mail: erkang@issp.u-tokyo.ac.jp

The magnetic damping parameter is of great importance in magnetic dynamics. Damping enhancement is observed in ferromagnet/non-magnetic metal multilayers [1] and is well explained by the spin-pumping model [2]. Non-magnetic heavy metals such as Pt have been extensively studied and have been shown to largely enhance the damping of the ferromagnet [3-4]. In our research, we investigate both thickness and sequence dependence to study the intrinsic and extrinsic damping in Fe/Pt systems.

We fabricate V/Fe/Pt/MgO and V/Pt/Fe/MgO multilayer using molecular beam epitaxy method. The sample schematic is shown in Fig. 1(a). The damping is measured using the time-resolved magneto-optical Kerr effect (TRMOKE). The TR-MOKE schematics is shown in Fig. 1(b). Pump light is normally incident on the sample to induce demagnetization in the ferromagnet. Probe light detects the Kerr rotation, and the time-dependent oscillation is shown in Fig. 1(c). We find that both the effective and intrinsic damping constants of Fe/Pt/MgO are much larger than those of Pt/Fe/MgO. The difference could originate from the difference in interface condition between Fe/Pt and Pt/Fe.

This work was partly supported by JSPS KAKENHI, Spin-RNJ, JST-Mirai Program, JST-ASPIRE, and X-NICS.

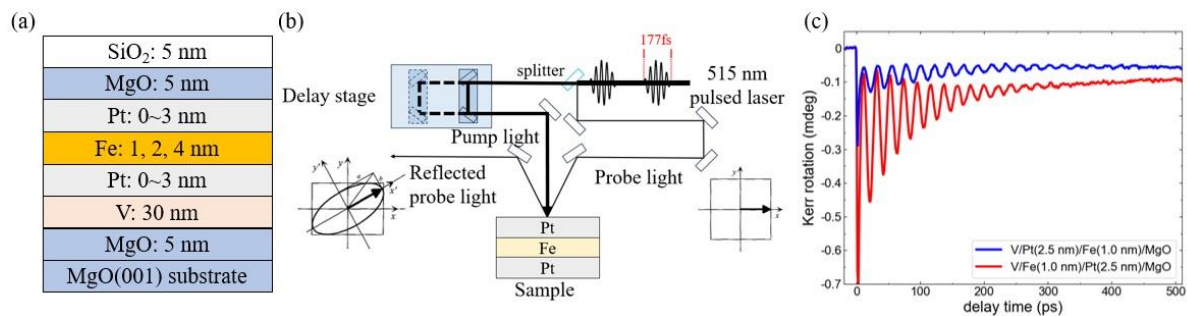


Fig. 1 (a) Sample schematics. (b) Time-resolved magneto-optical Kerr effect measurement schematics. (c) Typical TR-MOKE oscillation pattern with same Pt thickness but different stacking order.

References

- [1] S. Mizukami *et al.*, Jpn. J. Appl. Phys. **40**, 580 (2001).
- [2] Y. Tserkovnyak *et al.*, Phys. Rev. B **66**, 224403 (2002).
- [3] S. Azzawi *et al.*, Phys. Rev. B **93**, 054402 (2016).
- [4] C. Swindells *et al.*, Phys. Rev. B **99**, 064406 (2019).

Magnetic damping of NiFe thin films grown on two-dimensional chiral hybrid lead-iodide perovskites

東大物性研¹, 理研 CEMS², 香港中文大³, 東大 TSQS⁴

畑尻 天平¹, 坂本 祥哉¹, 甲崎 秀俊¹, Zikang Tian¹, 田中 未羽子¹, 井手上 敏也¹,
井上圭一¹, 宮島大吾^{2,3}, 〇三輪 真嗣^{1,4}

ISSP-UTokyo¹, CEMS-RIKEN², CUHK³, TSQS-UTokyo⁴

T. Hatajiri¹, S. Sakamoto¹, H. Kosaki¹, Z. Tian¹, M. Tanaka¹, T. Ideue¹,

K. Inoue¹, D. Miyajima^{2,3}, and 〇S. Miwa^{1,4}

E-mail: miwa@issp.u-tokyo.ac.jp

Spin polarization in chiral molecules, extensively explored under the framework of chirality-induced spin selectivity (CISS), has attracted significant attention in recent research [1]. Predominantly, CISS investigations have utilized system incorporating electric current, typically through a two-terminal device that combines a chiral molecule with a ferromagnetic metal. A notably perplexing issue is the observed substantial variance in magnetoresistance ratios between spin-polarized conductive atomic force microscopy measurements and multilayer device assessments, despite using identical material systems [2]. Because this discrepancy might be linked to pinholes within multilayer film devices, in this study, we investigated CISS-related phenomena in the absent of electric current injection into chiral molecules.

Our approach involves a bilayer system composed of two-dimensional chiral hybrid lead-iodide perovskite ((*R*)-(+)- or (*S*)-(–)- α -methylbenzylammonium lead iodide ((*R*- or *S*-MBA)₂PbI₄)) [2] (Fig 1(a)) and NiFe, where spin pumping facilitates the pure spin current injection into chiral molecules. The process is analyzed by evaluating the magnetic damping constant of NiFe using the time-resolved magneto-optical Kerr effect (TRMOKE) as shown in Fig. 1(b).

This work was partially supported by JSPS-KAKENHI, Spin-RNJ, X-NICS, and CURE.

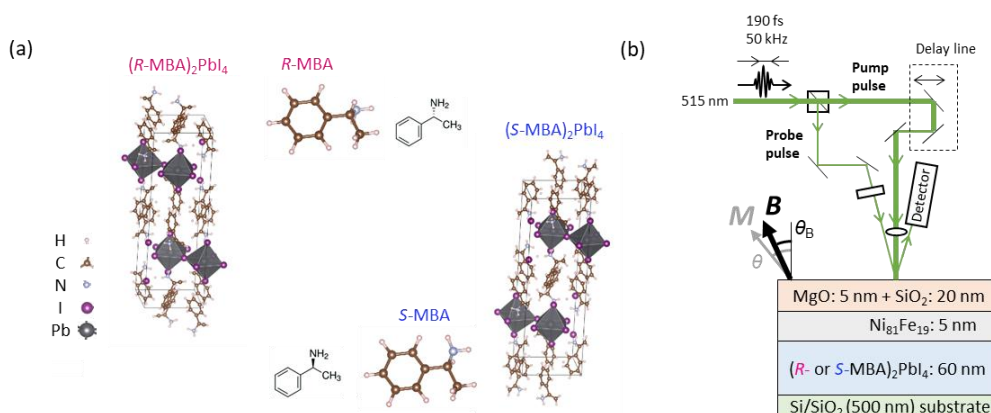


Fig. 1 **a**, Structure of chiral hybrid lead-iodide perovskites. **b**, Schematic of the experimental setup.

[1] R. Naaman *et al.*, Nat. Rev. Chem. **3**, 250 (2019). [2] H. Lu *et al.*, Sci. Adv. **5**, eaay0571 (2019).

静磁モードスピン波におけるマグノンホール効果の観測

Observation of the magnon Hall effect of magnetostatic spin waves

○谷口卓也¹, Christian Riedel², Franz Vilsmeier², 岡本聡^{3,4}, Christian Back²

Tohoku Univ.¹, TU Munich², Tohoku Univ. CSIS³, NIMS⁴, ○Takuya Taniguchi¹, Christian Riedel²,

Franz Vilsmeier², Satoshi Okamoto^{3,4}, Christian Back²

E-mail: takuya.taniguchi.c1@tohoku.ac.jp

スピン波の準粒子であるマグノンに対するホール効果は、マグノンホール効果と呼ばれ、ジャロシンスキー・守谷相互作用によって発現することが実験的に報告された[1]。その後、理論研究によりジャロシンスキー・守谷相互作用が存在しない系においても面直磁場下で励起された静磁モードスピン波に対してマグノンホール効果が発現し得ることが予言された[2]。しかし、不完全に面直磁化した YIG を用いた静磁スピン波のマグノンホール効果は観測されているものの、磁場方向に依存した熱勾配のみが観測されており、静磁スピン波におけるマグノンホール効果の立証には至っていなかった[3]。本研究では、電気測定や光学測定により静磁モードスピン波におけるマグノンホール効果の観測を試みた。

実験には、GGG 基板上に液相成長した YIG(200 nm)薄膜を幅 6 μm の細線状に加工した試料を用いた。同試料を面直磁化させた後交流磁場によりスピン波を励起し、スピン波の伝播過程を時間分解磁気光学 Kerr 顕微鏡 (TR-MOKE) によって観測した (図 1a)。その結果、磁場方向が同じ場合には磁場の大きさに依存してスピン波の波長のみが変化する一方で、磁場方向を反転するとスピン波の波面が大きく変化することが明らかになった。本講演では、マイクロマグネティックシミュレーションや電気測定の結果も併せて議論する。

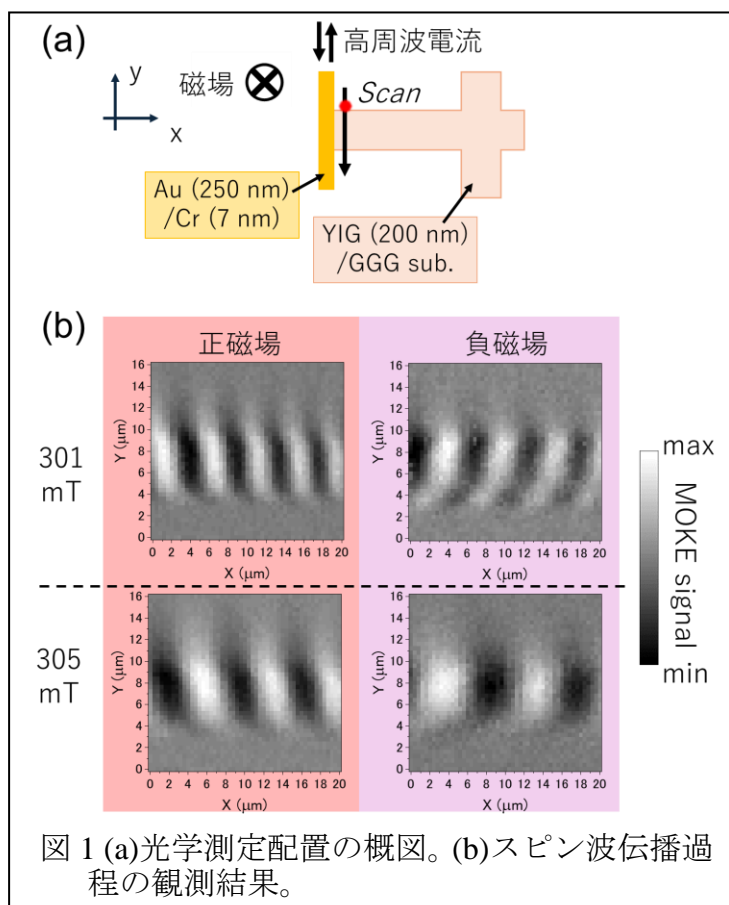


図 1 (a)光学測定配置の概図。(b)スピン波伝播過程の観測結果。

[1] Y. Onose *et al.*, Science **329**, 297 (2010). [2] R. Matsumoto and S. Murakami, Phys. Rev. Lett. **106**, 197202 (2011). [3] K. Tanabe *et al.*, Phys. Status Solidi B **253**, 783 (2016).

イットリウム鉄ガーネットを用いた 完全バンドギャップを示す二次元マグノニック結晶

Two-Dimensional Magnonic Crystals Exhibiting Complete Band Gaps

Using Yttrium Iron Garnets

○後藤 太一^{1,*}, 森 冠太¹, 渡邊 聡明², 高口 拓己¹, 宮下 響¹, 井上 光輝¹, 石山 和志¹

(¹東北大通研, ²信越化)

○Taichi Goto^{1,*}, Kanta Mori¹, Toshiaki Watanabe², Takumi Koguchi¹,

Hibiki Miyashita¹, Mitsuteru Inoue¹, Kazushi Ishiyama¹

(¹RIEC, Tohoku Univ., ²Shin-Etsu Chem.)

E-mail: * taichi.goto.a6@tohoku.ac.jp

1. 背景

スピン波デバイスは、位相干渉を利用したロジック回路などが開発され、次世代の波動型情報処理デバイスとして注目されている[1,2]。このスピン波を使った集積回路を実現するには、スピン波を回路内で自在に操作できる技術、いわゆるスピン波配線が必須である。このために、理論的にスピン波の伝搬制御が予想されている二次元マグノニック結晶に着目し、開発を進めている[3,4]。しかし、バンドギャップ幅が狭く、膜面内のいずれの方向へもスピン波の伝搬を許さない完全バンドギャップの発現には至っていない現状にある。そこで、本研究では、完全バンドギャップを発現可能な二次元マグノニック結晶を探した。

2. 計算方法・結果

Fig. 1 に示すような六方格子状に、イットリウム鉄ガーネット (YIG) 上の金膜に穴を開けた構造について調べた。すべての穴は互いに空隙によって繋がった。穴直径 d 、空隙幅 g を変化した本構造体の三次元モデルを計算機上で再現し、有限積分法を用いてスピン波伝搬特性を計算した。この結果、従来研究 [3] よりもマグノニックバンドギャップ幅が広がった。スピン波入射角度の依存性を調べたところ、入射角

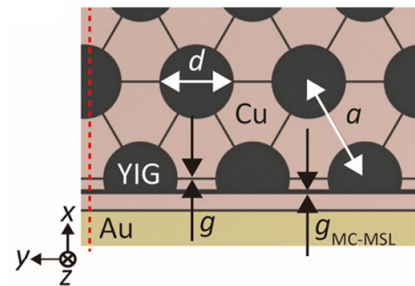


Fig. 1. Two-dimensional magnonic crystal with a hexagonal lattice structure. A gold film with holes covered a 10 μm thick YIG film. All holes were connected with g-gap slits. The hole diameter is d , and the gap between the magnonic crystal and microstrip line is $g_{\text{MC-MSL}}$.

度 0 度から 30 度の範囲で、 -20dB 以上のスピン波透過率スペクトルが局所的に減少するバンドギャップが重なることが確認できた。すなわち、構造の対称性から、完全バンドギャップが生じることが分かった。

3. まとめ

六方格子状に穴の空いた金属膜を YIG 上に作製することで完全バンドギャップを発現可能な二次元マグノニック結晶となることを示した。

[1] T. Goto, et al, Sci. Rep., **9**, 16472 (2019).

[2] 後藤太一, 応用物理, **90**, 172, (2021).

[3] K. Mori, et al., Phys. Rev. Appl., **21**, 014061, (2024).

[4] T. Goto, et al., Phys. Rev. Appl., **11**, 014033 (2019).

Dynamic control of spin wave propagation by electric field in space inversion symmetry broken Iron Oxide Garnet thin films

Univ. Tokyo¹, ^o (D) EMK Ikball Ahamed^{1*}, Md Shamim Sarker¹, Hiroyasu Yamahara¹,
Haining Li¹, Siyi Tang¹, Munetoshi Seki¹, Hitoshi Tabata¹

*E-mail: ahamedikball@g.ecc.u-tokyo.ac.jp

The aim of this study is to control spin wave propagation in Rare-earth Iron Garnet (RIG) thin films by the electric field. Due to the existence of cubic inversion symmetry in garnets, the electromechanical and electromagnetic coupling effects are very small. To overcome this weakness, we have broken the spatial inversion symmetry by introducing long-range strain gradient, which allows the coexistence of magnetic and electric dipole polarizations due to the Flexoelectricity effect [1]. We fabricated 85 nm and 120 nm-thick $\text{Y}_3\text{Fe}_5\text{O}_{12}$ (YIG, 12.376Å bulk) thin films on lattice matched $\text{Ga}_3\text{Gd}_5\text{O}_{12}$ (GGG, 12.38Å) and ~1% lattice mismatched $\text{Gd}_{2.6}\text{Ca}_{0.4}\text{Ga}_{4.1}\text{Mg}_{0.25}\text{Zr}_{0.65}\text{O}_{12}$ (SGGG, 12.50Å) substrates by pulsed laser deposition (PLD) technique. X-ray diffraction (XRD) and reciprocal space mapping (RSM) revealed strained epitaxy indicating that the in-plane lattice of YIG is matched with GGG and elongated to align with SGGG (Fig.1(a)). X-ray absorption spectroscopy (XAS) and X-ray magnetic circular dichroism (XMCD) were measured at room temperature and magnetic moments were calculated using the XMCD sum rule (fig. 1(b)-(c)) and found low orbital moment in YIG/GGG indicates low crystal distortion. However, large orbital momentum of 0.15 in YIG/SGGG films indicates the quenching of orbital moment sum is alleviated by the reduction of crystal symmetry from cubic to tetragonal. Finally, Au co-planner waveguides (CPWs) and Pt interdigital electrodes were fabricated by photolithography and sputtering techniques as in Fig.1(d). Spin wave transmission characteristics was measured using vector network analyser (VNA) with microwave techniques. Fig.1(e) summarizes the shift in spin wave transmission resonance frequency (Δf) as a function of the electric field (E). In tensile strained YIG (120nm)/SGGG, the spin wave transmission spectra exhibit a significant rightward shift with the application of an electric field, whereas a similar investigation on lattice-matched YIG (120nm)/GGG samples subjected to a large electric field of up to 800kV/cm showed a very small response. It is expected that the SW frequency shift is originated from the electrical response of the polarized domains in tensile strained RIG thin films that eventually modulates the magnetic anisotropy of insulating thin films via spin orbit coupling. This dynamic magnon control by electric field will represent a groundbreaking advancement in magnonics, offering the potential for implementing low-power consumption logic devices through the utilization of the spin wave.

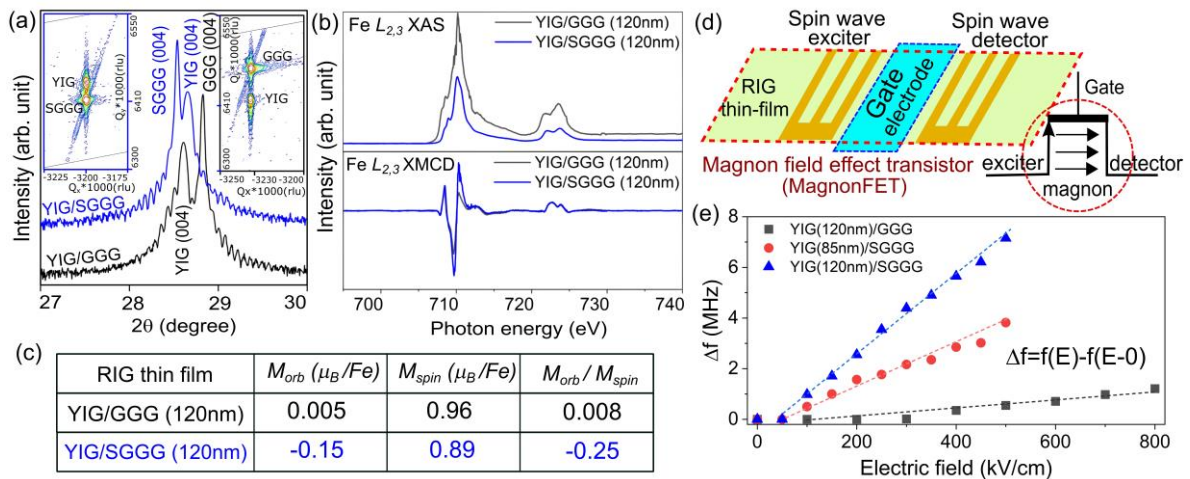


Fig. 1. (a)-(c) Structural and magnetic properties of lattice matched YIG/GGG (001) and tensile strained (~1%) YIG/SGGG (001) thin films, (a) XRD 2θ - ω scan (inset: RSM), (b) XAS and XMCD, (c) moments calculated from XMCD sum rule, (d) schematic of fabricated spin wave devices on RIG thin films (e) spin wave transmission resonance frequency shift [$\Delta f(E) = f_{res}(E) - f_{res}(E=0)$] versus applied electric field (E)

This research was supported by Institute for AI and Beyond for the University of Tokyo, JST, CREST Grant Number JPMJCR2202, Japan, AMED under Grant Number JP22zf0127006, JSPS KAKENHI Grant Number JP20H05651, JP22K18804, JP23H04099. XMCD was Measured in BL25SU X-ray beam line at SPring-8. We are very grateful to Professor Kinoshita and Dr. Yamagami for their support and help.

References: (1) H. Yamahara. et al., *Comm. Mater.* 2, 95 (2021)

Magnonic Band Gap Control by The Wall Width Modulation in a 1D Magnonic Crystal

Fukuoka Univ., °Taisuke Horaguchi, Yuma Takeda, Takushi Manago

E-mail: t.horaguchi@fukuoka-u.ac.jp

【Background and Objective】

Spin waves (SWs), which are waves of precessional motion of magnetization propagating through magnetic materials, have been actively studied as a novel medium for data transport and processing. In homogeneous magnetic materials, the band structure of SWs is determined by material parameters such as saturation magnetization and exchange stiffness constant, which limits the controllability of the band structure. However, in magnetic materials with artificially introduced micro-periodic structures (magnonic crystals: MC), the propagation of SWs can be selectively controlled by wavenumber. The potential for the versatile applicability for new magnetic logic devices [1] has stimulated active researches on MC.

In a one-dimensional MC with periodic walls along the x -axis, as shown in Fig. 1(a), the propagation of SWs with wavelengths close to the structural period is suppressed, resulting in a band gap (BG) within the band structure [2]. However, the detailed relationship between the structure of the MC and the central frequency or width of the BG remains unclear. Therefore, this study aims to control the spin wave band structure through structure modulation by using micromagnetic simulations to investigate the correlation between the wall width w and the band structure.

【Calculation Model and Results】

We calculated the spin wave propagation in MCs with various wall widths w and clarified the band structures of each MC by performing FFT processing on the spatial distribution and time evolution of magnetization. We assumed the application of a static magnetic field in the y -direction and an impulse magnetic field for spin wave excitation, setting the conditions to excite the MSSW mode.

Figure 1(b) shows the calculated band structures for MCs with $w = 0.2, 1.0, 1.8 \mu\text{m}$. The period of one set of wall and valley was fixed at $2.0 \mu\text{m}$. It was found that the central frequency f_{BG}^{1st} of the 1st. band gap around $k \approx \pi/2 \mu\text{m}^{-1}$ was increased with the wall width, and the BG width maximized at $w = 1.0 \mu\text{m}$. This increase in f_{BG}^{1st} can be related to the increase in the average thickness of the MC. Interestingly, we additionally found that the width of the 2nd. BG around $k \approx \pi \mu\text{m}^{-1}$ varied periodically with w . We will discuss the detailed wall width dependency within the range $0.2 \mu\text{m} \leq w \leq 2.0 \mu\text{m}$.

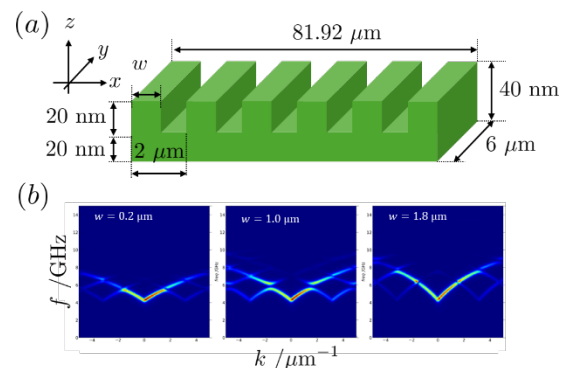


Figure 1 (a) Schematic image of 1D magnonic crystal. (b) Band structures of spin waves for MCs with $w = 0.2, 1.0$, and $1.8 \mu\text{m}$. The simulations were performed by mumax³[3] and python.

References: [1] A. V. Chumak *et al.*, Nat. Commun. **5**, 4700(2014). [2] S. A. Nikitov *et al.*, JMMM **236**, 320–330 (2001). [3] A. Vansteenkiste *et al.*, AIP Adv. **4**, 107133(2014).

Enhanced non-linear growth of magnon transconductance in a Bi-doped YIG with a perpendicular anisotropy

R. Kohno^{1*}, K. An¹, E. Clot¹, V. V. Naletov¹, N. Thiery¹, L. Vila¹, R. Schlitz², N. Beaulieu³, J. Ben Youssef³, A. Anane⁴, V. Cros⁴, H. Merbouche⁴, T. Hauet⁵, V.E. Demidov⁶, S.O. Demokritov⁶, G. de Leubens⁷, and O. Klein¹

¹Université Grenoble Alpes, CEA, CNRS, Grenoble INP, Spintec, Grenoble, France

²Department of Materials, ETH Zürich, Zürich, Switzerland

³Lab-STICC, CNRS, Université de Bretagne Occidentale, Brest, France

⁴Unité Mixte de Physique, CNRS, Thales, Université Paris Saclay, Palaiseau, France

⁵Université de Lorraine, CNRS Institut Jean Lamour, Nancy, France

⁶Department of Physics, University of Münster, Münster, Germany

⁷SPEC, CEA-Saclay, CNRS, Université Paris-Saclay, Gif-sur-Yvette, France

*E-mail: ryohei.kohno.d4@tohoku.ac.jp

Spin wave, or its quanta magnon, is expected to be an efficient information carrier flowing in an insulating media alternative to electrical charge current that has Joule loss. To realize functional magnonic circuits, non-linear transport behavior of magnons is essential considering that semiconductor diodes revolutionized our society. In fact, magnons do show such behavior, however it suffers from an intrinsic limitation, i.e., a saturation of non-linear growth of magnon transconductance due to magnon-magnon scattering process, as we reported in the previous JSPS meeting (19a-A201-2). Using non-local devices consisting of two parallel Pt electrodes deposited on (Bi-doped) YIG films as shown in Fig.1(inset)[1-4], we experimentally report two times more enhancement of non-linear growth of magnon transconductance in a Bi-doped YIG with a perpendicular anisotropy compared to that in a normal YIG[5,6] (Fig1(a) and (b)).

The motivation comes from the fact that in in-plane magnetized systems, the magnetic precession in a thin film follows an elliptic orbit due to the demagnetizing field, which induces twice the frequency of longitudinal oscillating magnetization along the equilibrium axis. This cause additional channel of the magnon interaction (three-magnon scattering process). By using a material with a perpendicular uniaxial anisotropy, it can compensate the demagnetizing field and thus reduces the magnon interaction, which increase the upper limit of the saturation.

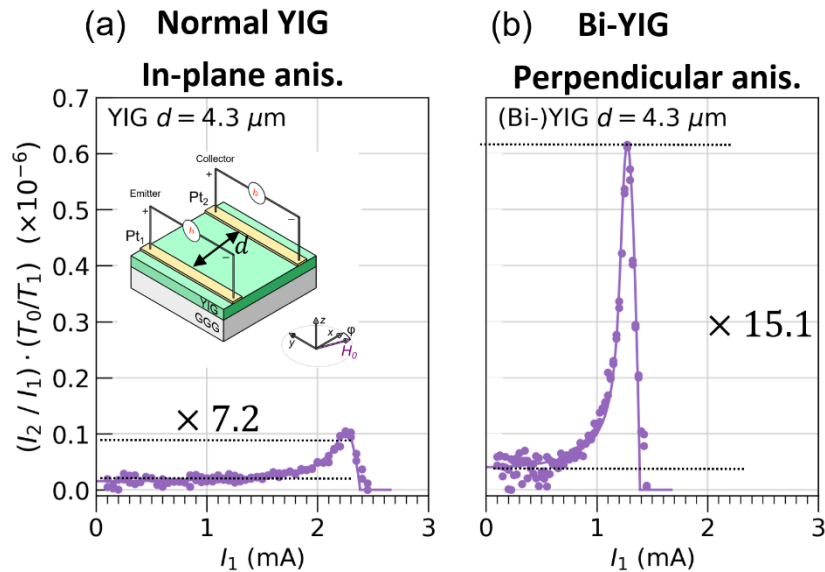


Fig.1: Magnon transconductance in (a) YIG and (b) Bi-doped YIG films in a non-local device (inset)

[1] L. J. Cornelissen *et.al.*, *Nat. Phys.* (2015), [2] Y. Kajiwara *et.al.*, *Nature* (2010), [3] S.T.B. Goennenwein *et.al.*, *Appl. Phys. Lett.* (2015), [4] M. Althammer, *Phys. Status Solidi rapid research letters* (2021), [5,6] R. Kohno *et.al.*, *Phys. Rev. B* 108, 144410 (Paper I) and 144411 (PartII)

Magnetoelastic transmission of surface acoustic-waves on a YIG/GGG substrate

○D. Hatanaka, M. Asano, M. Kurosu, Y. Taniyasu, H. Okamoto, and H. Yamaguchi

NTT Basic Research Laboratories

e-mail: daiki.hatanaka@ntt.com

Magnon polarons, which are coupled excitations between magnons and phonons, enable their advanced controls such as magnetically tunable and nonreciprocal phonon propagations, as well as improved coherence of magnons. These capabilities hold promise for extending the functionality of conventional magnonic and phononic systems in microwave information processing applications. However, the generation of magnon polarons, specifically the strong coupling between magnons and phonons, has been reported only in bulk acoustic wave-based systems [1,2]. Inspired by recent experimental efforts to demonstrate this coupling using planar magnomechanical platforms [3,4], we fabricated a surface acoustic wave (SAW) system on a YIG/GGG substrate. We investigated the interaction between highly coherent resonant spin and acoustic waves at room temperature.

The device consists of piezoelectric interdigitated transducers (IDTs) made from aluminum nitride (AlN) and is constructed on a YIG/GGG substrate, as shown in Fig. (a). Surface acoustic waves (SAWs) generated from one IDT travel through the YIG film, where they interact magnetostriictively with magnons (spin waves). The frequency response of the SAW transmission ($|S_{21}|^2$) at 1.16 GHz is measured from the other IDT while sweeping the strength of an external magnetic field ($\mu_0 H_{ex}$) applied parallel to the SAW direction, as shown in Fig. (b). Multiple absorption dips appeared in the S_{21} , and especially at ± 43 mT, avoided-crossing peak repulsions with large absorption windows were observed. The observed field dependence of the SAW transmission spectrum shows the feature of coherent transduction between high-quality magnons and phonons, which will lead to the realization of strongly coupled planar magnomechanical systems. In the presentation, we will also discuss the underlying mechanism of our observations.

This work was partially supported by JSPS KAKENHHI Grant Number JP21H05020, JP23H05463, and JP24H02235.

[1] T. Kikkawa et al., Phys. Rev. Lett., 117, 207203 (2016). [2] V. J. Gokhale et al., IEEE Trans. Ultra. Ferr. Freq. Contr., 70, 8 (2023). [3] D. Hatanaka et al., Phys. Rev. Appl., 17, 034024 (2022). [4] Y. Hwang et al., Phys. Rev. Lett., 132, 056704 (2024).

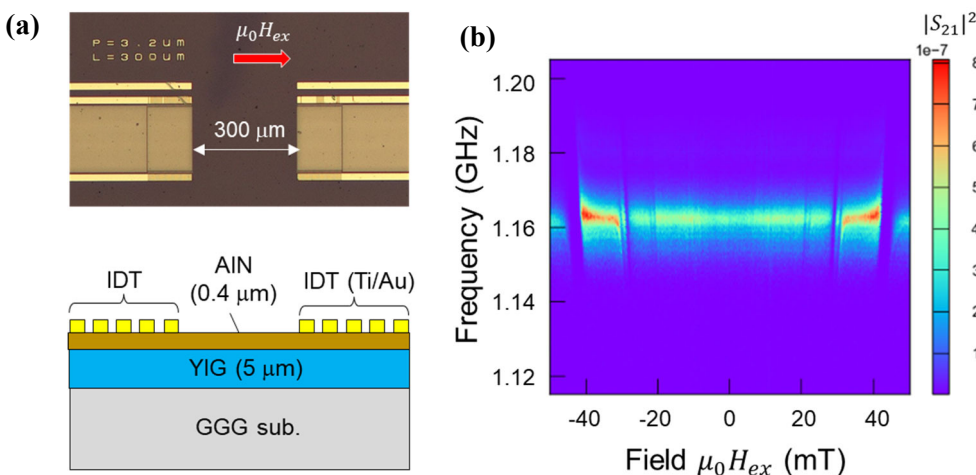


Fig. (a) Schematic of YIG-based SAW magnomechanical system and its film structure. **(b)** Field ($\mu_0 H_{ex}$) dependence of SAW transmission $|S_{21}|^2$.

Anomalous Nernst effect in Fe/Au/Fe trilayers

Nagoya Univ., °(D)Junwei Zhang, Bowen Qiang, Toshio Miyamachi, and Masaki Mizuguchi

E-mail: mizuguchi.masaki@material.nagoya-u.ac.jp

Introduction

The anomalous Nernst effect (ANE), one of the thermoelectric effects in a magnet, is recently attracting growing interest as it has great potential for the next generation of high-efficiency energy harvesting applications^[1]. However, reported thermopower of ANE is not enough for the applications to date. Thus, it is important to design a new class of materials that exhibit a large ANE. It has been reported that the ANE is enhanced by employing multilayer structures^[2]. In addition, the interlayer exchange coupling (IEC) is also interesting phenomenon in multilayer structures. Therefore, we are studying the effect of IEC on ANE in multilayer structures with different thicknesses of nonmagnetic spacer layer. In this contribution, the relationship between the AHE, ANE and IEC in Fe/Au/Fe trilayers is studied.

Research method

Fe/Au/Fe trilayers with several thicknesses of Au layer were prepared by using a magnetron sputtering. A Physical Property Measurement System (PPMS) was used for the measurement of magnetoresistance (MR), AHE and ANE. MR was measured by applying a direct current of 0.1 mA at room temperature to estimate saturation magnetic field. AHE and ANE were also measured by applying an external magnetic field of -50,000 to 50,000 Oe along the out-of-plane direction to samples.

Results

All the Fe/Au/Fe thin films with different Au thicknesses exhibited the AHE, ANE and IEC. With the change of the thickness of Au, the change of magnitude of the AHE and ANE was also observed. This implies that IEC affects the ANE and AHE. Relation between the ANE and the magnetization configuration will be also discussed in detail.

References

- [1] M. Mizuguchi *et al.*, Sci. Tech. Adv. Mater., **20**, 262 (2019).
- [2] K. Uchida *et al.*, Phys. Rev. B, **92**, 094414 (2015).

Thickness dependence of the anomalous Nernst effect in Co thin films studied by local laser heating

Soichiro Mochizuki¹, Itaru Sugiura², Tetsuya Narushima¹, Teruo Ono²,
Takuya Satoh¹, and Kihiro T. Yamada¹

¹ Department of Physics, Tokyo Institute of Technology, Tokyo 152-8551, Japan

² Institute for Chemical Research, Kyoto University, Uji, Kyoto 611-0011, Japan

The anomalous Nernst effect (ANE) generates electromotive forces orthogonal to thermal gradients and magnetizations. Whereas the ANE is quantitatively studied using homogeneous thermal gradients prepared by heaters [1], local heating by laser irradiations is mainly used to visualize local magnetizations through the ANE [2]. In this research, we would like to demonstrate the usefulness and limitations of local heating by laser irradiations for the quantitative study of the ANE.

Here, we report the thickness dependence of ANE induced by laser irradiation in Co thin films with various thicknesses. Because the laser intensity exponentially decays within tens of nanometers, the thickness dependence is suitable for testing the method's effectiveness. We fabricated magnetic bilayers with structures of Ru(5 nm)/ Co(*t*) (*t* = 3, 5, 7, 10, 20, 40, 60 nm) on sapphire (0001) substrates at room temperature by dc sputtering. These magnetic thin films were processed to Hall devices with a size of 0.4 mm × 0.4 mm by a standard photolithography technique. A green continuous wave laser beam was focused with a radius of 15 μm on the center of the Hall cross to create the thermal gradient in the thickness direction. The laser intensity was set at 70 mW and modulated at 85 kHz. We measured laser-induced electric voltages orthogonal to an in-plane magnetic field of ±800 Oe [3]. Furthermore, thermal gradients were simulated using a finite element method with COMSOL Multiphysics equipped with the wave optics module. The peak amplitude of the calculated anomalous Nernst coefficient (Q_{ANE}) is 0.015 μV/(K·T). The calculated values of Q_{ANE} are of the same order of magnitude as those in a quantitative previous study using homogeneous thermal gradients [4]. In this presentation, we would like to show more experimental details and discuss the results.

References

- [1] K. Uchida et al., Phys. Rev. B **92**, 094414 (2015).
- [2] M. Weiler et al., Phys. Rev. Lett. **108**, 106602 (2012).
- [3] S. Mochizuki et al., 2023 IEEE International Magnetic Conference - Short Papers (INTERMAG Short Papers), Sendai, Japan, 2023, pp. 1-2, doi: 10.1109/INTERMAGShortPapers58606.2023.10308523.
- [4] T. C. Chuang et al., Phys. Rev. B **96**, 174406 (2017)

熱流センシングのための Gd-Co 合金における異常ネルンスト効果

Anomalous Nernst effect in Gd-Co alloys for heat flux sensing

豊田工大¹, リーズ大学², 九州大学³ °田辺 賢士¹, 小田切 美穂¹,

今枝 寛人¹, Ahmet Yagmur^{1,2}, 黒川 雄一郎³, 鷲見 聡¹, 栗野 博之¹

Toyota Tech. Inst.¹, Univ. Leeds², Kyushu Univ.³, °Kenji Tanabe¹, Miho Odagiri¹,

Hiroto Imaeda¹, Ahmet Yagmur^{1,2}, Yuichiro Kurokawa³, Satoshi Sumi¹, and Hiroyuki Awano¹

E-mail: tanabe@toyota-ti.ac.jp

熱流センサーは、熱の流れを可視化できるセンサーであり、廃熱マネジメント社会に必要な要素技術として期待されている。一般に、ゼーベック型熱流センサーは非常に高価であり、応用先が限定されている。一方、最近 Zhou らによって異常ネルンスト型熱流センサーが提案され、安価なセンサーの可能性が示された[1]。熱流センサーの感度は、センサー面を通過する熱流密度あたりの熱電場 (E/j) で表現される。この式は、(横ゼーベック係数 S_{ANE}) / (熱伝導率 κ) と表すことができ、高感度化のためには大きな S_{ANE} と低い κ を有する材料が求められることが分かる。そこで我々は、高感度化を目指して、熱伝導率が低いとされるアモルファス Gd-Co 合金に注目して研究を行った[2]。

SiN(10 nm)/Gd_xCo_{100-x}(20 nm)/SiN(3 nm)の多層膜を、スパッタ装置を用いて SiO₂ ガラス基板上に成膜した。GdCo 層はコスパッタ法を利用して組成変調し、15 種類の異なる組成比を有する試料を作製し、異常ネルンスト効果の組成依存性を包括的に調査した。すべての試料に対して、熱電気輸送係数を計測した。その結果、Gd-Co 合金は磁化補償点を含む広い組成領域で、0.2 $\mu\text{m}/\text{A}$ 以上の大きな感度を示した (Fig. 1(a))。最高感度は Gd₂₄Co₇₆ の 0.23 $\mu\text{m}/\text{A}$ であり、これはそれまでの最高感度であった Co₂MnGa に匹敵する[3]。また先行研究では正の感度しかなかったが、Gd-Co 合金は磁化補償点を境に正負両方の感度を示すことが明らかになった (Fig. 1(b))。このことはサーモパイル構造を作製した際に大きなメリットになり、正負を合わせた両極性感度で考えると、先行研究の約 2 倍の感度が期待される。大きな感度の原因は、1.0 $\mu\text{V}/\text{K}$ 以上の組成において、比較的大きな S_{ANE} を示すことと、 $x > 20$ 以上の組成において、 κ が 5 W/mK 以下に低く抑えられているためであることが明らかになった。さらに詳細な解析から、 S_{ANE} は主に intrinsic な寄与に基づくこと、 κ は主に伝導電子の寄与に基づくことが明らかになった。

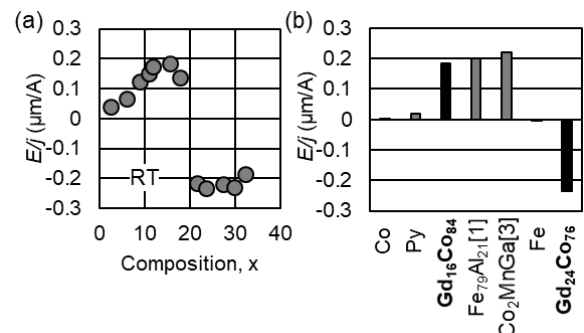


Fig. 1 (a)感度の Gd 組成依存性. (b)ほかの材料との感度比較.

[1] W. Zhou et al., APEX 13, 043001 (2020).

[2] M. Odagiri et al., arXiv:2402.04259.

[3] K. Uchida et al., APL 118, 140504 (2021).

複合構造を利用した高感度異常ネルンスト型熱流センサの無磁場動作

Magnetic field-free operation of highly sensitive anomalous Nernst-type heat flux sensors using composite structures

豊田工業大学, [○](M2)今枝寛人, 樋田怜史, 竹内恒博, 栗野博之, 田辺賢士

Toyota Tech Inst., H. Imaeda, R. Toida, T. Takeuchi, H. Awano and K. Tanabe

E-mail: sd23403@tti-j.net

熱流センサは、熱エネルギーの流れの見える化が可能であり、排熱マネジメントの要素技術として期待されている。特に、異常ネルンスト効果（ANE）を利用した熱流センサは、磁化と熱流の垂直方向に起電力が発生するため、従来のゼーベック型と比べ、フレキシブル化や小型化、低い熱抵抗などの点から注目されている[1]。ANE を利用した熱流センサの実用化のためには、感度（熱流密度 j あたりの発生する電場 $E: E/j$ ）[2]の向上や、磁場なしでのセンサ動作が必要になる。これまでに我々は、凹凸構造を持つ基板を用いることで高感度化を実現した[3]。この研究では 10 kOe 以上の大きな外部磁場を必要とするという欠点があったことから、我々は大きな保磁力を有するアモルファス希土類遷移金属合金（amo-Tb_{20.6}Co_{79.4}）と複合構造を利用した。その結果、無磁場下での高感度化に成功したのでここで報告する。

マグネトロンスパッタ装置を用いて、凹凸構造（幅: 5 μm , 高さ: 2, 5, 10 μm ）を持つプラスチック基板に SiN (10 nm)/ Tb_xCo_(100-x) (40 nm)/ SiN (10 nm)を成膜し、ポリマー樹脂をスピコート法によって塗布した（Fig. 1）。試料垂直方向に熱流を、面内方向に磁場を印加したときの ANE 電圧を測定した。Fig. 2 は、組成比 $x = 20.6$ の場合の結果である。5 kOe 程度の大きな保磁力を示し、無磁場下でも高磁場領域と同程度の感度があること分かる。これは凹凸構造側面に成膜された Tb-Co 薄膜の容易軸が、凹凸構造側面に対し垂直方向であることが原因だと考えられる。

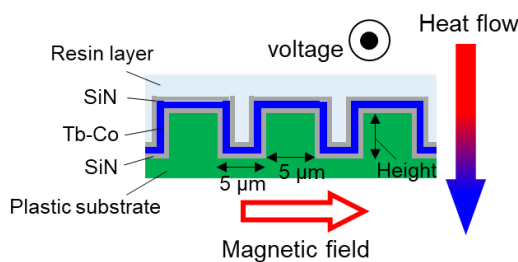


Fig. 1 Schematic of sample cross section. The Tb-Co layer on the side of the unevenness induces a large voltage.

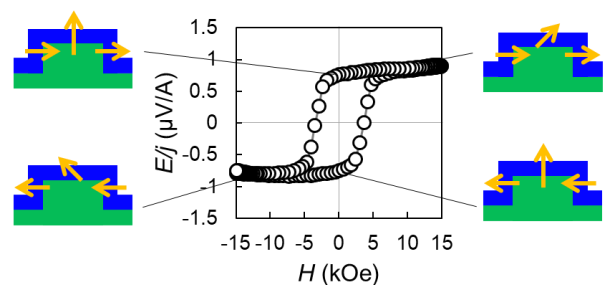


Fig. 2 H dependence of E/j and schematic of magnetization directions. The substrate has 10 μm uneven height. The arrows indicate the magnetization directions.

参考文献

- [1] W. Zhou *et al.*, Appl. Phys. Express **13**, 043001 (2020).
- [2] M. Odagiri *et al.*, arXiv:2402.04259.
- [3] H. Imaeda *et al.*, arXiv:2405.07758.

10 スピントロニクス・マグネティクス | 一般セッション(口頭講演) : 10.3 スピンデバイス・磁気メモリ・ストレージ技術

[17a-D61-1~10] 10.3 スピンデバイス・磁気メモリ・ストレージ技術

[17a-D61-1]

Searching for Cu-X spacers with a half-metallic $\text{Co}_2\text{FeGa}_{0.5}\text{Ge}_{0.5}$ electrode to boost magnetoresistance in CPP-GMR devices using first-principles calculations

○(D)Kodchakorn SIMALAOTAO^{1,2}, Ivan Kurniawan², Yoshio Miura^{2,3}, Yuya Sakuraba^{1,2} (1.Univ. of Tsukuba, 2.NIMS, 3.KIT)

[17a-D61-2]

Theoretical approach for the TMR oscillation as a function of the barrier thickness

○Keisuke Masuda¹, Thomas Scheike¹, Hiroaki Sukegawa¹, Yusuke Kozuka¹, Seiji Mitani¹, Yoshio Miura^{1,2} (1.NIMS, 2.KIT)

[17a-D61-3]

Ab-initio study on spin-transport properties of Fe/Mn/MgO/Mn/Fe and Co/Mn/MgO/Mn/Co magnetic tunnel junctions

○Tufan Roy¹, Masahito Tsujikawa², Masafumi Shirai^{1,2} (1.CSIS, Tohoku Univ., 2.RIEC, Tohoku Univ.)

[17a-D61-4]

Enhanced tunnel magnetoresistance of $\text{Fe/MgGa}_2\text{O}_4/\text{Fe}(001)$ magnetic tunnel junctions using MgO terminations as a Ga diffusion barrier

○(D)Rombang Rizky Sihombing^{1,2}, Thomas Scheike¹, Zhenchao Wen¹, Jun Uzuhashi¹, Tadakatsu Ohkubo¹, Seiji Mitani^{1,2}, Hiroaki Sukegawa¹ (1.NIMS, 2.Univ. Tsukuba)

[17a-D61-5]

磁気トンネル接合のフラッシュランプアニーリングと微細構造観察

○今井 亜希子¹、太田 進也^{1,2}、山崎 順³、荒木 徹平¹、金井 康^{1,4,6}、小山 知弘^{1,5,6}、関谷 毅¹、千葉 大地^{1,4,5,6} (1.阪大産研、2.東大物工、3.阪大電顕セ、4.東北大SRIS、5.阪大CSRN、6.阪大OTRI)

[17a-D61-6]

Low magnetic damping recording layer for reducing write-errors in voltage-driven magnetization switching

○Tatsuya Yamamoto¹, Tomohiro Ichinose¹, Takayuki Nozaki¹, Shingo Tamaru¹, Kay Yakushiji¹, Hitoshi Kubota¹, Shinji Yuasa¹ (1.AIST)

[17a-D61-7]

Probabilistic computing accuracy with various types of random telegraph noise from stochastic magnetic tunnel junctions

○Haruna Kaneko^{1,2}, Shun Kanai^{1,2,3,4,5,6,7}, Hideo Ohno^{5,8}, Shunsuke Fukami^{1,2,5,6,8,9} (1.RIEC, Tohoku Univ., 2.Grad. School of Eng., Tohoku Univ., 3.JST PRESTO, 4.DEFS, Tohoku Univ., 5.CSIS, Tohoku Univ., 6.WPI-AIMR, Tohoku Univ., 7.QST, 8.CIES, Tohoku Univ., 9.InaRIS)

[17a-D61-8]

Chaotic dynamics of spintronic oscillator with tunable anharmonic potential

○(M1)Ryo Tatsumi¹, Takahiro Chiba¹, Takash Komine², Hiroaki Matsueda¹ (1.Tohoku Univ., 2.Ibaragi Univ.)

[17a-D61-9]

Microwave control of chiral spin rotation in a non-collinear antiferromagnet Mn_3Sn

○Shoya Sakamoto¹, Takuya Nomoto², Tomoya Higo^{3,1}, Yuki Hibino⁴, Tatsuya Yamamoto⁴, Shingo Tamaru⁴, Yoshinori Kotani⁵, Hidetoshi Kosaki¹, Masanobu Shiga¹, Daisuke Nishio-Hamane¹, Tetsuya Nakamura^{6,5}, Takayuki Nozaki⁴, Kay Yakushiji⁴, Ryotaro Arita^{2,7}, Satoru Nakatsuji^{3,1,8,9}, Shinji Miwa^{1,8} (1.ISSP, Univ. of Tokyo, 2.RCAST, Univ. of Tokyo, 3.Phys. Dept., Univ. of Tokyo, 4.AIST, 5.JASRI, 6.SRIS, Tohoku Univ., 7.RIKEN, 8.TQSI, Univ. of Tokyo, 9.Johns Hopkins Univ.)

[17a-D61-10]

Co/Ni積層膜における磁歪効果に起因した垂直スピン軌道トルクの生成

○杉本 聡志¹、塩田 陽一²、小野 輝男²、葛西 伸哉¹ (1.物材機構、2.京大化研)

Searching for Cu-X spacers with a half-metallic $\text{Co}_2\text{FeGa}_{0.5}\text{Ge}_{0.5}$ electrode to boost magnetoresistance in CPP-GMR devices using first-principles calculations

University of Tsukuba¹, NIMS², Kyoto Institute of Technology³

[○]Kodchakorn Simalaotao^{1,2}, Ivan Kurniawan², Yoshio Miura^{2,3}, Yuya Sakuraba^{1,2}

E-mail: s2330100@u.tsukuba.ac.jp

Current-perpendicular-to-plane giant magnetoresistive (CPP-GMR) devices are considered promising candidates for the next-generation magnetic read heads in hard disk drives (HDDs). These devices benefit from a small resistance-area product (RA), which is advantageous for compact read heads and high-speed reading. $\text{Co}_2\text{FeGa}_{0.5}\text{Ge}_{0.5}$ (CFGG) is a prominent half-metallic Heusler alloy known for achieving a high magnetoresistance (MR) ratio in CPP-GMR devices with Ag spacers¹⁻³. To further enhance the MR ratio in CPP-GMR devices, we investigate the potential of Cu-based binary alloys (Cu-X) as spacers compared to a traditional Ag spacer. To this end, we employ first-principles calculations to compare the interface resistance in CFGG/Ag/CFGG(001) and CFGG/Cu-X/CFGG(001) trilayers. We focus on majority-spin interface ballistic conductance, which is inversely proportional to the interface resistance, based on the Landauer formula. Our calculations show that Cu-X spacers exhibit a lower interface RA compared to the Ag spacer, indicating a significant improvement in the MR ratio. In particular, the RA of the CFGG/CuZn(001) interface is about 30% smaller than that of the CFGG/Ag(001) interface in all the interfacial terminations at its maximum difference, indicating the advantage of the CuZn spacer for obtaining a large MR ratio in the CPP-GMR devices. Fig. 1 indicates a significant conductive predominance of the CuZn spacer, especially around the $k_{\parallel} = (0,0)$ in the Brillouin zone, with a good Fermi surface matching with the CFGG electrode. In addition, CFGG/CuZn/CFGG(001) exhibits lower formation energies in all interfacial terminations, indicating superior structural stability compared to CFGG/Ag/CFGG(001). Consequently, among the various Cu-X spacers examined, CuZn emerged as the most optimal candidate for a half-metallic CFGG electrode.

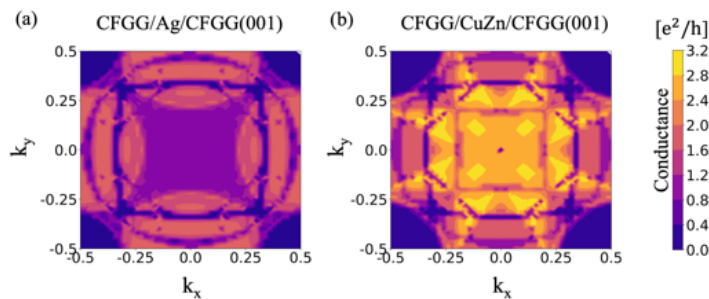


Fig. 1 In-plane wave vector dependence of the majority-spin conductance of (a) CFGG/Ag/CFGG(001) and (b) CFGG/CuZn/CFGG(001) trilayers.

References

1. S. Li, *et al.*, Appl. Phys. Lett., **103**, 042405 (2013).
2. Jung, J.W., *et al.*, Appl. Phys. Lett., **108**, 102408 (2016).
3. Büker, B., *et al.*, Phys. Rev. B, **103**, L140405 (2021).

TMR のバリア膜厚振動に対する理論アプローチ

Theoretical approach for the TMR oscillation as a function of the barrier thickness

NIMS¹, 京都工繊大²○増田 啓介¹, Scheike Thomas¹, 介川 裕章¹, 小塚 裕介¹, 三谷 誠司¹, 三浦 良雄^{1,2}NIMS¹, KIT²○K. Masuda¹, T. Scheike¹, H. Sukegawa¹, Y. Kozuka¹, S. Mitani¹, and Y. Miura^{1,2}

E-mail: MASUDA.Keisuke@nims.go.jp

Oscillation of the tunnel magnetoresistance (TMR) ratio as a function of the insulating barrier thickness called the “TMR oscillation” was firstly observed by Yuasa *et al.* in an Fe/MgO/Fe(001) magnetic tunnel junction (MTJ) with a high TMR ratio [1]. Subsequent experiments have also observed the similar TMR oscillation with a universal period of $\sim 3\text{\AA}$ [2,3]. However, the underlying mechanism of this phenomenon has yet to be clarified. Although previous theoretical studies have considered possible additional effects, such as interference of evanescent states [4] and nonspecular tunneling [5], based on the Δ_1 coherent tunneling theory, resistance oscillations in both the parallel and antiparallel magnetization states, leading to the TMR oscillation, have not been explained satisfactorily. To elucidate the origin of the TMR oscillation will deepen our fundamental understanding not only on the TMR effect but also on the quantum tunneling itself.

In this work, we propose a possible mechanism of the TMR oscillation in the Fe/MgO/Fe(001) MTJ [6]. Our idea is to consider the superposition of wave functions with opposite spins and different Fermi momenta for the tunneling problem, which is easily justified due to the existence of the spin-flip scattering around the interface of the MTJ. Assuming the superposition of the majority-spin Δ_1 and minority-spin Δ_2 wave functions for the transmission wave, we solved the tunneling problems for the parallel and antiparallel magnetization states of the Fe electrodes. The obtained transmittances in both the magnetization states and the resultant TMR ratio were found to oscillate with a period of $\sim 3\text{\AA}$ by varying the insulating barrier thickness, consistent with experimental observations. From the obtained analytical expressions, we also found that the period of the TMR oscillation is determined by the difference in the Fermi momenta between the majority-spin Δ_1 and minority-spin Δ_2 states. Finally, we directly compared our calculation results with our experimental results obtained for the

high-quality single-crystalline MTJ. We found that the calculation results [Fig. 1(a)] reproduce the characteristic sawtooth-like shape in the experimentally observed TMR oscillation [Fig. 1(b)]. This work was supported by Grant-in-Aids for Scientific Research (22H04966, 23K03933, and 24H00408) and MEXT Program: Data Creation and Utilization-Type Material Research and Development Project (JPMXP1122715503).

[1] S. Yuasa *et al.*, Nat. Mater. **3**, 868 (2004). [2] R. Matsumoto *et al.*, Appl. Phys. Lett. **90**, 252506 (2007). [3] T. Scheike *et al.*, Appl. Phys. Lett. **118**, 042411 (2021). [4] W. H. Butler *et al.*, Phys. Rev. B **63**, 054416 (2001). [5] X.-G. Zhang *et al.*, Phys. Rev. B **77**, 144431 (2008). [6] K. Masuda *et al.*, arXiv:2406.07919.

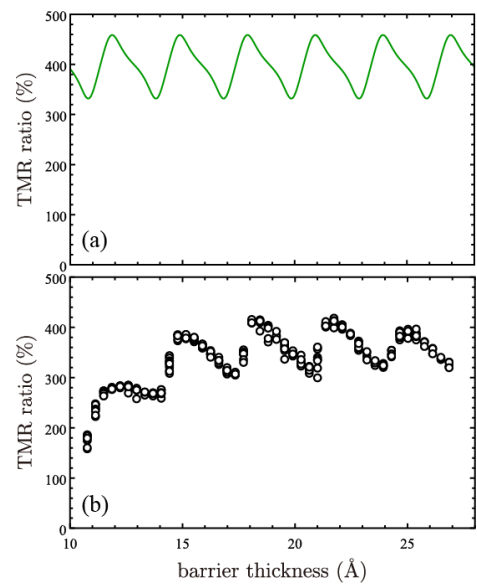


Fig. 1 (a) Theoretically calculated and (b) experimentally obtained TMR ratios as a function of the insulating barrier thickness. From Ref. [6].

***Ab-initio* study on spin-transport properties of Fe/Mn/MgO/Mn/Fe and Co/Mn/MgO/Mn/Co magnetic tunnel junctions**

CSIS, Tohoku Univ.¹, RIEC, Tohoku Univ.², °Tufan Roy¹, Masahito Tsujikawa², Masafumi Shirai^{1,2}

E-mail: roy.tufan.a3@tohoku.ac.jp

In spintronics applications, magnetic tunnel junctions (MTJs) with a high tunneling magneto-resistance (TMR) ratio ($\sim 1000\%$) at low temperatures (LT) as well as at the room temperature (RT) are desirable. There have been an enormous amount of studies in the search of suitable electrode materials whereas MgO is largely used as an insulating barrier of MTJs. Indeed, Fe(*bcc*)/MgO/Fe(*bcc*) and Co(*bcc*)/MgO/Co(*bcc*) are amongst the most studied MTJs, which show a large TMR ratios at LT owing to the coherent tunnelling of electrons with Δ_1 symmetry [1,2]. However, because of thermal fluctuation of interfacial spin-moments, the TMR ratio falls rapidly with increasing temperature [3]. In a recent experimental study, CoMnFe(*bcc*)/MgO/CoMnFe(*bcc*) is reported to show high TMR ratio at LT (1002%) and it is reduced to 350% at RT [4]. It is also found that Mn atoms are located at the interfacial region with MgO [4].

In this *ab-initio* study, we show the impact of Mn monolayer (1ML) insertion at the interface with MgO in pristine Co/MgO/Co and Fe/MgO/Fe MTJs. Figure 1 shows the TMR ratio and the resistance-area (RA) product of studied MTJs. Although the TMR ratio remains in the range of a few 1000%, the RA-product is much reduced after the Mn (1ML) insertion. However, oxidization of the interfacial Mn (1ML) remarkably deteriorates the spin-filtering property. We also evaluate the exchange stiffness constant and magnetic anisotropy energy of the MTJs to discuss the temperature dependence of TMR ratio with and without interfacial Mn (1ML). The thermodynamic stability of the Mn (1ML) formation at the interface is also discussed energetically.

The authors thank S. Mizukami for fruitful discussions. This work was partially supported by CREST (Grant No. JPMJCR17J5) from JST and X-NICS (Grant No. JPJ011438) from MEXT.

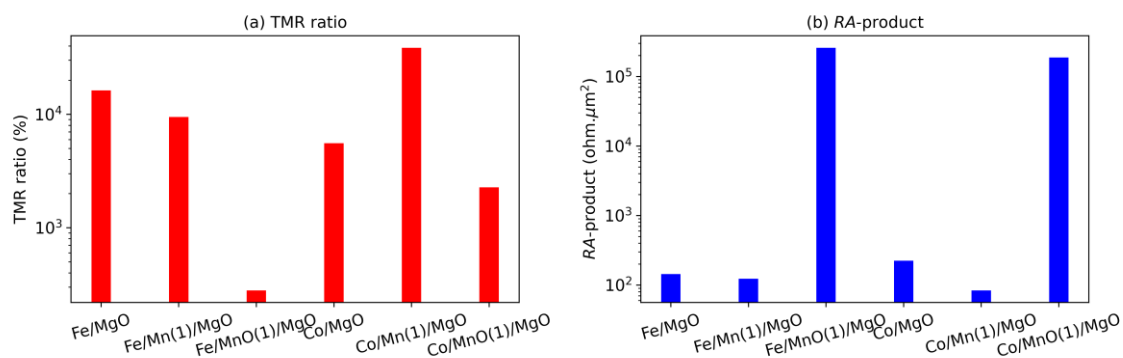


Figure 1: (a) TMR ratio (b) RA-product of studied MTJs.

- [1] W. H. Butler *et al.*, Phys. Rev. B **63**, 054416 (2001). [2] S. Yuasa *et al.*, Appl. Phys. Lett., **89**, 042505 (2006).
 [3] Y. Miura *et al.*, Phys. Rev. B **83**, 214411 (2011). [4] T. Ichinose *et al.*, J. Alloys Compd. **960**, 170750 (2023).

**Enhanced tunnel magnetoresistance of Fe/MgGa₂O₄/Fe(001)
magnetic tunnel junctions using MgO terminations as a Ga diffusion barrier**

NIMS¹, Univ. Tsukuba², ○Rombang Rizky Sihombing^{1,2}, Thomas Scheike¹, Zhenchao Wen¹, Jun
Uzuhashi¹, Tadakatsu Ohkubo¹, Seiji Mitani^{1,2}, and Hiroaki Sukegawa¹

E-mail: s.rombangrizky@nims.go.jp

Magnetic tunnel junctions (MTJs) are widely used in spintronic applications, including tunneling magnetoresistive (TMR) heads in hard disk drives and magnetoresistive random access memory (MRAM) cells. To maintain the scaling of these devices, it is necessary to reduce the resistance area product (RA) while maintaining the barrier thickness. MgGa₂O₄ (MGO) is a promising candidate for a low RA barrier due to its low band gap (~ 4.7 eV) and relatively large TMR ratios of over 120% at room temperature (RT) [1]. Recently, it has been reported that MgO insertion at both the upper and lower MGO interfaces in CoFeB/MGO/CoFeB MTJs is effective to enhance the interfacial perpendicular magnetic anisotropy and TMR ratio [2]. However, the mechanism of the improvement by the insertion remains to be elucidated. In this study, we developed Fe/MGO/Fe(001) epitaxial MTJs to investigate the effect of the MgO termination.

MTJ stacks were deposited by ultra-high vacuum magnetron sputtering. The typical structure is MgO(001) substrate/Cr buffer/Fe(50)/bottom MgO/MGO (1.7)/top MgO/Fe (5)/IrMn (10)/Ru (10), (unit: nm). The MgO and MGO layers were deposited using MgO and MgGa₂O₄ sintered targets. The stacks were post-annealed at 200°C under a magnetic field of 2 kOe. Magnetotransport properties were characterized by dc four-probe method after patterning into micrometer-scale MTJs.

The insertion of MgO ~ 0.3 nm for the bottom and top MGO interfaces and post-annealing processes resulted in an enhanced TMR ratio of 151% at RT. The value increases up to 291% at 5 K. Scanning transmission electron microscopy and energy dispersive X-ray spectroscopy of the MTJ cross-section revealed that Ga diffusion from the MGO to the Fe layers is suppressed by the MgO insertion, resulting in the improvement of the TMR ratio.

This work was partially executed in response to support of KIOXIA Corporation and supported by MEXT Program: Data Creation and Utilization-Type Material Research and Development Project Grant Number JPMXP1122715503, and JSPS KAKENHI (Grant Nos. 21H01750, 22H04966, and 24H00408).

References:

- [1] H. Sukegawa *et al.*, Appl. Phys. Lett. **110**, 122404 (2017).
- [2] S. Mertens *et al.*, Appl. Phys. Lett. **118**, 172402 (2021).

磁気トンネル接合のフラッシュランプアニーリングと微細構造観察

Microstructure observation of magnetic tunnel junctions treated by flash lamp annealing

阪大産研¹, 東大物工², 阪大電顕セ³, 東北大 SRIS⁴, 阪大 CSRN⁵, 阪大 OTRI⁶ ○今井 亜希子¹,
太田 進也^{1,2}, 山崎 順³, 荒木 徹平¹, 金井 康^{1,4,6}, 小山 知弘^{1,5,6}, 関谷 毅¹, 千葉 大地^{1,4,5,6}
SANKEN, Osaka Univ.¹, The Univ. of Tokyo², UHVEM, Osaka Univ.³, SRIS, Tohoku Univ.⁴,
CSRN, Osaka Univ.⁵, OTRI, Osaka Univ.⁶ ○Akiko Imai¹, Shinya Ota^{2,1}, Jun Yamasaki³, Teppei
Araki¹, Yasushi Kanai^{1,4}, Tomohiro Koyama^{1,5,6}, Tsuyoshi Sekitani¹, Daichi Chiba^{1,4,5,6}
E-mail: aimai@sanken.osaka-u.ac.jp

磁気トンネル接合 (MTJ) は最も代表的なスピントロニクス素子であり、中でも広く普及している CoFeB/MgO 系 MTJ は高いトンネル磁気抵抗 (TMR) 比を得るために熱処理が必須である。一般的には、熱処理炉内で 300°C 以上かつ 1 時間を超える熱処理を行うことで、大きな TMR 比を持つ MTJ が作製されてきた[1]が、一方で、分単位・秒単位での熱処理を実現する、それぞれラピッド・サーマル・アニーリング[2]や、フラッシュ・ランプ・アニーリング (FLA) などの短時間熱処理の手法がある。FLA はキセノンランプの強烈な閃光を試料表面に照射する手法で、試料表面が瞬時に極めて高温となり、その後数十秒程度で室温に下がる。我々は、CoFeB/MgO 系 MTJ に FLA を行い、トータル 1.65 s、正味 3.3 ms の照射時間で、周囲の配線にもダメージなく、100%に迫る TMR 比を得た。

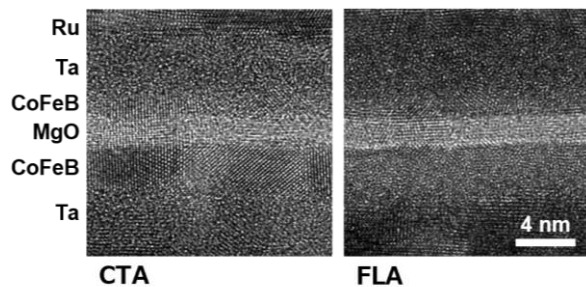


Fig. HRTEM images of the conventional thermal annealing (CTA) and FLA MTJs.

CoFeB/MgO 系 MTJ における TMR 比の向上は、熱処理時の B の原子拡散やそれに伴う CoFeB および MgO の結晶化の促進と深く関わっている[3]。FLA による結晶化過程や原子拡散の理解がさらなる TMR 比向上のカギであると考え、透過電子顕微鏡により微細構造観察と元素分析を行った。FLA することで CoFeB/MgO/CoFeB 層の結晶化が起きていることが確認し、従来法のアニール処理試料と比較すると結晶化や元素拡散に違いがあることが分かった。

本研究は、科研費 基盤研究(A)、挑戦的研究(萌芽)、JST A-STEP、CREST、COI-NEXT、X-NICS、the Spintronics Research Network of Japan、大阪大学超高压電子顕微鏡センター「文部科学省ナノテクノロジープラットフォーム事業微細構造解析プラットフォーム」(JPMXP09A21OS0030)、ARIM (JPMXP1222OS0039)の支援を受けて行われた。

[1] S. Ikeda et al., Appl. Phys. Lett. **93**, 082508 (2008). [2] W.G. Wang et al., Appl. Phys. Lett. **92**, 152501 (2008). [3] D.D. Djayaprawira, et al., Appl. Phys. Lett. **86**, 092502 (2005).

Low magnetic damping recording layer for reducing write-errors in voltage-driven magnetization switching

○Tatsuya Yamamoto, Tomohiro Ichinose, Takayuki Nozaki, Shingo Tamaru,

Kay Yakushiji, Hitoshi Kubota, and Shinji Yuasa

National Institute of Advanced Industrial Science and Technology (AIST),

E-mail: yamamoto-t@aist.go.jp

Introduction Electrical control of magnetization in magnetic tunnel junctions (MTJs) is the key technology for developing magnetoresistive random access memory (MRAM). Among a variety of techniques, the use of voltage-controlled magnetic anisotropy (VCMA) effect allows for switching the magnetization with a minimal energy and is thus regarded as a promising alternative to the spin-transfer-torque (STT) technology used in the state-of-the-art MRAMs [1]. Regardless of the remarkable advantage in the energy efficiency, it is not straightforward to replace the STT-MRAM by the VCMA-MRAM; a substantial reduction in the write-error rate (WER) of the VCMA-driven magnetization switching is strongly demanded for the practical application. While WERs of lower than 10^{-6} have been demonstrated by using a precisely controlled write pulse with a duration t_p as short as 0.2 ns [2], it is quite challenging to achieve low WERs in the practical ($t_p > 1$ ns) regime because the magnetization is subject to the thermal noise which randomly fluctuates the orbital motion during t_p and that results in the write-errors.

In this work, we develop perpendicularly magnetized MTJs consisting of an $\text{Mg}_{40}\text{Fe}_{10}\text{O}_{50}/\text{Co-Fe-B}/\text{MgO}$ multilayer as a recording layer. The nonmagnetic insulators on both sides of the Co-Fe-B layer effectively eliminates the spin pumping effect to reduce the effective magnetic damping a_{eff} . We show that the lower magnetic damping reduces the thermal fluctuation during t_p , and a fairly low WER of the order of 10^{-3} is achieved for $t_p > 1$ ns.

Experiments MTJ films consisting of a Co-Fe-B (0.8)/ $\text{Mg}_{40}\text{Fe}_{10}\text{O}_{50}$ (2.0)/Co-Fe-B (1.4)/Mo (0.3)/MgO (0.8) (thicknesses in nm) junctions were prepared on 300 mm Si wafers with a buffer layer. The magnetic properties of MTJ films were characterized by using a vibrating sample magnetometer and a vector network analyzer ferromagnetic resonance (FMR) measurement apparatus. To investigate the magneto-transport properties, the MTJ films were microfabricated into $\phi 60$ nm nanopillar devices using electron-beam lithography. The WER was calculated from 2×10^5 trials for various t_p under an in-plane magnetic field H_{ip} .

Owing to the superior wettability of Co-Fe-B on $\text{Mg}_{40}\text{Fe}_{10}\text{O}_{50}$ [3], the Co-Fe-B recording layer exhibits a low a_{eff} of 0.01 while avoiding FMR linewidth broadening arising from the structural inhomogeneity, as shown in Fig. 1(a). In fact, the obtained a_{eff} is about one-third that of a conventional Ta/Co-Fe-B/MgO recording layer. Figure 1(b) shows the WER as a function of t_p . The WER exhibits a clear minimum at a certain t_p corresponding to half of the magnetization precession period and the position shifts to the longer t_p side as the applied H_{ip} is reduced. Meanwhile, the WER dip structure of t_p -WER curve is broadened for the lower H_{ip} , and more importantly, the present MTJ maintain WER $< 10^{-3}$ even for $t_p > 1$ ns, which is 3-orders of magnitude lower than conventional MTJs. We discuss the reduction of WER in terms of reduced thermal fluctuation during t_p owing to the reduced a_{eff} in the recording layer [4].

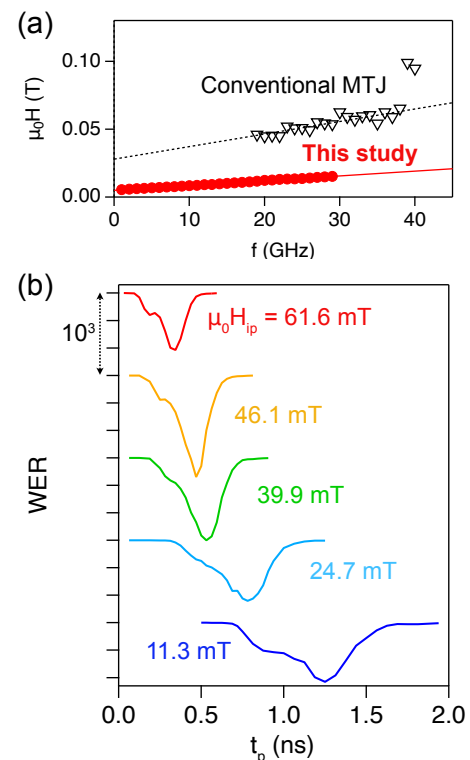


Figure 1 (a) FMR linewidth of recording layers in MTJ films. (b) WER as a function of t_p .

This presentation was partly based on results obtained from projects JPNP16007 and JPNP20017 commissioned by the New Energy and Industrial Technology Development Organization (NEDO), Japan.

References [1] T. Nozaki et al., *Micromachines* **10**, 327 (2019). [2] T. Yamamoto et al., *J. Phys. D: Appl. Phys.* **52**, 164001 (2019). [3] T. Yamamoto et al., *Acta Mater.*, **267**, 119749 (2024). [4] T. Yamamoto et al., *Phys. Rev. Applied*, **21**, 054008 (2024).

Probabilistic computing accuracy with various types of random telegraph noise from stochastic magnetic tunnel junctions

⁰(M2) Haruna Kaneko,^{1,2} Shun Kanai,¹⁻⁷ Hideo Ohno,^{5,8} and Shunsuke Fukami^{1,2,5,6,8,9}

¹RIEC, Tohoku Univ., ²Graduate School of Engineering, Tohoku Univ., ³JST PRESTO, ⁴DEFS, Tohoku Univ., ⁵CSIS, Tohoku Univ., ⁶WPI-AIMR, Tohoku Univ., ⁷QST, ⁸CIES, Tohoku Univ., ⁹InaRIS

E-mail: haruna.kaneko.t3@dc.tohoku.ac.jp

Probabilistic computers (p-computers) with probabilistic bits (p-bits) are expected to address some computationally hard problems for conventional deterministic computers, and stochastic magnetic tunnel junctions (s-MTJs) show promise as the crucial constituent of the p-bits [1,2]. Here, we study the computational accuracy as a function of the statistical properties of random telegraph noise (RTN) from s-MTJs [3-8].

We investigate the accuracy of p-computing based on the Ising model in terms of (i) frequent appearance of the lowest energy (E) states (correct solutions) compared to the incorrect ones in the statistics and (ii) low variation of probabilities among the lowest energetically equivalent states. We simulate the NAND-gate operation [9] using experimentally obtained RTN of s-MTJs [8] with various statistical properties (amplitude, distribution, etc.), where the amplitude (distribution) is mainly determined by the tunneling magnetoresistance ratio (magnetic anisotropy) of the s-MTJ. We also test two extreme cases: binary and continuous random numbers [Fig. 1a]. The interaction between p-bits is implemented by sending a signal given by $-I_0 \partial E / \partial x_i$ to i th p-bit, where I_0 is the inverse temperature representing the strength of interaction and x_i is the binary state of i th p-bit. We define I_0^* as I_0 to achieve the highest accuracy of p-computing. We find a positive correlation between the RTN amplitude and I_0^* for all types of random numbers [Fig. 1b], indicating that I_0 should be adjusted depending on the amplitude. We also find a systematic variation of operational window with the nature of RTN to obtain high accuracy. The obtained results provide a guideline to design and operate the s-MTJ-based p-computer.

This work is supported in part by JST-CREST JPMJCR19K3, JST-PRESTO JPMJPR21B2, JST-ASPIRE JPMJAP2322, and Takano Research Foundation.

- [1] K. Y. Camsari *et al.*, Phys. Rev. X **7**, 031014 (2017).
- [2] W. A. Borders *et al.*, Nature **573**, 390 (2019).
- [3] S. Kanai *et al.*, Phys. Rev. B **103**, 094423 (2021).
- [4] K. Hayakawa *et al.*, PRL **126**, 117202 (2021).
- [5] K. Kobayashi *et al.*, PRAppl. **18**, 054085 (2022).
- [6] K. Y. Camsari *et al.*, PRAppl. **15**, 044049 (2021).
- [7] K. Selcuk *et al.*, PRAppl. **21**, 054002 (2024).
- [8] R. Ota *et al.*, arXiv 2405.20665 (2024).
- [9] N. A. Aadit *et al.*, Nat. Electron. **5**, 460 (2022).

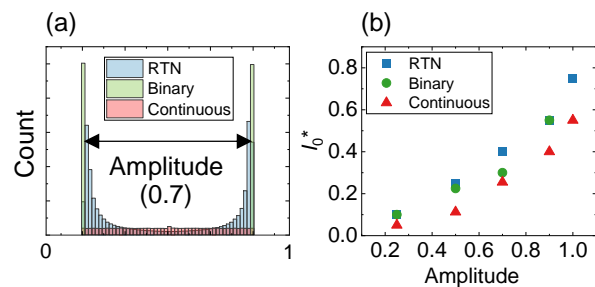


Fig. 1 (a) Histogram of the random telegraph noise (RTN) and binary/continuous random number. (b) I_0^* for each amplitude of RTN and binary/continuous random numbers.

制御可能な非調和磁気ポテンシャルを持つスピントロニクス振動子のカオスダイナミクス

Chaotic dynamics of spintronic oscillator with tunable anharmonic potential

東北大工¹, 茨城大工², 辰巳 僚¹, 千葉 貴裕¹, 小峰 啓史², 松枝 宏明¹

Tohoku Univ.¹, Ibaragi Univ.², R. Tatsumi¹, T. Chiba¹, T. Komine², H. Matsueda¹

E-mail: tatsumi.ryo.p6@dc.tohoku.ac.jp

Recently, physical reservoir computing, which is a neural network based on the nonlinear dynamics of physical systems, has much attention from information science and nonlinear physics. As a promising resource, spintronic devices have been actively studied, because magnetization dynamics allows low-power energy consumption and nanosecond-scale response on the device operation. It is known that reservoir computing shows high performance at the so-called “edge of chaos”, which is a transient state between periodic phase and chaos [1]. Accordingly, the chaotic dynamics of spin torque oscillator (STO) is theoretically investigated [2,3]. However, one of the studies reports that a typical STO requires a spin torque induced effective field with an order of several hundred mT for chaos [3], which hinders an application of the edge of chaos to spintronic reservoir devices.

In this study, we propose a spintronic Duffing oscillator that realizes chaotic magnetization dynamics in the spin-torque ferromagnetic resonance. Figure 1(a) shows a schematic illustration of our model characterized by the magnetic potential with the uniaxial magnetic anisotropy. The shape of the potential is similar to that of the Duffing equation which represents chaotic dynamics in a particle system. That is the key to realize the chaotic dynamics. Based on the Landau-Lifshitz-Gilbert (LLG) equation, we investigated the magnetization dynamics by means of the Lyapunov exponent λ (fig. 1(b)) and bifurcation diagram. Figure 1(b) shows that chaotic dynamics occurs when spin torque induced effective field is around 20 mT, whose value is about 1/10 of the previous study [3]. In the presentation, we will discuss the mechanism of low-power energy consumption of the proposed model and how to tune the potential shape.

[1] R. Legenstein, *et al.*, Neural Networks **20**, 323-334 (2007).

[2] T. Taniguchi, *et al.*, J. Magn. Magn. Mater. **563**, 170009 (2022).

[3] T. Yamaguchi, *et al.*, Phys. Rev. B **100**, 224422 (2019).

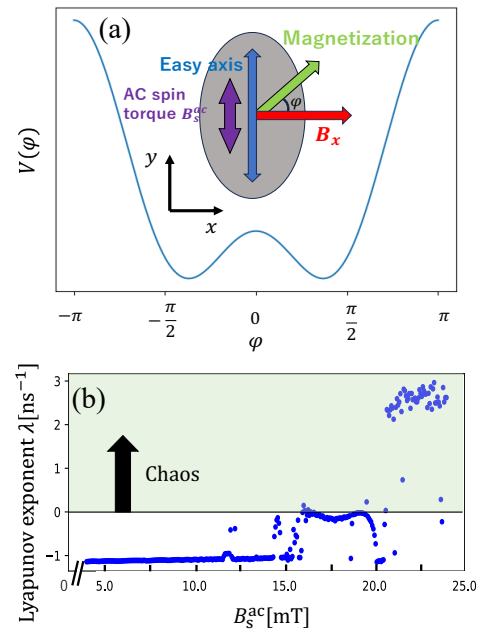


FIG. 1. (a) The shape of magnetic potential for the magnetization angle ϕ and a schematic illustration of our model. The external magnetic field B_x is 165 mT. (b) Lyapunov exponent as a function of the magnitude of spin torque induced effective fields B_s^{ac} [mT] with the resonance frequency 3.22 GHz

Microwave control of chiral spin rotation in a non-collinear antiferromagnet Mn₃Sn東大物性研¹, 東大先端研², 東大理³, 産総研新原理⁴, JASRI⁵, 東北大 SRIS⁶,理研 CEMS⁷, 東大 TQSI⁸, ジョンズホプキンス大⁹,○坂本祥哉¹, 野本拓也², 肥後友也^{3,1}, 日比野 有岐⁴, 山本竜也⁴,田丸慎吾⁴, 小谷佳範⁵, 甲崎秀俊¹, 志賀雅亘¹, 浜根大輔¹,中村哲也^{5,6}, 野崎隆行⁴, 薬師寺啓⁴, 有田亮太郎^{2,7}, 中辻知^{3,1,8,9}, 三輪真嗣^{1,8}ISSP, Univ. of Tokyo¹, RCAST, Univ. of Tokyo², Dept. of Phys., Univ. of Tokyo³, RCECT, AIST⁴,JSARI⁵, SRIS, Tohoku Univ.⁶, CEMS, RIKEN⁷, TQSI, Univ. of Tokyo⁸, Johns Hopkins Univ.⁹,°Shoya Sakamoto¹, Takuya Nomoto², Tomoya Higo^{3,1}, Yuki Hibino⁴, Tatsuya Yamamoto⁴,Shingo Tamaru⁴, Yoshinori Kotani⁵, Hidetoshi Kosaki¹, Masanobu Shiga¹,Daisuke Nishio-Hamene¹, Tetsuya Nakamura^{5,6}, Takayuki Nozaki⁴, Kay Yakushiji⁴,Ryotaro Arita^{2,7}, Satoru Nakatsuji^{3,1,8,9}, and Shinji Miwa^{1,8}

E-mail: shoya.sakamoto@issp.u-tokyo.ac.jp

Spintronics based on ferromagnets has led to the development of microwave spin-torque oscillators and diodes [1]. In these devices, magnetization precession frequencies reach several tens of GHz. Utilizing antiferromagnet holds promise as they may operate at much higher frequencies. In the present study, we explore the dynamics of antiferromagnetic spin structure in Mn₃Sn, known as chiral spin rotation [2-5], with concomitant application of DC and microwave current.

We fabricated Mn₃Sn (7 nm)/W (6 nm) epitaxial bilayers on MgO(110) substrates using molecular beam epitaxy [6,7]. The fabricated thin films were patterned into Hall bar devices by photolithography and Ar ion etching. A DC bias current and microwave current with amplitude modulation were applied through a bias-tee, and resultant DC Hall voltages were measured with a lock-in amplifier. We observed the emergence of DC Hall voltages upon concurrent application of microwave and DC bias currents. Through numerical simulations, we revealed that the rectified signals stem from the injection locking of chiral spin rotation to the microwave spin-orbit torque, which is similar to the spin-torque diode effect in ferromagnet.

This work was supported by JSPS KAKENHI (Nos. JP19H05825, JP21H04437, JP22H00290, 22H04964, 23H01833), JST CREST (JPMJCR18T3), JST Mirai Program (JPMJMI20A1), MEXT-Xnics (No. JPJ011438), JST-PRESTO (JPMJCR18T3), JST-ASPIRE (No. JPMJAP2317), and Spin-RNJ.

Reference

[1] A. A. Tulapurkar *et al.*, Nature **438**, 339 (2005). [2] O. V. Gomonay and V. M. Loktev, Low Temp. Phys. **41**, 698-704 (2015). [3] H. Fujita, Phys. Status Solidi PRL **11**, 1600360 (2017) [4] H. Tsai *et al.*, Nature **580**, 608-613 (2020). [5] Y. Takeuchi *et al.*, Nat. Mater. **20**, 1364 (2021). [6] T. Higo *et al.*, Nature **607**, 474 (2022). [7] S. Sakamoto *et al.*, Phys. Rev. B **104**, 134431 (2021).

Out-of-plane spin-orbit torque induced by magnetostriction for Co/Ni multilayers

○(P)S. Sugimoto^{1,3}, Y. Shiota^{2,3}, T. Ono^{2,3}, and S. Kasai^{1,3}

(1. NIMS, 2. Kyoto Univ., 3. JST CREST)

E-mail: SUGIMOTO.Satoshi@nims.go.jp

Design of spin polarization direction is an essential agenda for further developments of spin-orbit torque (SOT)-induced magnetization switching. Especially, out-of-plane (OOP) SOT enables zero-field switching of perpendicular magnetization with solving geometric constraints of in-plane SOT [1]. Generations of such OOP SOTs have principally required additional symmetry breaking for thin-film layered structures, and device engineering [2] and spin-injections by low-symmetry crystals [3] have been investigated so far. In this study, we newly introduce an alternative approach for inducing huge OOP-SOT for Co/Ni multilayers, attributed to strong magnetostriction of nonequilibrium Ni films.

Films with a structure of surface oxidized Si(100) substrate //Ta(2)/Pt(10)/Co(0.6)/Ni(t_{Ni})/Co(0.6)/Pt(t_{Pt}) were fabricated using a magnetron sputtering system. The robust perpendicular magnetic anisotropy (PMA) was sustained close to $t_{\text{Ni}} = 7$ nm, far beyond the typical ferromagnetic thickness limits of interfacial PMA such like Pt/Co and CoFeB/MgO. Our structure analyses revealed strong negative magnetostrictions unique to Ni [4] have resulted in heterogeneous magnetic microstructures with finite lattice relaxation along the perpendicular direction. Figure 1(a) shows FMR spectra for in-plane Co/Ni multilayers for opposite field directions. Clear nonreciprocity against field inversion ($V_{\text{STFMR}}(\mu_0 H) \neq -V_{\text{STFMR}}(-\mu_0 H)$) indicated unconventional SOT applications there.

The in-plane torque profiles revealed the emergence of strong OOP fieldlike and dampinglike SOTs, and their spin-to-charge (SC) conversion efficiencies ζ_i ($i = x, y, z$) were boosted up at in-plane SOT cancellation limit

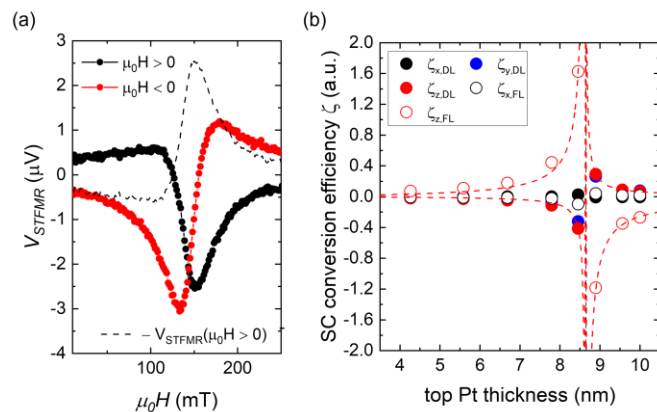


Fig. 1 (a) Nonreciprocal FMR spectra for Ni/Co multilayers.

between top and bottom Pt layers as $t_{\text{Pt}} \sim 8.6$ nm. This divergence of $\zeta_{z,\text{DL(FL)}}$ supports intrinsic OOP-SOT unique to nonequilibrium Ni films.

This work was partially supported by JSPS KAKENHI Grant Number 20K14419, and JST, CREST Grant No. JPMJCR21C1, Japan.

[1] I. M. Miron *et al.*, Nature (London) **476**, 189 (2011). [2] Y. W. Oh *et al.*, Nat. Nanotechnol. **11**, 878 (2016). [3] D. MacNeill *et al.*, Nat. Phys. **13**, 300 (2017). [4] G. Matsumoto *et al.*, J. Phys. Soc. Jpn. **21**, 882 (1996).

10 スピントロニクス・マグネティクス | 一般セッション(口頭講演): 10.4 半導体・トポロジカル・超伝導・強
相関スピントロニクス

[18p-D61-1~21] 10.4 半導体・トポロジカル・超伝導・強相関スピントロニクス

[18p-D61-1]

Giant Odd-parity Magnetoresistance in an α -Sn / (In,Fe)Sb Heterostructure

○Harunori Shiratani¹, Yuta Okuyama¹, Le Duc Anh^{1,2}, Masaaki Tanaka^{1,2} (1.Department of Electrical Engineering and Information Systems, The Univ. of Tokyo, 2.CSRN, The Univ. of Tokyo)

[18p-D61-2]

Fe₃Si/FeSi₂超格子の温度と磁場による磁気構造変化

○花島 隆泰¹、鈴木 淳市¹、加倉井 和久^{2,3,1}、宮田 登¹、堺 研一郎⁴、出口 博之⁵、原 嘉昭⁶、竹市 悟志⁷、吉武 剛⁸ (1.CROSS、2.東北大、3.理研、4.久留米高専、5.九工大、6.茨城高専、7.佐世保高専、8.九州大学)

[18p-D61-3]

Magnetoelectric switching phenomena in electron-doped hexagonal improper ferroelectrics displaying topologically protected magnetoelectric vortex state

○Hena Das^{1,2} (1.Kanagawa Institute of Industrial Science and Technology (KISTEC), 705-1 Shimoimaizumi, Ebina 243-0435, Japan, 2.Laboratory for Materials and Structures, Tokyo Institute of Technology, 4259 Nagatsuta, Midori-ku, Yokohama, Kanagawa 226-8503, Japan)

[18p-D61-4]

Interlayer electron transfer from WS₂ monolayers to III-V semiconductor substrates enhanced by surface treatments

○Takeshi Odagawa¹, Sota Yamamoto¹, Chaoliang Zhang¹, Kazuki Koyama¹, Jun Ishihara¹, Giacomo Mariani², Yoji Kunihashi², Haruki Sanada², Junsaku Nitta^{1,2}, Makoto Kohda^{1,3,4} (1.Grad. Sch. Eng., Tohoku Univ., 2.NTT Basic Research Laboratories, 3.CSIS, Tohoku Univ., 4.QST)

[18p-D61-5]

Observation of superconducting diode effect in a Fe(Se,Te)/FeTe heterostructure device

○塩貝 純一^{1,2}、小林 友祐¹、野島 勉³、松野 丈夫^{1,2} (1.阪大理、2.阪大OTRI、3.東北大金研)

[18p-D61-6]

Nonreciprocal transport in FeSe superconducting thin films

○(M2)Mio Hashimoto¹, Tomoki Kobayashi¹, Tomoyuki Yokouchi¹, Takako Konoike², Shinya Uji², Atsutaka Maeda¹, Yuki Shiomi¹ (1.The Univ. of Tokyo, 2.NIMS)

[18p-D61-7]

Oscillatory conduction behavior and its magnetic-field-induced enhancement in an all-epitaxial La_{2/3}Sr_{1/3}MnO₃/SrTiO₃/Nb:SrTiO₃ tunneling heterostructure

○(DC)Tatsuro Endo¹, Masaaki Tanaka^{1,2}, Shinobu Ohya^{1,2} (1.EEIS, Univ. of Tokyo, 2.CSRN, Univ. of Tokyo)

[18p-D61-8]

Electron spin dynamics in dilute nitride InGaAsN quantum dots grown at different temperatures

○Ayano Morita¹, Satoshi Hiura¹, Junichi Takayama¹, Akihiro Murayama¹ (1.Hokkaido Univ.)

[18p-D61-9]

Room temperature voltage control of optical spin polarization maintaining photoluminescence intensity using 0D-2D semiconductor nanostructure

○Hiroto Kise¹, Satoshi Hiura¹, Junichi Takayama¹, Kazuhisa Sueoka¹, Akihiro Murayama¹ (1.IST, Hokkaido Univ.)

[18p-D61-10]

Effect of spin diffusion on spin dynamics under persistent spin helix regime in a GaAs/AlGaAs semiconductor quantum well

○Koga Akagi¹, Jun Ishihara¹, Sota Yamamoto¹, Yuzo Ohno², Makoto Kohda^{1,3,4,5} (1.Grad. Sch. of Eng., Tohoku Univ., 2.Univ. of Tsukuba, 3.CSIS, Tohoku Univ., 4.DEFS, Tohoku Univ., 5.QUARC, QST)

[18p-D61-11]

Drift-Induced Wavelength Modulation of Electron Spin Waves in Quasi-One-Dimensional GaAs/AlGaAs Quantum Well

○Futa Sugawara¹, Keito Kikuchi¹, Jun Ishihara¹, Sota Yamamoto¹, Yuzo Ohno², Makoto Kohda^{1,3,4,5} (1.Grad. Sch. of Eng., Tohoku Univ., 2.Univ. of Tsukuba, 3.CSIS, Tohoku Univ., 4.DEFS, Tohoku Univ., 5.QUARC, QST)

[18p-D61-12]

Enhancement of Rashba Spin-Orbit Interaction Based on Quaternary InGaAsP/InGaAs Single Quantum Well by Bayesian Optimization

○Keito Kikuchi¹, Kohei Yoshizumi¹, Sota Yamamoto¹, Jun Ishihara¹, Makoto Kohda^{1,2,3,4} (1.Grad. Sch. of Eng., Tohoku Univ., 2.CSIS, Tohoku Univ., 3.DEFS, Tohoku Univ., 4.QUARC, QST)

[18p-D61-13]

Optical Observation of Electron Spin Wave Interference in a GaAs/AlGaAs Quantum Well

○Miari Hiyama¹, Keito Kikuchi¹, Sota Yamamoto¹, Jun Ishihara¹, Yuzo Ohno², Makoto Kohda^{1,3,4,5} (1.Grad. Sch. of Eng., Tohoku Univ., 2.Univ. of Tsukuba, 3.CSIS, Tohoku Univ., 4.DEFS, Tohoku Univ., 5.QUARC, QST)

[18p-D61-14]

Spin-orbit-torque magnetization switching in a ferromagnetic SrRuO₃ single layer with a spontaneous oxygen atomic displacement

○(D)Hiroto Horiuchi¹, Wakabayashi Yuki K.², Araki Yasufumi³, Ieda Jun'ichi³, Yamanouchi Michihiko⁴, Kaneta-Takada Shingo¹, Taniyasu Yoshitaka², Yamamono Hideki², Krockenberger Yoshiharu², Tanaka Masaaki^{1,5}, Ohya Shinobu^{1,5} (1.The Univ. of Tokyo, 2.NTT BRL, 3.JAEA, 4.Hokkaido Univ., 5.CSRN)

[18p-D61-15]

Spin injection through a ferromagnetic Fe/Mg/Si/n-Si tunnel junction with ohmic-like current-voltage characteristics for non-degenerated n-Si

○Shoichi Sato^{1,2}, Masaaki Tanaka^{1,2}, Ryosho Nakane^{3,1} (1.Tokyo Univ., 2.CSRN, 3.d.lab)

[18p-D61-16]

Spin-valve effect with two easy-magnetization axes in a spin-MOSFET based on perovskite-oxide La_{0.67}Sr_{0.33}MnO₃ with a LaMnO₃ buffer layer

○Aoi Nakamura¹, Tatsuro Endo¹, Masaaki Tanaka^{1,2}, Shinobu Ohya^{1,2} (1.Tokyo Univ., 2.CSRN, Tokyo Univ.)

[18p-D61-17]

Long-lived valley-polarization in suspended WSe₂ monolayers strained by electrostatic pressure

○Giacomo Mariani¹, Yoji Kunihashi¹, Louis Smet¹, Taro Wakamura¹, Satoshi Sasaki¹, Jun Ishihara², Makoto Kohda², Junsaku Nitta^{1,2}, Haruki Sanada¹ (1.NTT-BRL, 2.Tohoku Univ.)

[18p-D61-18]

Electrical spin injection into GaAs from perpendicularly magnetized Mn/Co bilayers

○(M2)Kotaro Nara¹, Mineto Ogawa¹, Michihiko Yamanouchi¹, Tetsuya Uemura¹ (1.IST. Hokkaido Univ.)

[18p-D61-19]

遷移金属ダイカルコゲナイド層間における異種磁性原子の磁性相互作用 II

○備前 匠光¹、大根 誓哉¹、中村 太一¹、小矢野 幹夫¹ (1.北陸先端大)

[18p-D61-20]

トポロジカル結晶絶縁体Pb_{1-x}Sn_xTeにおける非線形プラナーホール効果

○玉井 優¹、西嶋 泰樹¹、小林 純也²、庄司 啓人²、安藤 裕一郎³、大島 諒¹、黒田 眞司²、白石 誠司¹ (1.京大院工、2.筑波大院数理物質、3.大公大院工)

[18p-D61-21]

Observation of bulk and multiple surface states in a thick topological Dirac semimetal α -Sn film by quantum transport

○牧 秀樹¹、堀田 智貴¹、福岡 蒼一郎¹、Le Duc Anh^{1,2}、田中 雅明^{1,2} (1.東大工、2.東大CSRN)

Giant Odd-parity Magnetoresistance in an α -Sn / (In,Fe)Sb Heterostructure

Harunori Shiratani¹, Yuta Okuyama¹, Le Duc Anh^{1,2} and Masaaki Tanaka^{1,2}

Department of Electrical Engineering and Information Systems, The University of Tokyo¹,

Center for Spintronics Research Network (CSRN), The University of Tokyo²,

E-mail: shiratani-harunori2121@g.ecc.u-tokyo.ac.jp

The magnetoresistance is usually an even function of a magnetic field according to Onsager's theorem [1]. However, when time reversal symmetry (TRS) is broken, the magnetoresistance may have an odd-function component of a magnetic field. This phenomenon is called odd-parity magnetoresistance (OMR). OMR is theoretically predicted to occur in Weyl semimetals (WSM) with tilted Weyl cones [2]. WSM is characterized by the spin-splitting Dirac cone (Weyl cones) and may be achieved by introducing TRS breaking such as magnetization into topological Dirac semimetals (TDS). Here, we focus on α -Sn / (In_{1-x}Fe_x)Sb heterostructures, where α -Sn is known as a TDS [3], while (In_{1-x}Fe_x)Sb is a ferromagnetic semiconductor (FMS) [4]. In this heterostructure, the TRS in α -Sn is expected to be broken by the magnetic proximity effect from the magnetization of underlying (In_{1-x}Fe_x)Sb, enabling us to observe OMR.

In this study, an α -Sn / (In_{1-x}Fe_x)Sb heterostructure was grown by molecular beam epitaxy. The sample structure was (from top to bottom) AlO_x (3 nm) / α -Sn (6.5 nm) / (In_{1-x}Fe_x)Sb ($x = 15\%$, 20 nm) / InSb (100 nm) on an InSb (001) substrate. The ferromagnetism was measured by magnetic circular dichroism (MCD), which indicates that the Curie temperature of the (In,Fe)Sb is 120 K. For transport measurements, we fabricated a 50×400 μm^2 Hall bar (Fig.1 a). When a magnetic field B was applied parallel to the current, we observe a giant OMR as large as 170 % at $B = 1$ T, 5.5 K (Fig.1 b). Moreover, the signs of OMR (R_1 and R_2 in Fig 1b) are different when being measured at the opposite edges, which suggests that the OMR occurs in the transport channels at the Hall bar edges. The origin of this OMR might be explained by opposite tilting of the Weyl cones at the opposite edges. This large OMR possibly provides a deeper insight into MPE in topological materials and practical spintronic applications.

This work was partly supported by Grants-in-Aid for Scientific Research, CREST program and PRESTO Program of JST, UTEC-UTokyo FSI, Murata Science Foundation and Spintronics Research Network of Japan (Spin-RNJ).

[1] L. Onsager, Phys. Rev. **37**, 405 (1934). [2] A. Kundu et al., New J. Phys. **22** 083081 (2020).

[3] L. D. Anh, et al., Adv. Mat. **33**, 2104645 (2021). [4] N. T. Tu, et al., Appl. Phys. Express **11**, 063005 (2018).

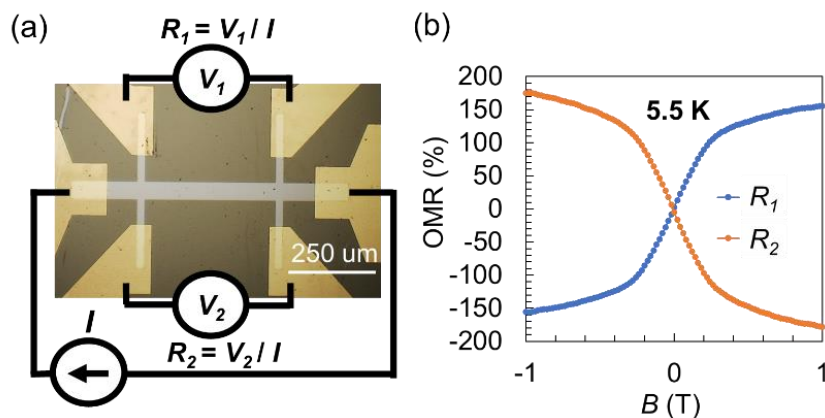


Fig. 1 (a) Top view of the Hall bar device, taken by optical microscopy, and measurement setup. $R_i = V_i / I$ ($i = 1, 2$) is defined as the resistance measured at each edge. (b) Odd-parity magnetoresistances (OMRs) of R_1 and R_2 at 5.5 K when the magnetic field B is applied parallel to the current.

Fe₃Si/FeSi₂ 超格子の温度と磁場による磁気構造変化

Temperature- and magnetic field-induced magnetic structural changes in the Fe₃Si/FeSi₂ superlattice

CROSS¹, 東北大², 理研³, 久留米高専⁴, 九工大⁵, 茨城高専⁶, 佐世保高専⁷, 九州大⁸,
 °花島隆泰¹, 鈴木淳市¹, 加倉井和久^{2,3,1}, 宮田登¹, 堺研一郎⁴, 出口博之⁵, 原嘉昭⁶,
 竹市悟志⁷, 吉武剛⁸

CROSS¹, Tohoku Univ.², Riken³, Kurume College⁴, Kyushu Institute of Technology⁵, Ibaraki College⁶,
 Sasebo College⁷, Kyushu Univ.⁸, °T. Hanashima¹, J. Suzuki¹, K. Kakurai^{2,3,1}, N. Miyata¹,
 K. Sakai⁴, H. Deguchi⁵, Y. Hara⁶, S. Takeichi⁷ and T. Yoshitake⁸

E-mail: t_hanashima@cross.or.jp

半導体スペーサーと磁性層からなる人工格子は、その電子状態によって磁気構造が変化することが期待される。温度と光照射により半導体スペーサーの電子状態を変化させられるため、その結果生じる層間結合の変化が注目されている。Fe₃Si/FeSi₂ 人工格子は磁性層 (Fe₃Si) と非磁性半導体スペーサー(FeSi₂)から構成される。上記の化合物は電気伝導性が近く、キュリー点が高いという特長を持つうえ、Fe と Si は、資源のカントリーリスクとコストが低く、持続可能性が高く、環境安全性が高い。

非磁性で半導体の FeSi₂ スペーサー層と磁性層の Fe₃Si からなる [Fe₃Si/FeSi₂]₂₀ 超格子の面内磁気構造の温度 (T) と磁場 (H_{ext}) 依存性を磁化測定と偏極中性子反射率測定 (PNR) を用いて調べた。 $H_{\text{ext}}=5$ mT のとき、4 K から 298 K までほぼコリニアな反強磁性 (AF) 構造が観測された。通常の PNR 解析では単一の磁気構造を仮定するが、ドメインが形成されていると考えられるため、複数構造を平均する必要があるがあった。 $H_{\text{ext}}=1$ T のとき、 H_{ext} に沿った強磁性成分と横方向の AF 成分を示すノンコリニア AF 構造が低 T で観測された。以上のことからこの物質では、反強磁性 (AF) 層間結合の大きいことが判った。

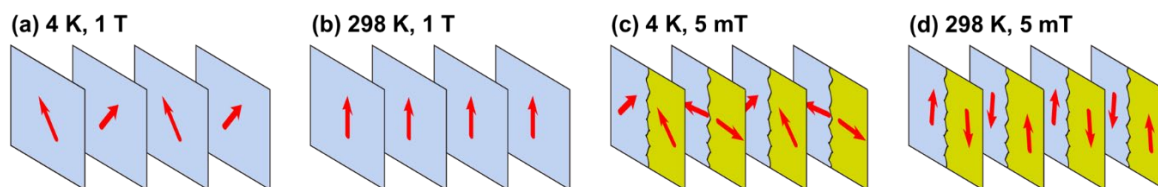


図 1. [Fe₃Si/FeSi₂]₂₀ 超格子の磁気構造の模式図。(a) $T=4$ K、 $H_{\text{ext}}=1.0$ T、(b) 298 K、1.0 T、(c) 4 K、5 mT (Canted-AF 構造)、(d) 298 K、5 mT (AF 構造)

**Magnetoelectric switching phenomena in electron-doped hexagonal improper ferroelectrics
displaying topologically protected magnetoelectric vortex state**

**Kanagawa Institute of Industrial Science and Technology (KISTEC), 705-1 Shimoimaizumi, Ebina
243-0435, Japan¹, Laboratory for Materials and Structures, Tokyo Institute of Technology, 4259
Nagatsuta, Midori-ku, Yokohama, Kanagawa 226-8503, Japan²**

◦Hena Das^{1,2}

E-mail: das.h.aa@m.titech.ac.jp

Magnetoelectric (ME) multiferroic systems hold promise to facilitate fast, ultra-low energy consuming memory and logic devices. However, for technological applications we need to ensure low coercive fields and maintain the desired ME functionality at nanoscale and above room temperature. Despite significant research developments, the number of technologically relevant room-temperature magnetoelectrics are still limited and hinders the design of practical magnetoelectric memories. Also, ME switching kinetics and dynamics are poorly understood. Here, we will discuss an idea to realize noncollinear ferrimagnetic orders with a considerably high magnetization M ($\sim 1.2 \mu_B/\text{f.u.}$) and magnetic transition temperature ($\sim 290 \text{ K}$) and strong ME coupling in an improper ferroelectric oxides forming topologically protected magnetoelectric vortex state [Hena Das *et al.*, Nat. Commun. **5**, 2998 (2014), Yanan Geng, Hena Das *et al.*, Nat. Mater. **13**, 163 (2014), Hena Das, Phys. Rev. Research **5**, 013007 (2023)]. We will elucidate the microscopic mechanisms of electric field induced magnetic phase transitions and ME coupling processes and the chemical and structural control over these phenomena. We will also discuss interactions between oxygen vacancies and the multiferroic order in these systems, giving new opportunities for deterministic defect-enabled property control in oxide heterostructures (K. A. Hunnestad, Hena Das *et al.*, Nat. Commun. (<https://doi.org/10.1038/s41467-024-49437-0>) (2024)).

Acknowledgements: Research at the Tokyo Institute of Technology is supported by the Ministry of Education, Culture, Sports, Science and Technology, Japan Grants-in-Aid No 24H00374 and JST-CREST (JPMJCR22O1). H.D. also acknowledges computational support from TSUBAME supercomputing facility.

Interlayer Electron Transfer from WS₂ Monolayers to III–V Semiconductor Substrates Enhanced by Surface Treatments

Grad. Sch. Eng., Tohoku Univ.¹, NTT Basic Research Laboratories², CSIS, Tohoku Univ.³, QST⁴,

◦Takeshi Odagawa^{1,*}, Sota Yamamoto¹, Chaoliang Zhang¹, Kazuki Koyama¹, Jun Ishihara¹,

Giacomo Mariani², Yoji Kunihashi², Haruki Sanada², Junsaku Nitta^{1,2}, and Makoto Kohda^{1,3,4}

*E-mail: tkod@dc.tohoku.ac.jp

Van der Waals heterostructures based on two-dimensional (2D) semiconducting transition metal dichalcogenides (TMDCs) and three-dimensional (3D) semiconductors are promising platforms for optoelectronics, owing to the spin–valley coupled physics in 2D TMDCs and the well-developed doping technologies for 3D semiconductors. To date, a variety of state-of-the-art devices have been realized, including a subthermionic tunnel field effect transistor [1] and a spin light-emitting diode [2]. For such 2D/3D semiconductor heterostructures, the surface of 3D semiconductors can play a critical role in modifying the transfer of charge, spin and valley currents between the constituent 2D and 3D semiconductors. Here, we present an enhanced static electron transfer from WS₂ monolayers to III–V semiconductors [3].

The monolayer WS₂/III–V semiconductor heterostructures studied were fabricated by transferring WS₂ monolayers on III–V semiconductor substrates. For the III–V substrates, an n-type In_{0.04}Ga_{0.96}As substrate and a semi-insulating GaAs substrate were used. The surface of the III–V substrates was of three types: (i) The substrates were covered with a native oxide layer of ~2.5 nm in thickness; (ii) The native oxides were reduced; (iii) After the native oxides were reduced, the substrate surface was sulfur passivated.

The excitonic species in the WS₂ monolayers were identified by polarization-resolved photoluminescence (PL) measurements at $T = 4$ K under 2.21 eV excitation, where the valley decoherence pathways are effectively suppressed. Figure 1 shows the horizontally (H) and vertically (V) polarized PL components in the WS₂ monolayers under the simultaneous photoexcitation of the K and K' valleys by H polarized light. In the WS₂ monolayers on the native oxide-covered III–V substrates (top, purple), the amplitudes of the H and V components were identical, indicating negatively charged exciton emission. Meanwhile, in the WS₂ monolayers on the reduced (middle, orange) and sulfur-passivated (bottom, green) III–V substrates, the V components were weaker than the H components, indicating neutral exciton emission. This reflects the enhancement of interlayer electron transfer from the WS₂ monolayer to the III–V substrates induced by the surface treatments. These results provide a novel approach to control the carrier density of 2D semiconductors, and to facilitate the interlayer transfer of charge, spin and valley currents.

This work was supported by the JSPS KAKENHI (grant no. 21H04647), JST-FOREST (grant no. JPMJFR203C), JST-CREST (grant no. JPMJCR22C2) and JST-SPRING (grant no. JPMJSP2114) programs, and the Asahi Glass Foundation. T.O. and K.K. acknowledge the financial support from GP-Spin at Tohoku University.

[1] D. Sarkar *et al.*, Nature **526**, 91–95 (2015).

[2] Y. Ye *et al.*, Nature Nanotech. **11**, 598–602 (2016).

[3] T. Odagawa *et al.*, APL Materials (accepted).

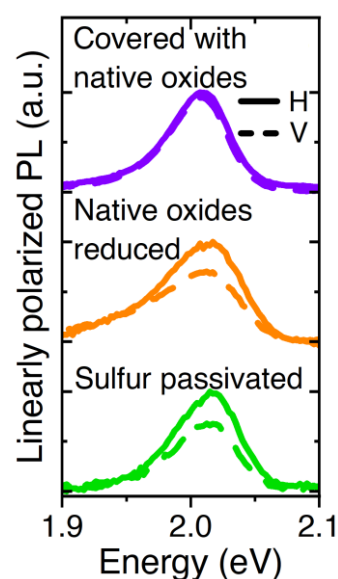


Fig. 1: Polarization-resolved PL spectra for the WS₂ monolayers.

Observation of superconducting diode effect in a Fe(Se,Te)/FeTe heterostructure device

Dept. of Phys., Osaka Univ.¹, OTRI, Osaka Univ.², IMR, Tohoku Univ.³

◦Junichi Shiogai^{1,2}, Yusuke Kobayashi¹, Tsutomu Nojima³, Jobu Matsuno^{1,2}

E-mail: junichi.shiogai.sci@osaka-u.ac.jp

Superconducting diode effect (SDE), *i.e.*, non-reciprocal response of the superconducting critical current, has attracted growing interests owing to its potential application to superconducting devices [1]. The mechanisms of SDE have been discussed among spin-orbit interaction induced by microscopic spatial inversion asymmetry, macroscopic imbalance of the device structure, and geometrically anisotropic defects. An iron-based superconductor Fe(Se,Te) is a good candidate material for exploring SDE because of its high superconducting critical parameters [2] and strong spin-orbit interaction [3]. In this study, we demonstrated SDE in a Fe(Se,Te)/FeTe thin-film heterostructure [4].

The Se capped 23.3-nm-thick Fe(Se,Te)/20-nm-thick FeTe heterostructure was grown by pulsed-laser deposition. We confirmed *c*-axis oriented growth of the Fe(Se,Te) and FeTe layers by x-ray diffraction pattern. To evaluate the superconducting critical current (I_c), the heterostructure was patterned into a 50- μm -wide rectangular-shaped device with four Pt/Ti electrodes as shown in Fig. 1(a). From temperature dependence of the sheet resistance, we determined onset $T_c = 13.5$ K. Figure 1(b) shows I - V characteristics when the in-plane magnetic fields $\mu_0 H = \pm 5$ T were applied. In addition to the non-linear feature indicating superconductivity, we observed that I_c for a positive bias is larger than that for a negative bias when $\mu_0 H = +5$ T. Such a relationship was reversed for $\mu_0 H = -5$ T, which is consistent with the previous report [1]. In this talk, we will discuss the origin of SDE observed in our Fe(Se,Te)/FeTe heterostructure device based on temperature and magnetic field dependences of the diode efficiency as well as second harmonic resistance [4].

Reference [1] F. Ando *et al.*, Nature **584**, 373 (2020). [2] Y. Imai *et al.*, Proc. Natl. Acad. Sci. USA **112**, 1937 (2015). [3] P. Zhang *et al.*, Science **360**, 182 (2018). [4] Y. Kobayashi, J. Shiogai *et al.*, to be submitted.

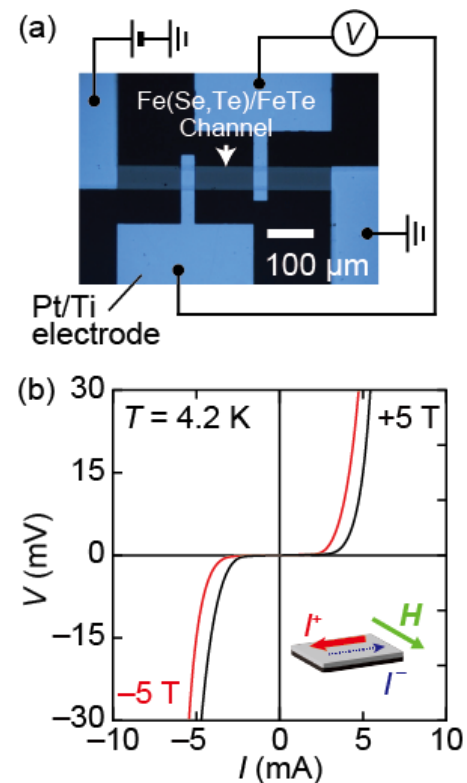


Fig. 1 (a) Optical micrograph of the Fe(Se,Te)/FeTe heterostructure and setup for critical current measurement. (b) I - V characteristics at $T = 4.2$ K when in-plane magnetic field of +5 T (black solid curve) and -5 T (red) is applied perpendicular to the current.

FeSe 超伝導薄膜における非相反伝導現象

Nonreciprocal transport in FeSe superconducting thin films

東大院総合¹, 物材機構²

○(M2) 橋本 滯¹, 小林 友輝¹, 横内 智行¹, 鴻池 貴子², 宇治 進也², 前田 京剛¹, 塩見 雄毅¹

The Univ. of Tokyo¹, NIMS²

○Mio Hashimoto¹, Tomoki Kobayashi¹, Tomoyuki Yokouchi¹, Takako Konoike², Shinya Uji²,

Atsutaka Maeda¹, Yuki Shiomi¹

E-mail: mhashimoto@g.ecc.u-tokyo.ac.jp

Nonreciprocal transport is one of the diode effects where current flows easily in one direction but not the other. Recently, this topic has attracted attention because it is unique to low symmetric materials, which requires both inversion and time-reversal symmetry breaking within a crystal. This effect has been observed in several superconducting materials [1~3] until now. However, for practical applications such as diode elements, it is desired to study this effect in simpler structures. In this study, we report nonreciprocal transport in FeSe thin films below the superconducting transition temperature $T_C \sim 3$ K despite the fact that the crystal structure of FeSe possesses inversion symmetry.

We grew FeSe films with a thickness of 26 nm on a LaAlO₃ substrate by pulsed laser deposition (PLD) and subsequently deposited amorphous Si as a protective capping layer. All of the transport properties were measured using the DC four-terminal method under magnetic fields to break time-reversal symmetry. The nonreciprocal component was obtained by taking the difference between the voltages for left-going and right-going currents. The current dependence of the voltage $V_{xx}(\pm I)$ and nonreciprocal voltage, $\Delta V = (V_{xx}(+I) - |V_{xx}(-I)|)/2$ under an in-plane magnetic field -0.6 T, perpendicular to the current, are shown in Fig. 1. A finite value of the $V_{xx}(\pm I)$ was observed in the superconducting state at 2.1 K when the current was applied. This is attributed to superconducting vortices driven by the current. As the current increases, ΔV becomes evident and shows a broad peak at around 8 mA in the superconducting state. Broken spatial inversion symmetry at LaAlO₃/FeSe and FeSe/Si interfaces may cause vortices to move asymmetrically in direction perpendicular to the current. In the presentation, we will discuss vortex dynamics and mechanisms of the nonreciprocal phenomenon.

[1] R. Wakatsuki *et al.*, Sci. Adv. **3**, e1602390 (2017).

[2] E. Zhang *et al.*, Nat. Commun. **11**, 5634 (2020).

[3] M. Masuko *et al.*, npj Quantum Mater. **7**, 104 (2022).

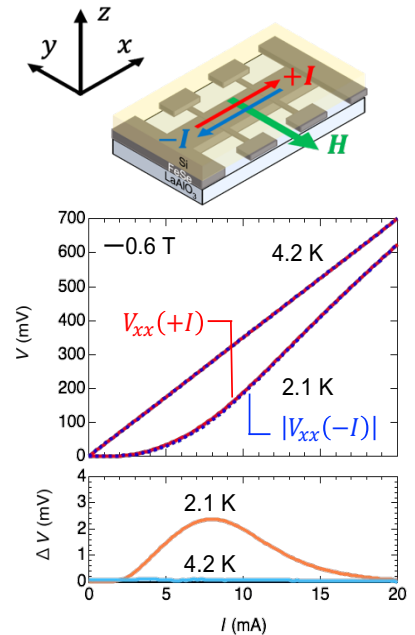


Figure 1. Current dependence of the voltage and nonreciprocal voltage at -0.6 T.

Oscillatory conduction behavior and its magnetic-field-induced enhancement in an all-epitaxial $\text{La}_{2/3}\text{Sr}_{1/3}\text{MnO}_3/\text{SrTiO}_3/\text{Nb}:\text{SrTiO}_3$ tunneling heterostructure

Tatsuro Endo,^{1,*} Masaaki Tanaka,^{1,2} and Shinobu Ohya^{1,2}

¹ Department of Electrical Engineering and Information Systems, The University of Tokyo

² Center for Spintronics Research Network, School of Engineering, The University of Tokyo

*E-mail: tatsuro-endo@g.ecc.u-tokyo.ac.jp

Resonant tunneling (RT), which reflects the coherence of electrons in quantum wells, has been demonstrated in heterostructures using various materials. Among them, there are several reports of negative differential resistance (NDR) related to the resonant states and RT in perovskite-oxide-based heterostructures. For example, there are reports on NDR in heterostructures where defects or impurities are deliberately introduced [1,2] and on RT in heterostructures with thin layers of electron gas formed either by δ -doping [3] or by utilizing a spontaneously formed charged ferroelectric domain wall [4]. These reports on RT, however, are either too complicated for straightforward analysis or give too little room for engineering. Here, we report a clear oscillation of electrical conductivity in a simple oxide-based tunnel diode with a SrTiO_3 (STO) barrier between ferromagnetic $\text{La}_{2/3}\text{Sr}_{1/3}\text{MnO}_3$ (LSMO) and Nb:STO electrodes.

We epitaxially grew a heterostructure composed of 12-nm-thick $\text{La}_{2/3}\text{Sr}_{1/3}\text{MnO}_3$ (LSMO) / 10-nm-thick STO on a Nb-doped STO (001) substrate with a Nb concentration of 0.5 wt% using molecular beam epitaxy (MBE) [Fig. 1(a)]. After electrode patterning with electron beam lithography and Ar milling etching, the sample was annealed under pure oxygen at atmospheric pressure to remove oxygen vacancies. In this heterostructure, differential conductivity oscillations with multiple conduction peaks are visible [Fig. 1(b,c)]. Resonant states arising from carriers confined in the LSMO layer between the STO barrier and the sample surface are probably the cause of this oscillation. The current-voltage curves of our heterostructure show no hysteresis, unlike the heterostructures with oxygen vacancies. We also report the response to the magnetic field, where the differential conductivity oscillation is enhanced when it is placed in the magnetic field applied perpendicular to the film plane [Fig. 1(d)]. Our results show that the simple oxide structure obtained by MBE is capable of oscillatory conduction.

This work was partly supported by Grants-in-Aid for Scientific Research, CREST and ERATO of JST, and the Spintronics Research Network of Japan (Spin-RNJ).

[1] J. Son and S. Stemmer, Phys. Rev. B **80**, 035105 (2009). [2] Y. Hikita *et al.*, Phys. Rev. B **77**, 205330 (2008). [3] W. S. Choi *et al.*, Nat. Commun. **6**, 7424 (2015). [4] G. Sanchez-Santolino *et al.*, Nat. Nanotech. **12**, 655 (2017).

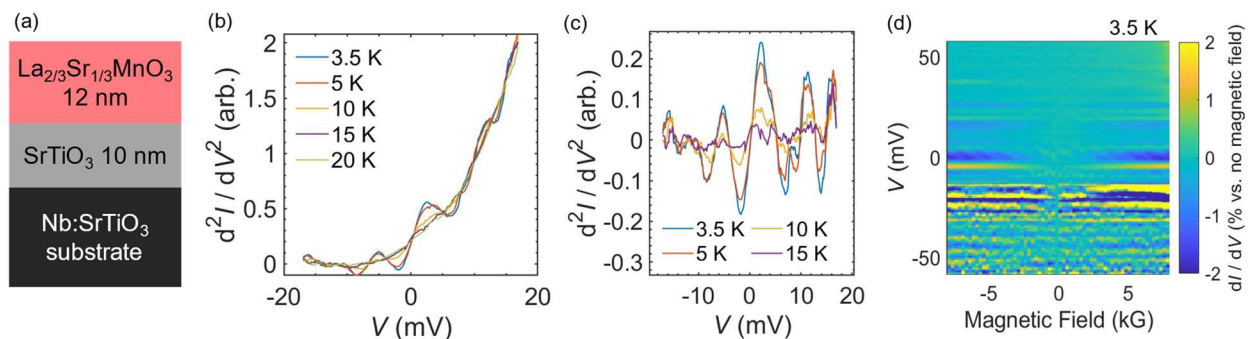


Fig. 1 (a) Schematic cross-sectional illustration of the LSMO/STO/Nb:STO tunneling diode heterostructure used in this study. (b) Derivative of the tunneling conductance obtained at various temperatures. (c) Derivative of the tunneling conductance at 3.5 K, 5 K, 10 K, and 15 K, after subtracting the data obtained at 20 K. (d) Ratio of the differential conductivity to the one at the zero magnetic field under various bias voltages.

Electron spin dynamics in dilute nitride InGaAsN quantum dots grown at different temperatures

Faculty of Information Science and Technology, Hokkaido Univ.

○A. Morita, S. Hiura, J. Takayama and A. Murayama

E-mail: yuzu0226lavendar@eis.hokudai.ac.jp

III-V semiconductor quantum dots (QDs) have attracted much attention as active layers of spin-polarized light-emitting diodes that convert the spin-polarized electrons into the corresponding circularly polarized light [1]. However, the QD luminescence intensity and its circular polarization degree (CPD) are significantly reduced at room temperature due to the escape of electrons from the QDs and the reinjection of spin-depolarized electrons into the QDs [2]. Recently, we found that dilute nitride InGaAsN QDs show strong luminescence at and above room temperature owing to the downward shift of conduction band, which can significantly suppress the electron escape [3]. In this study, we focus on the spin polarization properties of electrons in the dilute nitride InGaAsN QDs, which have not been sufficiently explored. The electron spin dynamics in InGaAsN QDs grown at different temperatures is investigated, because low temperature growth can introduce Ga^{2+} interstitial defects with spin-filtering functions as in dilute nitride GaNAs [4].

Figure 1 shows a schematic illustration of the sample structure. Two types of $\text{In}_{0.4}\text{Ga}_{0.6}\text{As}_{0.98}\text{N}_{0.02}$ QD samples were prepared by RF-plasma-assisted molecular beam epitaxy, in which the QD growth temperatures were 480°C and 420°C. Circularly polarized time-resolved photoluminescence (PL) measurement was performed at 300 K. Spin-polarized carriers were generated by excitation of GaAs barriers with σ^+ circularly polarized laser. Figures 2(a) and 2(b) show the circularly polarized PL time profiles and the corresponding CPD of the 480°C and 420°C samples, respectively. Here, the CPD is defined as $(I_{\sigma^+} - I_{\sigma^-}) / (I_{\sigma^+} + I_{\sigma^-})$ using the circularly polarized PL intensity $I_{\sigma\pm}$, which corresponds to the electron spin polarization at QD states. The 480°C sample indicates a rapid CPD decay from 30% to 5%, which originates from the usual spin relaxation in the QDs. However, the 420°C sample shows a temporarily suppressed CPD decay in the initial time region. This result suggests a selective removal of minority spins from the QD emissive states.

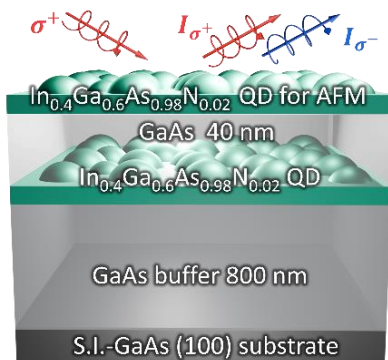


Fig. 1 Schematic illustration of InGaAsN QD sample structure.

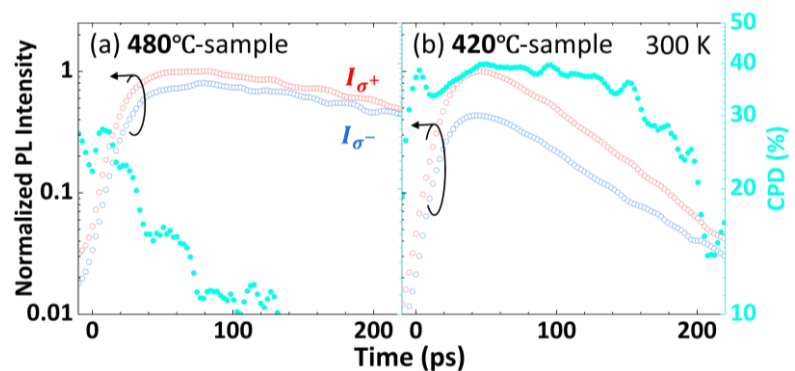


Fig. 2 Circularly polarized PL time profiles and corresponding CPD of dilute nitride InGaAsN QDs grown at (a) 480°C and (b) 420°C.

References:

- [1] K. Etou et al., Phys. Rev. Appl. **19**, 024055 (2023).
- [2] S. Sato et al., Appl. Phys. Lett. **116**, 182401 (2020).
- [3] A. Morita et al., J. Appl. Phys. **134**, 224303 (2023).
- [4] X. J. Wang et al., Nat. Mater. **8**, 198 (2009).

Room temperature voltage control of optical spin polarization maintaining photoluminescence intensity using 0D-2D semiconductor nanostructure

Faculty of Information Science and Technology, Hokkaido Univ.

○Hiroto Kise, Satoshi Hiura, Junichi Takayama, Kazuhisa Sueoka, and Akihiro Murayama

E-mail: h.kise@eis.hokudai.ac.jp

III-V semiconductor quantum dots (QDs) have attracted attention as active layers of optical spin devices owing to the suppressed spin relaxation and high luminescence efficiency. We have focused on the tunnel-coupled structures of QDs and quantum well (QW) [1], and the circular polarization degree (CPD) of photoluminescence (PL) has been manipulated by controlling the injection efficiency of carriers into QDs with an applied electric field [2]. The CPD, which corresponds to the electron spin polarization at the QD states, was defined as $(I_{\sigma^+} - I_{\sigma^-}) / (I_{\sigma^+} + I_{\sigma^-})$, where $I_{\sigma^{\pm}}$ denotes the right/left handed circularly polarized PL intensity. In the previous study, the CPD was successfully modulated by the bias voltage, whereas the PL intensity was simultaneously modulated because carriers easily escape from the QDs depending on the bias condition [3]. In this study, we use InAs QDs as an active layer, which have largely discretized energy states and thus can suppress carrier escape. The bias dependence of circularly polarized PL for three repeats of InGaAs QW-InAs QD tunnel-coupled structure was investigated at room temperature.

Figure 1(a) shows a schematic illustration of the sample structure. The sample with three repeats of InGaAs QW-InAs QD tunnel-coupled structure was grown on a *p*-GaAs(100) substrate by molecular beam epitaxy, and the electrode was fabricated on its surface by standard microfabrication. Figures 1(b) and 1(c) show the circularly polarized PL spectra and corresponding CPD with an excitation laser wavelength of 935 nm (QW excitation) at bias voltages of +0.8 V and -1.6 V, respectively. Focusing on the QD excited state (ES) at around 1.10 eV, there is no PL intensity change between these two conditions, whereas the CPD decreases at a negative bias voltage. Here, the conduction-band potential of the QW is expected to be largely tilted toward the QD side at -1.6 V with respect to the relatively flat band potential at +0.8 V. This band-potential slope can induce the faster drift of electrons, and thus can promote the Dyakonov-Perel spin relaxation in the QW [4]. Therefore, we expect that the depolarization of electrons during injection into the QDs is enhanced.

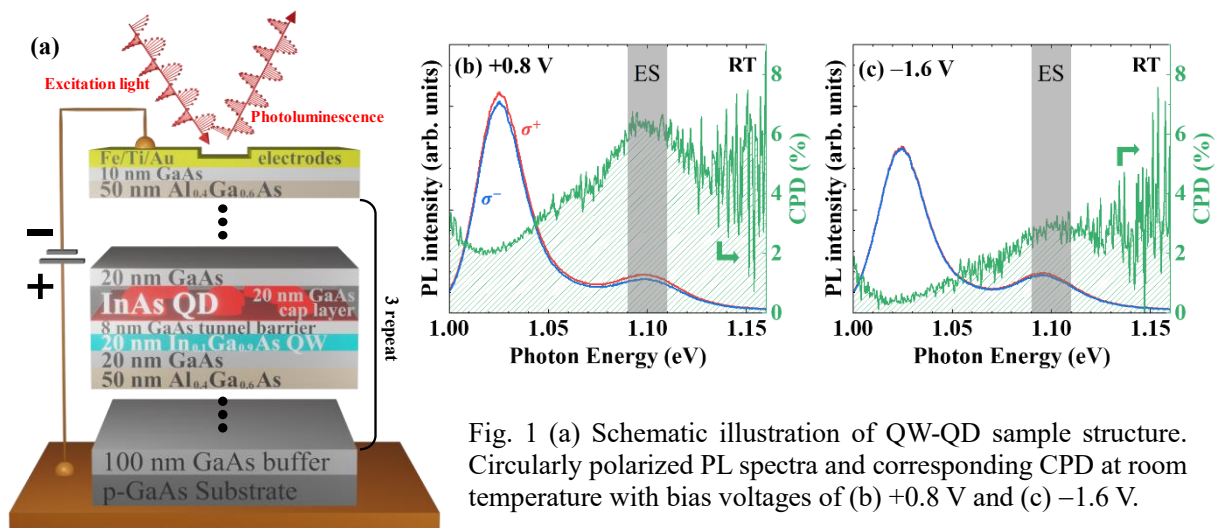


Fig. 1 (a) Schematic illustration of QW-QD sample structure. Circularly polarized PL spectra and corresponding CPD at room temperature with bias voltages of (b) +0.8 V and (c) -1.6 V.

References:

- [1] X. Yang et al., Appl. Phys. Lett. **104**, 012406 (2014).
- [2] H. Chen et al., Appl. Phys. Lett. **114**, 133101 (2019).
- [3] S. Park et al., Nanoscale **15**, 16784 (2023).
- [4] H. Sanada et al., Appl. Phys. Lett. **81**, 2788 (2002).

Effect of spin diffusion on spin dynamics under persistent spin helix regime in a GaAs/AlGaAs semiconductor quantum well

Grad. Sch. of Eng., Tohoku Univ.¹, Univ. of Tsukuba², CSIS, Tohoku Univ.³, DEFS, Tohoku Univ.⁴,
QUARC, QST⁵, °K. Akagi¹, J. Ishihara¹, S. Yamamoto¹, Y. Ohno², and M. Kohda^{1,3,5}

E-mail: akagi.koga.t3@dc.tohoku.ac.jp

In the persistent spin helix (PSH) state, the spin lifetime is ideally infinite, but in an actual system, the spin lifetime is limited by the higher-order Dresselhaus Spin-orbit (SO) field. Near the PSH state, the spin lifetime T_s is expressed as $T_s^{-1} = 6D_s m^2 \beta_3 / \hbar^4$, and is inversely proportional to the spin diffusion constant D_s [1]. D_s is determined by the electron momentum relaxation time τ_p and the electron-electron scattering time τ_{ee} as $D_s = v_F^2 / 2(\tau_p^{-1} + \tau_{ee}^{-1})$, where v_F is the Fermi velocity. Thus, these electron scattering mechanics affect the spin dynamics in the PSH state via the spin diffusion constant. In this work, we investigate the effects of the two types of electron scattering mechanisms on the spin dynamics in a GaAs/AlGaAs quantum well.

We used two samples with the same structure consisting of one-side modulation-doped (001) GaAs/AlGaAs quantum well, but with about a ten-fold difference in electron mobility. This indicates that the τ_p is expected to differ by a factor of ten. Furthermore, the τ_{ee} was modulated by changing the spin excitation density. The spin dynamics was measured at 15 K by the time- and spatially resolved magneto-optical Kerr rotation.

Figure 1 shows the time evolution of electron spins at different excitation densities at the low-mobility sample. The spin relaxation is suppressed by the increase in the excitation density. The observed spin relaxation here is mainly DP spin relaxation [2], in which the spin relaxation time is inversely proportional to D_s . At high excitation density, the electron-electron scattering time decreases and this leads to the reduction of D_s [3]. Assuming that the modulation of SO interactions due to the change in excitation density is negligible, the decrease in the spin diffusion constant due to the enhancement of the electron-electron scattering should cause an extension of the spin relaxation time. We also measure the excitation density dependence of spin dynamics in the high-mobility sample. We will discuss the SO parameters estimated using the spin diffusion method [4] and the effects of two types of electron scattering mechanisms on the SO parameters and the spin dynamics near the persistent spin helix.

This research was supported by JSPS KAKENHI Grant No. 21H04647, JST FOREST and CREST programs (Grant Nos. JPMJFR203C and JPMJCR22C2), and the Iketani Science and Technology Foundation, the Asahi Glass Foundation, and RIEC, Tohoku University.

- [1] S. Anghel *et al.*, J. Appl. Phys. **132**, 054301 (2022).
- [2] M. I. D'yakonov and V. I. Perel, Sov. Phys. JETP **33**, 1053 (1971).
- [3] J. Ishihara *et al.*, Phys. Rev. B **101**, 094438 (2020).
- [4] M. Kohda *et al.*, Appl. Phys. Lett. **107** 172402 (2015).

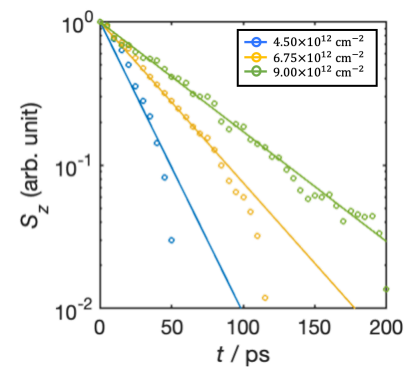


Fig. 1 Time evolution of spins on the low mobility sample at different excitation densities.

Drift-Induced Wavelength Modulation of Electron Spin Waves in Quasi-One-Dimensional GaAs/AlGaAs Quantum Well

Grad. Sch. of Eng., Tohoku Univ.¹, Univ. of Tsukuba², CSIS, Tohoku Univ.³, DEFS, Tohoku Univ.⁴, QUARC, QST⁵, °F. Sugawara¹, K. Kikuchi¹, J. Ishihara¹, S. Yamamoto¹, Y. Ohno², M. Kohda^{1,3,5}

E-mail: sugawara.futa.r6@dc.tohoku.ac.jp

A persistent spin helix state in a semiconductor quantum well suppresses the spin relaxation and forms a spatial spin structure [1], which can be regarded as electron spin waves. In the persistent spin helix, electron spin waves can be transported over distances of more than 100 μm via drift currents [2]. In addition, a previous study has reported the modulation of the spin precession frequency ω and the spatial precession length λ_{so} by the drift velocity based on a two-dimensional device [3]. In this study, we demonstrated the wavelength modulation in a quasi-one-dimensional wire device.

We demonstrate the spin dynamics simulation. We consider a sufficiently long, 5 μm wide wire channel structure in a two-dimensional electron gas in a (001) GaAs/AlGaAs quantum well. The wire width is comparable or less than the wavelength of electron spin wave, which is defined as a quasi-one-dimensional. Electron spins are continuously excited at the position $x = 0$ and transported by in-plane electric fields. We assume that the drift velocity within the channel is constant. The spin precession dynamics are calculated using a Monte-Carlo method based on a drift-diffusion model. We map the time average of spin states up to 1 ns at each coordinate within the channel after calculating the spin dynamics.

Figures 1(a) and (b) show maps of the drifted spin polarization under different simulation conditions. Here, red and blue represent the spin-up state and spin-down state, respectively. For the drift velocity of $v_{\text{drift}} = 1.0 \times 10^4$ m/s, corresponding to the ratio of the drift to the Fermi velocity $v_{\text{drift}}/v_{\text{Fermi}}$ is approximately 0.04, the electron spins are transported along the x -direction with a precession as shown in Fig. 1(a). The spatial precession length of the electron spins, λ_{so} , is 12.30 μm . When the drift velocity is increased 5 times, a phase shift of the spatial precession is observed in the transported electron spins as shown in Fig. 1(b). The λ_{so} in this case is about 13.00 μm , indicating a wavelength modulation of about 6% compared to that in the case of $v_{\text{drift}} = 1.0 \times 10^4$ m/s. This is because the amount of modulation of λ_{so} is expressed as $\Delta\lambda_{\text{so}} = -\pi\hbar^2 (v_{\text{Fermi}}/v_{\text{drift}})^2 / 6m^* \beta_3$, where β_3 is the cubic Dresselhaus coefficient. Then, we will discuss the comparison with the experimental results.

This research was supported by JSPS KAKENHI Grant No. 21H04647, JST FOREST and CREST programs (Grant Nos. JPMJFR203C and JPMJCR22C2), and the Iketani Science and Technology Foundation, the Asahi Glass Foundation, and RIEC, Tohoku University.

[1] M. P. Walser *et al.*, Nature phys. **8**, 757 (2012).

[2] Y. Kunihashi *et al.*, Nat. Commun. **7**, 10722 (2016).

[3] P. Altmann *et al.*, Phys. Rev. Lett. **116**, 196802 (2016).

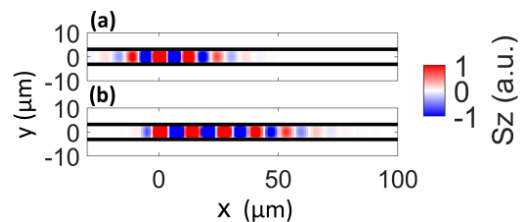


Fig. 1. Map of calculated electron spins under drift transport with $\beta_3 = 0.41 \times 10^{-13}$ eVm. (a) $v_{\text{drift}} = 1.0 \times 10^4$ m/s, (b) $v_{\text{drift}} = 5.0 \times 10^4$ m/s.

Enhancement of Rashba Spin-Orbit Interaction Based on Quaternary InGaAsP/InGaAs Single Quantum Well by Bayesian Optimization

Grad. Sch. of Eng., Tohoku Univ.¹, CSIS, Tohoku Univ.², DEFS, Tohoku Univ.³, and QUARC, QST⁴

○Keito Kikuchi¹, Kohei Yoshizumi¹, Sota Yamamoto¹, Jun Ishihara¹, and Makoto Kohda^{1,2,3,4}

Email: keito.kikuchi.t5@dc.tohoku.ac.jp

In two-dimensional electron gases (2DEGs), the Rashba spin-orbit interaction (SOI) is induced by internal electric fields influenced by band bending in the quantum well (QW) and heterointerface band offsets. These fields can be controlled by an external gate bias [1], allowing spin control without magnetic fields. Previous research shows that 2DEG structures based on InGaAsP/InGaAs are particularly effective in enhancing the internal electric field [2]. Improving our understanding and control of Rashba SOI is critical for the future of semiconductor technology and spintronics. However, enhancing Rashba SOI is challenging due to the many parameters involved in 2DEG structures. Therefore, we used Bayesian optimization to search for quantum structures that maximize Rashba SOI efficiently.

Our base structure is an i-HEMT InGaAsP/InGaAs QW structure with the following parameters: QW width w : 3-20 nm; composition ratio of the barrier layer $((\text{In}_{0.53}\text{Ga}_{0.47}\text{As})_x(\text{InP})_{1-x})$, quantum well layer $(\text{In}_y\text{Ga}_{1-y}\text{As})$, and barrier layer $((\text{Al}_{0.48}\text{In}_{0.52}\text{As})_z(\text{Ga}_{0.47}\text{In}_{0.53}\text{As})_{1-z})$ from the substrate side x, y, z : 0.00-1.00; Si doping concentration: $0.2\text{-}4.0 \times 10^{18} \text{ cm}^{-3}$; and a top gate voltage of $-0.3\text{-}0.3\text{ V}$. Using this structure, we calculated the wave function in the quantum well and the band structure with distortion using nextnano, a semiconductor quantum structure simulation. We then calculated the Rashba SOI, using theoretical calculations [3], and performed Bayesian optimization with the maximization of Rashba SOI as the objective function.

Figure 1 shows the optimized quantum structure obtained in this study. In this structure, Rashba SOI was maximized with a composition such that the barrier layer on the substrate side and the quantum well layer interface were InP/InAs. This structure is characterized by a large valence-band offset (ΔE_{Γ_8}) at the InP/InAs interface, indicating that the interface-induced Rashba SOI has a significant effect. Furthermore, as shown in Figure 2, the Rashba SOI parameter of this structure is optimized about twice as large as that of the previous quantum structure [2] (solid line for this study and dashed lines for Ref. [2]). Our Bayesian optimization successfully optimizes the quantum well structure with large Rashba SOI by the enhancement of the internal electric field generated at the interface. These results demonstrate the effectiveness of our approach using Bayesian optimization.

This research was supported by JSPS KAKENHI Grant No. 21H04647 and JST FOREST and CREST programs (Grant Nos. JPMJFR203C and JPMJCR22C2).

[1] J. Nitta *et al.*, Phys. Rev. Lett. **78**, 1335 (1997).

[2] M. Kohda and J. Nitta, Phys. Rev. B **81**, 115118 (2010).

[3] Th. Schäpers *et al.*, J. Appl. Phys. **83**, 4324–4333 (1998).

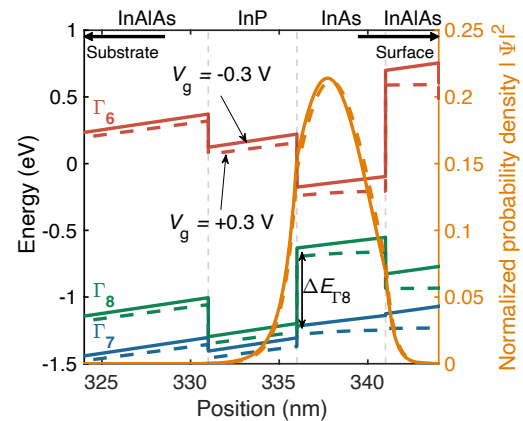


Fig 1: Band structure and wave function of optimized quantum structures and their gate modulation dependence.

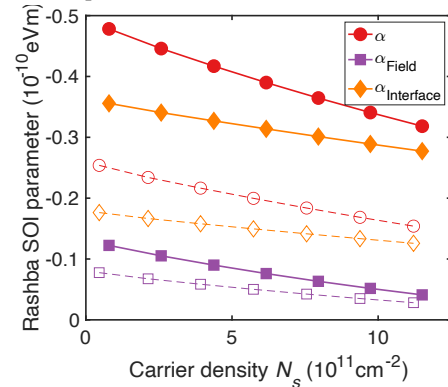


Fig 2: Dependence of Rashba SOI parameter on carrier density. (Solid line) Calculation result for optimized quantum structure. (Dashed line) Calculation result for conventional quantum structure.

GaAs 量子井戸における電子スピン波干渉の光学的観測

Optical Observation of Electron Spin Wave Interference in a GaAs/AlGaAs Quantum Well

○(M1) 檜山未有¹, 菊池奎斗¹, 山本壮太¹, 石原淳¹, 大野裕三², 好田誠^{1,3,4,5}

Grad. Sch. of Eng., Tohoku Univ.¹, Univ. of Tsukuba², CSIS, Tohoku Univ.³, DEFS, Tohoku Univ.⁴, QUARC, QST⁵,

°Miari Hiyama¹, Keito Kikuchi¹, Sota Yamamoto¹, Jun Ishihara¹, Yuzo Ohno², Makoto Kohda^{1,3,4,5}

E-mail: hiyama.miari.q3@dc.tohoku.ac.jp

Electron spin wave (ESW), a spatially structured electron spin polarization resulting from the persistent spin helix, can be exploited as a new information carrier due to its wave-like properties [1]. Here, we demonstrate the interference of ESWs, which is crucial for the realization of ESW-based information processing.

Spatially resolved Kerr rotation microscopy was used to probe the spatial distribution of electron spins in a (001) GaAs/AlGaAs quantum well at 10 K. Figure 1(a) shows the *in-phase* interference of two ESWs: the excitation positions of the ESWs by two pump lasers were separated by an integer multiple of the wavelength of the ESW (in this case the integer is 1), and the excitation helicities of the two pump lasers were the same. As shown in Fig. 1(b), the total spin distribution shown in Fig. 1(a) is deconvolved into two signals corresponding to two different ESWs, each described by the product of Gaussian and sinusoid of position x . At $x = 0$, the spin polarizations generated by the two ESWs are both down. Thus, the enhancement of the spin polarization was observed as a larger Kerr signal at $x = 0$ than the signal expected for the single ESW. On the other hand, Figure 1(c) shows the *anti-phase* interference of two ESWs: the excitation positions of two pump lasers were separated by one ESW wavelength as in Fig. 1(d), but the excitation helicities were opposite to each other. In this case, the direction of spin polarization at $x = 0$ is different depending on the source ESWs. Namely, the spin polarization originating from the left ESW was down at $x = 0$ while that from the right ESW was up at $x = 0$ as shown Fig. 1(d), where deconvolved ESW signals are shown. As a result, the destructive interference was observed as a smaller Kerr signal at $x = 0$ than the signal expected for the single ESW. These experimental results confirm that the interference of ESW as a wave like property is observed, and thus, that the ESW-based information processing can be realized.

This research was supported by JSPS KAKENHI Grant No. 21H04647, JST FOREST and CREST programs (Grant Nos. JPMJFR203C and JPMJCR22C2), and the Iketani Science and Technology Foundation, the Asahi Glass Foundation, and RIEC, Tohoku University.

[1] M. Kohda *et al.*, Appl. Phys. Lett. **123**, 190502 (2023).

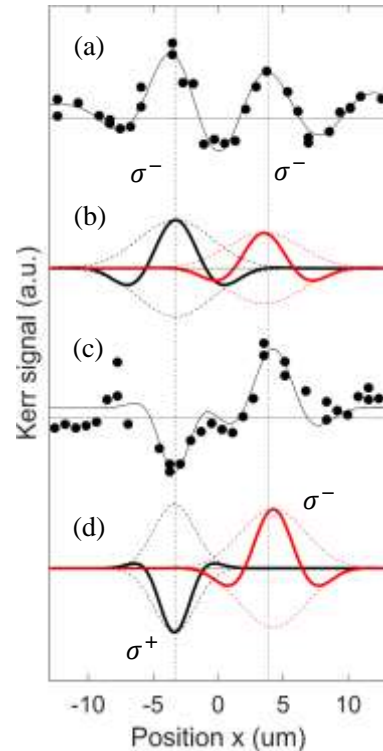


FIG. 1. (a) The in-phase interference of two ESWs. The markers and solid curve indicate the experimental data and fitting, respectively. (b) Deconvolution of two ESWs in (a). The red (black) curve is fit for the Kerr signal of the right (left) ESW. (c) The anti-phase interference of two ESWs. The markers and solid curve indicate the experimental data and fitting, respectively. (d) Deconvolution of two ESWs in (c). The red (black) curve is fit for the Kerr signal of the right (left) ESW. Unlike case (b), the Kerr signals at the excitation positions indicated by the vertical broken lines are opposite for left and right ESWs each other since these were excited by the opposite helicity.

Spin-orbit-torque magnetization switching in a ferromagnetic SrRuO₃ single layer with a spontaneous oxygen atomic displacement

○H. Horiuchi¹, Y. K. Wakabayashi², Y. Araki³, J. Ieda³, M. Yamanouchi⁴, S. Kaneta-Takada¹, Y. Taniyasu², H. Yamamoto², Y. Krockenberger², M. Tanaka^{1,5} and S. Ohya^{1,5}

¹Department of Electrical Engineering and Information Systems, The University of Tokyo

²NTT Basic Research Laboratories, NTT Corporation

³Advanced Science Research Center, Japan Atomic Energy Agency

⁴Division of Electronics for Informatics, Graduate School of Information Science and Technology, Hokkaido University

⁵Center for Spintronics Research Network (CSRN), The University of Tokyo

E-mail: h-horiuchi22@g.ecc.u-tokyo.ac.jp

Perovskite oxide SrRuO₃ (SRO), which is also known as a ferromagnetic Weyl semimetal [1–3], is promising for realizing efficient spin-orbitronics devices. In SRO, large Berry curvature arises due to oxygen octahedral rotation. Such a mechanism to enhance Berry curvature is promising for inducing strong spin-orbit torques (SOTs) that make the manipulation of magnetization efficient [4]. Among applications of SOTs, magnetization switching in a single-layer ferromagnet has been studied recently. However, breaking spatial inversion symmetry, for example, by intentionally introducing a composition gradient, is needed to obtain non-zero net SOT [5, 6]. This makes the crystal growth process difficult while maintaining film quality. Here, we studied an SOT-induced magnetization switching in an epitaxial ferromagnetic SRO *single* layer.

We grew an SRO layer on a SrTiO₃ (STO) (001) substrate using our machine-learning-assisted molecular beam epitaxy system [7]. An important finding is that 7.5 – 10 % of the magnetization in the 26 nm-thick SRO film is stably switched by the in-plane-current injection (Fig. 1). The switching current density of 3.1 ~ 5.3 MA cm⁻² is one order of magnitude smaller than conventional SOT systems consisting of a ferromagnet/heavy metal *bilayer*, indicating the existence of the large SOT. To clarify the reason for the obtained SOT in our SRO single layer, where spatial inversion symmetry seemingly is maintained, we closely analyzed the crystal structure using annular bright-field scanning transmission electron microscopy (ABF-STEM). We found that oxygen octahedral rotation (~5°) occurs especially near the interface between SRO and STO (Fig. 2). Considering also the results of our theoretical calculations based on the tight-binding model [8], the observed partial single-layer magnetization switching can be attributed to the octahedral rotation and the associated large intrinsic spin Hall effect near the interface. These results imply that only a tiny spontaneous displacement of atoms in perovskite oxides plays a pivotal role in spin-orbitronics device applications.

This work was partly supported by Grants-in-Aid for Scientific Research, JST CREST, JST ERATO, and Spintronics Research Network of Japan (Spin-RNJ).

References: [1] G. Koster *et al.*, Rev. Mod. Phys. **84**, 253-298 (2012). [2] K. Takiguchi *et al.*, Nat. Commun. **11**, 4969 (2020). [3] Y. Chen *et al.*, Phys. Rev. B **88**, 125110 (2013). [4] X. Hang *et al.*, APL **118**, 120502 (2021). [5] Q. Huang *et al.*, ACS Nano **16**, 12462 (2022). [6] Y. Joe *et al.*, Nano Lett. **24**, 7100 (2024). [7] Y. Wakabayashi *et al.*, APL Mater. **7**, 101114 (2019). [8] Carter, J.-M. *et al.*, Phys. Rev. B **85**, 115105 (2012).

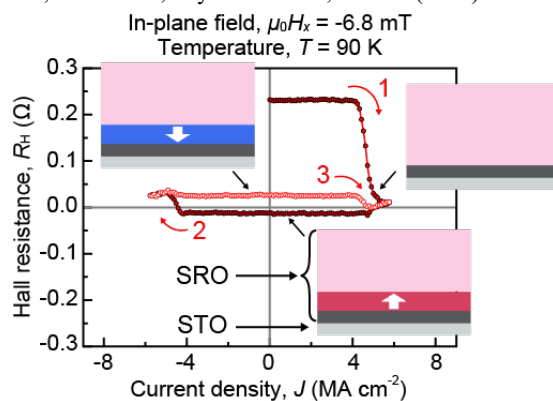


Fig. 1 SOT-induced partial magnetization switching. The insets are the schematic side views of the SRO/STO heterostructure, in which the expected magnetization distributions (red and blue) of our SRO film are indicated. Pink area is in a multidomain state, and gray part illustrates a dead layer of SRO.

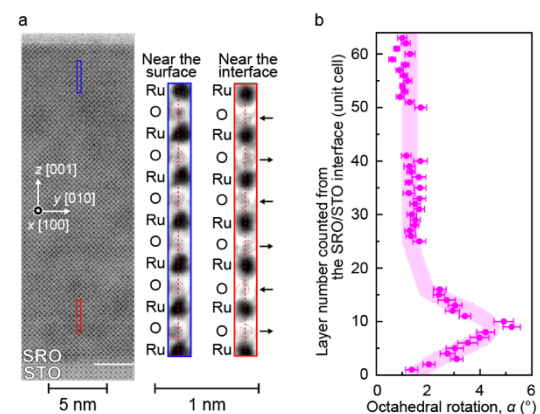


Fig. 2 a, ABF-STEM image of the SRO/STO heterostructure. The right images are the magnified views of the area within the blue and red frames in the main image. **b**, Distribution of the oxygen octahedral rotation angle α along the direction perpendicular to the film.

Spin injection through a ferromagnetic Fe/Mg/SiN/*n*-Si tunnel junction with ohmic-like current-voltage characteristics for non-degenerated *n*-Si

Shoichi Sato^{1,2}, Masaaki Tanaka^{1,2}, and Ryosho Nakane^{1,3}

¹Dept. of Electrical Eng. and Information Systems, ²Center for Spintronics Research Network (CSRN),

³Systems Design Lab (d.lab), The University of Tokyo, 7-3-1 Hongo, Bunkyo-ku, Tokyo 113-8656, Japan

Spin injection into Si using a ferromagnetic metal(FM)/insulator(I)/*n*⁺-Si tunnel junction has been actively studied in recent decades to realize Si-based spin transport devices utilizing spin-polarized electrons [1-4]. It is well known that the spin polarization decreases through stronger spin relaxation in Si as the donor doping concentration N_D is increased [5]. However, in almost all the studies on spin injection so far, a *n*⁺-Si region at the I/Si interface or a *n*⁺-Si substrate has been used to obtain sufficiently large currents for clear spin signals. This is because *n*⁺-Si can supply a large number of electrons in the forward bias regime as well as it can exclude a thick depletion region in the reverse bias regime even when the work function of the FM layer is located in the Si band gap. Thus, it is fundamentally hard to achieve the junction characteristics required for high-performance spin transport devices, i.e., a high-current capability and a high spin polarization in both forward and reverse bias regimes, as long as FM/I/*n*⁺-Si junctions are used. Here, we study a novel approach using a Fe/Mg/SiN/*n*-Si tunnel junction with a low donor concentration N_D . This junction structure can realize both the Fermi-level depinning effect of SiN and the low work function of Mg [6], leading to good electron charge and spin transport characteristics at the same time. This perspective is based on our previous demonstration of spin injection using Fe/Mg/SiO_xN_y/*n*⁺-Si tunnel junctions [3].

We prepared a non-degenerate *n*-Si substrate with a low phosphorus doping concentration of $N_D = 4.3 \times 10^{16} \text{ cm}^{-3}$. After the thermal cleaning of the Si surface, an amorphous SiN layer was formed by direct nitridation process using N₂ RF plasma [3]. Subsequently, Mg ($t_{\text{Mg}} = 0 - 2 \text{ nm}$), Fe (6 nm), and contact metal layers were successively deposited in the same vacuum system. Then, a three-terminal (3T) device schematically shown in Fig. 1(a) was fabricated by photolithography, Ar ion milling, and the deposition of a top Al layer. Figure 1(b) shows room-temperature current-voltage (I_B - V_J) characteristics of 3T devices with various Mg thicknesses ($t_{\text{Mg}} = 0, 0.5$, and 2 nm). The devices with $t_{\text{Mg}} = 0 \text{ nm}$ (black curves) exhibit the rectification characteristics, whereas the devices with $t_{\text{Mg}} = 0.5$ (green curves) and 1.0 nm (red curves) exhibit ohmic-like characteristics. These results indicate the difference in the work function between Fe and Mg, i.e., ohmic-like characteristics are realized through Fermi-level depinning and Mg. Figure 1(c) shows room-temperature 3T Hanle signals [3] (red solid curves) with various I_B ($= -5 - +5 \text{ mA}$), where $t_{\text{Mg}} = 2 \text{ nm}$. The spin lifetime τ_s was estimated from the fittings (black curves) and compared with τ_s estimated by electron spin resonance (ESR). The spin injection into the *n*-Si is strongly supported by the fact that $\tau_s \sim 3.2 \text{ ns}$ is comparable to an ESR-estimated τ_s value for a bulk Si material with a similar N_D value [5]. Unlike our previous study [3], the 3T Hanle signals were clearly observed in both $I_B > 0$ (the spin injection bias (the reverse bias) regime) and $I_B < 0$ (the spin extraction bias (forward bias) regime), which likely originates from the ohmic-like I_B - V_J characteristics of the device.

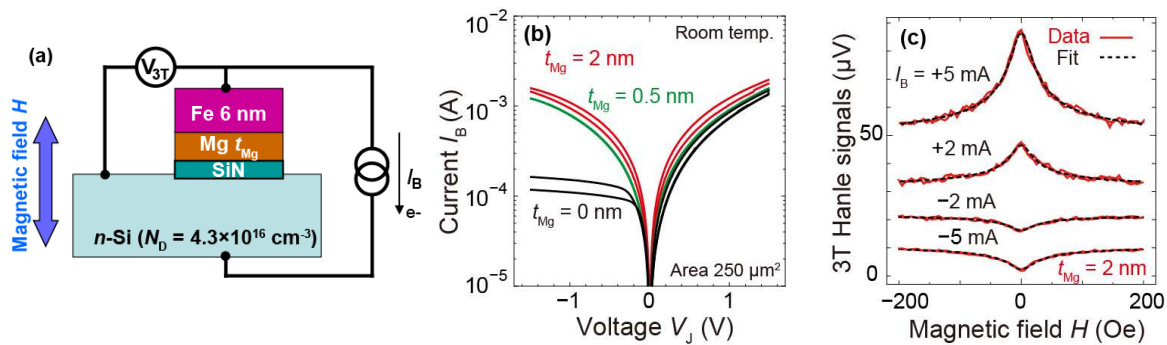


Figure 1 (a) Schematic device structure and 3T Hanle measurement setups. (b) Current-voltage (I_B - V_J) characteristics of the device with the Mg thickness $t_{\text{Mg}} = 0, 0.5$, and 2 nm. (c) 3T Hanle signals (red curves) for $t_{\text{Mg}} = 2 \text{ nm}$ with bias currents $I_B = -5 - +5 \text{ mA}$ and the fitting result for each signal (a black dashed curve).

Acknowledgements This work was partially supported by Grants-in-Aid for Scientific Research (20H05650, 23K17324), CREST Program (JPMJCR1777), and Spintronics Research Network of Japan (Spin-RNJ).

References [1] S. Sugahara and M. Tanaka, Appl. Phys. Lett. **84**, 2307 (2004). [2] H. Koike et al., Appl. Phys. Exp. **13**, 083002 (2020). [3] R. Nakane et al., Appl. Phys. Lett. **112**, 182404 (2018). [4] S. Sato et al., Phys. Rev. B, **102**, 035305 (2020). [5] D. J. Lépine, Phys. Rev. B, **2**, 2429 (1970). [6] D. Connelly et al., Appl. Phys. Lett. **88**, 012105 (2006).

Spin-valve effect with two easy-magnetization axes in a spin-MOSFET based on perovskite-oxide $\text{La}_{0.67}\text{Sr}_{0.33}\text{MnO}_3$ with a LaMnO_3 buffer layer

[○]Aoi Nakamura¹, Tatsuro Endo¹, Masaaki Tanaka^{1,2}, Shinobu Ohya^{1,2}

Department of Electrical Engineering and Information Systems, The University of Tokyo¹,
Center for Spintronics Research Network, School of Engineering, The University of Tokyo²,
E-mail: aoi-nakamura@g.ecc.u-tokyo.ac.jp

Exploring efficient spin-dependent transport is key to realizing next-generation ultra-low-power information processing devices. In particular, a spin MOSFET is expected to be a new nonvolatile device that can significantly reduce the power consumption in logic circuitry. In our previous study, we obtained an extremely high magnetoresistance (MR) ratio of up to 140% at 3 K in a spin MOSFET device based on single-crystal perovskite oxide ($\text{La}_{0.67}\text{Sr}_{0.33}\text{MnO}_3$) (LSMO) [1]. This MR ratio is 10–100 times larger than that reported for semiconductor-based spin-MOSFETs. In this device, we formed a nanometer-sized semiconducting channel by irradiating this region of the LSMO film with Ar ions to introduce oxygen vacancies [2]. By analyzing the I - V characteristics and the back-gate modulation, we clarified that the conduction occurs near the interface between Ar-irradiated LSMO and a SrTiO_3 (STO) substrate. In this presentation, we show the spin-dependent transport properties in a new device, in which a ferromagnetic LaMnO_3 (LMO) layer is inserted between the LSMO layer and the STO substrate. LMO has an electronic structure similar to Ar-irradiated LSMO, thus it is expected that the channel properties are more controllable. An LMO layer has also demonstrated strengthened magnetism in LSMO especially near the interface [3].

We grew an LSMO (12 nm)/ LMO (6 nm) heterostructure on an STO (001) substrate using molecular beam epitaxy (MBE) [Fig. 1(a)]. Our magnetization measurements showed that the Curie temperature of the thin LMO layer in our device is 110 K. We prepared a spin MOSFET device using the same procedure as described in Ref. [1] and measured the spin-dependent transport by varying an in-plane applied magnetic field. Fig. 1(b) and (c) show a representative MR curve and the plot of MR curves relative to the applied magnetic-field direction θ measured from the [100] direction, respectively. We observed large MR ratios of up to 10%. The color map shows anisotropic peaks of the MR ratio at $\theta = 60^\circ$, 105° , 240° , and 285° [red circles in Fig. 1 (c)]. This feature may be explained by a combination of the easy magnetization axes of LSMO and LMO, which are [110] and [010], respectively. Fitting Simmons' equation [4] to the experimental I - V curve yields that the barrier height formed near the LSMO/LMO interface is 81 meV, the length of the channel region is 4.4 nm, and its thickness is 1.2 nm. The obtained barrier height that is larger than that obtained in Ref. [1] (55.5 meV) suggests that the barrier height is increased by inserting the LMO layer [5].

This work was partly supported by Grants-in-Aid for Scientific Research, CREST and ERATO of JST, and the Spintronics Research Network of Japan (Spin-RNJ).

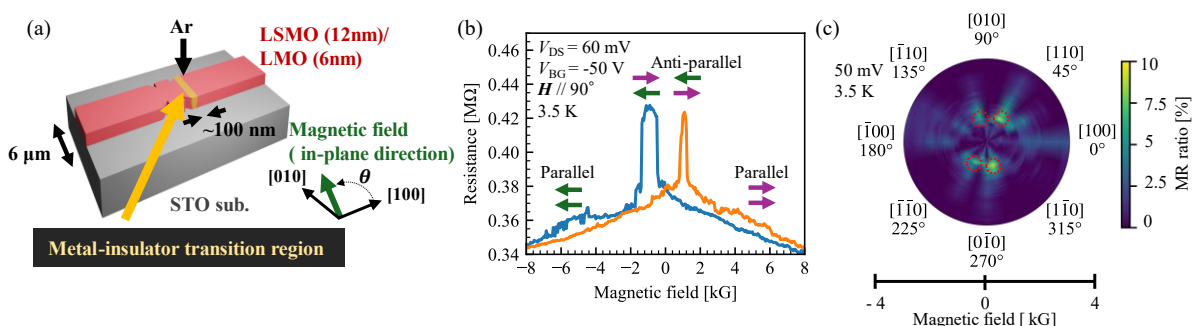


Fig. 1 (a) LSMO/LMO electrodes (red) separated by a tunnel barrier (yellow). The tunnel region is insulating LSMO/LMO made by introducing oxygen vacancy into LSMO/LMO using Ar ion irradiation. (b) Magnetic-field dependence of the resistance when the magnetic field was applied at $\theta = 90^\circ$. A back-gate voltage of -50 V was applied. Green and purple arrows show schematic directions of the magnetization in electrodes. (c) Color map of the MR ratio of our device with respect to the applied magnetic field direction θ . The angle θ of the applied magnetic field is defined in Fig. 1 (a). The MR ratios of up to 10% were observed.

- [1] T. Endo *et al.*, Adv. Mater. **35**, 2300110 (2023).
- [2] L. Cao *et al.*, Phys. Stat. Solidi. Rapid Res. Lett. **15**, 2100278 (2021).
- [3] T. Matou *et al.*, Appl. Phys. Lett. **110**, 212406 (2017).
- [4] J. G. Simmons, J. Appl. Phys. **34**, 1793 (1963).
- [5] P. Jha *et al.*, J. Appl. Phys. **112**, 063714 (2012).

Long-lived valley-polarization in suspended WSe₂ monolayers strained by electrostatic pressure

NTT 物性基礎研¹, 東北大院工² °G. Mariani¹, 国橋 要司¹, L. Smet¹, 若村 太郎¹, 佐々木 智¹,
石原 淳², 好田 誠², 新田 淳作^{1,2}, 眞田 治樹¹

NTT-BRL¹, Tohoku Univ.², °G. Mariani¹, Y. Kunihashi¹, L. Smet¹, T. Wakamura¹, S. Sasaki¹,
J. Ishihara², M. Kohda², J. Nitta^{1,2} and H. Sanada¹

E-mail: giacomo.mariani@ntt.com

Transition-metal dichalcogenides (TMDs) monolayers have been emerging as a platform for hybridizing spintronics, valleytronics, and optoelectronics because of their direct bandgap and spin-valley-dependent optical transitions. However, the properties of TMD monolayers are sensitive to the interfacial inhomogeneities with their supporting substrate. Impurities and strain puddles create potential traps for charges which can affect the valley polarization. Previous studies evidenced that suspended monolayers have improved carrier mobility and are less sensitive to the dielectric screening of the substrate [1]. The dynamics of the valley polarization of suspended monolayers have been mainly studied by photoluminescence (PL) spectroscopy, which limits the analysis to short-lived bright excitons and radiatively recombined carriers. Here, we report the long lifetime of the valley polarization in a suspended WSe₂ monolayer by a pump-probe Kerr rotation (KR) spectroscopy, measured at a temperature of 7 K. Suspended monolayers avoid the screening of photo-excited charged defects, that in the supported or encapsulated monolayers causes a distortion of the voltage-dependent lifetime of the valley polarization. Compared to PL analysis, the KR signal is sensitive to both the radiative and non-radiative recombinations and thus can measure the valley polarization of long-lived complexes such as trions or resident carriers.

Large-area undoped WSe₂ monolayers were prepared by an Au-assisted exfoliation and directly transferred over a hole etched in a Silicon substrate (Fig. 1a). The vertical gap between the Ti-Au top electrode and the doped Si, which serves as a back gate, allows the suspension of the monolayer (Fig. 1b, inset). The back-gate voltage allows a simultaneous control of strain and doping of the monolayer, which is not in direct contact with any material [2]. The maximum deflection at the center of the hole as a function of the voltage is extracted from reflectance spectra (Fig. 1b). The dynamics of the neutral or charged complexes were measured by a two-color time-resolved KR spectroscopy, which uses a circularly-polarized pump pulse (1.734 eV) from a Ti:Sapphire laser to initialize the valley polarization. Linearly polarized probe pulses (1.655 eV, near trion resonance) from another synchronized laser were focused on the pump beam spot and the KR angle of the reflected probe beam was measured to investigate the transient dynamics of the valley polarization after the excitation. The delay between pump and probe pulses was scanned and the KR signal was measured at different gate voltages (Fig. 1c). The maximum measured delay of ~12 ns is set by the repetition rate of the laser. The negative and positive voltages induce a *p*- or *n*-doping of the monolayer, respectively. Different KR offsets and lifetimes, which are V_g -dependent, inferred the existence of a long-lived valley polarization possibly associated with different trion complexes [3].

We demonstrated the long lifetime of the valley polarization in suspended WSe₂ monolayers, revealing dynamics more complex than that detected by only PL analysis. Monolayers suspended over long trenches with lateral confinement may exhibit enhanced diffusion of valley-polarized resident carriers, which can be detected by our technique.

References

- [1] T. Jin, *et al.*, J. Appl. Phys. **114**, 164509 (2013).
- [2] P. Hernández López, *et al.*, Nat. Commun. **13**(1), 7691 (2022).
- [3] M. Ersfeld, *et al.*, Nano Lett. **20**(5), 3147-3154 (2020).

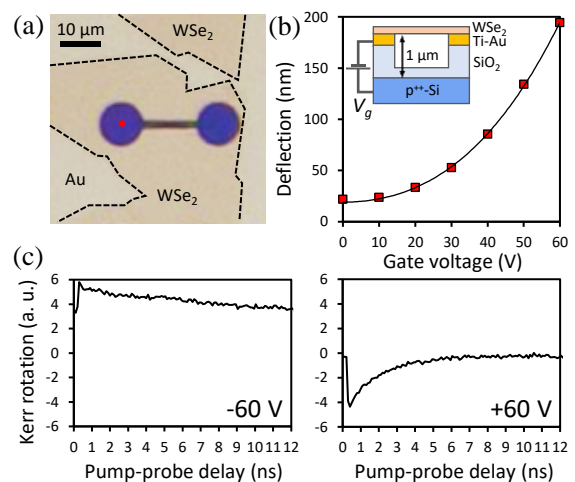


Fig.1: (a) Optical microscope image of a WSe₂ monolayer suspended over holes in a Si substrate. The monolayer over the right hole was opened to create an air vent. (b) Deflection measured at the center of the device (red point in (a)), as a function of the gate voltage V_g . The inset shows the schematic of the device. (c) Time-resolved Kerr rotation near the trion resonance, measured at gate voltages of -60 and +60 V.

Electrical spin injection into GaAs from perpendicularly magnetized Mn/Co bilayers

Grad. School of Information Science and Technology, Hokkaido University.

°Kotaro Nara, Mineto Ogawa, Michihiko Yamanouchi, and Tetsuya Uemura.

E-mail: nara18140148@eis.hokudai.ac.jp

Spin injection from perpendicularly magnetized ferromagnetic materials into semiconductors is an important technique for the realization of semiconductor spintronics devices, such as spin transistors and surface emitting spin lasers. Recently clear perpendicular magnetic anisotropy (PMA) was reported in Co-based ferromagnetic thin films induced by antiferromagnetic δ -Mn [1]. In this study we report on the electrical spin injection into GaAs from perpendicularly magnetized Mn/Co bilayers using a nonlocal detection method.

A layer structure consisting of (from the surface side) Ru cap (2 nm)/Mn (1.7 nm)/Co (1 nm)/ n^+ -GaAs (Si = $7 \times 10^{18} \text{ cm}^{-3}$, 30 nm)/ n^- -GaAs (Si = $5 \times 10^{16} \text{ cm}^{-3}$, 2000 nm)/undoped GaAs (250 nm) was grown on a GaAs(001) single-crystalline substrate. A Hall bar and non-local four terminal devices were fabricated by using electron beam lithography and Ar ion milling. The magnetic properties of Mn/Co bilayer were evaluated by anomalous Hall effect, and spin injection properties were measured by four-terminal non-local geometry.

Fig. 1 shows a transverse resistance R_{yx} of the Hall bar measured at 77 K as a function of out-of-plane magnetic field, $\mu_0 H_z$, where μ_0 is the permeability of the vacuum. The Mn/Co bilayer has a clear PMA with its coercive field of approximately 0.41 T. Fig. 2(a) shows a non-local resistance, R_{NL} , at 77K as a function of $\mu_0 H_z$. Since almost quadratic response to H_z is dominant in R_{yx} due to the magnetoresistance of GaAs, quadratic signal proportional to H_z^2 was subtracted from R_{NL} . As a result, clear spin-valve signals were observed at $|\mu_0 H_z| \approx 0.41$ T as shown in Figs. 2(b) and (c). These results suggest the injection, transport and detection of perpendicular spins in a Mn/Co/GaAs lateral junction.

This work was supported in part by JSPS KAKENHI (22K18961), MEXT X-NICS (JPJ011438), MEXT ARIM (JPMXP1224HK0020), JST CREST (JPMJCR22C2), and JST SPRING (JPMJSP2119).

[1] R.K. Han *et al.*, Phys. Rev. Applied. **19**, 024033 (2023).

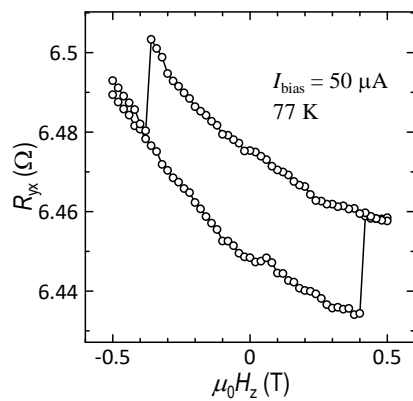


Fig. 1 R_{yx} as a function of $\mu_0 H_z$

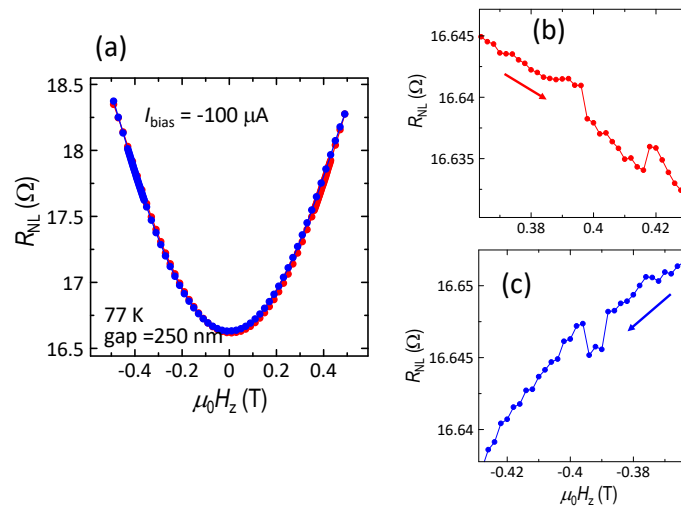


Fig. 2(a) R_{NL} as a function of $\mu_0 H_z$, (b), (c) spin valve signal in R_{NL} observed at $|\mu_0 H_z| \approx 0.41$ T.

遷移金属ダイカルコゲナイド層間における異種磁性原子の磁性相互作用 II

Magnetic interaction of co-intercalated magnetic atoms in transition metal dichalcogenide layers II

北陸先端大 [○](M2) 備前 匠光, 大根 誓哉, 中村 太一, 小矢野 幹夫

JAIST, [○]Takumi Bizen, Seiya One, Taichi Nakamura and Mikio Koyano

E-mail: s2310135@jaist.ac.jp

遷移金属ダイカルコゲナイド(Transition Metal Dichalcogenides; TMD)のひとつである TiS_2 層間に単一ゲストを挿入した磁性層間化合物 M_xTiS_2 の磁性や伝導物性について多くの研究が行われている。特に Fe_xTiS_2 は強磁性やスピングラスを示し、大きな異常ホール効果を示すことが報告されている。本研究では、 TiS_2 層間を“磁氣的相互作用の場”ととらえ異種磁性原子(Fe と Co または Mn)を co-intercalation することで、Fe の異常ホール効果が Co または Mn への置換によってどのような変化を示すか調査することを目的とする。

封管ヨウ素化学気相輸送法を用いて $(\text{Fe}_y\text{M}_{1-y})_{0.33}\text{TiS}_2$ ($\text{M} = \text{Co or Mn}, 0 \leq y \leq 1$) 単結晶を合成した。試料の組成評価には EDX を、結晶構造の評価には XRD を用いた。さらに Quantum Design 社の MPMS を用いて結晶試料の磁化測定および磁気異方性の調査を行った。また同社の PPMS を用いて $(\text{Fe}_y\text{Co}_{1-y})_{0.33}\text{TiS}_2$ ($0 \leq y \leq 1$) のホール効果の温度および磁場依存性を測定した。

Figure 1 に $(\text{Fe}_y\text{M}_{1-y})_{0.33}\text{TiS}_2$ ($\text{M} = \text{Co or Mn}, 0 \leq y \leq 1$) の常磁性 Curie 定数 C の y 依存性を示す。 (Fe, Co) 系の場合、 y (Fe 濃度) が減少するにしたがって C は直線的に減少し、 $y = 0$ でほぼゼロとなる。これは Fe の減少に伴ってモーメントの数が減少することを示している。一方 (Fe, Mn) 系ではその減少は小さく Mn も Fe と同程度の磁気モーメントを持っていることがわかる。Figure 2 に $(\text{Fe}_y\text{Co}_{1-y})_{0.33}\text{TiS}_2$ ($0 \leq y \leq 1$) のホール係数の温度依存性を示す。 $y = 1$ (橙) は 40 K にピークを持つ非常に大きな異常ホール効果を示すが、 y の減少(Fe の減少)とともに異常ホール効果が消失することが分かる。これは Fig. 1 の常磁性 Curie 定数の y 依存性と無矛盾である。

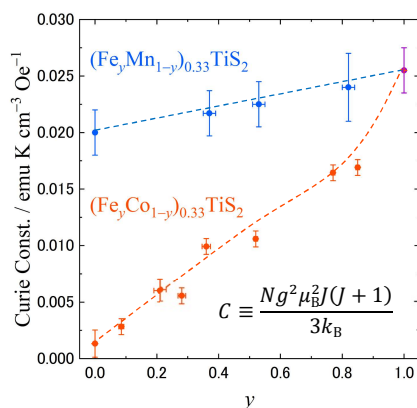


Fig.1 y -dependence of Curie constant C for $(\text{Fe}_y\text{M}_{1-y})_{0.33}\text{TiS}_2$ ($\text{M} = \text{Co and Mn}, 0 \leq y \leq 1$).

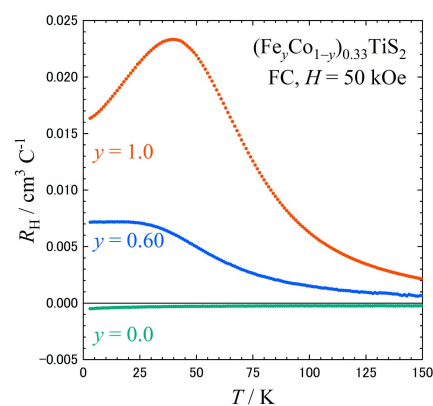


Fig.2 Temperature dependence of Hall coefficient for $(\text{Fe}_y\text{Co}_{1-y})_{0.33}\text{TiS}_2$ ($0 \leq y \leq 1$).

[1] H. Negishi *et al.*, *J. Magn. Magn. Mater.*, **67**, 179 (1987). [2] H. Negishi *et al.*, *J. Magn. Magn. Mater.*, **60**, 259 (1986).

トポロジカル結晶絶縁体 $\text{Pb}_{1-x}\text{Sn}_x\text{Te}$ における非線形プラナーホール効果 Nonlinear planar Hall effect in topological crystalline insulator $\text{Pb}_{1-x}\text{Sn}_x\text{Te}$

京大院工¹, 筑波大院数理物質², 大公大院工³,

○(M2)玉井 優¹, 西嶋 泰樹¹, 小林 純也², 庄司 啓人²,

安藤 裕一郎³, 大島 諒¹, 黒田 眞司², 白石 誠司¹

Kyoto Univ.¹, Univ. Tsukuba², Osaka Metropolitan Univ.³,

°Yu Tamai¹, Taiki Nishijima¹, Junya Kobayashi², Keito Shoji²,

Yuichiro Ando³, Ryo Ohshima¹, Shinji Kuroda², Masashi Shiraishi¹

E-mail: tamai.yu.28c@st.kyoto-u.ac.jp

$\text{Pb}_{1-x}\text{Sn}_x\text{Te}$ (PST)はその組成比により物性が大きく変化し、特に $x > 0.25$ の条件では、バルク内部は絶縁体であるが、その表面は金属的であるトポロジカル結晶絶縁体(TCI)となることが知られている。光電子分光等を用いた研究については複数報告があるが[1], その電気伝導特性、磁気抵抗特性については実験的に未検討な点が多い。我々は、これまでに PST におけるノンリニアホール効果について評価し、室温で極めて巨大であること、更にはその極性をパルス電界印加により不揮発に制御可能であることを報告した[2]。本研究では、運動量空間における非自明なスピントクスチャを探る手法として期待されている非線形プラナーホール効果^[3,4]に着目し、TCI である SnTe と PST, 及びバルク絶縁体である PbTe について評価した。

実験には GaAs 基板上にエピタキシャル成膜された SnTe, PST, 及び PbTe 薄膜を、アルゴンイオンミリングによりホールバー形状に加工した試料を用いた。作製した各デバイスにおいて、非線形プラナーホール効果の有無を確認するため、2 次高調波ホール電圧測定を行った。Fig.1 に SnTe における 2 次の縦方向電圧 $V_{xx}^{2\omega}$ と横方向電圧 $V_{yx}^{2\omega}$ の磁場依存性を示す。 $V_{xx}^{2\omega}$, $V_{yx}^{2\omega}$ とともに先行研究と同様の磁場依存性と角度依存性を持つことが確認された。また、ホールバーの形状を考慮した $V_{xx}^{2\omega}$ と $V_{yx}^{2\omega}$ の振幅比較により、得られた信号は非線形プラナーホール効果が支配的であることが判明した。発表では PST と PbTe の結果についても報告し、非線形プラナーホール効果の起源について議論する。

[1] Y. Tanaka *et al.*, Phys.

Rev B. **87**, 155105 (2013)

[2] T. Nishijima *et al.*, Nano

Lett. **23**, 2247(2023).

[3] P. He *et al.*, Phys. Rev

Lett. **123**, 016801 (2019)

[4] Y. Kozuka *et al.*, Phys.

Rev Lett. **126**, 236801

(2021).

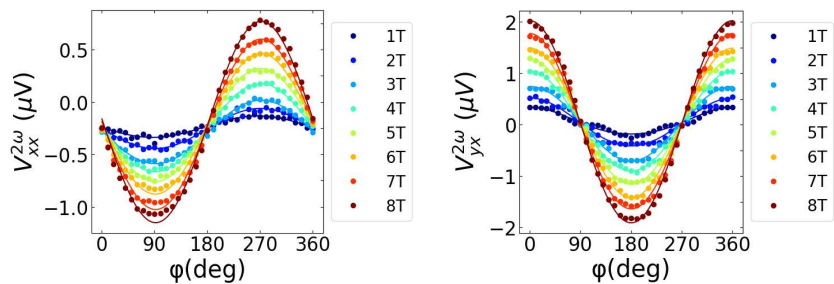


Fig.1 Magnetic field dependence of longitude ($V_{xx}^{2\omega}$) and transverse ($V_{yx}^{2\omega}$) voltage in SnTe.

Observation of bulk and multiple surface states in a thick topological Dirac semimetal α -Sn film by quantum transport

Hideki Maki¹, Tomoki Hotta¹, Soichiro Fukuoka¹, Le Duc Anh^{1,2}, and Masaaki Tanaka^{1,2}

Dept. of Electrical Engineering and Information Systems, The University of Tokyo¹,

Center for Spintronics Research Network, The University of Tokyo²

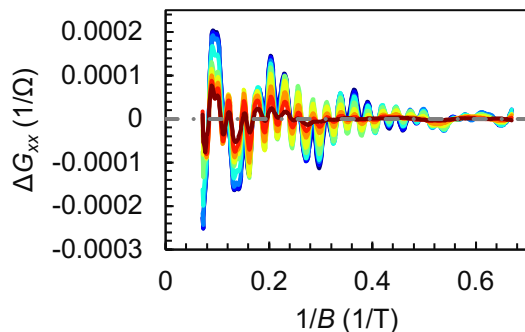
E-mail: maki-hideki725@g.ecc.u-tokyo.ac.jp

Topological materials have recently attracted much attention for spintronics applications due to the spin-momentum-locking nature of their topological surface state. α -Sn under in-plane compressive strain is an elemental topological Dirac semimetal (TDS), which is a parent phase that can be transformed to many other topological phases [1]. The Fermi surface of TDS α -Sn has a multiple-band structure, which was revealed recently to include a linear-dispersion bulk state, a topological surface state (TSS) and a Rashba-like surface state (RSS) with spin-polarization originated from a large Rashba effect on the α -Sn surface [2]. Due to these multiple spin-polarized surface states, TDS α -Sn has potential for spintronics applications. While the linear-dispersion bulk state and TSS of TDS α -Sn have been observed in quantum transport measurements [1], the RSS has never been observed.

We grew a 40 nm-thick α -Sn film on an InSb (001) substrate by molecular beam epitaxy. Through magnetotransport measurements, clear Shubnikov-de Haas (SdH) oscillations are observed (Fig.1). Fourier-transformed spectra of the SdH oscillations exhibit four oscillation components (Fig.2). The observed SdH oscillations are fitted with Lifshitz-Kosevich formula and band parameters such as the relaxation time and mobility are obtained. By comparing the present results with our previous study [1], one of the observed SdH oscillations can be attributed to the RSS of α -Sn, in addition to those corresponding to the InSb, the bulk linear heavy hole (HH) and the TSS of α -Sn. The obtained transport properties of the RSS, relaxation time (215 fs) and mobility (9400 cm²/Vs), are useful for spintronics application using the α -Sn surface states.

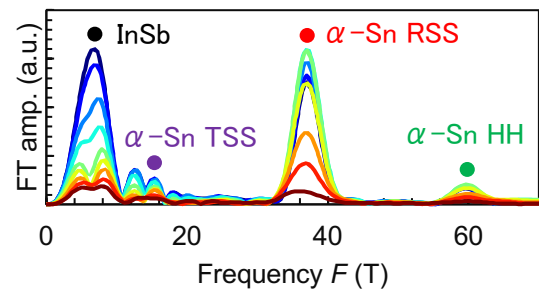
This work was partly supported by Grants-in-Aid for Scientific Research, CREST program and PRESTO Program of JST, and Spintronics Research Network of Japan (Spin-RNJ).

[1] L. D. Anh, *et. al.*, Adv. Mater. **33**, 2104645 (2021). [2] K. H. M. Chen, *et. al.*, PRB **105**, 075109 (2022).



— 2K — 3K — 4K — 5K — 7K
— 10K — 15K — 20K — 30K

Fig.1 Conductance oscillation part ΔG_{xx} of SdH oscillation at various temperatures (2 – 30 K).



— 2K — 3K — 4K — 5K — 7K
— 10K — 15K — 20K — 30K

Fig.2 Fourier transformed (FT) spectra of ΔG_{xx} in Fig.1. Four oscillation peaks are observed, derived from InSb and three α -Sn bands.

10 スピントロニクス・マグネティクス | 一般セッション(口頭講演): 10.5 磁場応用

[19a-C301-1~7] 10.5 磁場応用

[19a-C301-1]

高勾配磁気分離におけるフィルターワイヤー上への粒子堆積過程に関する研究

○廣田 憲之¹、伊藤 永遠²、安藤 努² (1.NIMS、2.日大)

[19a-C301-2]

Fe基アモルファス合金に対する磁場中低温焼鈍の効果

○小野寺 礼尚¹、喜多 英治²、高橋 弘紀³ (1.茨城高専、2.筑波大数理、3.東北大金研)

[19a-C301-3]

Change of Enhancement/Suppression Effects on Solid-phase Reaction on Mn-Sb under High Magnetic Field

○Kosuke Saito¹, Ryota Kobayashi², Yoshifuru Mitsui¹, Rie Umetsu³, Kohki Takahashi³, Keiichi Koyama¹ (1.Kagoshima Univ., 2.NIT, Kurume college, 3.IMR, Tohoku Univ.)

[19a-C301-4]

In situ X 線回折測定による変調回転磁場及び等速回転磁場下での 2 軸性結晶 $\text{DyBa}_2\text{Cu}_4\text{O}_8$ 及び $\text{Dy}_{0.5}\text{Y}_{0.5}\text{Ba}_2\text{Cu}_4\text{O}_8$ の磁気異方性○木村 史子¹、カハガッラ ピュマーリ パモータ¹、足立 伸太郎¹、堀井 滋¹ (1.京都先端科学大工)

[19a-C301-5]

ゼオライト含有高分子複合膜の磁場配向と気体透過特性

○山登 正文¹、牛島 栄造¹、高橋 弘紀² (1.都立大院都市環境、2.東北大金研)

[19a-C301-6]

量子化学計算を援用したセルロース合成酵素サブユニットの三次元磁場配向NMRシミュレーション

○久住 亮介¹ (1.森林総研)

[19a-C301-7]

交流磁場下における液中磁性ナノ粒子の配向運動に及ぼす粒子間相互作用の観測

○諏訪 雅頼¹、塚原 聡¹ (1.阪大理)

高勾配磁気分離におけるフィルターワイヤー上への粒子堆積過程に関する研究

In-situ observation of particles deposition process on filter wires during High Gradient Magnetic Separation

NIMS¹, 日大² °廣田 憲之¹, 伊藤 永遠², 安藤 努²

NIMS¹, Nihon Univ.², °Noriyuki Hirota¹, Towa Ito², Tsutomu Ando²

E-mail: hirota.noriyuki@nims.go.jp

高勾配磁気分離では、磁性ワイヤーで編まれたフィルターを用い、外部から磁場を印加することで磁化されたワイヤー周囲に形成される急峻な磁場勾配を利用して流体中に分散した粒子をその磁性に応じて分離する手法である。粒子は磁気力によりフィルターワイヤー上に捕集されるので、サイズ分離とは異なり、フィルターの目開きを粒子サイズよりも格段に大きくとることが出来るため、目詰まりしにくく、圧損の少ない高速な分離が実現するほか、磁場を取り去ると堆積粒子がフィルター上から脱着するので、フィルターの再利用が可能でコストの低減にもつながり、また、環境にも優しい。しかし、その分離プロセスにおける粒子堆積過程がよく理解されていないため、必要以上に余裕をもった条件による分離が行われていることが多い。粒子堆積過程の理解が深まり、条件の最適化が出来れば、高勾配磁気分離のさらなる普及につながると期待される。そこで本研究では高勾配磁気分離におけるフィルターワイヤー上への粒子堆積過程のその場観察をこうなうことで、その理解を深めることを目指した。

実験では、フィルターワイヤーの表面が観測しやすいよう、CCD カメラとフィルターワイヤー間の障害物や媒体の屈折率変化をもたらす部材をできるだけ排除した。実験にはマグネステン製の線径 1.0 mm、3.5 メッシュのフィルターを用いた。平均粒径 5 μm のフェライト粒子を蒸留水中に分散させたものを試料とした。超伝導磁石中に設置した流路中にフィルターを設置し、気泡が入らないように流路を蒸留水で満たしたのち、所定の磁場を印加し、チューブポンプにより流量を一定として流体試料を流した。この時、フィルター真横と流路中の上流側に設置した CCD カメラにより粒子堆積過程を観測した。図にはフィルター真横から観察した粒子堆積過程の一例を示す。



す。フィルターに到達する以前の段階で、外部印加磁場により粒子が磁化され、粒子間の相互作用によってチェーン状の構造が形成されることがわかった。粒子濃度や印加磁場強度に依存して粒子挙動に違いがみられた。これらの詳細については当日報告する。

図 高勾配磁気分離におけるフィルターワイヤー上への粒子堆積過程のその場観察結果例

Fe 基アモルファス合金に対する磁場中低温焼鈍の効果

Low Temperature Annealing in a Magnetic Field for an Iron-based Amorphous alloy

茨城高専¹, 筑波大数理², 東北大金研³ ○小野寺 礼尚¹, 喜多 英治², 高橋 弘紀³NIT Ibaraki Coll.¹, Univ. of Tsukuba², IMR, Tohoku Univ.³°Reisho Onodera¹, Eiji Kita², Kohki Takahashi³

E-mail: onodera@ibaraki-ct.ac.jp

特定の組成を持つ Fe 基アモルファス合金を適切に熱処理し結晶化させると、軟磁気特性に優れ、かつ高い飽和磁束密度を持つナノ結晶合金を得る[1]. このナノ結晶合金は優れた磁気特性から、トランスやインダクタのコア材料として注目を集めている. ナノサイズの α -Fe 結晶, 狭い粒径分布, 高密度で分散した結晶粒, 粒間アモルファスの存在, の全てを満たすことで優れた磁気特性を獲得するが, そのためには高度な結晶化制御が必要となる.

一方, Fe 基アモルファス合金の結晶化は磁場中熱処理で誘起できると明らかになっており, その起源は磁気エネルギー利得による核形成頻度の増加であると理解されている[2]. この磁場効果は結晶化制御に有効であるが, 20 T 級の磁場が必要であり産業応用できるプロセスではない.

本研究では, 磁場強度を 10 T 以下に抑制する一方で, 熱処理を多段階化し, 結晶化に対する磁場効果を有効に活用する手法の開発を目的としている. 今回, ナノ結晶合金の前駆アモルファス合金に対して, 結晶化に至らない低温での熱処理(低温焼鈍)を無磁場, 磁場中でそれぞれ実施した. 焼鈍温度 T_a は, $T_a = 0.85T_x$, $0.9T_x$ と結晶化温度 T_x の 85, 90%として選択した. 低温焼鈍後のアモルファス合金について, X線構造解析(XRD), メスbauer分光, 示差走査熱量測定(DSC)をそれぞれ実施したため報告する.

Figure 1(a)は低温焼鈍アモルファス合金の XRD, (b)は DSC の結果の一部である. XRD プロファイルにはアモルファスのハローパターン中に僅かに Fe (110) の回折ピークが確認でき, 結晶相がごくわずかに存在していることがわかる. その一方で, DSC で観測できる α -Fe の結晶化ピークは, 低温焼鈍および, 磁場印加によってピークオンセット(結晶化温度: T_x), ピーク温度(結晶化ピーク温度: T_p)は変化しなかった. メスbauer分光の結果については当日報告する.

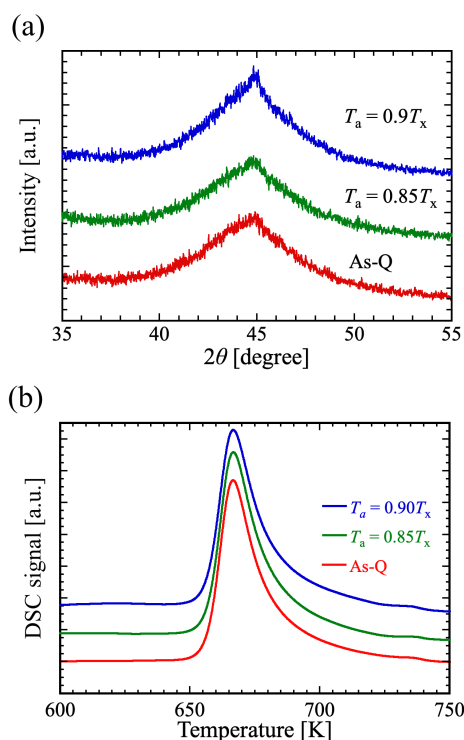


Fig. 1(a) XRD profiles and (b) DSC curves of as-Q and annealed amorphous alloys.

[1] A. Makino, T. Kubota, K. Yubuta, A. Inoue, A. Urata, H. Matsumoto, S. Yoshida, J. Appl. Phys. **109** (2011) 07A302.

[2] R. Onodera, S. Kimura, K. Watanabe, Y. Yokoyama, A. Makino, K. Koyama, J. Alloys Comp., **637** (2015) 213-218.

Change of Enhancement/Suppression Effects on Solid-phase Reaction on Mn-Sb under High Magnetic Field

Kagoshima Univ.¹, NIT, Kurume college², IMR, Tohoku Univ.³

°Kosuke Saito¹, Ryota Kobayashi², Yoshifuru Mitsui¹, Rie Y. Umetsu³, Kohki Takahashi³,

Keiichi Koyama¹

E-mail: k9576360@kadai.jp

Phase transformation and reactions to ferromagnetic phases are enhanced by magnetic fields, which was explained by gain of Zeeman energy [1]. Reactive sintering of ferromagnetic MnBi from nonferromagnetic Mn and Bi powders was enhanced by the magnetic field [1]. It is pointed out for crystallization of Fe-based amorphous, a high magnetic field has an enhancing effect on the nucleation [2,3], while has a suppressing effect on the grain coarsening [2]. It is difficult to evaluate the kinetics of solid-phase reactions in Bi-Mn system due to the low melting point of Bi. To evaluate the kinetics of solid-phase reactions, it is necessary to conduct experiments with raw materials that have higher melting points than Bi. We focused on Mn-Sb alloys which is similar system to Bi-Mn. So far, we found that 5 T magnetic field reduced both preexponential factor f and activation energy Q , resulting the enhancement of reaction [4]. In this study, we found the complex enhancement/suppression effect on the in-field reaction of MnSb alloys for $\mu_0 H \leq 15$ T.

Figure 1 shows the reacted fraction of $\text{Mn}_{1.1}\text{Sb}$ in the function of magnetic field intensity at 673 K (paramagnetic region) and 523 K (ferromagnetic region). It is found that the reacted fraction tends to reduce with applying magnetic field at 673 K. In 523 K, reaction was enhanced by applying 5 T, whereas the reaction was suppressed at 10 and 15 T. This behavior is due to the competition of the change of f and Q of the rate constant. It is found that magnetic state and magnetic field intensity contribute to the enhancement/suppression effect on the reaction. In the presentation, we will show f and Q and discuss in the viewpoint of the relationship between magnetic field and proceeding of the reactive sintering.

[1] Y. Mitsui, *et al.*, J. Alloys. Compd. **615** (2014) 131–134.

[2] H. Fujii, *et al.*, J. Mater. Sci. **43** (2008) 3837–3847.

[3] R. Onodera, *et al.*, Mater. Trans. **54**, (2013) 1232–1235.

[4] K. Saito, *et al.*, Abstract of Joint Conf. of Kyushu Branches of JIMM, ISIJ, and JILM (2024).

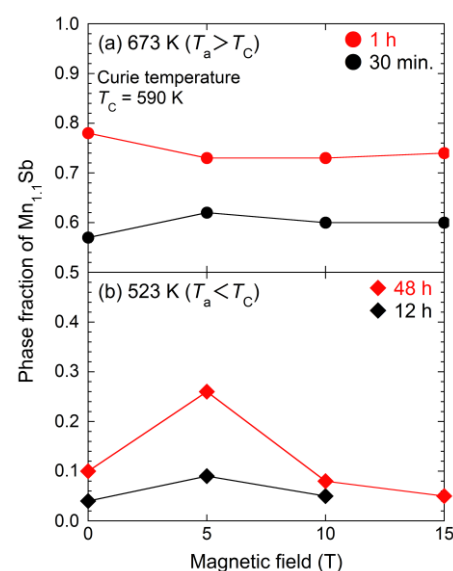


Fig. 1. Relationship between reacted fraction and magnetic field intensity at 673 K (a) and 523 K (b).

In situ X 線回折測定による変調回転磁場及び等速回転磁場下での 2 軸性結晶 $\text{DyBa}_2\text{Cu}_4\text{O}_8$ 及び $\text{Dy}_{0.5}\text{Y}_{0.5}\text{Ba}_2\text{Cu}_4\text{O}_8$ の磁気異方性

Magnetic anisotropy of biaxial crystalline $\text{DyBa}_2\text{Cu}_4\text{O}_8$ and $\text{Dy}_{0.5}\text{Y}_{0.5}\text{Ba}_2\text{Cu}_4\text{O}_8$ under modulated and uniform rotating magnetic fields by in situ X-ray diffraction measurements

京都先端科学大工^o木村史子, カハガッラ ピュマーリ パモーダ, 足立伸太郎, 堀井滋

Kyoto Univ. Adv. Sci., ^oFumiko Kimura, Pamoda Piyumali Kahagalla, Shintaro Adachi,

Shigeru Horii

E-mail: kimrua.fumiko@kuas.ac.jp

1. はじめに

$\text{REBa}_2\text{Cu}_3\text{O}_y$ (RE123, RE:希土類元素, $y=6\sim7$)は, 液体窒素温度以上の高い臨界温度(T_c)と磁場中での高い臨界電流密度(J_c)を有する物質である. しかし, 実用化には結晶の2軸配向制御が必要である. その2軸結晶配向に, 我々は磁化率異方性を用いた磁場配向法を用いている. しかし, RE123は作製過程でtwin結晶を形成する. そのtwin構造過程を解明するためには, まず, twin結晶を有しない結晶を調べ, 比較する必要がある. 今回は, RE123(直方晶)の類縁物質である $\text{REBa}_2\text{Cu}_4\text{O}_8$ (RE124, 直方晶)を検討した. RE124は, twin構造を有さないだけでなく結晶格子内に不定酸素の層が存在しない安定した物質である.

既に, 我々は冷却プロセスの異なる Dy123 及び酸素アニールした Dy123 を用いて, 磁化率異方性比 $(\chi_2-\chi_3)/(\chi_1-\chi_3)$ を求め, 磁気異方性比から双晶組織の形成を論じた. ここで, $\chi_1>\chi_2>\chi_3$ の順で各結晶軸の磁化率を定義した. その結果, ①アニーリング温度 650°C , 0.1% 酸素雰囲気下, ②アニーリング温度 550°C , 0.1% 酸素雰囲気下, ③アニーリング温度 300°C , 100% 酸素雰囲気下の順で磁化率異方性比が減少した. また, $\text{Dy}_{247}(\text{Y}_2\text{Ba}_4\text{Cu}_7\text{O}_y(14<y<15))$ の磁化率異方性比の決定も試みた. 今回, Dy124 及び $\text{Dy}_{0.5}\text{Y}_{0.5}\text{124}$ の磁化率異方性比を求める試みを行い, 更に等速回転磁場下での挙動も検討したので報告する.

2. 実験方法

Dy124 及び $\text{Dy}_{0.5}\text{Y}_{0.5}\text{124}$ 試料作製 Dy124 及び $\text{Dy}_{0.5}\text{Y}_{0.5}\text{124}$ は, $\text{RE}(\text{RE}_2\text{O}_3):\text{Ba}(\text{BaCO}_3):\text{Cu}(\text{CuO})=1:2:4$ のモル比で混合し 880°C で 12 時間, 900°C で 12 時間仮焼し, $\text{RE123}+\text{CuO}$ を合成し, $(\text{RE123}+\text{CuO}):\text{KOH}=5:6$ の質量比で混合し, 700°C で 2 時間フラックス法で結晶育成した. 作製した結晶を粉砕し, 試料とした.

懸濁液の調整 微結晶 Dy124 及び $\text{Dy}_{0.5}\text{Y}_{0.5}\text{124}$ を粘度計校正用標準液 JS160000 (日本グリース(株)製, 粘度 $140\text{ Pa}\cdot\text{s}$) を媒体として約 $10\text{ mass}\%$ になるように懸濁液を調整した.

磁場印加 変調回転磁場印加は静磁場下で試料を 90° 毎に高速と低速回転を繰り返して変調磁場を発生させ印加した. 低速(ω_s)は 30 rpm に固定し, 高速(ω_h)は 37.5 rpm から 67.5 rpm まで変化させた. 等速回転磁場は, 0.09 から 180 rpm まで変化させた. 磁場強度は 1 T であった.

in situ X 線回折測定 Dy124 及び $\text{Dy}_{0.5}\text{Y}_{0.5}\text{124}$ 微結晶懸濁液に変調回転磁場及び等速回転磁場を印加しつつ X 線回折測定を行った. 線源は $\text{MoK}\alpha$ であった.

3. 結果と考察

Figure は, Dy124 及び $\text{Dy}_{0.5}\text{Y}_{0.5}\text{124}$ の $\chi_1\chi_2\chi_3$ 座標系での揺らぎをオイラー角で示したものを ω_h/ω_s に対してプロットした. Dy124 の半価幅は 1.6° から 1.8° で変化し, また, $\text{Dy}_{0.5}\text{Y}_{0.5}\text{124}$ の θ 角についても 2° 前後で変動が小さいため, 正確な磁化率異方性比 $(\chi_2-\chi_3)/(\chi_1-\chi_3)$ を求めることができなかった. しかし, $\text{Dy}_{0.5}\text{Y}_{0.5}\text{124}$ の ψ 角は Dy124 のそれより大きくなっていることから, 試料体積が同じと仮定すると, $(\chi_2-\chi_3)$ の磁化率差は Y の付加により小さくなっていることが分かる. 発表では, 等速回転磁場についても議論する.

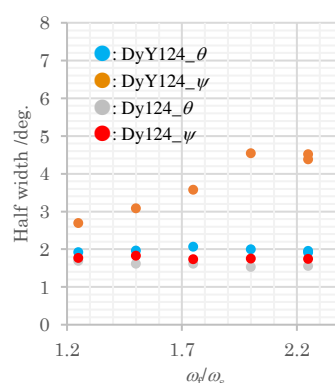


Figure Half width of diffraction spots for {200} and {0014} planes of Dy124 and $\text{Dy}_{0.5}\text{Y}_{0.5}\text{124}$ correspond to the fluctuations of the reciprocal lattice vectors on $\chi_2\chi_3$ (psi) and $\chi_1\chi_3$ (thita), respectively.

ゼオライト含有高分子複合膜の磁場配向と気体透過特性

Magnetic Alignment of Zeolite-Containing Polymer Composite Membranes and their Gas Permeation Properties

都立大院都市環境¹, 東北大金研² ○山登正文¹, 牛島栄造¹, 高橋弘紀²Tokyo Metro. Univ.¹, IMR², °Masafumi Yamato¹, Eizo Ushijima, Kohki Takahashi²

E-mail: yamato-masafumi@tmu.ac.jp

1. はじめに

十分な気体選択性と高気体透過性を有する次世代型 CO₂ 分離膜は地球温暖化抑制で求められる CO₂ 削減のキーマテリアルであり, その開発は喫緊の課題である. 一般に気体分離膜における透過係数と気体選択性は Trade-Off の関係があり, 高分子単独膜でそれを打破することは現状困難であると考えられている. [1]そのため気体選択性の高い無機多孔材料との複合化された Mixed Matrix Membrane(MMM)についての研究が盛んにおこなわれている. [2]ゼオライトに代表される多孔材料は結晶学的にも異方性を有するものも多く, 結晶内に存在する孔を適切に揃えることで, 気体透過における選択性の向上や透過係数の向上が期待できる. [3]ゼオライトの一種である ZSM-5 に注目し, MMM を磁場内で作製し, その配向と気体透過特性について検討したので報告する.

2. 実験

ゼオライトは東ソーの合成ゼオライトである HSZ-800 シリーズを用い, ゼオライト空孔内に存在するカチオンを銅イオンやコバルトイオンに置換したものを用いた. マトリクス高分子は配向を確認する際には PVA を, 気体透過測定する場合はポリエーテルブロックアミド共重合体である Pebax®MH1654 を用いた. MMM は溶媒キャスト法で作成した. 得られた膜の気体透過係数は差圧法により算出した.

3. 結果・考察

図1はイオン交換前の ZSM-5 と Co イオンに交換した ZSM-5 を含有した MMM の WAXD パターンである. Co イオンに交換したことにより磁化容易軸が a 軸から c 軸に変化したことがわかる.

表1は得られた MMM の N₂ と CO₂ の気体透過係数をまとめたものである. MH1654 単独膜と比較すると ZSM-5 を添加することで, N₂ も CO₂ も透過係数は増加した. 銅イオンやコバルトイオンを導入したものはプロトン型と比較するとその効果は小さいかった. これは空孔内の遷移金属イオンが気体透過を阻害していることが原因だと思われる.

一方, 磁場印可すると気体透過係数は大きく変化した. プロトン型では透過係数は減少する一方, 銅イオンやコバルトイオンを導入したものの透過係数は増加した. これはプロトン型 ZSM-5 と遷移金属イオンを導入した ZSM-5 では配向様式が異なるためである. プロトン型は c 軸が磁化困難軸であるのに対し, 遷移イオン置換型は c 軸が磁化容易軸である. 今回作成した膜は膜面内に平行に磁場を印加しているので, プロトン型は孔のない c 軸が面内方向に存在する. 一方, 遷移金属イオン型は孔のない c 軸が面に垂直に存在するため, 気体分子の拡散に大きく寄与したのと考えられる.

参考文献

- [1] L. M. Robeson, *J. Memb. Sci.*, **320**, 390 (2008).
[2] M. A. Aroon, A. F. Ismail, T. Matsuura, M. M. Montazer-Rahmati, *Sep. Purif. Technol.*, **75**, 229 (2010).
[3] M. Hussain, A. Konig, *Chem. Eng. Technol.*, **35**, 561 (2012).

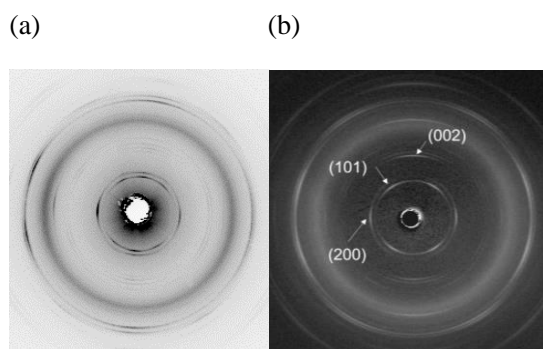


Figure 1. 2D-WAXD patterns of PVA/ZSM-5@H⁺ (a) and PVA/ZSM-5@Co²⁺ (b) prepared in a magnetic field of 10T.

Table 1. Summary of permeability of MMM.

Sample	Permeability /Barrer	
	N ₂	CO ₂
MH1654	1.1	53
MH1654/ZSM-5@H ⁺ 0T	27	120
MH1654/ZSM-5@H ⁺ 10T	2.0	98
MH1654/ZSM-5@Cu ²⁺ 0T	1.2	83
MH1654/ZSM-5@Cu ²⁺ 10T	5.0	92
MH1654/ZSM-5@Co ²⁺ 0T	1.1	62
MH1654/ZSM-5@Co ²⁺ 10T	1.6	69

量子化学計算を援用したセルロース合成酵素サブユニットの 三次元磁場配向 NMR シミュレーション

NMR spectral simulations for magnetically oriented microcrystal suspension of a domain in cellulose synthase

森林総研 久住 亮介

Forestry and Forest Research Products Institute, Ryosuke Kusumi

E-mail: rkusumi@ffpri.affrc.go.jp

二軸性の反磁性微粒子に変調回転磁場を印加すると、三次元的に配向させることができる¹⁾。この三次元磁場配向化法を核磁気共鳴 (NMR) 分光法に応用すれば、化学シフト (CS) テンソル、すなわち原子核周りの電子環境の情報を高精度に取得できる²⁾。特に、NMR 磁石内で試料の変調回転が可能で固体 NMR プローブ³⁾を使用すれば、三次元磁場配向した微結晶の懸濁体 (Magnetically Oriented Microcrystal Suspension, MOMS) の in situ 固体 NMR を通じて、液体中にある微結晶から CS テンソルを直接決定することも可能である⁴⁾。この MOMS-NMR では“微結晶の単結晶 NMR”を通じて対象の原子レベル構造情報を液体中で非破壊に抽出できるため、再結晶化溶液や生理環境下にあるタンパク質・生体化合物などへの応用が期待される。例えば、バイオマスの代表格であるセルロースの合成酵素は、生体内において複数のサブユニットからなる複合体 (CSC) として細胞膜に埋め込まれており、その全体像や産生セルロース繊維の排出機構などは未だ不明瞭なままである。ここに MOMS-NMR を適用すれば、天然の紡糸機構の解明につながる貴重な知見が得られる可能性がある。そこで本研究では、CSC の MOMS-NMR 実験に先立ち、量子化学計算 (密度汎関数法, DFT) を援用して三次元磁場配向した CSC サブユニットの NMR スペクトルのシミュレーションを行なった。

Fig. 1 に、CSC サブユニット (AxCesA) におけるセルロース合成活性部位 PilZ ドメインの Arg643 残基および Lys573 残基について、MOMS-NMR による実測を想定して得られた ^{13}C 化学シフトの振動パターンの例を示す。CS テンソルの計算には農林水産研究情報センターのスーパーコンピュータ上にて Gaussian 16 を使用し、構造モデルは同ドメインの結晶構造 (PDB : 4I86, P2₁2₁2₁)⁵⁾とした。汎関数および基底関数などの条件は B3LYP/6-311G++(2d, p)とした。AxcesA-PilZ ドメインは両残基を通じて環状二グアニルリン酸 (c-di-GMP) を認識し、セルロース合成が活性化されると報告されている⁵⁾。シミュレーションの結果、両残基の振動パターンは大きく異なり、かつ MOMS プローブにおける変調回転軸の傾斜角度に大きく依存することが分かった。CS テンソルは核周りの電子環境の変化を鋭敏に反映するため、c-di-GMP の作用前後における振動パターンの変化を追跡することで、セルロース合成の活性化機構を高精度で解析できる可能性が示唆された。

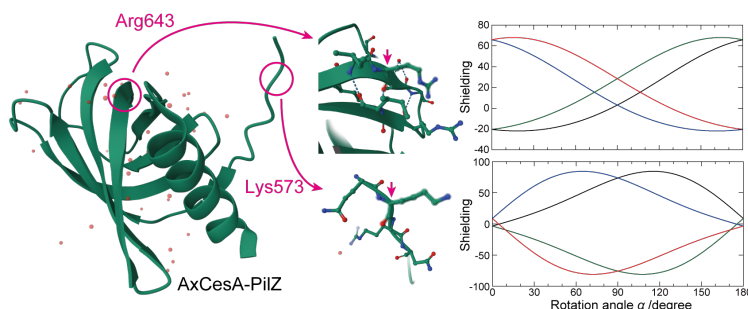


Fig. 1 Single-crystal rotation patterns for carboxyl carbons of Arg643 and Lys573 residues in AxcesA-PilZ. Rotation angle α means the orientation direction of PilZ domain around the modulated rotation axis of MOMS probe⁴⁾.

参考文献

- 1), T. Kimura et al., *Langmuir* **22**, 3464 (2006); 2), R. Kusumi et al., *J. Magn. Reson.* **223**, 68 (2012); 3), R. Kusumi et al., *J. Magn. Reson.* **309**, 106618 (2019); 4), R. Kusumi et al., ISMAR-APNMR 2021; 5), T. Fujiwara et al., *Biochem. Biophys. Res. Commun.* **431**, 802 (2013).

交流磁場下における液中磁性ナノ粒子の配向運動に及ぼす 粒子間相互作用の観測

Interparticle interaction in orientational motion of magnetic nanoparticles in liquid under alternating magnetic field

阪大院理¹ ○諏訪 雅頼¹, 塚原 聡¹

Osaka Univ.¹ ○Masayori Suwa¹, Satoshi Tsukahara¹

E-mail: msuwa@chem.sci.osaka-u.ac.jp

【序論】近年、磁気ハイパーサーミアや磁気粒子イメージングのような、交流磁場に対する磁性ナノ粒子 (MNPs) の応答を利用した医療診断技術の研究・開発が行われている。磁化信号や発熱効率の最適化は、数値計算で行われる場合が多い。しかし、MNP 濃度が高い場合、双極子相互作用を考慮する必要がある、計算コストが高くなる。従って、双極子相互作用を考慮すべき濃度範囲が明らかにする必要がある。我々は、磁場中で MNP 分散液に生じる光学異方性により、MNP 自体の配向ダイナミクスを観測できることを実証した[1]。本研究では、透過率の高い近赤外光を用い、交流磁場中において広い濃度範囲の MNP 溶液の磁気直線複屈折 (MLB) を測定し、配向運動に及ぼす粒子間相互作用の観測を試みた。

【実験】既報[1]の磁気直線二色性測定装置の光源を波長 785 nm の近赤外レーザー光に替え、試料とウォラストンプリズム間に 1/4 波長板を設置し、透過光の楕円率を測定、MLB を見積もった。交流磁場の振幅 $\mu_0 H_0$ は 3 mT 以下、周波数 f は 0.3 Hz ~ 100 kHz の間で測定を行った。MLB の $2f$ 振動成分 B_{2f} の振幅と位相をロックインアンプで測定し、同位相成分 (実部 B'_{2f}) と直交成分 (虚部 B''_{2f}) に分け、周波数に対してプロットした (MLB 周波数スペクトル)。試料として、共沈法で合成したマグヘマイトナノ粒子を用いた。ストック溶液の MNP 濃度は 81.2 mg/mL であり、イオン交換水で希釈して濃度を調節した。

【結果と考察】近赤外光を用いることにより、ストック溶液を試料として用いた場合でも、複屈折測定に十分な強度の透過光を観測できた。MLB 周波数スペクトルの濃度依存性を Fig.1 に示す。濃度の低い範囲では、単緩和型のスペクトルを示した。しかし、10 mg/mL 以上でピーク形状が変化し、低周波数側に広がった。これは粒子間相互作用磁場[2]と交流磁場の振幅が同等となる濃度であり、磁気双極子相互作用により MNP の配向運動が制限されることが示唆された。

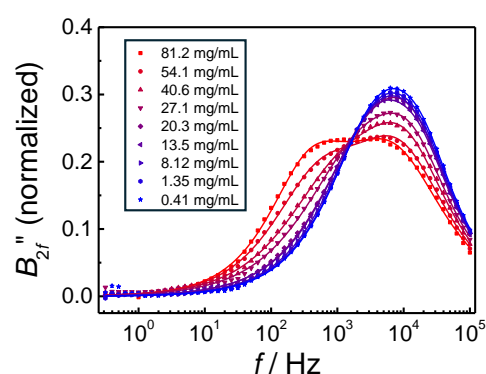


Fig. 1 The evolution of MLB frequency spectra on MNP concentration. For better overview, only imaginary parts were shown. $\mu_0 H_0 = 0.67$ mT.

[1] M. Suwa, S. Kawahigashi, H. Emura, S. Tsukahara, *J. Appl. Phys.* **134**, 233902 (2023)

[2] N. A. Usov, J. M. Barandiarán, *J. Appl. Phys.* **112**, 053915 (2012)